Marco Barla

Tunnels in Swelling Ground

SIMULATION OF 3D STRESS PATHS BY TRIAXIAL LABORATORY TESTING

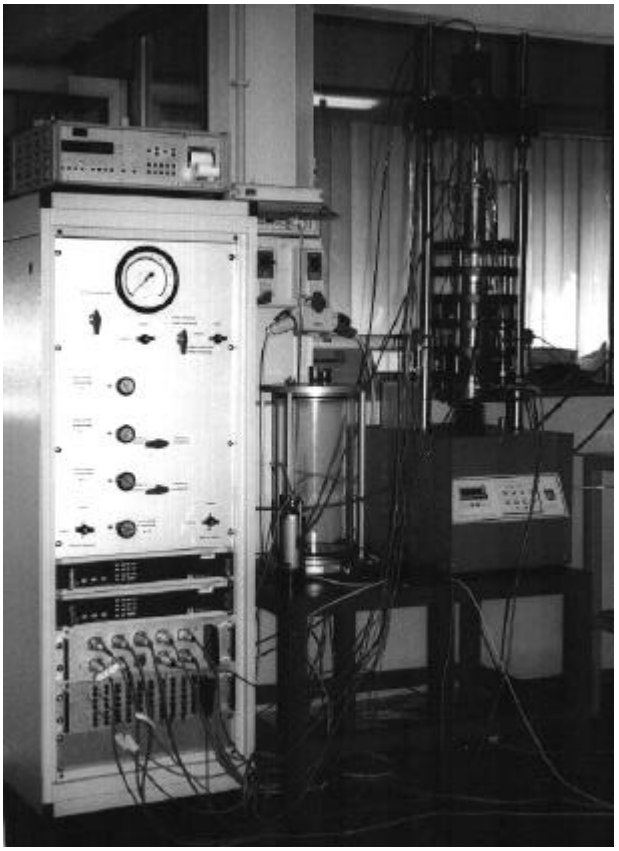

Dottorato di Ricerca in Ingegneria Geotecnica

Politecnico di Torino
Politecnico di Milano
Università degli Studi di Genova
Università degli Studi di Padova

Dottorato di Ricerca in Ingegneria Geotecnica (XII ciclo)

Politecnico di Torino
Politecnico di Milano
Università degli Studi di Genova
Università degli Studi di Padova

November 1999

TUNNELS IN SWELLING GROUND

SIMULATION OF 3D STRESS PATHS BY TRIAXIAL LABORATORY TESTING

……
Marco Barla
Author

…… …… ……
Prof. Michele Jamiolkowski Prof. Giovanni Barla Prof. Diego Lo Presti
Supervisors

……..
Prof. Renato Lancellotta
Head of the Ph.D. Programme in Geotechnical Engineering

“Peace cannot be kept by force,
it can only be achieved by understanding.”
Albert Einstein

SAN DONATO TUNNEL (FLORENCE, ITALY), 1986

SARMENTO TUNNEL (SINNI, ITALY), 1997

Abstract

The present thesis is to contribute to the understanding of the swelling behaviour of tunnels with a major interest being placed on the stress and deformation response in the near vicinity of the advancing face, i.e. in three dimensional conditions.
Following the introduction of the most recent developments, mostly based on contributions of the International Society for Rock Mechanics, the research examines the stress distribution around a circular tunnel by means of numerical methods. According to different stress conditions and stress-strain laws for the ground, the stress history of typical points around the tunnel (sidewalls, crown and invert) is described with the stress path method (Lambe 1967).
This allows one to evidence how the three dimensional analyses results are necessary to describe the ground behaviour. In particular, it can be observed that the excavation is accompanied by a continuous variation of the mean normal stress even for an isotropic initial state of stress. This behaviour cannot be identified by the corresponding two dimensional solutions.
With the stress paths computed, the thesis deals with the design, construction and calibration of a new triaxial apparatus developed with the intent to allow one to reproduce the proposed stress paths. This part of the thesis is intended to allow one to underline some peculiar aspects of the experimental programme: measurements of local deformations, ability to impose on the specimen the desired stress history, capability to assess different experimental quantities versus time.
The thesis continues with the characterisation of the swelling soil used for the testing programme. This soil is a stiff clay (Caneva clay) with samples retrieved by means of a triple tube sampler and also by a cubic sample. Geotechnical characterisation is given in terms of deformability and strength as well as swelling properties by means of the Huder & Amberg oedometer test.
Then the interest is moved to the innovative testing programme undertaken with the new triaxial apparatus and another triaxial cell having similar features. Specimens preparation and testing procedures are described in details. The specimens are submitted to the stress paths computed by numerical analyses with the intent to simulate, “at laboratory scale”, the ground behaviour around the tunnel during face advancement.
The “undrained phase” is initially considered with “compression” (to simulate the sidewall behaviour) and “extension” tests (to simulate the crown/invert behaviour). Then the “drained phase” is reproduced with the intent to study the time dependent response, when the excavation is completed (the head of the tunnel is far away from the section under study) or during a standstill.

The experimental testing allows one to draw some important conclusions on the excess pore pressure induced in the specimen. It has been shown how negative excess pore pressure can develop due to the “compression” stress paths and positive excess pore pressure due to the “extension” stress paths, for the stiff clay under study. This aspect is of a great importance from the engineering point of view, when the analysis is extended to simulate the swelling / consolidation phenomenon induced in the ground after tunnel excavation.
The above observations were compared with similar experiments undertaken at the Massachusetts Institute of Technology on an anisotropic shale. It has been possible to verify the non unique response around the tunnel, with the necessity to undertake additional tests of the same kind as those described above, prior to deriving any conclusions on the design analysis methodology to be adopted.
Some further recommendations are given at the end on the continuation of the research work undertaken with the present thesis. Considering the number of underground infrastructures in difficult conditions, that are nowadays at the design stage or under construction in Italy and around Europe, this continuation is highly desirable.

Sommario

La Tesi affronta un importante problema, di interesse applicativo nel settore dello scavo di gallerie, ricorrendo a metodi teorici e sperimentali propri dell'Ingegneria Geotecnica. Si tratta dell'analisi del comportamento di gallerie in terreni rigonfianti, durante lo scavo e nel lungo termine, ad opera ormai completata.
Dopo un primo inquadramento del problema, alla luce delle conoscenze disponibili e dei più recenti sviluppi sul tema, soprattutto a cura della International Society for Rock Mechanics, lo studio esamina per via teorica (mediante metodi numerici della meccanica del continuo) la distribuzione dello stato di sforzo nell'intorno di una galleria circolare.
Per diverse condizioni tensionali originarie e leggi sforzo-deformazione del terreno in cui avviene lo scavo, lo sviluppo dello stato di sforzo in punti caratteristici nell'immediato intorno della galleria (calotta, piedritti ed arco rovescio) viene rappresentato con il metodo dello *stress path* (Lambe 1967).
Questa procedura consente di evidenziare come i risultati delle analisi numeriche tridimensionali siano indispensabili al fine di descrivere congiuntamente l'evoluzione delle componenti di sforzo durante l'avanzamento del fronte di scavo. Si osserva come, anche nelle condizioni di stato tensionale originario di tipo isotropo, lo scavo sia accompagnato da una variazione continua del primo invariante degli sforzi, durante l'avanzamento del fronte, in contrasto con quanto consentono di prevedere le corrispondenti soluzioni bidimensionali. In particolare il primo invariante degli sforzi aumenta mentre il fronte della galleria si avvicina alla sezione di studio e subisce una consistente diminuzione subito dopo il suo passaggio, per poi aumentare nuovamente ritornando al valore iniziale.
Nella condizione di stato tensionale iniziale non isotropo ($K_o = 2$), per ciò che concerne la simulazione del comportamento dell'elemento sul piedritto, si osserva una diminuzione del primo invariante delle tensioni. In corrispondenza invece dell'arco rovescio si ha un aumento. In entrambi i casi, i percorsi di sollecitazione derivanti da un'analisi bidimensionale sono lineari mentre i risultati delle analisi tridimensionali descrivono andamenti diversi.
Introducendo nei modelli una legge di comportamento di tipo elasto-plastico rammollente, i percorsi di sollecitazione risultano più complessi e di difficile interpretazione. In entrambi i casi di condizione tensionale iniziale ($K_o = 1$ o $K_o = 2$), e per entrambe le situazioni (piedritto e arco rovescio) il valore del primo invariante delle tensioni diminuisce durante lo scavo, per effetto della plasticizzazione che si sviluppa sul contorno della galleria.
Stabilite in tal modo le condizioni di base per il successivo sviluppo della ricerca, la tesi affronta la progettazione, costruzione e taratura di una nuova apparecchiatura triassiale, con la quale riprodurre sperimentalmente gli *stress path* precedentemente calcolati. Si tratta di una parte

molto importante del lavoro, che consente di porre in luce alcuni aspetti rilevanti dell'attività sperimentale svolta: la misura delle deformazioni locali; la capacità di imporre al provino, in modo attento e rigoroso, la storia tensionale scelta; la possibilità di controllo preciso delle diverse grandezze sperimentali nel tempo. La nuova attrezzatura triassiale consente di raggiungere pressioni in cella di 2 MPa e carichi verticali di 50 kN. Può ospitare campioni di 50 e 70 mm di diametro. Il piedistallo su cui poggia il campione è costituito da un meccanismo di scivolamento che ne permette il libero movimento, virtualmente senza attrito, su di un piano orizzontale e si presta ad evitare gli effetti negativi dovuti alle bande di taglio durante la rottura. La cella è dotata di trasduttori di pressione per la misura delle pressioni interstiziali alla base e confinamento, di LVDT per la misura dello spostamento assiale esterno, di una cella di carico interna, di misuratori di deformazione locale assiale e radiale.

La tesi prosegue quindi con la caratterizzazione del terreno rigonfiante preso a riferimento per l'esecuzione delle prove in condizioni di *stress path* controllato. Si tratta di un'argilla consistente (argilla di Caneva), i cui campioni sono stati prelevati sia a mezzo di sondaggi stratigrafico-geotecnici accurati che con campione cubico in galleria. Oltre alla caratterizzazione geotecnica dello stesso materiale, in termini di deformabilità e resistenza, sono presentati i risultati di prove di rigonfiamento (in particolare, la prova di Huder & Amberg).

Si passa quindi alla parte preponderante della ricerca che presenta un articolato ed innovativo programma di prove, condotto ricorrendo alla nuova cella triassiale messa a punto e ad un'altra attrezzatura di caratteristiche analoghe. Sono descritti nel dettaglio la preparazione dei provini e la metodologia di prova attuata, che consiste nel sottoporre il terreno agli *stress path* prima sviluppati per via teorica. L'intento è quello di simulare, in cella triassiale, il comportamento di zone particolari situate in adiacenza al cavo, durante l'avanzamento del fronte. I percorsi di sollecitazione simulati sono quelli corrispondenti al caso elastico $K_o = 1$, sia per ragioni di semplicità che per l'impossibilità di confrontare i risultati con precedenti esperienze per prove che simulassero percorsi di sollecitazione diversi.

È dapprima considerata la cosiddetta "fase non drenata" in cui vengono eseguite prove di "compressione" (atte a simulare il comportamento del terreno in corrispondenza delle pareti della galleria) e prove in "estensione" (atte a simulare il comportamento del terreno in corrispondenza della volta e dell'arco rovescio), partendo da uno stato di sforzo iniziale isotropo; segue la "fase drenata", volta a simulare invece le conseguenti risposte del terreno nel tempo, quando il fronte di scavo è fermo o si è nella fase di avanzamento, con lo stesso fronte di scavo che si allontana gradualmente dalla sezione di interesse a una distanza tale da non influenzare più lo stato tensionale sul contorno nella sezione di studio.

Le prove sperimentali hanno consentito di raggiungere alcune conclusioni fondamentali sulle pressioni neutre indotte all'interno del provino. È stato messo in luce come, nell'argilla consistente oggetto di prova, si possano generalmente sviluppare pressioni neutre negative, a seguito degli *stress path* in "compressione", e positive, dopo quelli in "estensione". Questo aspetto del problema risulta di particolare interesse dal punto di vista applicativo, ove l'analisi venga concordemente estesa alla risposta della galleria durante lo scavo, nei termini di fenomeni di rigonfiamento e/o consolidazione indotti nel terreno.

Vale rilevare come le osservazioni conseguentemente sviluppate siano poste a confronto con i risultati di analoghe sperimentazioni condotte presso il Massachusetts Institute of Technology, su di un argillite a significativo comportamento anisotropo, almeno per la "fase non drenata" e

seguendo uno *stress path* di tipo bidimensionale. È stato così possibile verificare la non univocità della risposta intorno al cavo, con le esigenze di condurre ulteriori sperimentazioni dello stesso tipo di quelle proposte, prima di poter avanzare ipotesi definitive circa la metodologia di analisi progettuale da adottare in sede applicativa.
Infine, la tesi presenta una serie di suggerimenti e raccomandazioni per l'ulteriore sviluppo della ricerca, in un settore particolarmente importante, considerate le numerose costruzioni di infrastrutture sotterranee in condizioni difficili, in fase di progetto o realizzazione nel nostro Paese ed in Europa.
In allegato alla tesi sono inoltre riportati i dati relativi alle prove triassiali effettuate con la procedura proposta, sotto forma di grafici e tabelle in modo tale da rendere possibile un utilizzo degli stessi per successivi lavori di ricerca.

Acknowledgements

The work described in the present thesis has been developed with the financial support of the Ministry of University and Scientific Research (M.U.R.S.T.) of the Italian Government as part of the Research Program "Tunnelling in difficult conditions" (40%) co-ordinated by Prof. G. Barla.
Working at the Politecnico di Torino for three years was a great opportunity to get in contact with many people. A number of them have been taking part to some extent in my research work and I would like to acknowledge them.
Starting with Mr. Belloni, Carrara and Fuoco who took me to several sites, in the period when I was looking for samples to be used in the testing programme, I would also like to thank Mrs. Luisella Vai and Mr. Ugo Rabagliati of Geodes-Torino who introduced me to the geotechnical data of the Caneva clay and the "secrets" of numerical modelling.
When developing the new triaxial apparatus and carrying out the subsequent work, several italian and foreign students have been working with me in the laboratory. Above all I wish to remeber: Mrs. Michela Enzo, Mr. Guido Piasso, Michele Scioia and Nicolas Vandenbussche. A special thank should also be given to Mr. Adrian Grigore, a doctoral student from Roumenia who spent a year working at the Politecnico, and performed with me a part of the calibration testing programme on the new triaxial cell and experienced a couple of triaxial chamber explosions (!).
A special thank is due to Mr. Giuseppe Coenda, the man who manually manufactured the pieces of the triaxial cell in his little but very equipped workshop in Borgo San Paolo (a working-class neighbourhood in Torino). His devotion to work and attention on little aspects of mechanics has been very appreciated but also a great teaching.
Coming to my collegues, the doctoral students Antonella Chiappone, Sebastiano Foti, Ignazio Puci, who started with me, and also Herbert Sarri and Guido Musso, who came later, together with Monica Barbero and Stefania Borgna have been important in providing a friendly and cooperating atmosphere to the research group.
I would like to acknowledge the help of the technicians of the Geotechnical Laboratory, Mr. Roberto Maniscalco and Francesco Froio. Above all thanks are due to Renzo Pallara whose advice and constant presence has been definitely important during the development of the new apparatus and when performing the tests. He really spent a lot of time to introduce me to the experimental techniques and to follow the developing of the control program.
Since for a good habit Supervisors should not be acknowledged, I would like to thank my Dad and his friends Diego and Michele for having trusted and followed me during these three years. Their comments in the review of this thesis were very appreciated, but especially they have

provided me with invaluable encouragement and constant source of hope. In particular a great teaching was their will to continuously get insights into the geotechnical field that I could always feel during our private scientific meetings but also during the Doctoral Committee meetings. Definitely I came to the conclusion that they have a sort of research "instinct"!
And finally I must apologise to my mother and my brother Davide who have stood scientific discussions both at lunch and dinner time until Santina decided to marry me. A special thank is to be devoted to them for their patience and unconditional support. In particular to Santina, who assisted me during the up and down of the research work, being involved during the night experiments, following testing, preparing specimens during the summer holidays and, of course, for her love.

Contents

Chapter 1

Introduction

1.1 Framework

There are no clearly defined rules for design of tunnels in swelling ground. Difficulties are generally met for characterisation and testing of swelling soils and rocks and for prediction of the response to excavation and support loading. This is to be recognised even if significant efforts have been made in the recent past by many researchers, in particular by members of the Commission on Swelling Rocks of the International Society for Rock Mechanics (ISRM 1983, ISRM 1989, ISRM 1994a, ISRM 1994b).
Case histories have been reported where tunnels are shown to have experienced severe problems and difficulties, all caused by swelling during and long after excavation. To remain with important cases in Italy, relevant examples are the San Donato Tunnel, near Florence, and the San Vitale Tunnel, near Benevento, both excavated in clay-shales. Also to be mentioned is the recent costly reconstruction of the concrete invert in the Orte Tunnel, near Rome, which was excavated nearly 30 years ago in stiff clays.
It is as well known that severe difficulties are being met along the new tunnels of the Bologna to Florence high-speed railway line, where excavation takes place, at present, in the clay-shales of the Chaotic Complex. Also, problems are anticipated in connection with the excavation of tunnels in swelling ground along significant lengths of the Alp-Transit Project, in Switzerland, and of the Alpetunnel Project between France and Italy.
Considering the need, as emphasised by the current tunnel projects underlined above, and that additional development are required in the understanding of the swelling behaviour of soils and rocks during excavation, the present thesis is to address this behaviour and the underlying mechanisms, as they occur in argillaceous rocks in the near vicinity of the tunnel face.

1.2 Problem statement

The swelling behaviour in tunnels has been defined succinctly as the time dependent volume increase of the ground, leading to inward movement of the tunnel perimeter. This can be compared with the corresponding definition of squeezing, which underlines the time dependent shearing of the ground leading to inward movement of the tunnel perimeter (Barla G. 1993, Einstein 1996).
With tunnel excavation a stress relief will take place in the cross section considered at a certain distance from the advancing face. Two main types of deformation will occur, namely (1)

immediate and (2) time dependent deformations. The immediate deformation is due to the undrained response of the rock mass to excavation, which may result in negative excess pore pressures both at the sidewalls and in the invert (and crown) under a given primary stress state. The time dependent deformation occurs as the excess pore pressures are reduced leading to consolidation/swelling and creep.
The present thesis is intended to investigate this type of behaviour in argillaceous rocks by performing triaxial tests in which the entire stress history of a ground element located at a known distance from the advancing face will be duplicated. Considering the importance of three dimensional conditions at the tunnel face in determining the tunnel stability and the deformational response, this aspect of the problem need be studied from both the short term and long term points of view.

1.3 Thesis scope and objectives

The scope of the present thesis is to contribute to the understanding of the swelling behaviour of tunnels with major interest being placed on the stress and deformation response in the near vicinity of the advancing face, i.e. in three dimensional conditions. The problem will be analysed from the experimental point of view, by means of triaxial laboratory testing in closely controlled conditions. The stress paths imposed during testing were predicted on the basis of three dimensional stress analyses.
The following main tasks have been undertaken.

- Stress analysis carried out with the objective to define the stress history around a tunnel during excavation. The considered section of interest is placed at a known distance from the advancing face.
- Design, construction and calibration of a new triaxial apparatus for soft rocks, together with the development of software for automated testing and data acquisition. The intent has been centered on the simulation of stress paths as they occur around the excavation, at the sidewalls and in the invert (crown).
- Performance of laboratory tests on a stiff clay (Caneva clay), with emphasis on triaxial testing for a set of conditions (undrained, drained, time-dependent), as they occur during excavation in the vicinity of the tunnel face.
- Analysis and synthesis of the results obtained, with conclusions drawn on the swelling behaviour of argillaceous rocks.

1.4 Organisation of thesis

The thesis is divided into 7 chapters and one appendix. Following the present chapter, which is intended to provide a general introduction to the work carried out, Chapter 2 is to give a brief overview of the subject of swelling ground in tunnels, with emphasis on the swelling mechanism and the testing procedures developed so far, and the types of analyses which are generally carried out for design purposes.

Chapter 3 presents the results of the numerical analyses performed with the intent to study the problem of a circular tunnel in order to improve the understanding of the ground behaviour in two and in three dimensions around the opening, as the tunnel face advances.
Chapter 4 is devoted to a description of the triaxial testing equipment used during this thesis. In particular, the new triaxial apparatus developed is described taking into account its calibration and special features.
Chapter 5 describes the geotechnical characterisation of the Caneva clay, the soil used for testing.
The testing program itself, procedures and results obtained are illustrated in Chapter 6.
Finally some conclusions and suggestions for further work are made in Chapter 7.
Data from the triaxial testing program are listed in Appendix A.

Chapter 2

Swelling in tunnels, existing approaches

2.1 Introduction

Following a brief review of the swelling mechanism as defined by the Commission on Swelling Rock of the ISRM, the present chapter is to examine the existing methods for design and analysis of tunnels in swelling ground. The main purpose is to provide a background description for the subsequent development of this thesis, so that the results obtained can be put in the proper perspective. Reference will be made to ISRM (1989).

2.2 Swelling mechanism

According to the definition given by ISRM (1983), "*the swelling mechanism is a combination of physico-chemical reaction involving water and stress relief. The pysico-chemical reaction with water is usually the major contribution but it can only take place simultaneously with, or following, stress relief*". Einstein (1996) however notes that it would be probably better to modify the second sentence by saying that stress changes "usually" have a significant effect. Swelling can take place in soils and rocks where clay minerals, anhydrite or pirite / marcasite are present.
One can distinguish two typical mechanism: mechanical and physico-chemical.
Mechanical swelling, which occurs in most clays, silty clays, clayey silts and corresponding rocks, is an inverse consolidation or, otherwise expressed, it is caused by the dissipation of negative excess pore pressure. Physico-chemical swelling involves a chemical reaction that can develop between water and mineralogical constituents. This type of swelling depends on the minerals present in the ground.
In argillaceous rocks swelling is caused by one or a combination of three mechanisms: intracrystalline, osmotic and interparticle.
While intracrystalline swelling occurs by hydration of cations, in osmotic swelling water is adsorbed to the exterior surface of clay particles and water molecules are incorporated in the so called "double layer". In the case of interparticle swelling, water is absorbed into clay minerals having expandable layers such as smectites and mixed clay layers. Absorption depends on the distance of clay layers, which in turn depends on the applied stress.
Anhydrite swelling is less frequent than swelling of argillaceous rocks and involves a simple mechanism, hydration. The volume increase is caused by the transformation of anhydrite into gypsum. Calcium sulphate occurs in nature in two different modifications:
anhydrite = $CaSO_4$
gypsum = $CaSO_4 \cdot 2H_2O$

The stability of both modifications depends on the temperature, on the water available and on the applied pressure. At temperature higher than 58°C and at pressure of about 10 N/cm^2 only anhydrite is stable while under 38°C only gypsum can exist. Between the two temperatures, both are stable. Anhydrite can exist under 38°C but only in a metastable modification when water necessary to its transformation into gypsum is not available.
The chemical reaction is as follows:

$$\underset{(46\ cm^3)}{CaSO_4} + \underset{(36\ cm^3)}{2H_2O} \rightarrow \underset{(74\ cm^3)}{CaSO_4 \cdot 2H_2O}$$

If one compares the specific volumes, the cristallised gypsum shows a volume change ΔV:

$$\Delta V = \frac{74 - 46}{46} \cdot 100 = 61\%$$

which shows a higher volume with respect to the anhydritic modification. If the volume of the two molecules of water is taken into account, then the starting volume is 10% higher than the final one. Two cases must be distinguished:

- in a closed system, where anhydrite and water are present in quantity sufficient to the transformation, then the final volume is 10% lower after the transformation;
- in a rock mass, the water may not be present but can be supplied from fractures when a stress relief occurs. In this case the initial volume can increase up to 61%.

2.3 Laboratory techniques

Characterisation of a swelling soil or rock implies two stages, identification and quantification. Different laboratory techniques have been developed to this end and they are illustrated in recommendations of the Commission on Swelling Rock of the ISRM (ISRM 1989, Madsen 1999). As far as the identification of the swelling potential, a wide variety of index tests have been proposed, in addition to mineralogical analysis by X-ray diffrattometry. With reference to the quantification aspect, three tests are recommended as briefly described in the following (Madsen 1999).

Determination of Maximum Axial Swelling Stress
This test is conducted in a conventional oedometer. The sample is assembled under a seating load and water is added. The axial force and the axial displacement are measured and recorded as a function of the elapsed time. Small amounts of axial strain are compensated in a stepwise manner by increasing the axial force. The test continues until no more axial swelling displacement can be observed or the maximum axial force (maximum axial swelling stress) has been reached.

Determination of Axial and Radial Free Swelling Strain.
For this test, the sample is contained in a cell where water can be added. Radial deformation is not prevented as in the conventional oedometer. Axial displacement is measured and recorded. The axial swelling versus time curve can be determined with this test.

Determination of the Swelling Stress as a Function of Axial Swelling Strain.
This oedometer test is an improved version of the original one proposed by Huder & Amberg (1970). It is intended to measure the axial swelling strain necessary to reduce the axial swelling stress of a radially constrained specimen immersed in water from its maximum value to a value which is acceptable in the particular application. The sample is assembled in a conventional oedometer and loaded in a stepwise manner up to a load corresponding to a desired axial stress. The cell is then filled with water and the axial load is reduced in consistent decrements. The swell heave for each decrement is measured until no displacement can be observed for a particular load decrement. The swelling strain (subtracted of the elastic deformation due to unloading) versus axial stress can be determined.

It is noted that oedometers are and have been the traditionally used equipments of swell testing in tunnelling projects. This does not relate only to the history of soil and rock testing, but also to the fact that the arrangement represents a small scale model of a tunnel invert. Only in recent years, mainly with the works of Bellwald (1987) and Aristorenas (1992) at the Massachussets Institute of Technology, the attention has been dedicated to triaxial tests.
It has been progressively realised (Steiner 1993) that, in order to get a better understanding of the swelling mechanisms as they occur around a tunnel, it is essential to conduct triaxial tests. In this way one can duplicate reasonably well the entire history of a ground element around a tunnel, starting with natural state to tunnel excavation.

2.4 Empirical design approach

The empirical design approach is used primarily before construction, when limited geological information is available, or during construction when time is limited. With this approach the user is required to establish the existence of swelling rock through visual inspection, simple measurements and observations of quantifiable parameters or index tests. This qualitative or quantitative description is then directly related to support dimensions or support loads. These pressures or loads are used to determine the appropriate structural dimensions.
Amongst the many existing empirical methods developed (see Steiner 1980, for a complete review), two are often used in the design of tunnel supports in swelling rock, namely those by Terzaghi (1946) and by Peck (1969). Terzaghi listed swelling rock in Class 9 in his rock classification. The rock load for this class is equivalent to 250 feet (~75 m), independent of tunnel dimensions. Following Terzaghi's line of thought, Peck (1969), in his review of tunnelling in soft ground, also stated that the swelling pressure can exceed the overburden pressure. He suggests an equivalent support load corresponding to the pressure of $(\sigma_{vo}+\sigma_{ho})/2$ rather than to the overburden pressure, σ_{vo}, itself; σ_{ho} denotes the initial horizontal stress in the ground. This load assumes no radial deformation of the rock mass due to tunnel excavation, and thus represents the most unfavourable case of the immediate installation of a

perfectly rigid support. One should note that both these methods provide design radial stresses on the tunnel support which are independent of the rock properties and the tunnel dimensions.
Other empirical approaches have been developed in the past few years: e.g. Brekke & Howard (1973), Barton et al. (1974) (also see Franklin et al. 1974 and Barton 1976). Brekke & Howard (1973) developed a functional classification of gouge materials from seams and faults and discussed the appropriate tunnelling method in these materials. Severe swelling problems can be encountered in tunnelling if swelling pressures are greater than 0.25 MPa. The swelling pressure can be obtained either from a direct measurement of the swelling pressure by a laboratory swelling pressure test, or possibly from correlation with the liquid limit test, or from correlation with the percentage of imbibed water under 100% relative humidity. Barton et al.(1974), in their Q-method provide direct relationship between support dimensions and rock mass characteristics, typical of swelling rock. Description and rating with respect to swelling can be found for the parameters J_a and SRF. For swelling rock, the rating of both these parameters increases considerably, and the parameter Q decreases accordingly. Swelling rock is generally rated with the ”extremely poor” to ”exceptionally poor” rock mass quality parameter, Q.
Franklin et al. (1974) developed similar methods for preliminary design of underground openings. The proposed methods consider the swelling pressure as a parameter to determine a ground class; they are, however, not aimed at the design of tunnel support in swelling rock.

2.5 Analytical approach

The analytical approach provides models which describe the behaviour of the rock mass and its interaction with the tunnel support. These models are built within the framework of continuum mechanics and take into account the tunnel geometry, the initial state of stress, the rock properties obtained either from laboratory tests or from in-situ measurements, and possibly the excavation sequences. Three types of models can be distinguished: (1) models based on a swelling law, (2) rheological models, (3) mechanistic models.

2.5.1 Models based on swelling law

The models based on swelling law have been especially developed for tunnel design in swelling rock. They incorporate a swelling law in a classical linear elastic model. The swelling law assumes that, from a given pressure, called the swelling pressure, the material increases in volume as the applied stresses decrease. The main features of these models are summarised in **Table 2.1**.
The swelling law can be directly obtained from one-dimensional swelling tests. Although Terzaghi (1925) is believed to be the first to have used an oedometer test to obtain a relationship between swelling stress and strain, this test is often referred to Huder & Amberg (1970) or to Kovari et al. (1981). As previously described, the ISRM has suggested an improved version of the Huder & Amberg oedometer test.

Table 2.1 Swelling law models (from ISRM, 1989).

Model	Laboratory Test Type	Analytical method
Grob (1972)	1-D oedometer / H&A 1970	Inverse settlement
Einstein et al. (1972)	1-D oedometer / H&A 1970	Inverse settlement
Wittke & Rissler (1976)	1-D oedometer / H&A 1970	FEM
Gysel (1977)	1-D oedometer / H&A 1970	FDM
Gysel & Bellwald (1987)	1-D oedometer / H&A 1970	Closed form
Kovari et al. (1983)	1-D oedometer / H&A 1970	FEM
Schwesig & Duddeck (1985)	1-D oedometer / H&A 1970	FEM
Fröhlich (1986)	1-D oedometer / H&A 1970	FEM
Kovari et al. (1987)	1-D oedometer / H&A 1970	Inverse settlement
Kiehl (1990)	Triaxial / Pregl et al. 1980	FEM

In order to model swelling of the tunnel invert, Grob (1972) approximated field situations with one dimensional (1D) conditions and found relationship **(2.1)** between the axial strain and the axial stress based on oedometer test results, where W and K are material constants of the swelling rock.

$$\varepsilon_a = W - K \log_{10} \sigma_a \tag{2.1}$$

The floor heave is computed following essentially an inverse 1D settlement procedure.
Simultaneously, Einstein et al. (1972) hypothesised that the first invariant of the total stresses controls the volumetric swell deformations. They assumed that the swelling rock behaves as an isotropic linear elastic material, and the stress distribution is obtained accordingly for the oedometer. Results of 1D tests can be extrapolated to three dimensional (3D) conditions with relationship **(2.2)** where ν is the Poisson's ratio and σ_r and σ_a are, respectively, the radial and axial stress in the oedometer.

$$\sigma_r = \left(\frac{\nu}{1-\nu} \right) \sigma_a \tag{2.2}$$

These results are then used to determine the three dimensional state of stress around the tunnel. The assumption of linear elasticity represents a significant simplification, given that the stress strain relations are basically non-linear. The floor heave is evaluated following an inverse settlement computation which relates the change in the first invariant of stress to the volumetric swell deformation.
More recently, similar three dimensional extensions of the swelling law have been incorporated in various methods of analysis, using the finite difference or finite element method (Wittke & Rissler 1976, Gysel 1977, Kovari et al. 1983, Schweisig & Duddeck 1985, Barla G. et al. 1986, Fröhlich 1986) or closed form solutions (Gysel 1987).
Wittke & Rissler (1976), have extended Grob's swelling law to three dimensional conditions. The relationship was found thinking that the swelling deformation can be described, at least

approximately, as a form of true volume change, that can be described by the first stress invariant.
The relationship derived from the three dimensional volume change caused by swelling and the three dimensional stress state is equation **(2.3)**:

$$I_{1,e} = K\left[1 - \frac{1}{\log\left(I_{1,s_o}\,\frac{1-\nu}{1+\nu}\right)}\log\left(I_{1,s}\,\frac{1-\nu}{1+\nu}\right)\right] \tag{2.3}$$

While the 1D and 3D laws are reasonably useful to get first estimates, they are restricted in a number of ways. Examples of restrictions which apply to some of these laws are:
- the assumption of linear elasticity;
- only the strain state corresponding to the final equilibrium can be computed;
- if the initial state of stress in the ground is isotropic, the model predicts that no swelling occurs;
- generalisation of the oedometer test results to 3D.

Clearly, an improvement is possible by determining swelling laws in triaxial tests which better represent the actual stress conditions. Example of triaxial tests to determine the swelling behaviour can be found in Kiehl (1990). Predictive procedures are given by using swelling laws based on the true triaxial tests results of Pregl et al. (1980). In Kiehl's approach, the volumetric swelling strain is controlled by the third invariant of the total stress. Furthermore, a swelling strain-time relationship is derived from the test results and plastic deformations at high deviatoric stresses are introduced by relating them to the undrained shear strength of rock. Anisotropy can also be considered in Kiehl's approach. Although the approach is based on swelling laws rather than mechanistic models, it appears to give results which are consistent with the mechanistic interpretation of swelling which is associated with the dissipation of negative pore pressures.

2.5.2 Rheological models

Because of the observed time-dependency of the swelling and creep processes and the difficulties of understanding these mechanisms, a phenomenological approach, in the form of rheological models, appeared to be attractive. Rheological models are scale-independent representations of material behaviour. They are essentially stress-strain-time models which can describe various types of rock behaviour such as instantaneous and viscous behaviour. They are composed of three basic elements, namely the Hookean (spring) element, the Newtonian (dashpot) element, and the St. Venant (slider) element. The constitutive laws represented by these models depend on the type of elements contained in the model and on the manner in which these elements are combined. Several models have been applied in practice to describe the observed behaviour of swelling rocks (e.g. Lo et al. 1978, Gaudin et al. 1981, Lombardi 1974, Sun Jun et al. 1986, Nguyen Minh & Habib 1988).

Panet (1979) reported the limitations of rheological models used in underground works. It has been recognised that most of the rheological models developed until now deal only with the deviatoric component of the total stress behaviour, implying that the volumetric component is not taken into account. These models are adequate to describe the phenomenon of creep, but not swelling. Swelling around tunnels is a time-dependent volume increase of the ground produced by the adsorption of water in the zones directly adjacent to the excavation (Terzaghi 1936, Terzaghi 1946). Therefore, if one wants to be consistent, should also incorporate in these rheological models the time-dependent volumetric contribution to tunnel deformations. This volumetric contribution has been omitted in most of the previous studies. It has been introduced, however, in viscoelastic models by Sakurai (1977) and Lo & Yuen (1981). A solution for viscoplastic models has been also presented by Lombardi (1984), in which the amount of volumetric strain due to swelling is associated to a change of the stress field which corresponds to a final plastic state of the rock mass directly adjoining a tunnel.
A rheological model for the phenomena of swelling and creep has been developed in a separate study by Aristorenas (1989). Swelling is introduced through a variable bulk modulus, K, which is assumed to be finite (compressible material) and to vary over time whereas in conventional rheological (creep) models the bulk modulus, K, is assumed to be infinite (incompressible material). It is represented by a Burger model joined in series with an arrangement of a Bingham model. This new model has the capability of describing three stages, namely primary, secondary and tertiary, with both volumetric and deviatoric components and shows that the viscoelastic range of rheologic behaviour can be modelled by existing approaches, which do not take into account the volumetric component. This is however no longer correct for the viscoplastic range, where the volumetric component becomes important.
Another attempt by using rheological models has been made by incorporating laws which are obtained through curve fitting to results from either laboratory tests or in-situ convergence measurements. Semple et al. (1973) developed a creep equation for altered rocks, similar to that of Singh & Mitchell (1969). These creep equations were satisfactorily compared with tests on London clay and incorporated in a model for time-dependent behaviour of tunnels. Sulem (1983) and Sulem at al. (1987a, 1987b) analysed measurements of tunnel convergence with time and distance from the tunnel face and derived a time-function of tunnel convergence, through curve fitting. Bellwald (1990) studied this expression in more detail and concluded that the represented behaviour starts with convergence primarily due to consolidation/swelling followed by creep.

2.5.3 Mechanistic models

The models presented so far describe swelling largely without specifically considering the essential element of swelling: water. The mechanistic models directly incorporate the effect of water and thus provide a more rational approach. The mechanical response of a fluid-saturated porous material is characterised by deformation-diffusion processes, specifically consolidation, when there is a volume decrease, or swelling for a volume increase. Only mechanical swelling is assumed and not physico-chemical swelling.

Mechanistic models can be coupled or uncoupled. The uncoupled models were developed first by Terzaghi (1923) in one dimension and extended to three dimensions by Rendulic (1935). In these models, the solutions are obtained by solving the solid and matrix deformation independently of the hydraulic diffusion. In coupled models the deformation and diffusion are solved interactively. The simplest theory is the Biot's poroelasticity theory. Coupled models have been applied to tunnelling problems by Carter & Booker (1982), Detournay & Cheng (1988) for elastic conditions, and Carter (1988) for elasto-plastic conditions.
A further step in the use of coupled models have been made by Anagnostou (1991). He interprets the time-dependent development of swelling strain as a consequence of the dissipation of negative pore pressure. In addition, the flow of water within the rock mass is taken into consideration. This and the modelling of swelling rock as an anisotropic non-linear-elastic, perfectly plastic material appear to produce realistic predictions of swelling strain, specifically in the form of invert heave in tunnels.

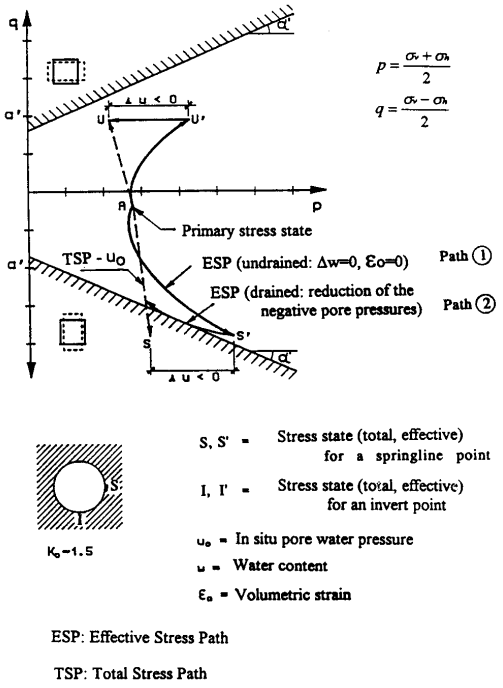

Figure 2.1 Stress path during unloading and swelling of a point of the tunnel invert for a circular tunnel with initial $K_o = 1.5$ (Bellwald 1987).

The latest development in the area of mechanistic modelling is the combination of mechanistic swelling/consolidation models with creep models. Bellwald (1987) has proposed the concept and Aristorenas (1992) has formulated such an approach. The concept simulates the occurrence of negative excess pore pressures associated with the volume increase of the rock

around a tunnel (ESP undrained in **Figure 2.1**) followed by a dissipation of the negative excess pore pressure (ESP drained in Figure 2.1). As negative pore pressures dissipate, the stress state moves closer to the failure state and creep may occur.

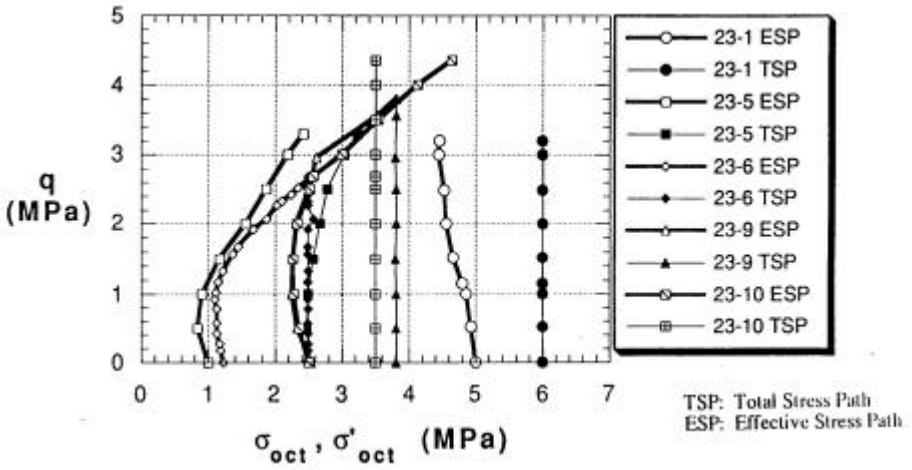

Figure 2.2 Stress paths during undrained compression tests (Aristorenas 1992).

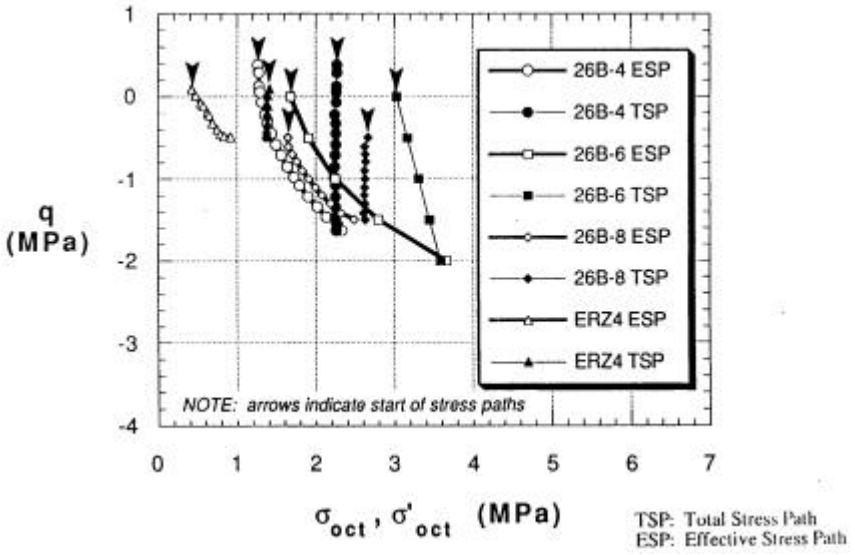

Figure 2.3 Stress paths during undrained extension tests (Aristorenas 1992).

The model developed by Aristorenas is based directly on observations from laboratory triaxial tests on shales. The triaxial undrained and drained tests were performed in a specially devised triaxial apparatus and followed pure shear stress paths in compression and extension. In

Figures 2.2 and **2.3** the total and effective stress paths for compression and extension tests are reported. In **Figure 2.4** stress paths for drained tests are also illustrated. Pure shear stress paths were followed after isotropic consolidation to reproduce the sidewall and the invert behaviour of a circular tunnel. Samples where brought up to failure and, most of them, exhibited a negative pore pressure during the undrained phase.

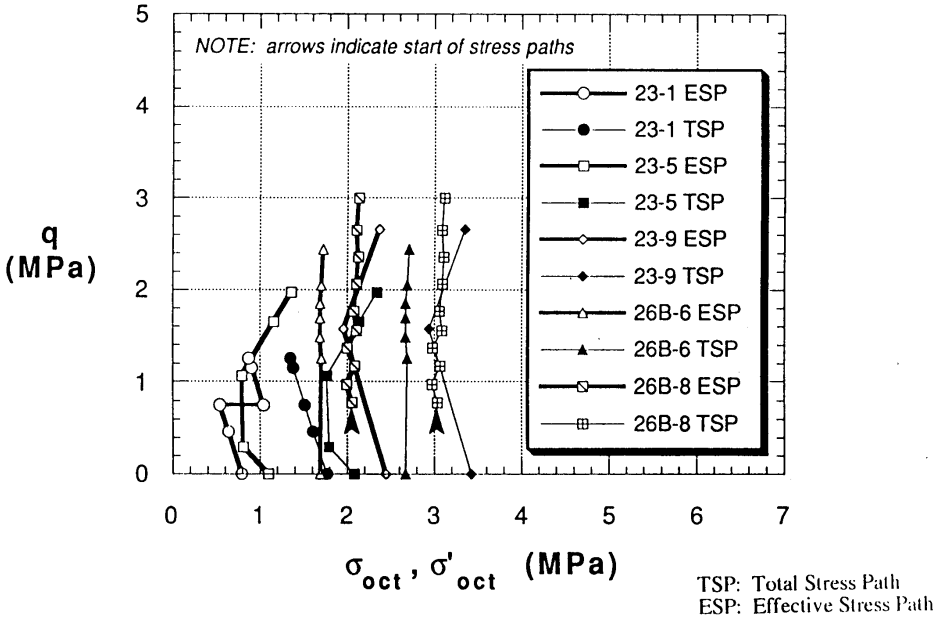

Figure 2.4 Stress paths during drained compression tests (Aristorenas 1992).

The model includes the basic behavioural characteristics of shales, such as anisotropy, plasticity, dilatancy, creep and failure. The evolution of the material deformation is controlled by consolidation (swelling) and creep phenomena. Volumetric strains in the form of contraction and swelling are produced by, respectively, the increase (loading) and decrease (unloading) of the octahedral effective stress. In addition, material expansion (dilatancy) also occurs during shearing and is considered. The analysis indicates that inclusion of creep in the simulation of tunnel excavation in essentially two dimensional conditions significantly increases convergence.

2.6 Determination of stress paths

The stress path, a tool introduced by Lambe (1967), allows the easy visualisation of stress changes in a soil or rock mass during a given event. The stress path is a locus of points in a two-dimensional stress space. Each point defines the current state of stress and the direction

of stress change. With reference to tunnel excavation, as the face is advanced, the initial stresses around the opening are progressively relieved. The state of stress at typical locations (sidewalls, crown, invert) will change continuously until a plane strain condition is attained as the face is at a distance of several times the radius of the tunnel past the section under consideration. If reference is made to design analyses of tunnels, the use of the stress path tool is limited to a number of studies which will be briefly reviewed in the following.

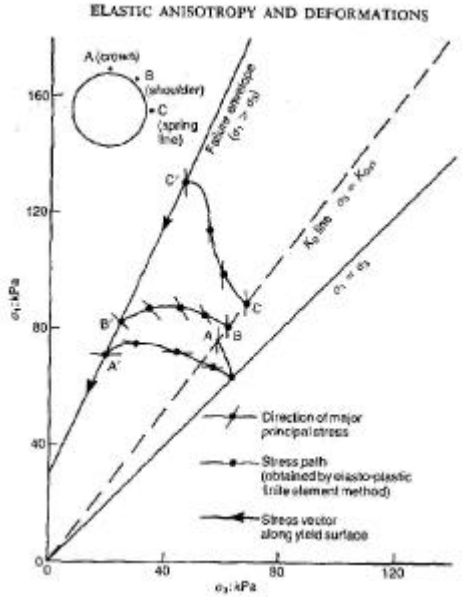

Figure 2.6 Stress paths for typical elements in soil due to tunnelling (Ng & Lo 1985).

Ng & Lo (1985) have studied the stress path at three typical points around a tunnel for the K_o = 0.75 condition using an elasto-plastic finite element analysis in which the excavation process is simulated by reducing the initial stresses. In **Figure 2.6** the stress paths calculated due to tunnelling are reported for three elements (A, B, C) around a circular tunnel.
Steiner (1992) has pointed out the behaviour at the sidewalls, crown and invert of a circular and of a horseshoe shaped tunnel by means of two dimensional computations for a linearly elastic isotropic medium. The stress paths were obtained for a tunnel 400 m below ground and an overburden stress equal to 10 MPa. The horizontal stress ratio varied from K_o = 0.7 to hydrostatic (K_o = 1) to K_o = 1.5. The stresses for the horseshoe shaped tunnel where obtained employing the boundary element code Examine2D and for the circular tunnel with the analytical solution for a hole in a plate. The results of this work are summarised in **Figure 2.7**.

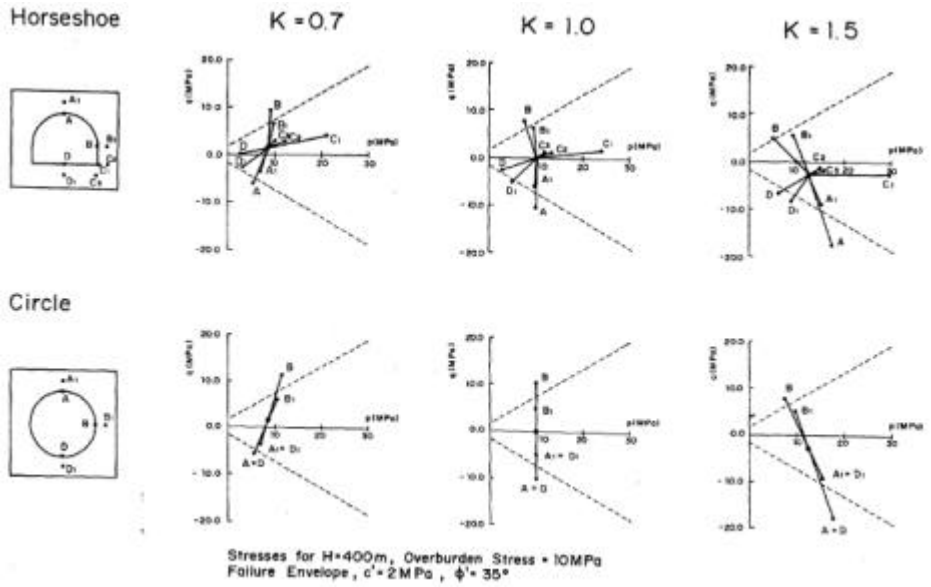

Figure 2.7 Stress paths for typical elements in soil due to tunnelling (Steiner 1992).

Bellwald (1990) and Aristorenas (1992) have examined the effective stress path around a tunnel by means of theoretical considerations. In Figure 2.1, described in the previous paragraph, the effective stress path has been drawn for the invert of a circular tunnel with K_o = 1.5 condition. Two phases can be distinguished, the undrained phase, during tunnel excavation and the drained phase, after excavation, when the negative excess pore pressure dissipates.

Chapter 3

Stress paths around a circular tunnel during face advancement

3.1 Introduction

It has been shown that swelling of soil and rock is a complex phenomenon with a number of important factors influencing it. One of such factors is the stress history at points in the tunnel surround as the face advance takes place. This can be well described by the use of the stress path representation, as proposed by Lambe (1967) for a number of applications to Geotechnical Engineering.
Therefore, it is of interest to develop in the present chapter typical stress paths as created during tunnel excavation, which can be adopted as appropriate input to laboratory testing in three dimensional (3D) conditions. This line of thoughts, which agrees with work previously performed by Ng & Lo (1985), Steiner (1992), Bellwald (1990) and Aristorenas (1992), is appealing with reference to engineering applications in tunnels, when consideration is to be given to 3D conditions and to the influence of the advancing face.

3.2 Influence of tunnel cross section

In this chapter numerical analyses will be performed on the 3D stress distribution around a tunnel as the face is advanced. The tunnel is treated as a circular opening excavated in an infinite medium. The diameter is taken equal to 10 m, which is typical for highway and railway tunnels.
It is realised that circular tunnels represent a simplification of the real problem, mainly if excavation takes place by the conventional method. In all cases, even if circular tunnels may have a simple cross section, they do behave in quite a complicated manner, as it will be shown in the following. As an additional simplification, it is assumed that no presupport/support is present in the tunnel, as the unloading process, although undertaken in multiple stages, will lead to a full stress relieved boundary condition around the tunnel.
It is expected that tunnels of more irregular cross sections will behave in a more complicated fashion. However, the analysis of tunnels with different cross sections is beyond the scope of this thesis. In all cases, it is found useful to derive in the following a few remarks on the influence of cross section on the stress distribution around tunnels in two dimensional (2D) conditions.
The tunnel cross sections investigated are shown in **Figure 3.1**. Four different cross sections have been considered. Cross section 1 is the typical horseshoe shaped tunnel, with vertical

sidewalls and invert arch. Cross section 2 is a horseshoe shaped tunnel, however with curved sidewalls. Cross section 3 is similar to the previous one with a flatter invert arch and with two small arches connecting the sidewalls to the invert, in order to avoid angular points. Cross section 4 is the circular tunnel.

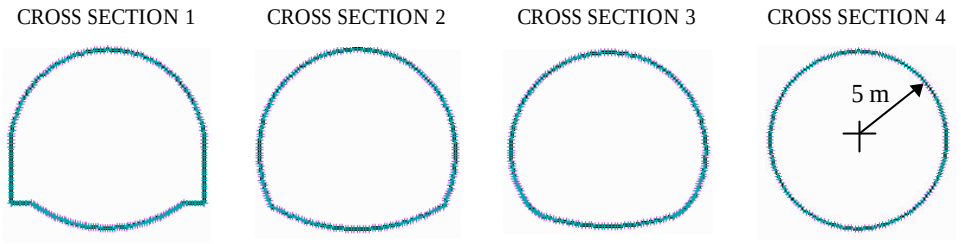

Figure 3.1 Different tunnel cross sections considered.

The ground around the tunnel is assumed to behave according to a linearly elastic, homogeneous and isotropic medium (ILE), with E (elastic modulus) = 400 MPa and ν (Poisson's ratio) = 0.3. The analyses have been performed with the Phase^2 Finite Element code (Rocscience 1999) for two different stress ratios (K_o = 1 and K_o = 2), with an initial vertical stress of 1 MPa.

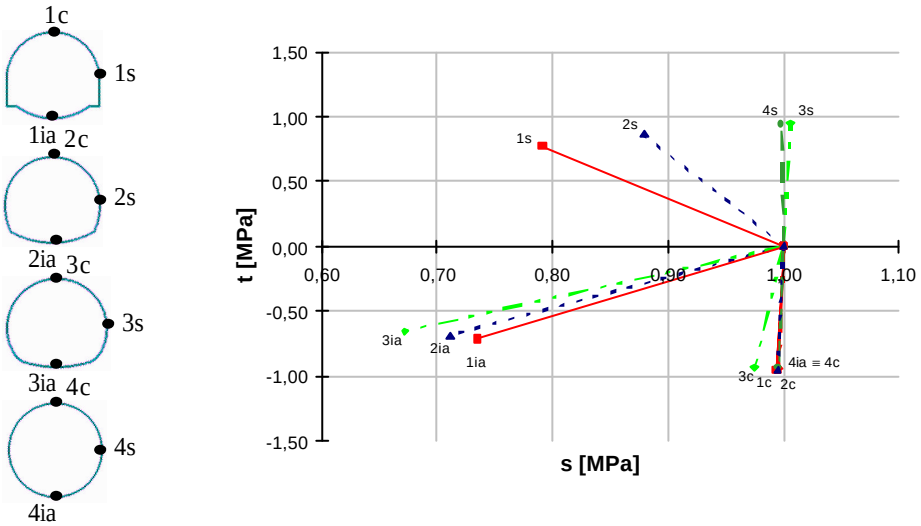

Figure 3.2 Stress paths around the tunnel for the different cross sections, K_o = 1.

The stress paths for some significant points around the tunnel and for the values of K_o considered, are illustrated in **Figures 3.2** and **3.3**. With the assumption that swelling will take

place where the first invariant of the induced state of stress is lower than the corresponding one computed for the initial state of stress, **Figures 3.4** and **3.5** show the zones where swelling is likely to occur.

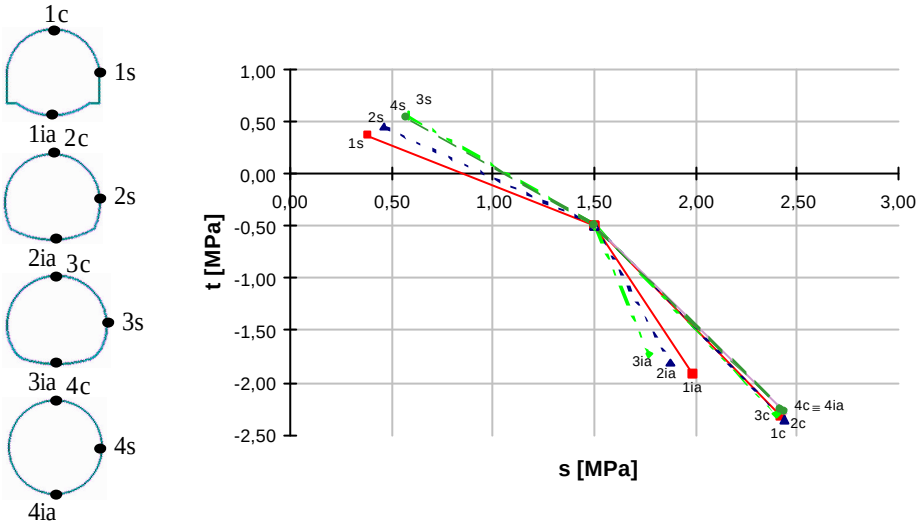

Figure 3.3 Stress paths around the tunnel for the different cross sections, $K_o = 2$.

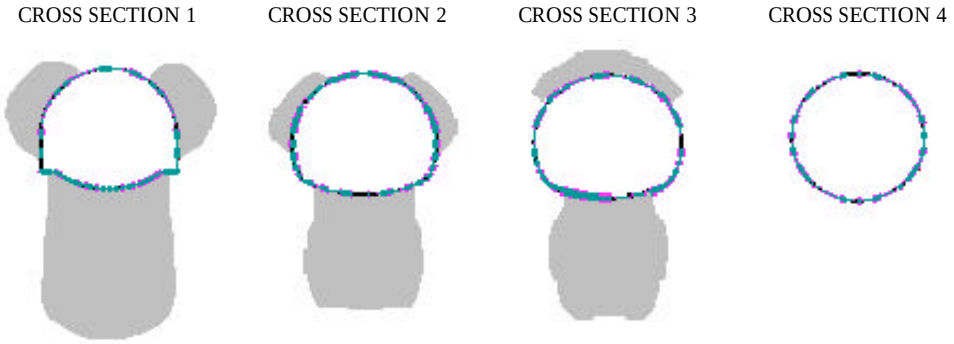

Figure 3.4 Swelling zones around the tunnel for the different cross sections, $K_o = 1$.

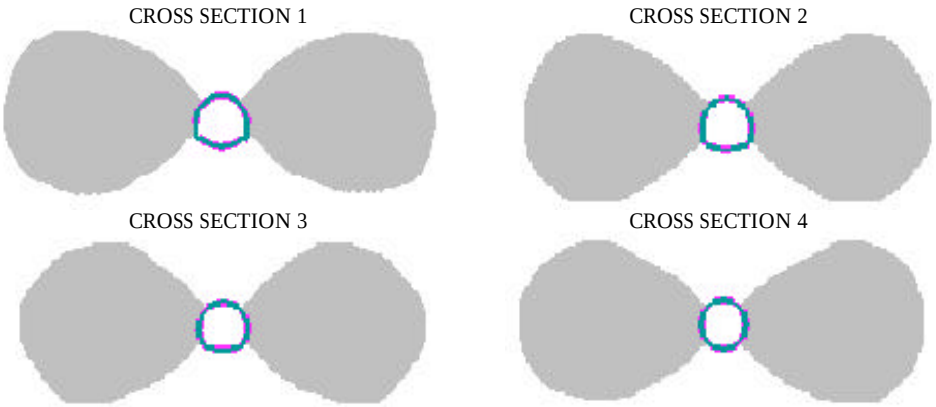

Figure 3.5 Swelling zones around the tunnel for the different cross sections, $K_o = 2$.

In order to underline the influence of curvature at the invert, **Figure 3.6** shows again the computed swelling zones for the two typical cross sections 1 and 2, however with a change in the invert radius.

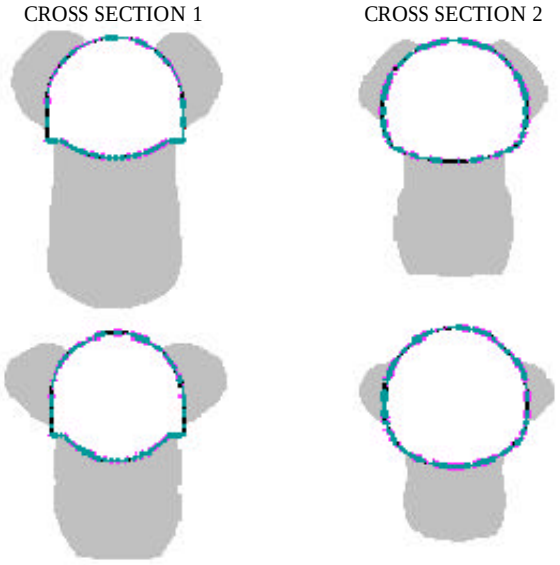

Figure 3.6 Swelling zones around the tunnel for different curvatures of the invert arch for cross sections 1 and 2, $K_o = 1$.

The obvious conclusion based on the above computations is that a circular tunnel is the preferable cross section to be chosen, whenever a swelling rock condition is expected to occur (Steiner 1992). However, it is to be remarked that the analyses performed up to now, and the stress paths derived hold true for plane strain conditions, i.e. the influence of the advancing face has been neglected.

3.3 The case of the circular tunnel

A more systematic numerical study has been performed in order to define the stress distribution around a deep circular tunnel during excavation. In the following paragraphs the circular tunnel is studied by means of two and three dimensional analyses in order to find out the stress path with more accuracy. The circular cross section has been chosen to simplify the problem and in order to allow to compare the numerical results obtained with closed form solutions.

3.3.1 Problem under study

The problem under study is illustrated in **Figures 3.7** and **3.8**, where shown is a 10 m diameter circular tunnel, with the surrounding elements where the stress path is computed. Attention has been posed on the behaviour of the elements at the sidewall (S = sidewall) and crown (C = crown), that due to the symmetry conditions is behaving as the invert arch.

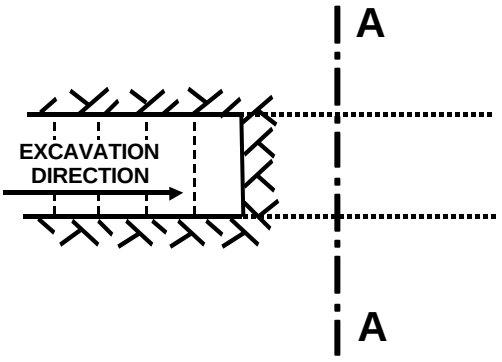

Figure 3.7 Longitudinal section of the circular tunnel.

The simulation of tunnel excavation proceeds from left to right (Figure 3.7). Before excavation, the stress state at points C and S depends on the depth of cover and the K_o condition considered. During excavation, the tunnel face advances, passes trough the A-A section and continues in the opposite direction. Finally, a new equilibrium condition is reached corresponding to the excavation completed with no support installed.

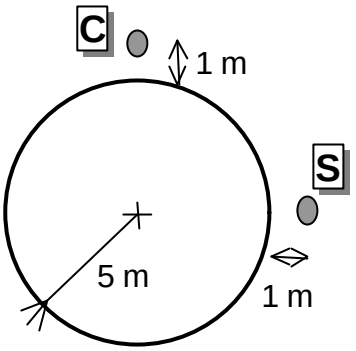

Figure 3.8 Cross section A-A of the circular tunnel.

3.3.2 Numerical analyses in 2D and 3D conditions

A number of numerical analyses have been performed using the finite difference element codes Flac and Flac3D (Itasca 1996) and the boundary element code Examine3D (Rocscience 1998). Due to the symmetry conditions it has been possible to create a mesh of a ¼ of the real problem in order to optimise computation time. In 2D analysis excavation has been simulated by gradually reducing to zero the forces due to excavation on the tunnel contour. For 3D analysis tunnel excavation has been simulated by removing elements in sequence, for steps of 0.5 m length in the longitudinal direction.

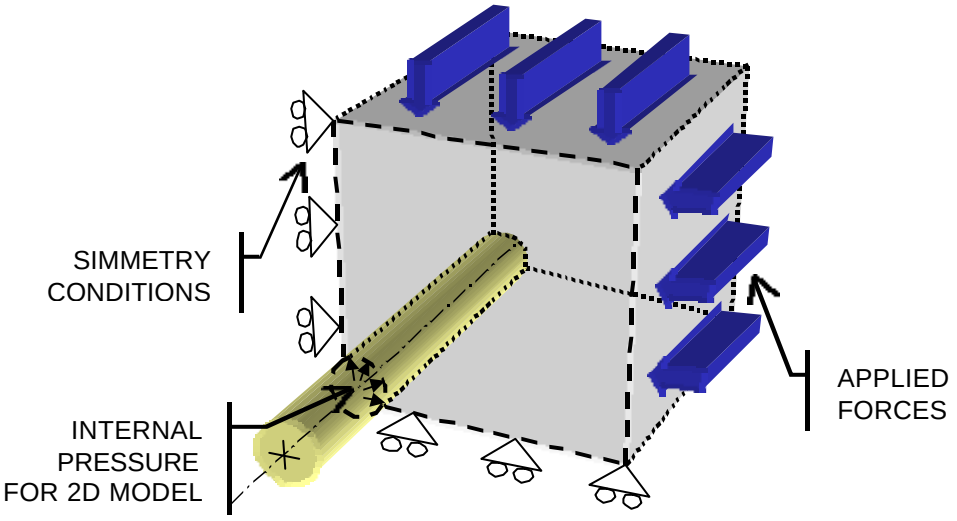

Figure 3.9 Boundary conditions and model.

In **Figure 3.9** a schematic description of the boundary conditions applied to the models is presented. The grey box (blocky light dotted line in figure) represents the three dimensional model with its boundary conditions and its applied forces. The model for two dimensional analysis has been obtained with a vertical section of the first one (dark dotted black line in figure). The mesh adopted for the analyses is plotted in **Figure 3.10**. For the 3D analyses it is assumed that the excavation has reached the A-A section (where stress paths are computed), which is located at half distance from the vertical limit faces of the model along the longitudinal axis.

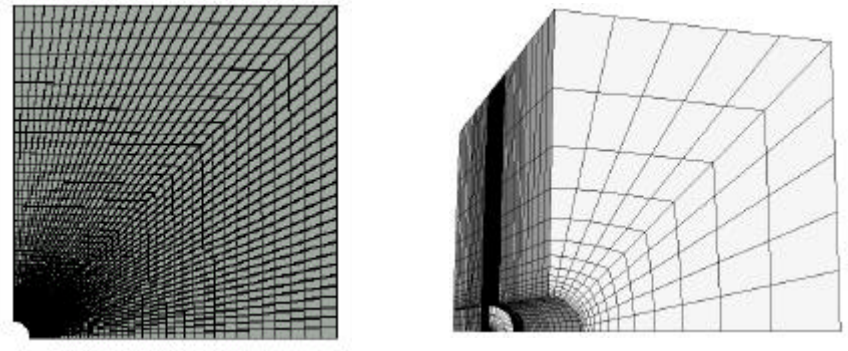

Figure 3.10 Mesh in two dimensions and in three dimensions when excavation has reached the A-A section.

Two different stress conditions, depending on the K_o ratio, have been simulated in the models. For each case a two dimensional and a three dimensional analysis have been performed and the results compared with the closed form solutions available.

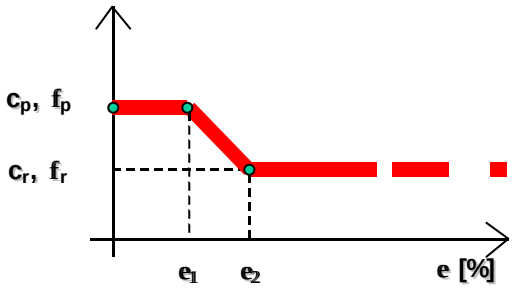

Figure 3.11 Peak and residual strength parameters c, ϕ versus axial strain ε.

The ground around the tunnel is assumed to behave according to a linearly elastic model (e, ILE), with E (elastic modulus) = 400 MPa and ν (Poisson's ratio) = 0.3, or an elasto-plastic model with strain-softening (p, ELPLA). In the latter case (as seen in **Figure 3.11**) a limit value

(ε_1) for the axial strain (ε) is defined below which the peak strength parameters (c_p = cohesion, ϕ_p = friction angle) apply. Then, for values of ε greater than ε_1, the strength parameters are taken to change linearly down to the residual strength parameters (c_r, ϕ_r), which hold true for ε greater than the limit value ε_2.
A summary of the analyses performed is shown in **Table 3.1**.

Table 3.1 Numerical analysis performed*.

Analysis	K_o	Initial σ_v	Model
2D-1e	1	1 MPa	ILE
3D-1e	1	1 MPa	ILE
2D-1p	1	1 MPa	ELPLA
3D-1p	1	1 MPa	ELPLA
2D-2e	2	1 MPa	ILE
3D-2e	2	1 MPa	ILE
2D-2p	2	1,5 MPa	ELPLA
3D-2p	2	1,5 MPa	ELPLA

* K_o is the horizontal stress ratio and σ_v is the vertical stress.

It is noted that the deformability properties assumed in the calculations are those of Bellwald (1990) and Aristorenas (1992). For the elasto-plastic analyses (for K_o = 2), reference is made instead to the parameters given by G.3S – Ecole Polytechnique (Bernaud et al. 1993) for the highly fracturated and tectonised clay-shale of the Chaotic Complex, as met during the excavation of the Raticosa tunnel in the Appennines.
The numerical results obtained in all the analyses performed are described below by depicting the stress path during excavation, which is drawn on the *t*-*s* plane, where:

$$t = \frac{\sigma_v - \sigma_h}{2}$$

$$s = \frac{\sigma_v + \sigma_h}{2}$$

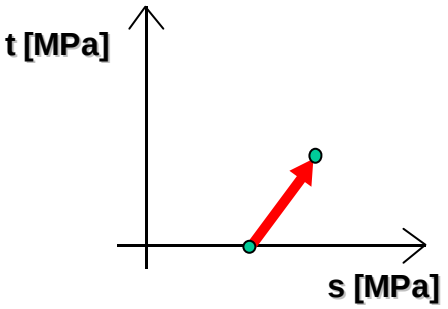

σ_v and σ_h are the vertical stress and the horizontal stress respectively. In case the horizontal stress becomes larger than the vertical one this results in a negative *t*.
The different stress paths obtained from 2D and 3D analyses are compared in the same picture. For purpose of comparison of the stress path computed by numerical methods, the closed form solution for a circular hole in a linearly elastic plate, subjected to an isotropic or

anisotropic state of stress is considered. Also plotted are the vertical (σ_v) and horizontal (σ_h) stresses as excavation takes place, versus the face position along the longitudinal axis of the tunnel.

3.3.3 Elastic analyses results

As shown in **Figure 3.12**, the results obtained for the 2D elastic $K_o = 1$ analyses exhibit a stress path which leads to the same state of stress as given by the closed form solution: as the mean normal stress remains constant, the maximum shear stress at the tunnel crown/invert and sidewall is shown to change accordingly.
The results of the 3D computations, which appear to be in good agreement when comparing the Flac3D and Examine3D stress values, exhibit a different trend of behaviour. As the tunnel face approaches the monitored section A-A the mean normal stress increases. An arrow, along the 3D stress path, shows the state of stress obtained when the face of the excavation crosses the A-A section. As soon as the face of the excavation overpasses the A-A section, the mean normal stress suddenly decreases and then goes back to the initial value. As shown in **Figure 3.13**, this takes place because of an abrupt decrease in the horizontal stress (σ_h). It is of interest to note that between the highest and the lowest value of *s*, the excavation proceeds for 2-3 meters only. The behaviour is similar, however with an opposite sign for the stresses, at the crown.

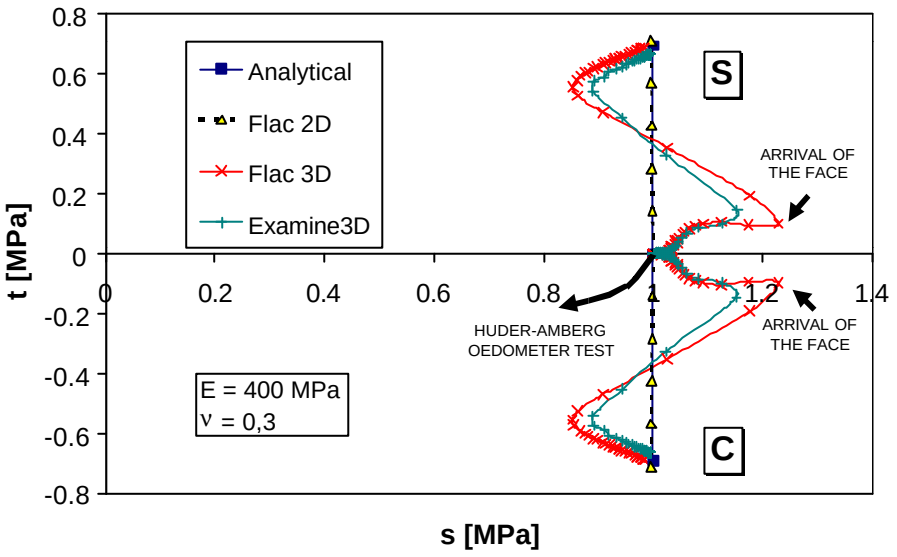

Figure 3.12. Stress paths for points S (sidewall) and C (crown/invert) for the elastic $K_o = 1$ analyses.

The results of the elastic $K_o = 2$ analyses show instead a different trend of behaviour between the sidewall and the crown (**Figure 3.14**). In the first case the mean normal stress decreases, in the second it increases. The 3D behaviour is non linear also in this case.

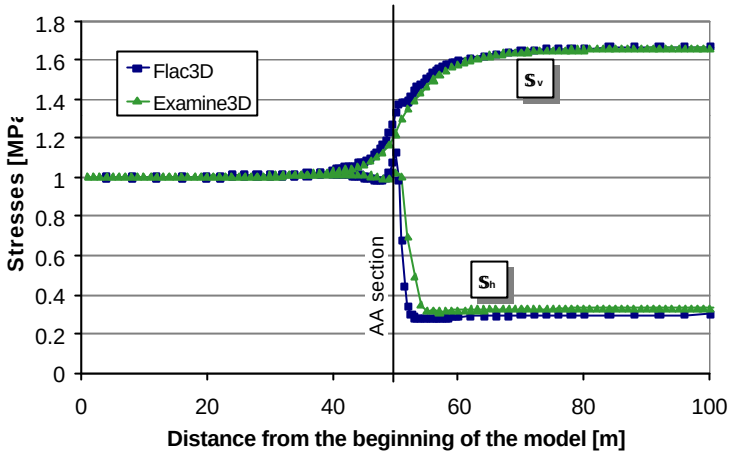

Figure 3.13 Stresses at point S (sidewall) for the 3D elastic $K_o = 1$ analyses.

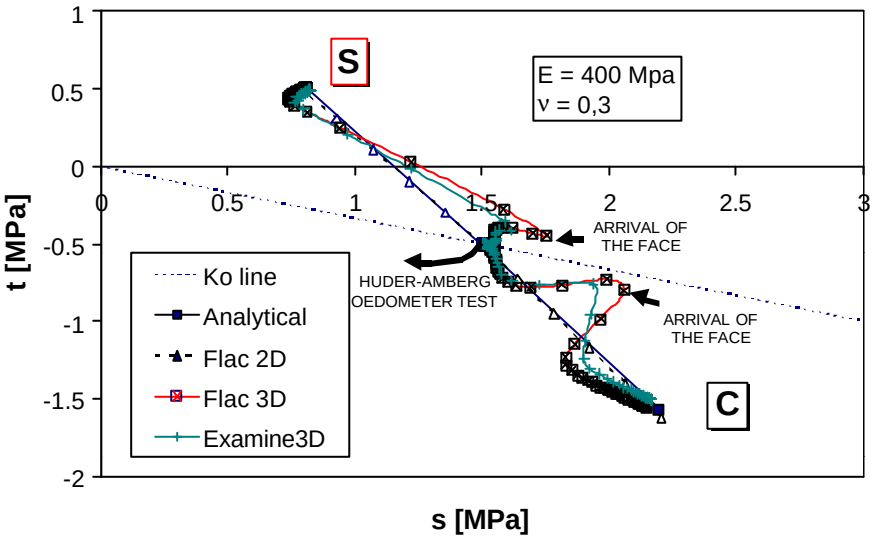

Figure 3.14 Stress paths for points S (sidewall) and C (crown/invert) for the elastic $K_o = 2$ analyses.

As shown in **Figure 3.15** the horizontal stress at the sidewall experiences a sudden decrease when the face of the tunnel reaches the monitored section while the vertical stress slightly increases during all the excavation process. In **Figure 3.16** the corresponding stresses at the crown are reported. It is possible to notice that the changes are less abrupt than for the sidewalls and that the change of *s* is limited to a few meters of excavation (when the face is near to the A-A section) and probably due to mesh discretization.

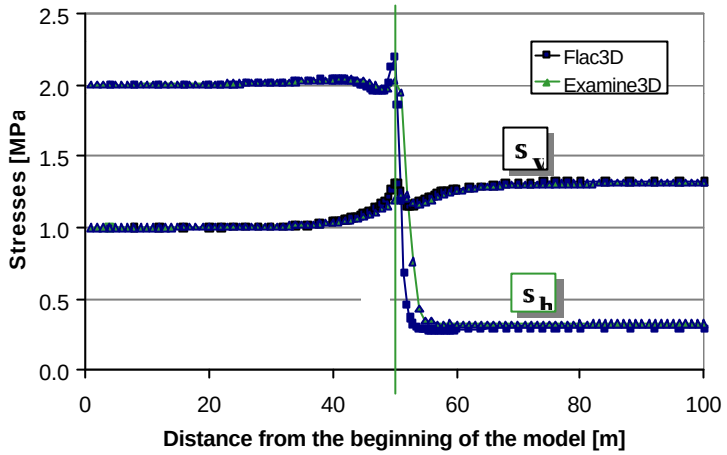

Figure 3.15 Stresses at point S (sidewall) for the 3D elastic $K_o = 2$ analyses.

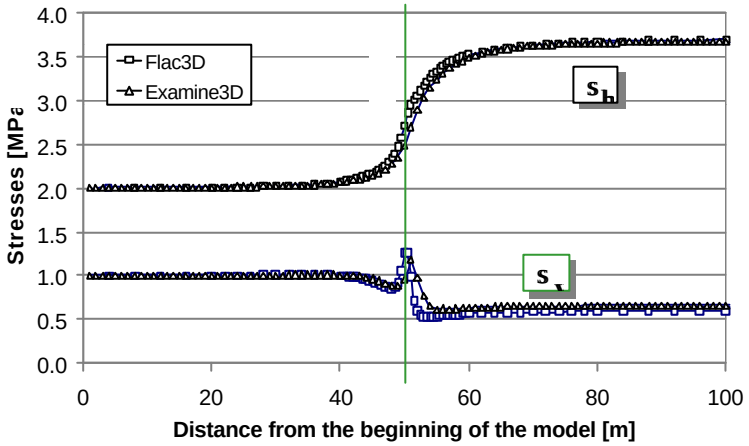

Figure 3.16 Stresses at point C (crown/invert) for the 3D elastic $K_o = 2$ analyses.

The numerical results obtained allow one to notice a significant difference between the stresses computed in three dimensional and two dimensional conditions, with a clear influence on the

stress path experienced around the tunnel. In order to emphasise this, Figures 3.12 and 3.14 also show the typical stress path as obtained in the modified Huder & Amberg oedometer test which is generally used to characterise the swelling ground behaviour. It is evident that the stress history around a tunnel, in particular near the heading, can be properly described only by simulating three dimensional conditions, which is possible in a triaxial apparatus, as will be discussed in the following.

3.3.4 Elasto-plastic analyses results

For the failure envelopes used in the computations, strength is exceeded and plastic deformation around the tunnel takes place.
In the elasto-plastic $K_o = 1$ analyses the *s* value decreases strongly with an initial increase for both points S and C (**Figure 3.17**).

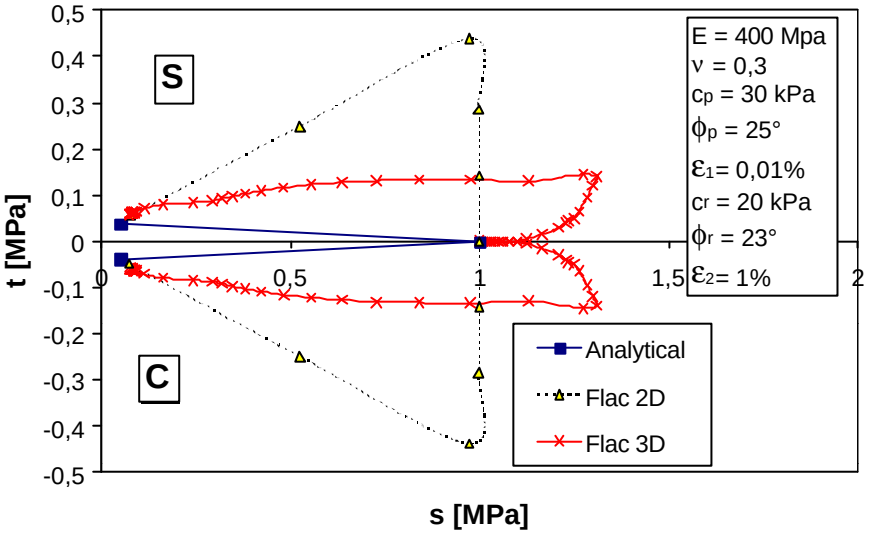

Figure 3.17 Stress paths for points S (sidewall) and C (crown/invert) for the elasto-plastic $K_o = 1$ analyses.

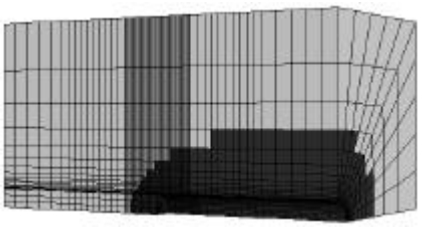

Figure 3.18 Plastic zones around the tunnel.

The decrease of *s* starts when the face of the excavation is still 5-6 m behind. The matter of fact is that a plastic zone is created around the tunnel during excavation (**Figure 3.18**). When the elements where stresses are computed change from elastic to plastic behaviour, as soon as the plastic zone (black zone in

Figure 3.18) gets through the A-A section, both the vertical and the horizontal stresses decrease to small values and determine the decrease of *s* (**Figure 3.19**). The change in the state of stress after the tunnel face crossing is small and when the face is just 2-3 m ahead the stresses have reached a new final equilibrium.

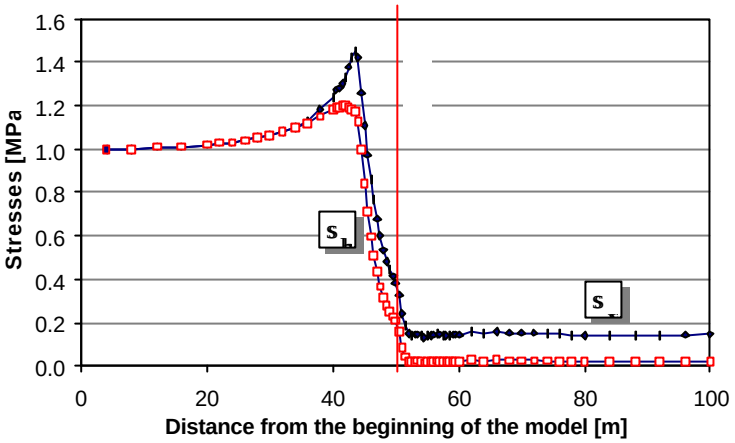

Figure 3.19 Stresses at point S (sidewall) for the 3D elasto-plastic $K_o = 1$ analysis.

In the elasto-plastic $K_o = 2$ analyses performed yielding takes place only at the crown/invert, while the walls are experiencing mainly an elastic behaviour, as well shown by the stress path which is nearly the same as for the elastic analysis (**Figure 3.20**).

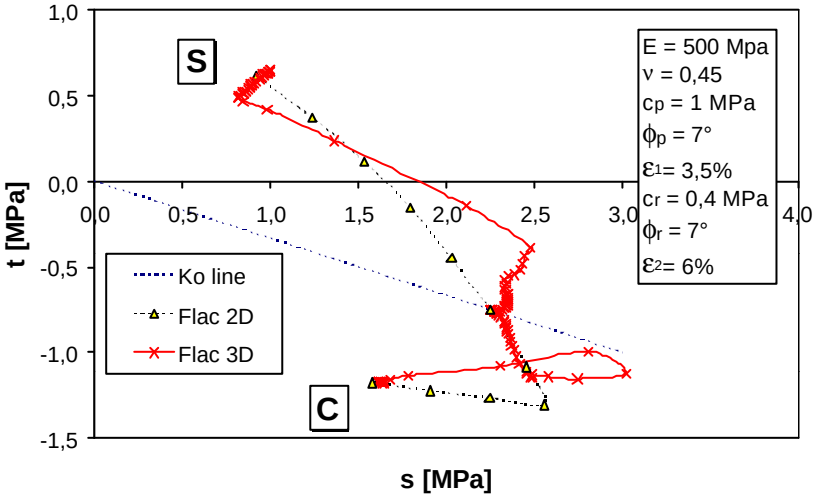

Figure 3.20 Stress paths for points S (sidewall) and C (crown/invert) for the elasto-plastic $K_o = 2$ analyses.

The plastic zone around the tunnel has the typical ear shape section as can be seen in **Figure 3.21**. Paying attention to point C (crown/invert), it is possible to see that the stress path has two changes in direction during excavation. The first change, where *s* increases, is due to the plastic zone that intercepts the A-A section, the second one, where *s* decreases is due to the crossing of the tunnel face (**Figures 3.22** and **3.23**). Also for this case the final equilibrium stress state is reached as soon as the face of the excavation is only a few meters ahead.

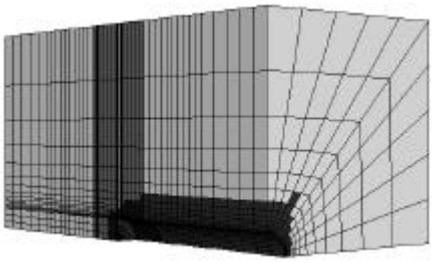

Figure 3.21 Plastic zones around the tunnel.

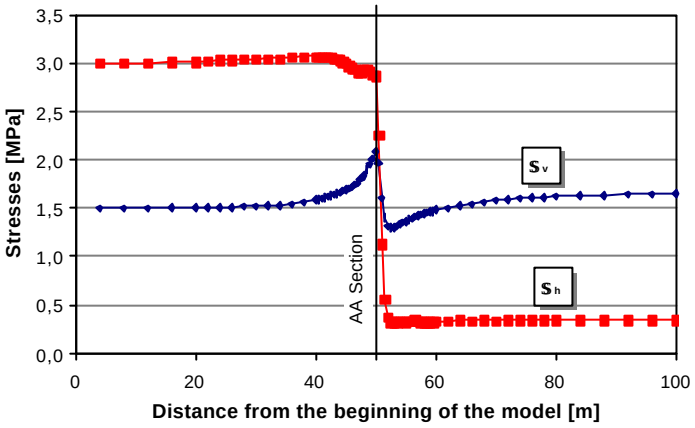

Figure 3.22 Stresses at point S (sidewall) for 3D elasto-plastic $K_o = 2$ analysis.

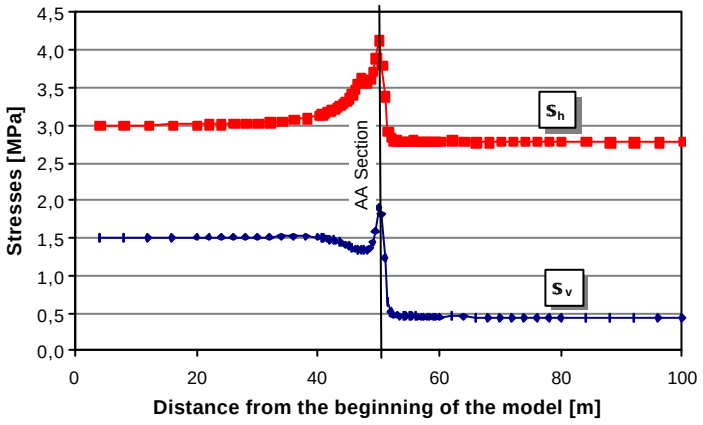

Figure 3.23 Stresses at point C (crown/invert) for 3D elasto-plastic $K_o = 2$ analysis.

3.4 Conclusions

The numerical results obtained allow one to notice a significant difference between the stresses computed in three dimensional and two dimensional conditions, with a clear influence on the stress path experienced around the tunnel. With the 3D analyses a change of the mean normal stress *s* is evidenced for all the cases under study.

For the results pertaining to the elastic $K_o = 1$ case, the 3D stress path for the sidewall and the crown/invert evidences a variation in the mean normal stress during excavation, which is not shown by the corresponding theoretical solution and 2D results. In the elastic $K_o = 2$ case, both elements around the tunnel give again a change in the *s* value: a decrease of *s* for the sidewall simulation and an increase for the crown/invert respectively.

In this case, the change is shown both by the two dimensional and the three dimensional analyses, even though the two dimensional stress path is linear. On the basis of these results, if the swelling behaviour of the tunnel is correlated to a decrease of the mean normal stress, this is much more likely for $K_o = 2$ analyses (at the sidewalls) but it can still occur for the $K_o = 1$ condition.

As the simulation comes near to the most likely behaviour of ground, as represented by an elasto-plastic constitutive law, the stress paths increase in complexity. For all the cases considered, a decrease of the first stress invariant is evidenced.

As shown in Figures 3.12 and 3.14 the modified Huder & Amberg oedometer test, which is generally used to characterise the swelling ground behaviour, is not able to reproduce the correct stress history experienced by the ground in the near vicinity of the tunnel. It becomes evident that this stress history, in particular near the face of the excavation, can be properly described only by simulating three dimensional conditions, which is possible in a triaxial apparatus, as will be discussed in the following.

Chapter 4

Testing equipment

4.1 Introduction

Triaxial tests were performed by means of two different apparatuses at Politecnico di Torino. The first one (GDS) is a triaxial apparatus available in the Soil Mechanics Laboratory. The second one (SRTA, Soft Rock Triaxial Apparatus) was designed and built in the Rock Mechanics Laboratory as part of the present thesis. In this chapter a brief description is given of the GDS apparatus (Puci 1993, Lo Presti et al. 1995) and a more comprehensive presentation is reported for the SRTA.

4.2 The GDS Triaxial Apparatus

4.2.1 General description and features

The GDS triaxial cell (**Figure 4.1**) is a hydraulic apparatus originally built by GDS Instrument Ltd. and usually used for clay testing at Politecnico di Torino. Later modifications in order to reduce system compliance, seating and bedding errors have been made in several years and have improved and changed substantially the apparatus original characteristics.
The triaxial apparatus has a maximum capacity of 5 kN for the vertical load and of 1.2 MPa for the pressure cell. The cell can host cylindrical samples of 71 mm diameter and 142 mm height and can reach maximum values of 2.5 MPa for the axial stress and 1 MPa for the confining pressure. The cell structure (**Figure 4.2**) can be divided in two parts. The lower one houses the loading piston and the set of ball bearings, the upper one is the confinement chamber where the specimen is positioned.
Bellofram diaphragms are used in order to separate the pressure chambers inside the loading piston. The cylinder section has been reduced to be identical to that of the specimen in order to make the axial pressure independent of the cell pressure and to enhance the actuators resolution in the case of local application under stress control. The cell structure has been stiffened starting from the original one. It consists of an iron ring connected to an iron plate by three internal tie rods located inside a perspex confinement cell. Sealing is guaranteed by lateral o-rings. The top cap of the sample is fixed to the top plate. The base pedestal is connected to the loading rod with the interposition of the load cell. The axial load is applied from the bottom.

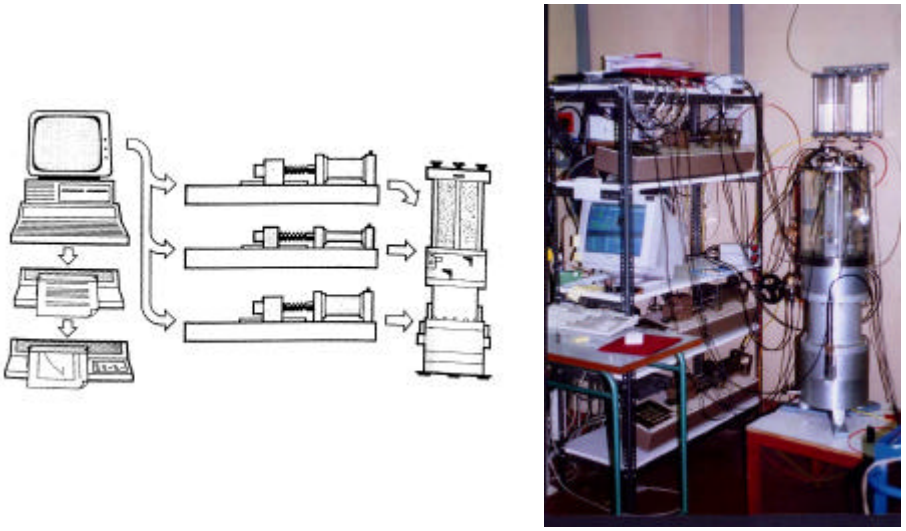

Figure 4.1 Scheme and photograph of the complete GDS apparatus.

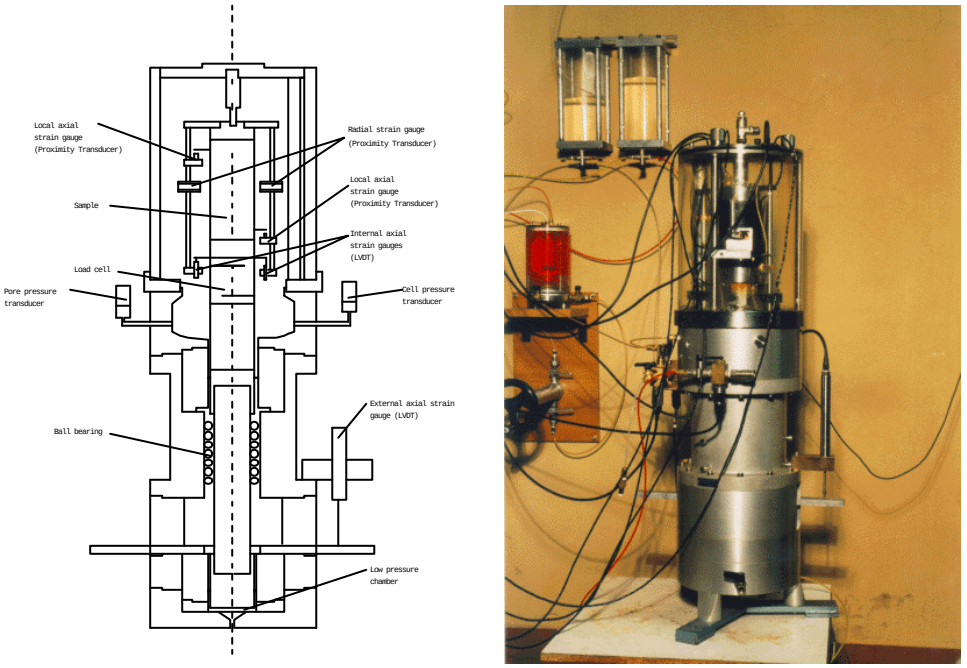

Figure 4.2 Section and photograph of the GDS triaxial cell.

4.2.2 Actuators and control system

For axial, lateral and pore pressure control the apparatus is equipped with three pressure controllers (GDS Digital Controller).
The Digital Controller (**Figure 4.3**) is a hydraulic actuator controlled by an internal microprocessor that measures and controls volume and pressure, due to movements of a step by step motor, of the liquid contained inside the hydraulic cylinder. Pressure of the liquid (distilled water) is generated by the movement of a piston inside the cylinder which is pushed by the rotation of a threaded rod led by the step by step engine. The resolution of the system is of 0.5 kPa. The Digital Controller has a capacity of 1000 cm^3 and a full scale of 2 MPa for both the cell and the axial pressure and of 200 cm^3 and again 2 MPa for the back pressure. This last Digital Controller uses silicon oil instead of distilled water as fluid. This necessity is dictated by the volume gauge adopted. This measuring device is described in the next section.

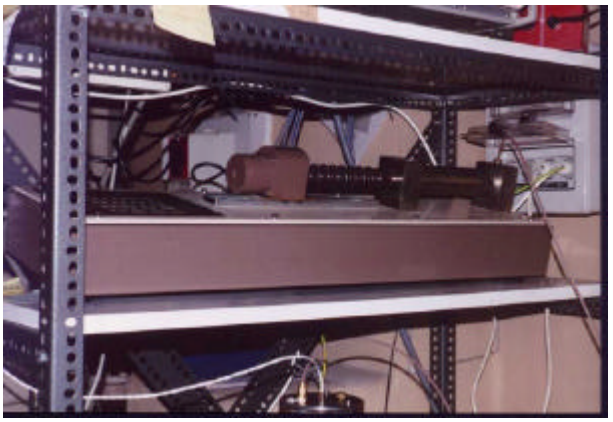

Figure 4.3 Photograph of the GDS digital controller.

The control system comprises a personal computer with a National Instruments AT-MIO-16X card used for data acquisition and its transformation from analogical to digital. The control software is LabView (National Instrument 1998). A user made programme enables one to control each phase of the test and to perform any desired stress path in very strictly controlled conditions.

4.2.3 Measurement systems adopted

An analogical digital converter and a personal computer are used for data acquisition. All data are automatically fed into the computer hard disk. The personal computer completely controls and drives the test (acquisition, control and loading).
In order to obtain a complete data acquisition, the GDS triaxial cell is equipped with the following sensors:

- a pair of inductive proximity transducers (Kaman) for the measurement of the local axial strain;

- a pair of submergible LVDTs for the internal measurement of the axial strain;
- a pair of inductive proximity transducers (Kaman) for the local measurement of the radial strain;
- a pair of LVDTs for the external measurement of the axial strain with target provided by two transversal rods directly connected to the central part of the loading piston;
- a load cell (Maywood Instrument 4958-5kN) located inside the confinement cell, between the pedestal and the iron loading rod;
- a pressure transducer to measure the pore pressure at the top of the specimen;
- a pressure transducer to measure the cell pressure;
- a volume variation indicator.

The volume change measurement is obtained with a special apparatus with a capacity of 45 cm^3 that uses a proximity sensor and a floating target that goes up and down depending on water entering or exiting the sample (**Figure 4.4**). The upper part of the tank is full of coloured silicon oil while the lower part, which is connected to the sample drainage system, is full of water.

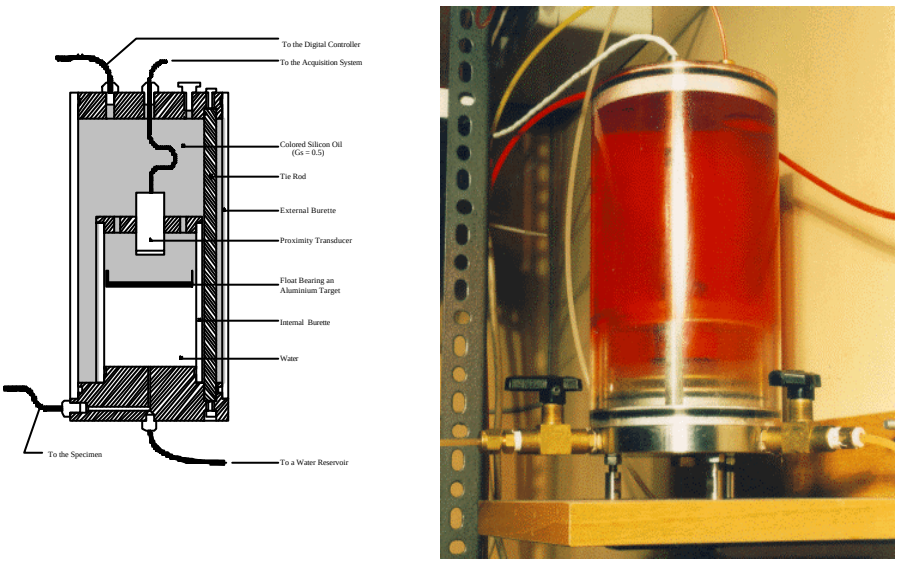

Figure 4.4 Scheme and photograph of the volume change measurement system.

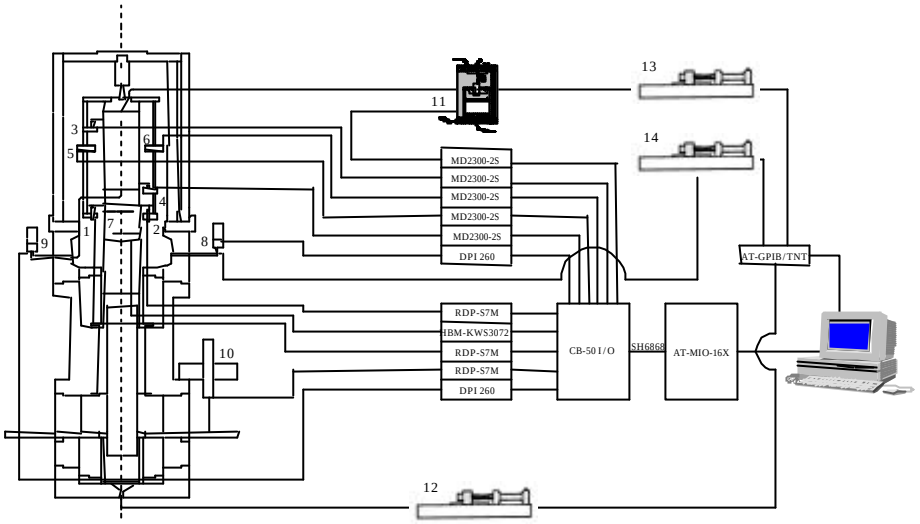

Legend:

1. LVDT transducer for internal axial strain
2. LVDT transducer for internal axial strain
3. Proximity sensor for local axial strain
4. Proximity sensor for local axial strain
5. Proximity sensor for local radial strain
6. Proximity sensor for local radial strain
7. Load cell
8. Pore pressure transducer
9. Confining pressure transducer
10. LVDT transducer for external axial strain
11. Volume measurement system
12. GDS digital controller 200 cm^3/2 MPa
13. GDS digital controller 1000 cm^3/2 MPa
14. GDS digital controller 1000 cm^3/2 MPa

Figure 4.5 Scheme of the GDS data acquisition system.

4.3 The Soft Rock Triaxial Apparatus

4.3.1 General description

The Soft Rock Triaxial Apparatus shown in **Figure 4.6** consists of the following components:

- triaxial cell,
- actuators,
- sensors,
- data acquisition and control system.

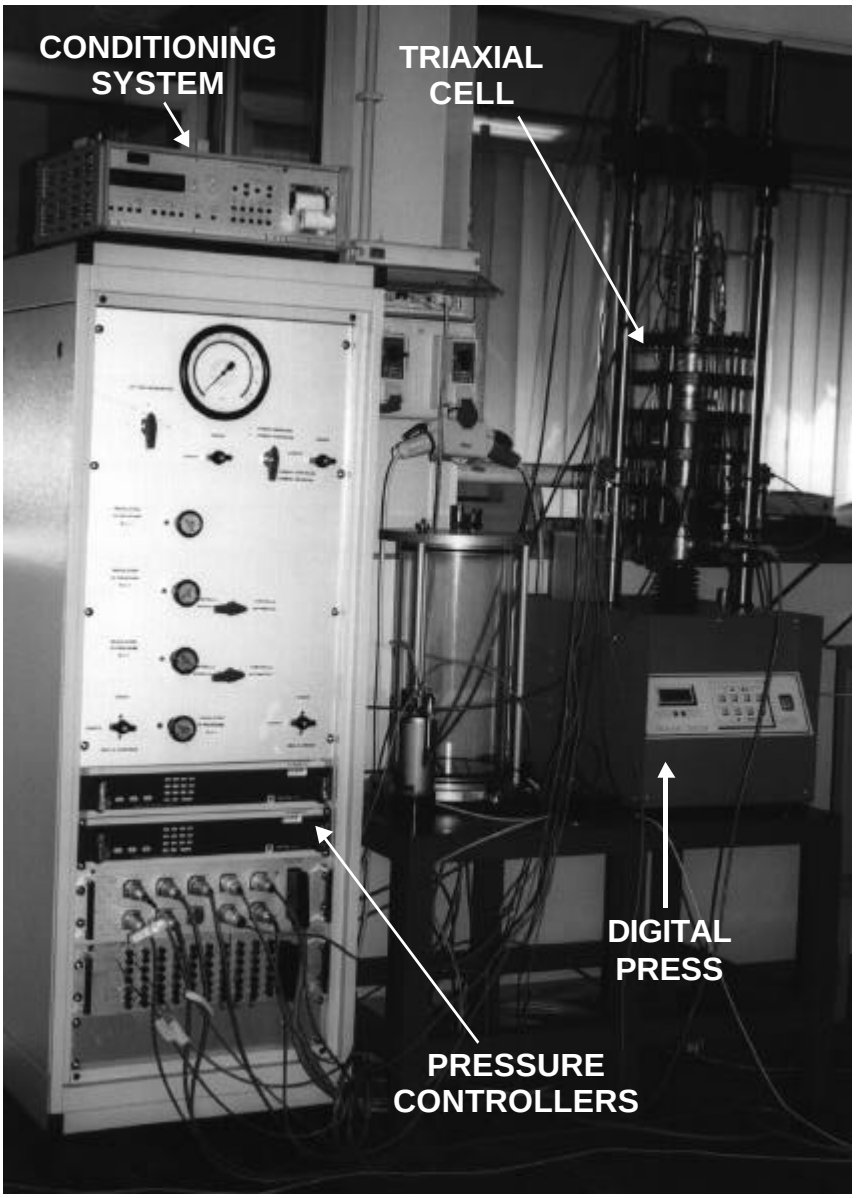

Figure 4.6 Photograph of the Soft Rock Triaxial Apparatus.

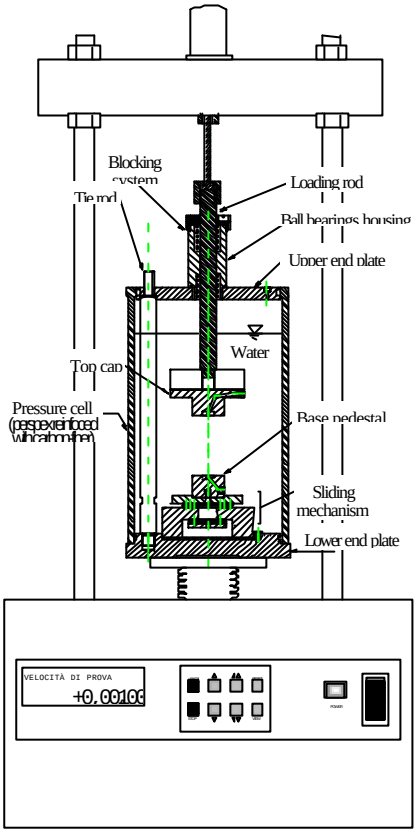

Figure 4.7 Layout of the triaxial cell.

4.3.2 The triaxial cell

The triaxial cell is the most important part of the whole apparatus. The cell structure (**Figure 4.7**) is very stiff and consists of two end platens connected by three tie rods located inside a 2 cm thick perspex pressure cell. This cell is reinforced by strips of carbon-fibers in order to withstand high cell pressures (up to 2 MPa). The three internal tie rods (20 mm of diameter located at 120°) allow the realisation of a stiff structure and a more efficient assembly of the apparatus before positioning the perspex cell.
The axial load during consolidation is applied from the top by a loading piston, connected to a loading rod (25.4 mm of diameter) virtually frictionless due to a double set of cylindrical ball bearings (XA 162536). Sealing is guaranteed by the 50 mm inox guiding system that has a tolerance of 1/100 mm. Therefore no o-ring is used. The top platen has different holes for electric cables and other kind of connections. Sealing, in these cases, is guaranteed by o-rings.

During shearing the axial load is applied from a digital loading machine. In this case some components are added to the loading rod in order to obtain contrast with the fixed bar of the loading press. For extension tests three rods are connected to the bottom plate and linked to the digital loading machine in order to convey traction.
The top cap is directly connected to the load cell. Drainage lines are present both in the top cap and in the base pedestal. The base pedestal is supported by a sliding mechanism which was designed according to the suggestions given by Hayano et al. (1997). This mechanism consists of two sets of ball bearings as shown in **Figure 4.8**. A screw links together the base pedestal with the connection to the bottom plate and a spring is used to fasten this connection so that extension tests can also be performed. Due to this mechanism, which is appropriate to mitigate the adverse effects of shear bands, the base pedestal is unrestrained in the horizontal direction. When the specimen is assembled in the triaxial apparatus, the base pedestal can be fixed in order to simplify operations. The blocking mechanism is removed before closing the confinement chamber.

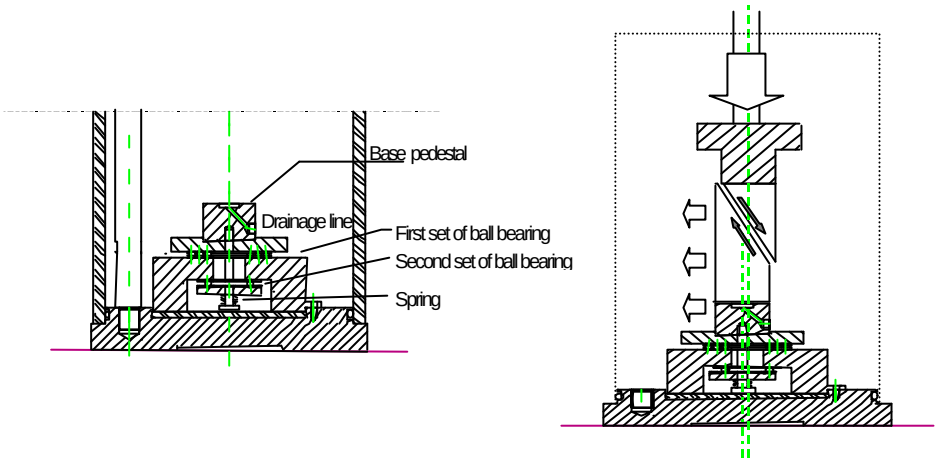

Figure 4.8 Schematic drawing showing the sliding mechanism and its effects.

The cell can host samples of 50 and 70 mm diameter and 100 to 140 mm height by changing the top and the base pedestal.

4.3.3 Actuators

The vertical load is applied by means of a double chamber air cylinder during consolidation and when the stress control phases are undertaken. A digital loading machine is used to apply the vertical load at a constant rate of displacement during the loading or unloading stress paths. For confining pressure and for back pressure, air pressure is used. The air pressure is compressed at 12 bar by a compressor and can get up to 25 bar when a pressure multiplier is connected on the line. For back pressure an air-water interface is present. At the air-water interface, volume variation can be measured. For confining pressure an air-oil interface is used,

directly in the cell chamber. The specimen is submerged into transparent silicon oil and air enters from the top plate of the chamber.

4.3.3.1 The control panel

The control panel has been organised in order to have an easy control of the pressure lines (**Figure 4.9**). Air pressure is used for cell pressure, for the vertical load during consolidation due to the double chamber air cylinder and for back pressure.
Due to the control panel it is possible for the user to open and close the air source and the pressure multiplier and regulate all the pressures (top and bottom chamber pressure of the loading piston, cell pressure, back pressure). The panel allows one to switch from automatic to manual regulation. Manual regulation is obtained due to Fairchild pressure regulators (50 bar maximum pressure) while automatic regulation is available for the cell pressure and one of the two chambers of the loading piston only. The functioning of the servo-control for pressure will be better described in the next paragraph. On the control panel a Budenberg standard test gauge has been mounted in order to control directly the output pressure of each line (one at the time).

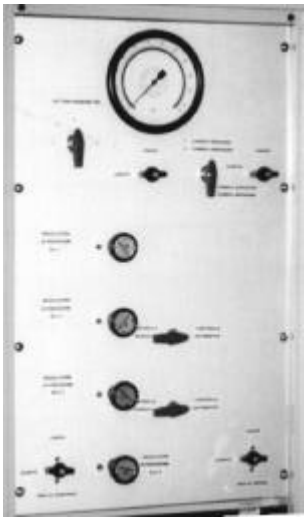

Figure 4.9 Photograph of the control panel.

4.3.3.2 Servo-control for pressures

The cell pressure and the air cylinder upper chamber are both governed by two programmable digital pressure controllers DPI520 (**Figure 4.10**). The DPI520 instrument is a single channel pneumatic pressure controller designed to be programmed by an external personal computer. Pressure demands via a digital interface IEEE488 are converted by the controller into a regulated pressure supplied by the line. The DPI520 used has respectively 10 bar full scale

output pressure, for the loading piston line, and 20 bar, for the cell pressure line. Technical characteristics are detailed in **Table 4.1**.

Table 4.1 Instrument specifications of the DPI520

Combined non linearity, hysteresis and repeatability	± 0.05% of full scale
Stability	± 0.015% of reading
Controller stability	± 40 ppm of full scale
Delivery at 1 bar operating pressure	1 l/min

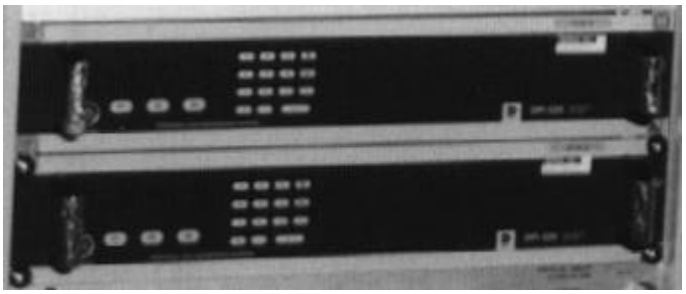

Figure 4.10. Photograph of the digital controllers.

4.3.3.3 The loading piston

The loading piston, a Bellofram diaphragm cylinder (model: D-6-f-BP-HFM), is an actuator made from elastomers, engineered metals and fabrics, which require no lubrication and are virtually frictionless. It consists of two pressure chambers divided by two Bellofram diaphragms. When pressure is supplied in the upper chamber, the cap diaphragm expands pushing down the piston rod. The head diaphragm follows the movements with no friction (**Figure 4.11**).

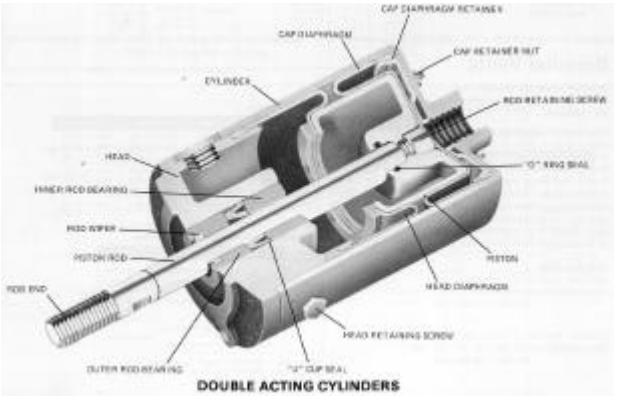

Figure 4.11 Section of the double acting cylinder.

4.3.4 Measuring system adopted

4.3.4.1 Sensors

The triaxial cell is equipped with the following sensors (**Figure 4.12**):
- a pair of LDTs for the local measurement of the axial strain;
- a pair of inductive proximity transducers (Kaman) for the local measurement of the radial strain;
- a pair of LVDTs for the external measurement of the axial strain;
- a load cell located inside the confinement chamber (Maywood Instrument 4958-50 kN);
- a pair of pressure transducers to measure the pore pressure at the top and bottom of the specimen;
- a pressure transducer to measure the cell pressure;
- a volume variation indicator.

Local deformation transducers (Tatsuoka 1988, Goto et al. 1991) are stripes of phosphorus bronze, a high elasticity material (Young's modulus = 120,000 GPa), 90 mm long, 45 mm large and 0.2 mm thick. Four strain gauges are glued on it, two for each size, electrically connected as a Wheatstone bridge. The LDTs are mounted on the membrane of the sample by two glued hinges. When the sample deforms the strips inflects and this changes the response signal of the strain gauges.

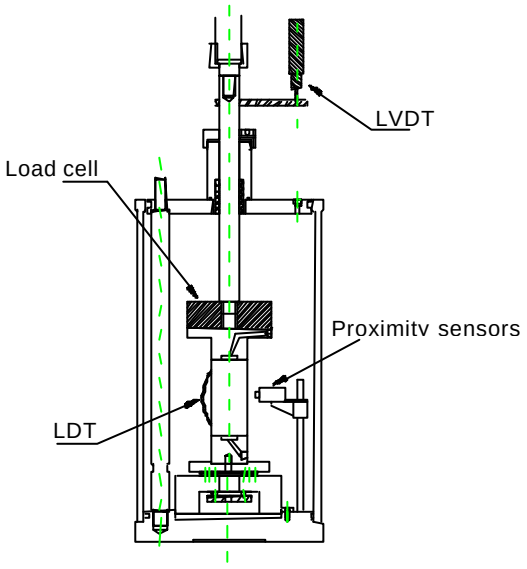

Figure 4.12 Schematic drawing showing the displacement transducers and the load cell.

The radial deformation is measured by means of two submergible proximity sensors mounted on a special apparatus at the specimen mid-height. The proximity sensors' target consists of a thin square of aluminium foil glued on the sample by means of grease. The horizontal position of the sensors can be adjusted by a screw located outside the cell. This allows one to reposition the sensors during a test. The local measurement of radial strain is very important in order to prevent specimen swelling during flushing as it will be better explained in Chapter 6.
An Imperial College volume gauge is used to measure volumetric strains. The volume variation is inferred from the LVDT measurement. This LVDT is mounted on the water-air interface used to apply back pressure. The two faces are separated by a diaphragm.

4.3.4.2 The multi-channel conditioning system

HBM-UPM60, a multi-point conditioning system is used for data acquisition. With the UPM60, up to sixty channels can be examined in sequence automatically. In the configuration of the SRTA measuring device, only eleven channels are used and a complete acquisition lasts for 2 seconds. The channels are connected to the UPM60 via scanning modules and data are then converted from analog to digital and transferred via HPIB connection from the conditioning system to the personal computer.

4.3.5 Data acquisition and control-system during testing

The HP-VEE (Hewlett Packard 1995) software is used to control the whole test procedure (data acquisition, pressure control and loading). A user made program has been developed by the author to control the different phases.
Developing the control program has requested a great amount of time. One subroutine for each phase of the test is present. A control panel (shown in **Figure 4.13**) was designed in order to have a visual control of the situation of the test in every moment.

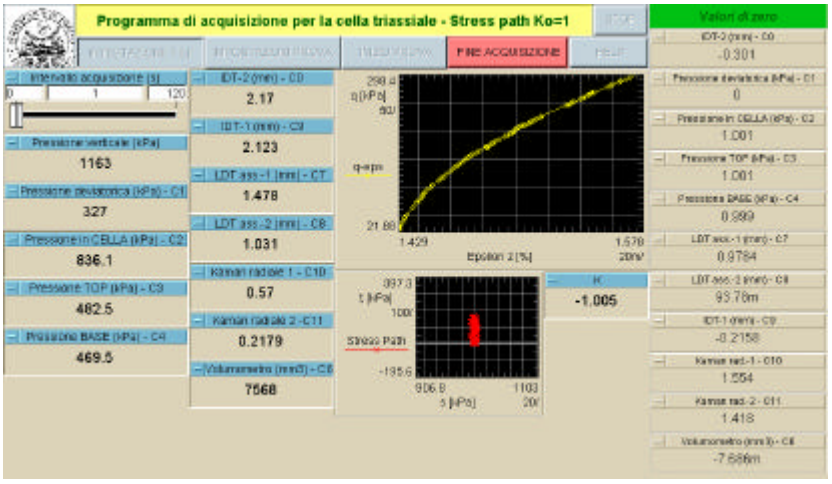

Figure 4.13 Screen view of the control program for the shearing phase as running on the PC.

When starting the program, the user is asked to introduce all the information regarding the geometry of the specimen. With this information, the program will execute mathematical operations to obtain correct stresses and strains after every acquisition.
Management of the test follows logical operations. Data are transmitted to the personal computer, which is able to compare actual values with the values set by the operator continuously and take decisions step by step acting on the servo-control system. Time elapsed between each cycle (acquisition-evaluation-decision) depends on the amount of data already recorded and can vary between 2 to 4 seconds.
In the flushing phase the program controls the height and diameter of the sample and keeps them to the initial value (with a tolerance of ± 0.0015%) by increasing or decreasing the applied pressures. During saturation the program is capable to perform B value check by increasing isotropically the applied pressures and evaluate the negative pore pressure increase. Drainage must be closed by the operator during the B check. Consolidation is governed by the program by increasing the confinement pressure and adjusting the axial load in order to get the desired K_o condition. During the stress path phase (i.e. shearing) the program requires information about the desired stress path and is able to follow it in a stepwise manner. After having completed the stress path the program can maintain the stresses constant so that creep and swelling deformations can be measured. Additional information about the stepwise procedure to control deformations during flushing and stress paths during shearing will be given in Chapter 6.

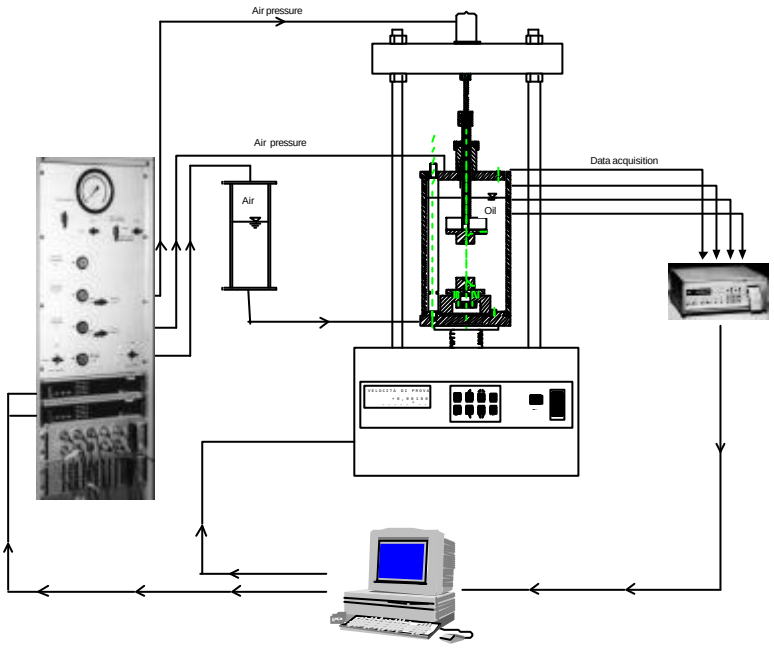

Figure 4.14 Schematic drawing of the data acquisition and control systems.

4.4 Evaluation of the Soft Rock Triaxial Apparatus

In order to evaluate the correct functioning of the apparatus before using it for testing samples which exhibit a swelling behaviour, a test program on soft rock specimens has been undertaken. In the following paragraphs this program is described with emphasis on the apparatus features and capabilities to correctly assess the stress-strain-strength behaviour. Additional information is available in two different papers: Lo Presti et al. (1998) and Barla M. et al. (1999). The test program was aimed at verifying the following aspects:

- importance of local strain measurements, when assessing stiffness characteristics and creep deformations (Matsumoto et al. 1999),
- effectiveness of the dry setting method in preventing specimen swelling,
- setting up of the experimental procedures.

4.4.1 Tests performed

Triaxial compression tests were performed on three soft rocks, pertaining to different sites.
a) The S. Raffaele Cimena site is a 23 million years Miocene geologic formation, which mainly consists of silty marl interbedded with sandstone. The tests were performed on sandstone specimens retrieved by means of a triple tube sampler from a depth of about 12 to 13 m (Barla G. et al. 1999). Typical grain size distribution curves are shown in **Figure 4.15**. The material resulted to be non plastic or with a maximum plasticity index of about 18%. The natural water content of the tested specimens resulted to be between 14 and 15%. The carbonate content ranged from 11 to about 24%.

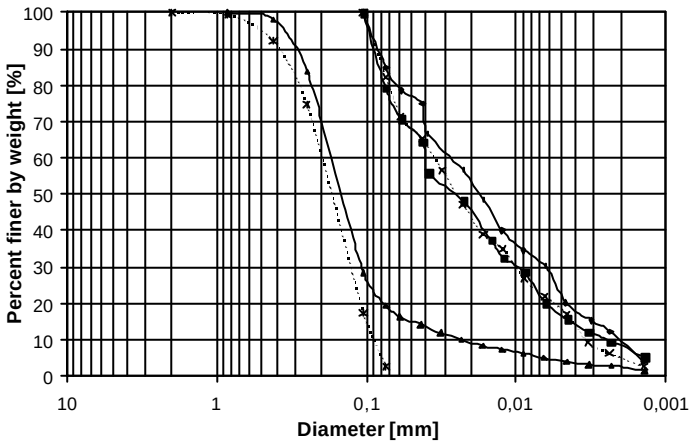

Figure 4.15 Typical grain size distribution curves of the S. Raffaele Cimena specimens.

b) The Sagamihara site is a late 1.5 million years Pleistocene geologic formation, which mainly consists of continuous unweathered soft sedimentary mudstone (Hayano et al. 1997). The tests were performed in the framework of a Round Robin Test program organised by TC29 of

ISSMGE which has kindly provided the specimens. The specimens were obtained from a block sample carved at a depth of about 50 m.
c) The Giaglione site is characterised by two different structural geologic formations, the Piedmontese zone and the Tectonic Breccia zone. The first one is composed with interbedding calcschists and micaschists; the latter one is composed with tectonized carbonatic breccia with inclusions of calcschists and micaschists blocks, which range from one to ten meters in height. Tests have been performed only on the second geologic formation. The specimens were obtained by means of a double tube sampler and were kindly provided by Alpetunnel-Geie.
The main characteristics of the tested soils are summarised in **Table 4.2**.

Table 4.2 Characteristics of the tested soils*.

Site	D_{50} [mm]	U_c [%]	$CaCO_3$ [%]	e [-]	w_n [%]
S. Raffaele Cimena	0.15	7.2-14	6-24	0.20-0.45	14-15
Sagamihara	0.006-0.02	-	1	0.98-1.26	22-28
Giaglione	0.26	-	-	0.35-0.39	-

* D_{50} = mean grain size; U_c = uniformity coefficient; $CaCO_3$ = calcium carbonate content; e = void ratio; w_n = natural water content.

Table 4.3 Testing conditions*.

(A)	(B)	(C)	(D)	(E)	(F)	(G)	(H)
SRC1	0	0.26	14.4	11.6	0.01	< 1	-
SRC2	0	0.34	15	23.7	0.25	< 2.7	-
SRC3	0	0.33	15	19.3	0.01	< 3.1	-
SRC4	466	0.23	-	23.5	0.01	< 1	C
SRC5	100	0.27	14.4	11.6	0.01	0.7	C
SRC6	0	0.43	1.55	5.7	0.01	-	-
SRC7	0	0.18	1.67	27	0.01	-	-
SRC8	100	0.48	10.8	7.1	0.01	-	C
SRC9	200	0.43	11.8	6.7	0.01	-	O
SGH1	470	0.74	25.0	1	0.01	-	C
SGH2	470	0.73	25.1	1	0.01	-	C
SGH3	472	0.70	24.1	1	0.01	-	O
SGH4	475	0.68	21.6	1	0.001	-	O
SGH5	470	0.70	25.5	1	0.01	-	C
GIA1	1000	-	-	-	0.01	2	-
GIA2	1000	-	-	-	0.01	2	-

* (A) Test No.; (B) σ'_c = effective isotropic consolidation pressure [kPa]; (C) e = void ratio; (D) w_n = natural water content [%]; (E) $CaCO_3$= calcium carbonate content [%]; (F) $\dot{\varepsilon}_a$ = axial strain rate [%/min]; (G) Clay fraction [%]; (H) Drainage valve: C = closed, O = open.

The $CaCO_3$ content in the case of Sagamihara mudstone was determined in our laboratory. The other data for the same Sagamihara mudstone shown in Table 4.2 are due to Hayano et al. (1997). It should be observed that the values of the void ratio also determined by us considering a specific gravity G_s = 2.765, were smaller than those indicated by the authors above. However, the dry unit weight of the tested samples ranged between 15.9 and 16.5 kN/m^3, in good agreement with the values reported by them.
Cylindrical triaxial specimens of S. Raffaele Cimena and Sagamihara were obtained by means of a lathe. This was necessary to obtain specimens with a diameter of about 70 mm (S. Raffaele Cimena) and 50 mm (Sagamihara) and a height to diameter ratio (H/D) of 2 for both rocks.
Specimens of Giaglione site were cut from samples of 57 mm diameter by a circular diamond saw to obtain a height of about 114 mm (H = 2 D). It is worthwhile to point out that a more precise parallelism of end faces and perpendicularity between end faces and longitudinal axis is obtained in the case of Sagamihara and S. Raffaele Cimena specimens than for Giaglione specimens.
Four triaxial compression tests were performed on specimens taken from Sagamihara, nine on specimens taken from S. Raffaele Cimena and two on specimens from Giaglione. Test SRC1 was carried out with a conventional triaxial apparatus equipped with LDTs. The testing conditions are summarised in **Table 4.3**.

4.4.2 The dry setting

In the dry setting procedure, the specimen is positioned in the triaxial cell without getting it in contact with water (dry porous stones). A flushing phase is then necessary to remove the air present in the circuits as well as back pressurisation is needed in order to saturate the specimen.

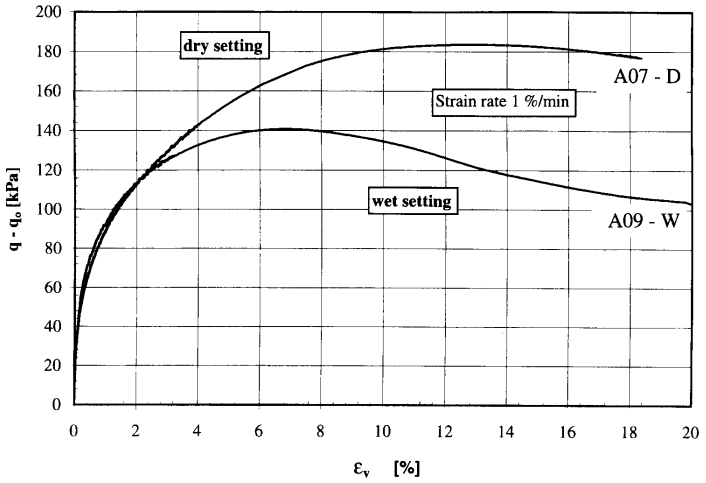

Figure 4.16 Impact of dry setting on stress-strain curve (Lo Presti et al. 1999).

In Lo Presti et al. 1999, the dry setting is compared with the wet setting method for two different Italian clays: Augusta clay and Pisa clay. These clays show that specimens that underwent wet setting developed very large swelling strains after saturation. The influence of dry setting on the stress-strain curve in the case of the Augusta clay is shown in **Figure 4.16**, where the results from two different tests (depending on the dry or wet setting method) are compared. The peak undrained strength of test A07-D is about 30% greater than that of test A09-W. A similar comparison for the Pisa clay did not show important differences in the stress-strain curves of specimens that underwent dry and wet setting. Thus, the authors stated that the dry setting procedure resulted quite effective in preventing specimen swelling which causes degradation of strength and large strain secant stiffness of overconsolidated clays. In the case of lightly overconsolidated clay specimens, the swelling deformations are not very important.
From the tests performed on our samples with the dry setting method, the above results appear to be confirmed and the dry setting method seems to be preferable compared with the conventional setting method for overconsolidated clays.

4.4.3 The soil stiffness from local measurements

In many cases, an accurate assessment of soil stiffness, from very small strains to peak, is of fundamental importance for the correct design of structure foundations. In fact, the observed settlements under working load conditions of well designed foundations on stiff soil are, generally, less than 0.1% (Simpson et al. 1979, Burland 1989, Tatsuoka et al. 1995a). Conventional laboratory tests greatly underestimate the soil stiffness for strain levels of less than 0.1%. The main consequence of such an underestimation is that the feasibility of very important constructions is not verified (Tatsuoka et al. 1995a) and for less important constructions the costs can greatly increase.

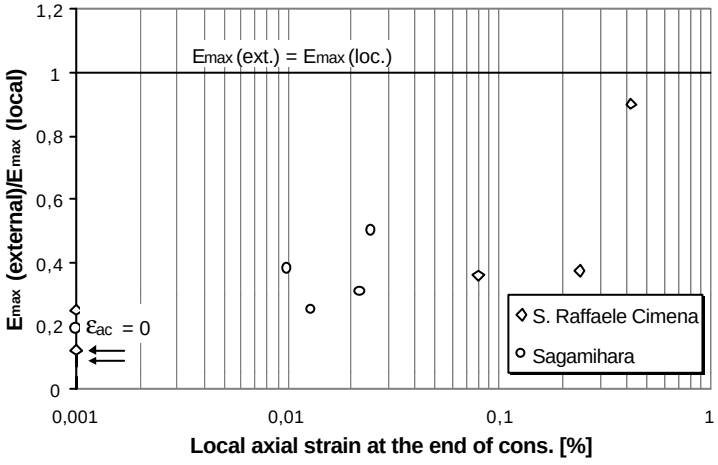

Figure 4.17 E_{max} (external) / E_{max} (local) vs. external axial strain at the end of consolidation.

The underestimation of stiffness from laboratory triaxial tests is mainly due to two different reasons: sample disturbance and bedding and seating errors in measuring the axial strains. The effects of sample disturbance can be mitigated using high quality samples (i.e. block samples) (Tatsuoka et al. 1997) and adopting appropriate reconsolidation techniques (Lo Presti 1997). The bedding and seating errors can be mitigated using specially devised triaxial equipment with local measurement of axial strain (Jardine et al. 1984, Symes & Burland 1984, Clayton & Khatrush 1986, Goto et al. 1991, Lo Presti et al. 1994). The impact of bedding errors on soil stiffness increases especially with a decrease of the axial strain experienced by the specimen during reconsolidation in the laboratory (Tatsuoka et al. 1995b).

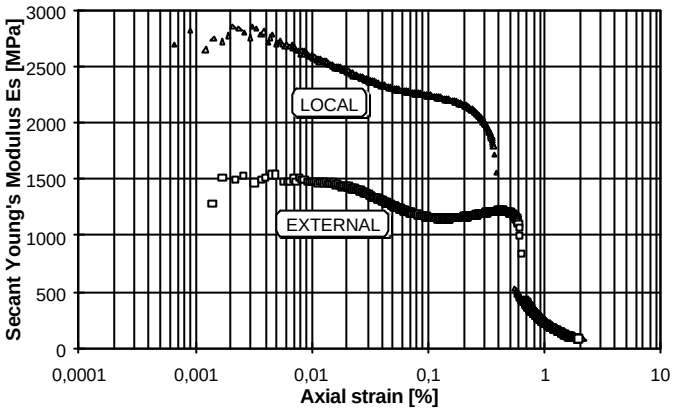

Figure 4.18 Secant Young's modulus vs. log axial strain. Test SGH1 on Sagamihara mudstone.

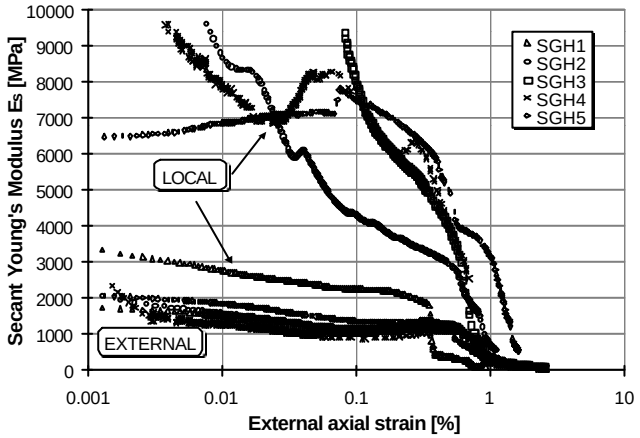

Figure 4.19 Secant Young's modulus vs. log axial strain for Sagamihara mudstone.

In the case of hard soils and soft rocks, a very large underestimation of the stiffness is expected, because of the very small axial strains usually experienced by the specimens during reconsolidation. Such an underestimation has been experimentally shown by Tatsuoka & Kohata (1995) for some Japanese sedimentary soft rocks. These data suggest that the use of specially devised triaxial equipment for hard soils and soft rocks testing is extremely important.
The data shown in **Figures 4.17**, **4.18**, **4.19**, **4.20** and **4.21** clearly confirm the importance of local axial strain measurements. This is especially relevant at very small strains. The ratio of the small strain Young's modulus, which was obtained from external axial strain measurements, to that determined from local axial strain measurements E_{max}(external)/E_{max}(local) is plotted in Figure 4.17 vs. the external axial strain at the end of consolidation.
The E_{max} values plotted in Figure 4.17 are the Young's moduli which were determined for an axial strain equal to 0.001%. It is possible to see that the underestimation of soil stiffness increases with a decrease of the axial consolidation strain. The greatest underestimation is observed in the case of unconfined compression with $\varepsilon_{ac} = 0$.
External axial strain measurements underestimate the stiffness also at large strains as shown in Figure 4.18. It is possible to see that the secant Young's modulus (E_s), obtained from local axial strain measurements, is equal to about 2800 MPa at $\varepsilon_a = 0.001\%$ and decreases to about 1800 MPa at peak. On the other hand, the secant Young's modulus from external axial strain measurements decreases from 1500 MPa to 1200 MPa for the same strain interval. Therefore, bedding and seating errors, which are more relevant at small strains, give a more or less constant secant stiffness over a wide strain interval. In reality, the soil stress-strain behaviour is highly non linear in this strain interval, as can be seen from the local measurements. In Figure 4.19 the secant Young's moduli inferred from local and external axial strains are compared for all the tests performed on Sagamihara mudstone. In Figures 4.20 and 4.21 the highly non linear stiffness is revealed for Sagmihara mudstone and for San Raffaele Cimena and Giaglione specimens by plotting normalised Young's modulus versus normalised deviator stress.

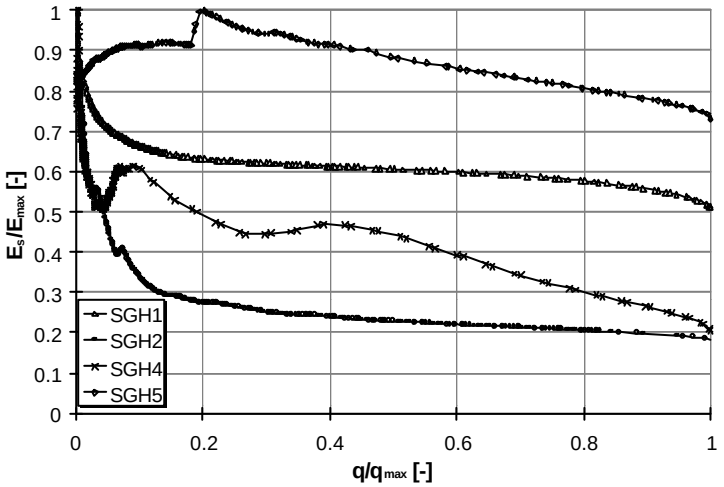

Figure 4.20 E_s/E_{max} vs. q/q_{max} for Sagamihara mudstone.

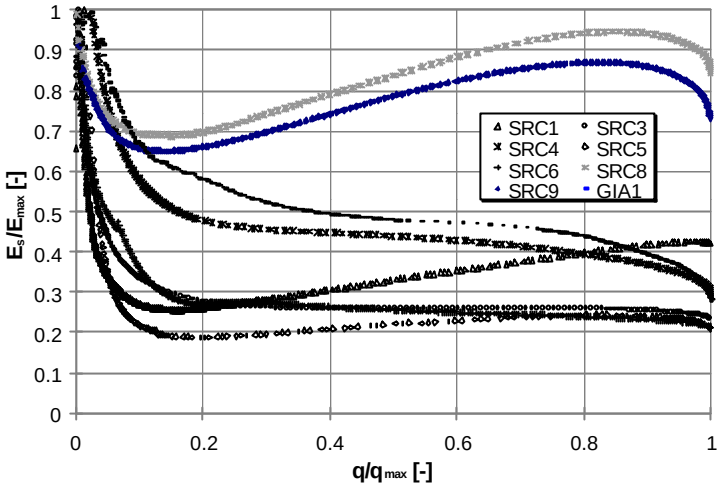

Figure 4.21 E_s / E_{max} vs. q / q_{max} for San Raffaele Cimena and Giaglione specimens.

The E_{max} values from all the tests performed are plotted vs. $q_{max} = (\sigma_1-\sigma_3)_{max}$ in a log-log scale (**Figure 4.22**). E_{max} values were inferred from local axial strain measurements. It is possible to notice that the E_{max} / q_{max} ratio mainly ranges from 1000 to 1500 in the case of Sagamihara mudstone and Giaglione carbonatic breccia. In the case of S. Raffaele Cimena samples the E_{max} / q_{max} ratio ranges from 500 to 700 when q_{max} is greater than 3 MPa. This ratio ranges from 200 to 500 when q_{max} is less than 3 MPa.

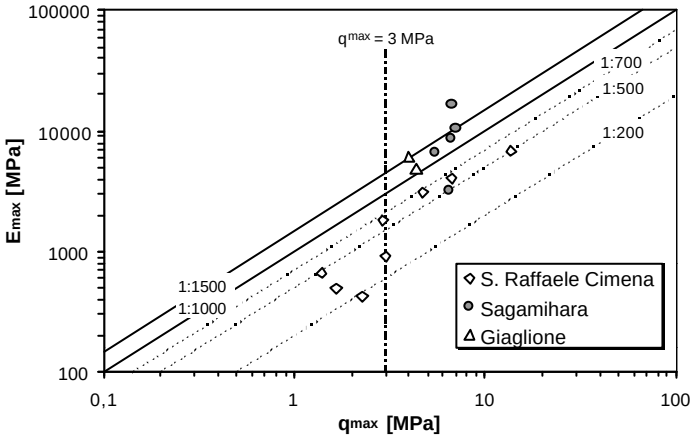

Figure 4.22 E_{max} vs. q_{max} for tested soft rocks.

Tatsuoka & Shibuya (1992) and Tatsuoka et al. (1995b) have shown that in the case of various sedimentary soft rocks the E_{max}/q_{max} ratio is equal to about 1000. Similar results have been reported by Fuoco et al. (1995) in the case of gneiss. Results shown by Tatsuoka & Shibuya (1992), Tatsuoka et al. (1995b) and Fuoco et al. (1995) refer to E_{max} values that have been inferred from local axial strain measurements.
As a general indication, the E_{max}/q_{max} ratio is equal to 1000 with the exception of specimens which exhibit q_{max} of less than 3 MPa.
As the E_{max}/q_{max} ratio is relatively constant, it is possible to evaluate the spatial variability of E_{max} from the assessment of q_{max} that is easily obtained in conventional equipment.

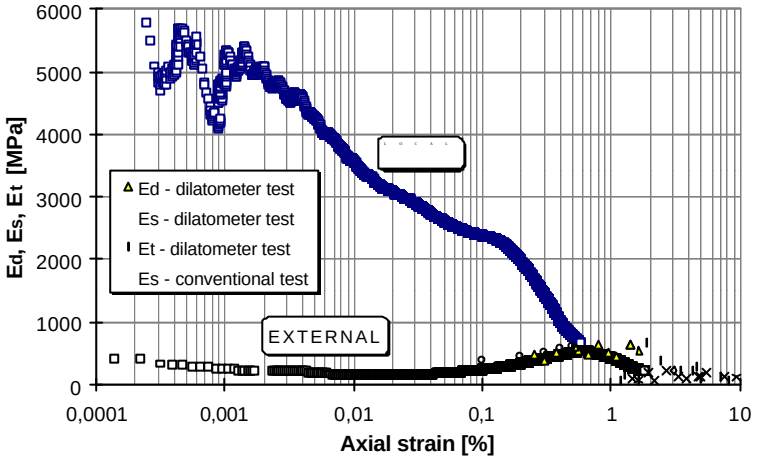

Figure 4.23 Young's moduli for carbonatic breccia in laboratory triaxial tests compared with dilatometer results at Giaglione site.

For the Giaglione site, values of the in situ deformation modulus (E_d) could be obtained from dilatometer tests. Moreover, the results of conventional triaxial compression tests were available. **Figure 4.23** compares the secant (E_s) and tangent (E_t) moduli evaluated by means of triaxial tests, performed in a conventional apparatus and in the previously described equipment, with the results obtained from in situ dilatometer tests.
For the tests performed with the apparatus described above, the secant Young's modulus was obtained from local and external axial strain measurements. Only external axial strain measurements were available for the conventional triaxial test. Specimens were isotropically reconsolidated in the triaxial cell at 1 MPa.
It is possible to notice that, up to large strains of about 0.5%, external or conventional measurements largely underestimate the soil stiffness. At large strains (ε_a > 0.5%) the same values of the secant modulus are obtained from conventional external and local axial strain measurements. A reasonable agreement between the in situ E_s and E_t values and the corresponding results from the conventional triaxial test for external axial strain measurement is noted.

4.4.4 The importance of the sliding mechanism

Figure 4.24 shows the specimens of the Sagamihara mudstone subsequent to triaxial compression. It is possible to see that all the specimens exhibit a single well defined rupture plane.

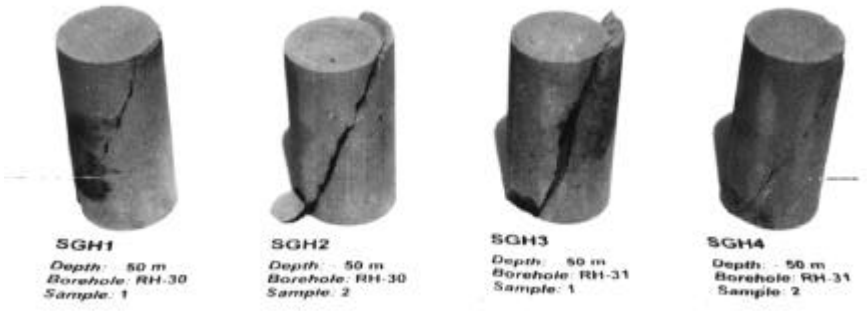

Figure 4.24 Sagamihara specimens after triaxial compression loading.

Unconfined compression tests were carried out on S. Raffaele Cimena specimens (tests SRC1 to SRC3). One test (SRC1) was performed by using a conventional apparatus with a fixed base pedestal.

Figure 4.25 shows the stress-strain curves for tests SRC1 and SRC3 obtained with local and external axial strain measurements respectively. If the attention is posed on the post peak stress-strain curve, the nearly brittle response of test SRC1 is in contrast with the softening behaviour shown for test SRC3.

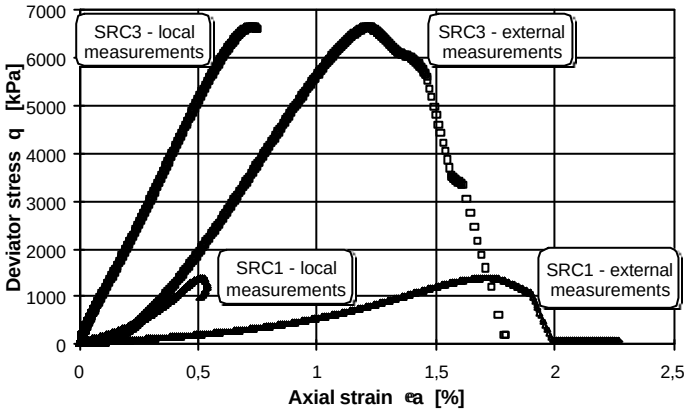

Figure 4.25 Stress-strain curves from unconfined compression tests on S. Raffaele Cimena specimens.

A comparison for the stress-strain curves of tests SRC1 and SRC5 is depicted in **Figure 4.26**. It is noted that both the specimens were obtained from the same samples, with the test SRC5 being isotropically consolidated to 100 kPa, unlike test SRC1. Whereas the importance of using the sliding mechanism is well reflected in the post peak stress-strain curve, due to the limited number of tests performed so far, this is not the case for the peak strength values.

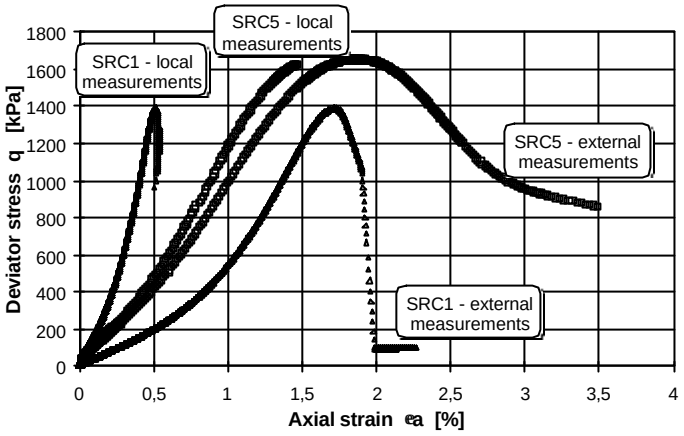

Figure 4.26 Stress-strain curves from compression loading triaxial tests on S. Raffaele Cimena specimens.

4.4.5 End capping

End capping with gypsum or other similar remedia is generally believed to be an effective countermeasure to reduce the bedding error. On the other hand, it has been shown that it is not possible to completely avoid bedding and seating errors, especially in the case of hard soils or soft rocks (Tatsuoka & Shibuya 1992, Tatsuoka et al. 1995b). End capping was not used for the tests described in this thesis except for tests GIA1 and GIA2 where a 3 mm thick rubber disk was interposed between the specimen and the inox steel cap and pedestal.

Figure 4.27 compares the axial displacements obtained with a pair of LDTs during tests SRC3 and SRC5. It is possible to notice that while for test SRC5 there is a very good agreement between the two LDT measurements, in the other case one sensor measures almost a nil displacement while the other one gives a displacement of about 0.02 mm. It is worthwhile to remember that the specimens are about 140 mm high and the LDTs are about 90 mm long. Moreover, test SRC3 is unconfined with zero axial strain before shearing, while the axial consolidation strain (ε_{ac}) is equal to about 0.42% for test SRC5. A similar comparison in the case of Sagamihara mudstone and Giaglione specimens is shown in **Figure 4.28**. In this case, the Sagamihara specimens are 100 mm high, while the LDTs are 90 mm long. The height of Giaglione specimens is 130 mm. However, also in this case the two independent measurements of axial displacement performed during a test are in agreement or not depending on the axial consolidation strain. The two measurements are not in agreement when ε_{ac} is very small.

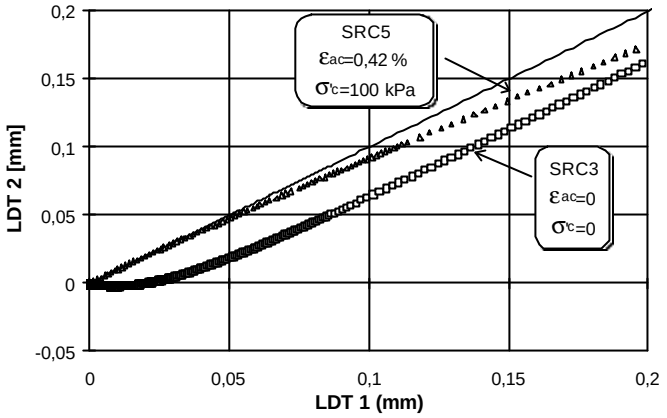

Figure 4.27 Axial displacement from two independent local measurements from S. Raffaele Cimena tests.

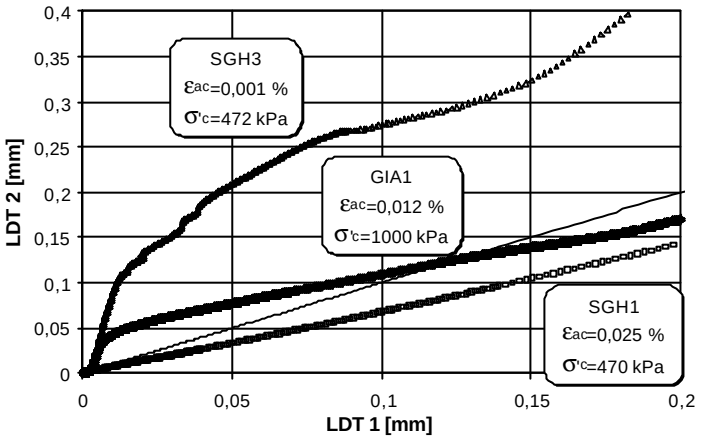

Figure 4.28 Axial displacement from two independent local measurements from Sagamihara and Giaglione tests.

On the basis of the results shown it is possible to state that capping may be important in the case of unconfined compression tests or when very small consolidation axial strains are expected. A great effort has to be done in trying to obtain good planar surfaces for the top and bottom end of the specimen. In tests GIA1 and GIA2 planarity was not easy to achieve and some bedding errors are present even though rubber end capping, as described above, was used. In this cases end capping cannot be avoided.

4.4.6 Some conclusions on the evaluation tests performed

On the basis of the experimental results reported, it is possible to draw the following conclusions.

- The dry setting method has been confirmed to be preferable to the conventional setting method.
- The local axial strain measurements are extremely important to correctly assess the stiffness of soft rocks from laboratory triaxial tests.
- The external axial strain measurements underestimate the stiffness from very small strains up to peak. A greater underestimation is observed at small strains. As a consequence, the external strain measurements obscure the highly non linear stress-strain response of soft rocks.
- The underestimation of stiffness increases with a decrease of the consolidation axial strain.
- The E_{max}/q_{max} ratio of the Sagamihara, S. Raffaele Cimena and Giaglione soft rocks, as inferred from local strain measurements, is equal to 1000 ± 500, in agreement with the results reported by Tatsuoka & Shibuya (1992).
- The sliding mechanism of the base pedestal is appropriate to mitigate the adverse effects of shear bands.
- To reduce seating and bedding errors a great effort need to be made to achieve good planar specimens surfaces. End capping or similar remedia are suggested to reduce these errors.
- Based on the laboratory results obtained in triaxial tests with local strain measurements, the use of the above values as input data in design might result in significant underestimates of stiffness for soft rocks if consideration is not given to strain level.
- The new triaxial apparatus is working satisfactorily in terms of both accuracy in measuring strains and capacity to perform triaxial tests in closely controlled conditions, as required for implementing the stress paths which were proposed in the previous chapter.

Chapter 5

Geotechnical characterisation of the Caneva stiff clay

5.1 Introduction

In order to simulate the ground behaviour around the tunnel in the triaxial apparatus, under closely controlled stress path conditions and to gain insights into the swelling phenomenon, an Italian stiff clay (Caneva clay) was chosen for testing as described in the following Chapter 6. The samples used are from the Caneva-Stevenà Quarry, near Pordenone, in the North-East of Italy.

As part of a geotechnical investigation on large-scale slope instabilities in the area (Barla G. et al. 1997), the room and pillar workings underground were visited. This allowed one to observe the exploratory adits in clays. These adits, which were excavated in 1970, have incurred in dramatic failures of the 30 cm thick unreinforced concrete liner, as illustrated in **Figure 5.1 (a)** to **(d)**.

The observation of the swelling induced deformations and instabilities in these adits and the easy access to the site were all considered to be favourable circumstances. At the same time, the results of the tests previously performed by ISMES (Barla G. et al. 1997) were further conditions to motivate the choice of the Caneva clay as representative soil for the testing programme to be carried out in this thesis.

The present chapter is to give few introductory remarks on the Caneva-Stevenà site. The physical and mineralogical composition of the clay under study and the results of oedometer and conventional triaxial tests will also be presented. Moreover, in the following Chapter 6 the attention will be posed on the triaxial tests in controlled conditions, performed with the aim to simulate the tunnel behaviour.

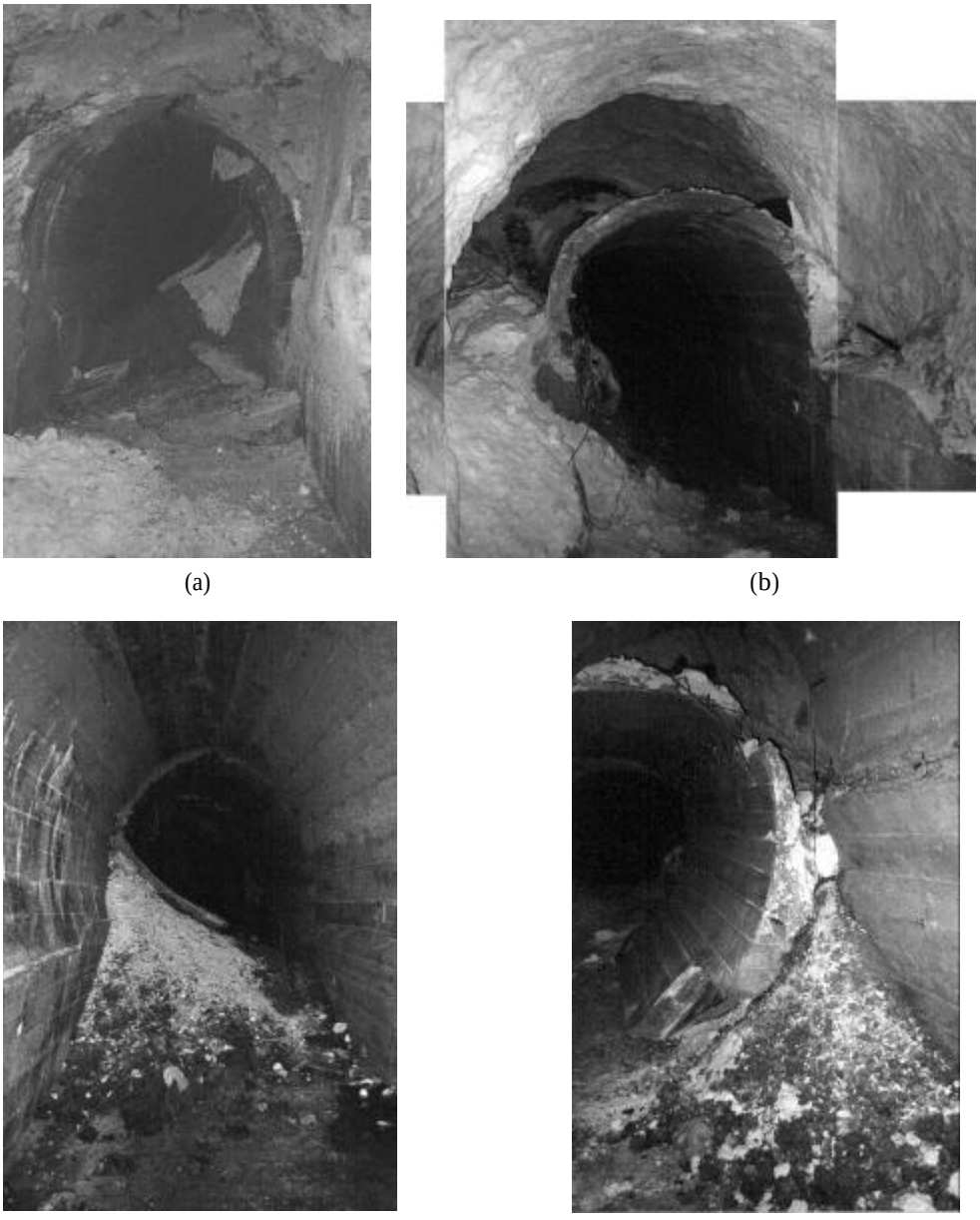

(a) (b)

(c) (d)

Figure 5.1 (a) to (d) – Typical conditions of the exploratory adit in the swelling zones at the Caneva-Stevenà Quarry.

5.2 Site conditions

Figure 5.2 illustrates a schematic cross section of the Caneva-Stevenà Quarry taken through boreholes CAEST3 and CAEST4, which were drilled with the main purpose to obtain representative samples of stiff clay. Based upon logging of these boreholes and other ones drilled at various locations in the area, in conjunction with detailed examination of the quarry face, the following geological formations were identified (Barla G. et al. 1997):

- Monte Cavallo Formation (Upper Jurassic-Upper Cretaceous) comprising:
  (a) the white limestone (local name: "marmorino bianco"), which is the rock being mined, composed of 99.9% calcium carbonate ($CaCO_3$);
  (b) the red limestone (local name: "marmorino rosso"), which sometimes is heavily fractured and faulted, with clay and iron oxide within the discontinuities as infilling;
  (c) the grey limestone, which is the upper rock formation characterised by layers of 1 m thickness.
- Flysch Complex (Eocene) consisting of sandstones, siltstones, marls, clays and silty-clays. The stiff clays pertain to this Complex and form the impervious substratum beneath the fractured limestone.

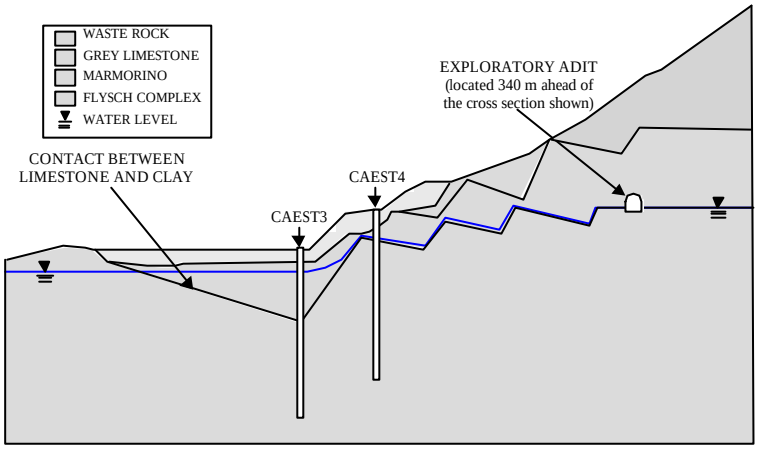

Figure 5.2 Schematic illustration of a typical cross section of the Caneva-Stevenà Quarry showing the boreholes CAEST3 and CAEST4 (not to scale).

Table 5.1 gives a list of the samples taken at various depths from the ground surface for boreholes CAEST3 and CAEST4 respectively. In order to obtain accurate undisturbed samples a triple-tube core barrel (NK3) was used incorporating a detachable PVC liner (length 1.50 m) so that the sample integrity could be preserved.
Also shown in Table 5.1 is a cubic sample (30 cm side) which was taken along the exploratory adit, in a side drift where the clay appeared not to be significantly disturbed by excavation. It is relevant to note that this sample pertains to the contact zone between the white limestone

(local name: "marmorino bianco") above and the Flysch Complex below. In all cases this sample was taken in the sidewall, following removal of the exposed clay.

Table 5.1 List of samples taken from the Caneva-Stevenà Quarry site.

Borehole N.	Sample N.	Depth [m]	Length [m]	Tests performed at
CAVA ROSS	CUBIC	-	-	Ismes
CAEST 3	1	44.65 – 45.55	0.90	Politecnico
CAEST 3	2	47.60 – 48.35	0.75	Ismes
CAEST 3	3	55.35 – 55.75	0.40	Ismes
CAEST 4	1	25.52 – 25.85	0.33	Ismes
CAEST 4	2	32.48 – 33.68	1.20	Ismes
CAEST 4	3	36.58 – 37.65	1.07	Politecnico
CAEST 4	4	45.94 – 47.15	1.21	-
CAEST 4	5	51.12 – 52.50	1.38	Politecnico
CAEST 4	6	58.95 – 59.80	0.85	Politecnico

5.3 Physical properties and mineralogical composition

The main characteristics of the Caneva clay are reported in **Table 5.2**. The available data for the plasticity index PI and liquid limit LL have been plotted in the plasticity chart (**Figure 5.3**). According to the USCS (Unified Soil Classification System) the clay can be classified as inorganic lean clay of medium plasticity. According to the Italian Geotechnical Society (A.G.I.), the soil can be classified as silty clay or clayey silt. In two cases it can be classified as silty sand.

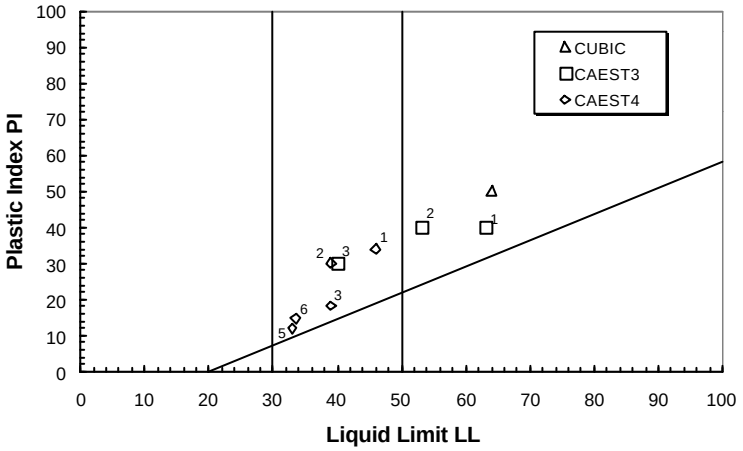

Figure 5.3 Plasticity Chart for the Caneva clay.

Grain size distributions are shown in **Figure 5.4** and appear to be variable, forming in general a poor basis for classification. The cubic sample is shown to consist of nearly 65% of particles less than 0.074 mm, in contrast with the CAEST4-5 sample which is characterised by a high sand content. In general, a significant heterogeneity in the size distribution is noted between the various samples. It is of interest to observe that the cubic sample, which pertains to the upper portion of the Tertiary Deposit, in the contact zone with the Cretaceous Limestone, has the highest clay content.

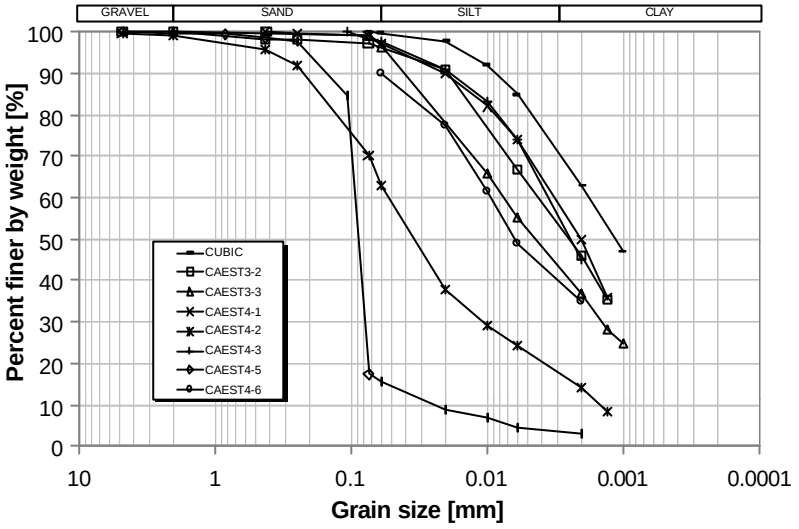

Figure 5.4 Typical particle size distribution curves of the Caneva clay.

Table 5.2 Physical properties of the stiff clays of the study*.

Sample	Depth [m]	w_n [%]	γ [kN/m^3]	G_s [-]	e [-]	LL [%]	LP [%]	PI [%]	$CaCO_3$ [%]
CUBIC	-	23.4	20.1	2.67	0.60	64	14	50	16.8
CAEST 3-1	44.65 – 45.55	16.2	21.4	2.69	0.53	63	23	40	1.9
CAEST 3-2	47.60 – 48.35	12.5	21.9	-	0.30	53	13	40	41.0
CAEST 3-3	55.35 – 55.75	-	20.5	-	-	40	10	30	-
CAEST 4-1	25.52 – 25.85	17.0	21.3	2.76	0.49	46	12	34	13.9
CAEST 4-2	32.48 – 33.68	10.7	22.9	-	0.29	39	9	30	-
CAEST 4-3	36.58 – 37.65	13.8	22.4	2.84	-	39	21	18	22.3
CAEST 4-4	45.94 – 47.15	-	-	-	-	-	-	-	-
CAEST 4-5	51.12 – 52.50	13.3	22.0	-	-	33	21	12	-
CAEST 4-6	58.95 – 59.80	11.9	23.2	2.83	-	34	19	15	23.9

* Where: w_n = natural water content, γ = specific gravity, G_s = grain density, e = void ratio, LL = liquid limit, LP = plastic limit, PI =plastic index, $CaCO_3$ = calcium carbonate content.

The natural water content (w_n) of the various samples, plotted in **Figure 5.5** versus depth below the limestone-clay contact, is shown to range between 8 and 17%, except for the cubic sample which exhibits a higher value, up to 25%. The tendency of the water content to decrease with depth, although exhibiting a large scattering of the data, is in line with the stratigraphic conditions of the site as shown in Figure 5.1.

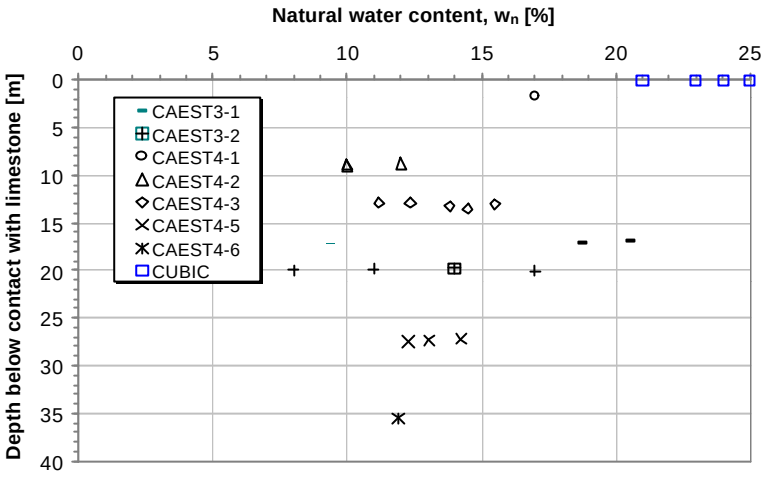

Figure 5.5 Natural water content versus depth for the Caneva clay.

Given the interest on the swelling behaviour of the Caneva clay, the presence of expandable clay minerals in the samples has been investigated by means of X-ray diffraction mineralogical analyses. The results obtained are summarised in **Tables 5.3** and **5.4**, depending on the laboratory used for the analyses.

Table 5.3 Data from mineralogical analyses performed at Ismes laboratory on the Caneva Clay.

Sample	Calcite [%]	Quartz [%]	Pyrite [%]	Plagioclase [%]	Dolomite [%]	Illite [%]	Kaolinite [%]	Clorite [%]	Smectite [%]
CUBIC	25	25	-	-	-	12.5	2.5	-	35
CAEST 3-2	20	15	-	-	15	7	-	3	40
CAEST 4-1	12	20	2	1	-	11.4	-	8.1	45.5

Table 5.4 Data from mineralogical analyses performed at Pavia University.

Sample	Dolomite [%]	Calcite [%]	Quartz [%]	Feldspar [%]	Chlorite [%]	Mica [%]	Smectite [%]
CAEST 3-1	24	23	15	4	12	7	15
CAEST 4-3	29	20	16	7	11	7	10
CAEST 4-5	26	18	19	4	13	8	12
CAEST 4-6	34	21	10	2	12	5	16

As an attempt to gaining insights into the likely swelling behaviour of the Caneva clay, the available data have been plotted on the diagram of **Figure 5.6**, which is generally used to identify the swelling potential of soft rocks. The triangular diagram combines together the mineralogical constituents of a rock. Each point is drawn by a definite percentage of clay minerals, quartz and carbonate content which is defined on each side of the triangle by a clockwise scale form 0 to 100% of the particular constituent. In order to compare the Caneva clay with other soils which are shown to exhibit a different degree of swelling (Barla G. et al. 1990), the data from two known argillaceous soft rocks (Varicolori clay shales and the Terraveccchia claystone) from Sicily are reported in the same diagram. Although some caution need be used, the data points confirm that the Caneva clay exhibits a swelling potential which is between medium and high potential.

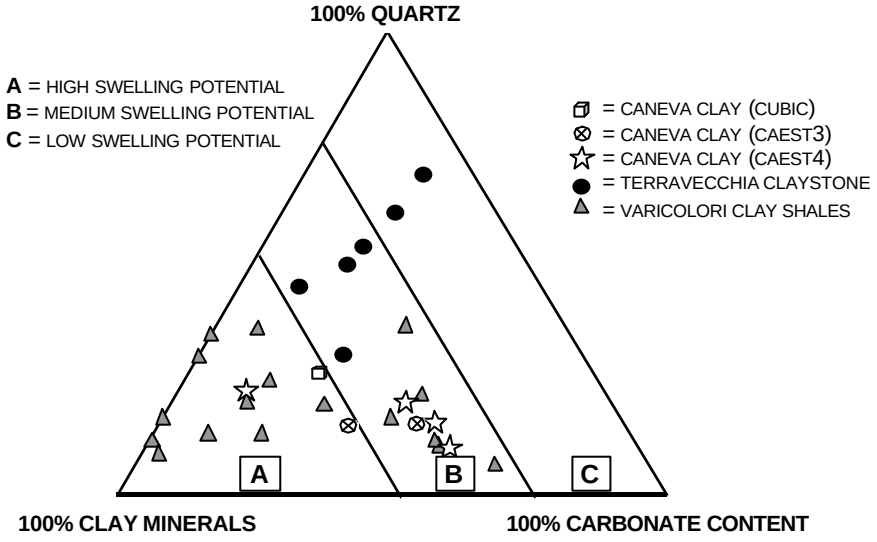

Figure 5.6 Diagram of the swelling potential for the Caneva clay.

5.4 Oedometer tests

Table 5.5 is a summary of the oedometer tests carried out at the ISMES and Politecnico di Torino laboratory respectively. The type of oedometer test performed is that of Huder & Amberg, with a testing procedure which is in line with the recent ISRM recommendations for determining the axial swelling stress as a function of the axial swelling strain (Madsen 1999). The tests have been carried out in a conventional oedometer, as used in Soil Mechanics, with the specimen being loaded in a stepwise manner up to the vertical stress level at the sample location and in dry conditions. After filling the oedometer cell with water, the swell heave for

each load decrement is measured until no displacement can be observed for a given load decrement. The result is a plot of the axial stress versus the axial strain.

Table 5.5 Oedometer tests performed on the Caneva Clay*.

Test code	Sample	Depth [m]	w_n [%]	Test type [%]	Laboratory where tests were performed
Edo1	CUBIC	-	25	Load – Unload	ISMES
Edo2	CUBIC	-	23	H&A	ISMES
Edo3	CUBIC	-	23	H&A	ISMES
Edo4	CUBIC	-	21	Load	ISMES
Edo5	CAEST 3-2	48.05	17	H&A	ISMES
Edo6	CAEST 4-1	25.73	17	H&A	ISMES
Edo7	CAEST 4-3	37.18	14	H&A	Politecnico
Edo8	CAEST 4-3	36.64	11	H&A	Politecnico
Edo9	CAEST 4-6	59.36	12	H&A	Politecnico

* Where: w_n = natural water content.

Figure 5.8 presents the swelling curves of the Caneva clay as obtained in all the tests performed except for the Edo1 and Edo4 tests, which are conventional loading or unloading oedometer tests (Table 5.5). The results are plotted by giving the total axial strain versus the applied vertical stress during the unloading stage. It is noted that the specimens taken from the cubic sample and from the CAEST4 sample exhibit a larger axial strain at the end of unloading down to a load corresponding to 28 kPa (complete unloading of the specimen was not carried out, in order to avoid upward bulging which may occur producing displacements which are not representative of swelling).

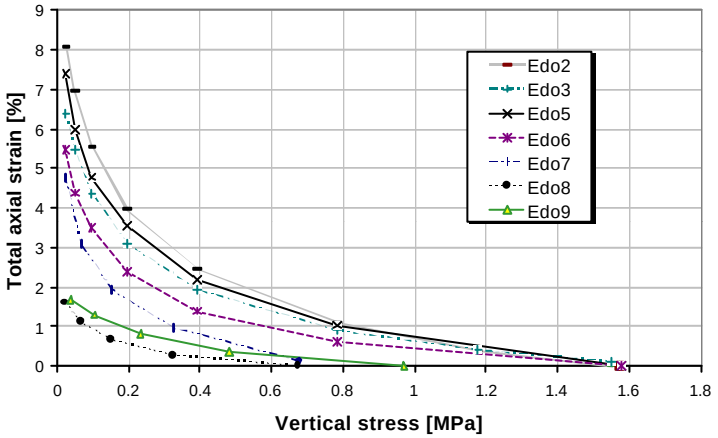

Figure 5.8 Axial strain versus vertical stress for the Caneva clay.

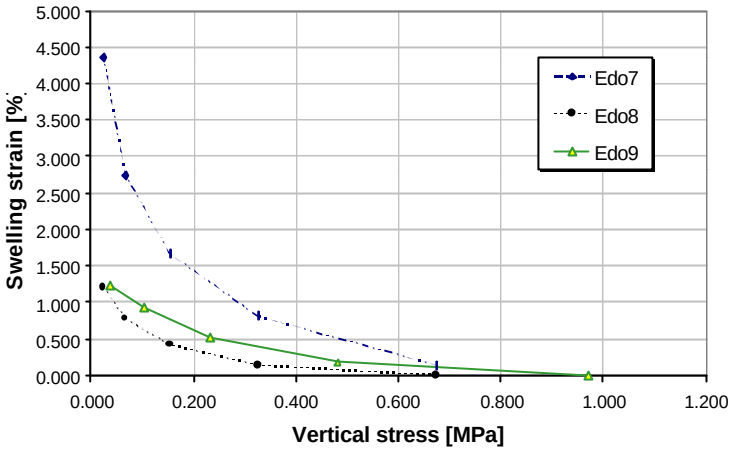

Figure 5.9 Swelling strain due to water adsorption versus vertical stress for the Caneva clay (only the tests carried out at the Politecnico laboratory are shown).

As recommended by Madsen (1999), **Figure 5.9** shows only the swelling strain caused by adsorption of water, which has been plotted versus the axial stress. This plot, which is presented only for the tests performed at the Politecnico laboratory, is to distinguish between the istantaneous strain related to the axial stress decrement through the matrix deformation and the swelling strain. The resulting curves are an indication of the swelling strains of the Caneva clays.

As an additional point of interest, **Figure 5.10** combines the data points of representative tests by giving the total axial strain versus clay mineral content determined by the X-ray diffraction mineralogical analyses. It is confirmed that higher total axial strains are associated with the presence of a more significant content of expandable clay minerals.

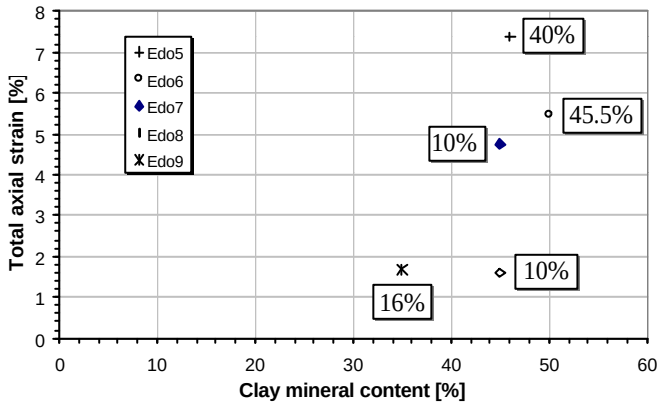

Figure 5.10 Total axial strain versus clay mineral content. Also given is the percentage of smectite.

5.5 Triaxial tests

With the main interest in determining representative shear strength parameters of the stiff clay of this study a number of conventional triaxial tests were performed as summarised in **Tables 5.6** and **5.7**. A total of twelve undrained compression tests were carried out by considering specimens taken from the cubic sample and drilled boreholes.

Table 5.6 CIU-CL triaxial tests performed on the Caneva Clay*.

Test code	Sample	Depth [m]	Test type [%]	w_n [%]	e [-]
Tx1	CUBIC	-	CIU-CL	25	0.67
Tx2	CUBIC	-	CIU-CL	24	0.64
Tx3	CUBIC	-	CIU-CL	24	0.64
Tx4	CUBIC	-	CIU-CL	23	0.59
Tx5	CUBIC	-	CIU-CL	24	0.62
Tx6	CUBIC	-	CIU-CL	22	0.57
Tx7	CAEST 3-2	47.77	CIU-CL	14	0.30
Tx8	CAEST 3-2	47.87	CIU-CL	11	0.28
Tx9	CAEST 3-2	47.97	CIU-CL	8	0.30
Tx10	CAEST 4-2	32.79	CIU-CL	12	0.32
Tx11	CAEST 4-2	32.89	CIU-CL	10	0.31
Tx12	CAEST 4-2	32.99	CIU-CL	10	0.22

* Where: w_n = natural water content, e = void ratio.

Table 5.7 CIU-CL triaxial tests results*.

Test code	Sample	B	σ'_{cons} [kPa]	B.P. [kPa]	t_{max} [kPa]	s'_{max} [kPa]
Tx1	CUBIC	0.95	800	200	151	723
Tx2	CUBIC	0.95	1920	280	379	1639
Tx3	CUBIC	0.97	1400	200	310	1281
Tx4	CUBIC	0.95	800	200	194	742
Tx5	CUBIC	0.95	1400	200	282	1234
Tx6	CUBIC	0.94	2000	200	310	1879
Tx7	CAEST 3-2	0.91	1350	350	3096	3863
Tx8	CAEST 3-2	0.93	777	400	3544	4653
Tx9	CAEST 3-2	0.90	2000	300	2569	4227
Tx10	CAEST 4-2	0.91	700	200	646	1484
Tx11	CAEST 4-2	0.73	1390	300	1011	2297
Tx12	CAEST 4-2	0.90	2000	400	1155	2803

* Where: B = Skempton's pore pressure parameter, σ'_{cons} = isotropic consolidation stress, B.P. = back pressure.

Each test involved isotropic consolidation of the specimen to the desired state of stress and shearing by compression loading in a conventional triaxial apparatus. The results obtained are illustrated in **Figure 5.11** which shows the stress state at failure. It is noted that all the tests were performed under the same constant displacement rate ($15 \cdot 10^{-3}$ mm/min) except for the TX11 test ($2 \cdot 10^{-3}$ mm/min).

If the data are fitted with straight lines as shown in the same Figure 5.11, the average failure envelopes are obtained. The failure lines intercepts and slopes determine the average cohesion c' and friction angle ϕ' respectively as shown in **Table 5.8**. The data given in Figure 5.11 and Table 5.8, which are fitting well for the results of testing on the CUBIC and the CAEST4-2 samples, are quite scattered and further testing should be carried out to assess the failure envelope for that pertaining to CAEST3-2 sample.

Table 5.8 Strength parameter from triaxial testing*.

Sample	c' [kPa]	ϕ' [°]
CUBIC	76	10.0
CAEST4-2	84	25.6

* Where: c' = effective stress cohesion intercept, ϕ'= friction angle in terms of effective stresses.

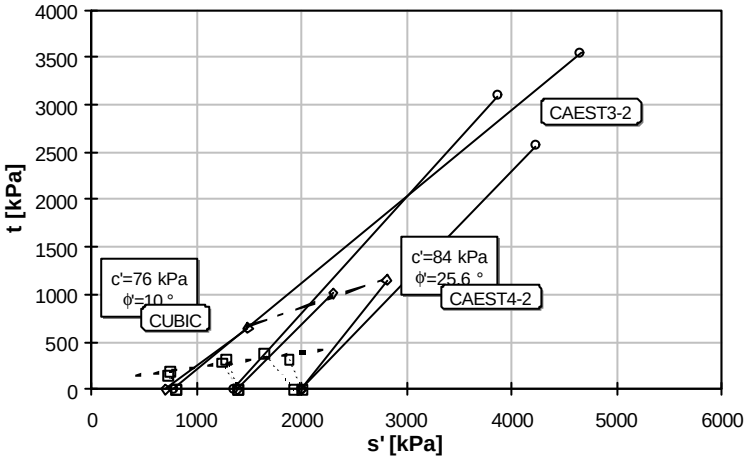

Figure 5.11 Failure envelopes from conventional triaxial testing.

It is shown that the shear strength parameters of the clays tested are highly different, closely dependent on the specimens tested, and the sample location and depth. It appears in general that the clays with higher calcium carbonate content (the $CaCO_3$ content of the CAEST3-2 sample is more than twice that of the cubic sample) have significantly higher shear strength parameters.

It is of interest to bring the attention on the undrained shear strength (c_u) as determined by interpreting the results of triaxial testing in terms of total stresses, as described in Table 5.9, where the Skempton's A parameter is also given together with the isotropic consolidation stress (σ'_c).

Table 5.9 Undrained shear strength for conventional triaxial tests performed*.

Test code	Sample	IC	A	c_u	σ'_c [kPa]	c_u / σ'_c [kPa]
Tx1	CUBIC	0.78	0.76	151	800	0.189
Tx2	CUBIC	0.80	0.87	379	1920	0.197
Tx3	CUBIC	0.80	0.69	310	1400	0.221
Tx4	CUBIC	0.82	0.65	194	800	0.242
Tx5	CUBIC	0.80	0.79	282	1400	0.201
Tx6	CUBIC	0.86	0.70	310	2000	0.155
Tx7	CAEST 3-2	0.97	0.09	3096	1350	2.293
Tx8	CAEST 3-2	1.05	-0.05	3544	777	4.561
Tx9	CAEST 3-2	1.13	0.07	2569	2000	1.285
Tx10	CAEST 4-2	0.90	-0.11	646	700	0.923
Tx11	CAEST 4-2	0.97	0.05	1011	1390	0.727
Tx12	CAEST 4-2	0.97	0.15	1155	2000	0.577

* Where: IC = consistency index, A = Skempton's parameter, c_u = undrained shear strength, σ'_c = isotropic consolidation stress.

Altough a certain degree of caution need be exercised, one may notice that the computed values of both the A parameter and the c_u / σ'_c ratio, as shown in the Table 5.9, would indicate that the samples taken at depth in the drilled boreholes are typical of a clay which is from lightly to highly over-consolidated. The geologic history of the site characterised by erosion/unloading and tectonic movements would confirm these assumptions. The lower values of the above parameters exhibited by the cubic sample could be due to fissures and discontinuities caused by different degree of disturbance developed during the unloading caused by the adit excavation or during sampling.

5.6 Conclusions

In order to provide an appropriate reference to the triaxial testing programme carried out on the Caneva stiff clay, as presented in the following Chapter 6, the attention was devoted to the results obtained in conventional tests. Following a list of the physical properties and of the mineralogical composition of the reference clay, also given are the results of conventional oedometer and triaxial tests, carried out for the purpose of geotechnical characterisation.
On the basis of the results obtained, one may draw the following conclusions.

- The Caneva clay is characterised by a significant heterogeneity of the samples tested (a cubic sample, taken from an exploratory adit in the Caneva-Stevenà Quarry; a number of samples taken in two boreholes, drilled to reach the Tertiary Flysch Complex, below the

Cretaceous Limestone Formation) in terms of the physical and mechanical properties and of the mineralogical composition.

- The identification of the swelling potential of the Caneva clay, as evaluated to different degrees (from medium to high potential) on the basis of mineralogical composition, is confirmed by the results of the oedometer tests carried out according to the Huder & Amberg procedure, as modified by ISRM recommendations (Madsen 1999). It is clearly shown that the Caneva clay exhibits a development of swelling strain as the axial stress applied to the specimen is gradually decreased.
- The results of conventional undrained compression triaxial tests confirm a significant degree of variability of the strength parameters (c_u, c', ϕ'), depending on the location and depth of the samples tested. In general, the strength parameters appear to be greater in terms of the calcium carbonate content; also, they are likely to be influenced by the size distribution in terms of clay content.

Chapter 6

Simulation of different stress path conditions by triaxial testing

6.1 Introduction

The Caneva clay has been characterised in the previous chapter by giving the physical and swelling properties, in addition to the representative strength parameters. It is the purpose of the present chapter to describe the results of the experimental programme carried out on the same clay by performing a number of triaxial tests with the equipment described in Chapter 4, including the newly developed triaxial apparatus. The main objective is to simulate the instantaneous excavation of a circular tunnel in a medium subjected to an isotropic initial state of stress, according to the stress path conditions presented in Chapter 3.
The study is intended to simulate, "at laboratory scale", the stress conditions experienced by a ground element around the tunnel as the excavation process takes place. In addition to paying attention to the instantaneous response to excavation and the influence of face advancement, the tests will be continued following the undrained phase, in order to gaining insights into the behaviour in drained conditions, when the consolidation/swelling phase is to occur.

6.2 Specimen preparation and testing procedure

The testing procedure adopted is quite complicated and time consuming. It has been defined as consisting of six phases: specimen preparation and set-up, flushing, saturation, consolidation, shearing and swelling/consolidation.

6.2.1 Specimen preparation and set-up

Specimen preparation has been carried out with great care in order to avoid any disturbance, including free swelling. To this end, the specimens were always cut from each sample and preserved in a cellar where temperature and humidity are reasonably constant. Each specimen was carefully wrapped in a plastic foil and covered with a paraffin layer, to be again wrapped in a second plastic foil, in order to avoid any possible contact with air. The three protecting layers were removed only at the time of inserting the specimen in the triaxial cell for testing.

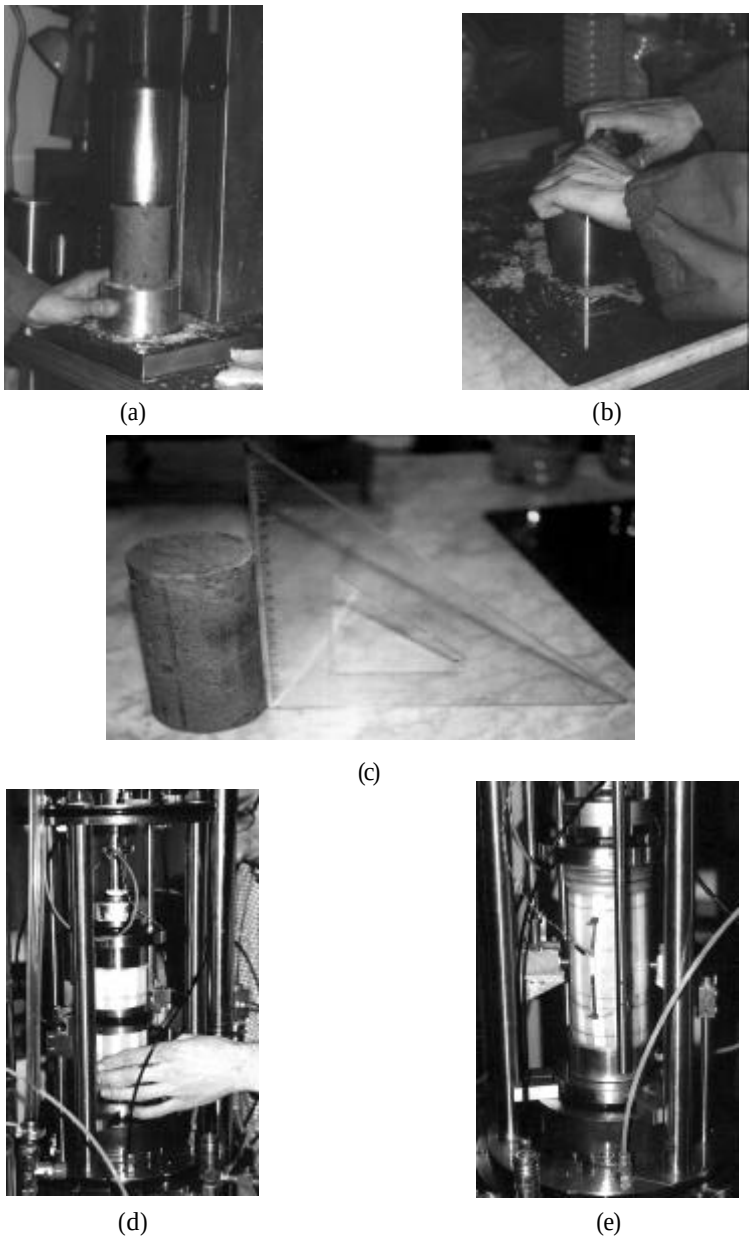

(a) (b)

(c)

(d) (e)

Figure 6.1 Specimen preparation and set-up. (a) Preparation of the lateral surfaces. (b) Preparation of the end surfaces. (c) Specimen ready to be introduced in the triaxial cell. (d) Membrane set-up. (e) Specimen ready, with measurement systems already positioned.

Each specimen was always finished by hand in order to obtain good planar surfaces at the top and bottom ends and a satisfactory normality with the lateral surfaces. Final dimensions of each specimen are 70 mm in diameter and 140 mm in height approximately. The specimen is set-up in the triaxial cell by using the dry setting method, in order to minimise swelling, which needs be prevented from taking place during the flushing and saturation phases. A few selected photographs taken during specimen preparation and the set-up phase are shown in **Figure 6.1**.

6.2.2 The flushing phase

In order to achieve the desired saturation of the pore pressure circuits, considering that the specimen was set-up by the dry setting method, which makes dry circuits mandatory (i.e. no water is to be in contact with the specimen), a flushing phase was always required. Moreover, before starting the flushing phase, the water used for back pressure was deaired. Then, a small pressure gradient of the order of 5 kPa (≅ 50 cm water height) was applied between the bottom and the top pore pressure circuits by leaving open the exit tap, so that a flow through the specimen could develop.

During the flushing phase the axial and radial deformations were measured with the intent to keep them within a target value (0±0.0015%). This could be obtained by the closed circuit control system with the computer making the servo-valve to change the applied pressures value, in order to keep the strains as desired. The vertical pressure was used to avoid axial deformation, as the confining pressure was used to control the radial deformations. Both systems act simultaneously and independently, so that if the specimen is to swell, the pressure is increased incrementally. It is obvious to note that the flushing phase duration was not the same for all the specimens tested, being closely dependent on permeability. Nevertheless, 24 hours flushing was always attained.

6.2.3 The saturation phase

The saturation of a specimen is achieved on the basis of the principle that air is soluble into water. Since solubility increases as air pressure is increased, the saturation phase will be characterised by a back pressure increase in the specimen. Considering that with the flushing phase an effective state of stress, able to avoid swelling, has been obtained, during the saturation phase any back pressure increase is to take place with a corresponding increase in the total state of stress in order to maintain the achieved effective stress constant. This is done by a stepwise procedure. The degree of saturation is controlled by means of the Skempton's pore pressure parameter B, which is computed for each step.

The procedure to be adopted implies that a given total isotropic stress increment $\Delta\sigma$ is applied to the specimen in undrained conditions. By measuring the corresponding variation of the pore pressure Δu, the B value is calculated with equation **(6.1)**.

$$B = \frac{\Delta u}{\Delta s} \tag{6.1}$$

Then, the back pressure is increased of the same increment as the drainage valve is open. This condition is maintained for at least 10 hours, in order to allow the air to dissolve into water, before initiating the next step.
It is noted that for the Caneva clay the saturation phase was lengthy and complete saturation was difficult to obtain, as shown in **Table 6.2**, where the values of B computed in each test are reported.

6.2.4 The consolidation phase

Following the saturation phase, each specimen is to be consolidated to the initial state of stress. In the tests performed, considering that this state of stress is unknown, the assumption of an isotropic state of stress was introduced for simplicity, with the vertical effective stress equal to the corresponding gravity component in situ and the K_o ratio equal to unity.
As the state of stress resulting from the flushing and saturation phases is not necessarily isotropic, the first step in the consolidation phase of the test is to achieve an initially isotropic effective state of stress in the specimen. Then, this is to be increased to the consolidation state of stress, which is to be maintained constant for the time required to attain a creep rate of deformation lower than 0.05 %/day. In all cases, the time duration of loading was never smaller than 24 hours.

6.2.5 The stress path - shearing phase

The stress path phase of the test is the most relevant one, in line with the objectives of the present thesis. Given that the intention is to simulate, "at laboratory scale", the stress conditions in the near vicinity of the tunnel, during face advancement, each test was carried out in undrained conditions, by imposing to the specimens the typical stress paths computed in Chapter 3.
It is accepted that the issue of whether undrained or drained conditions are more applicable to the tunnel problem during face advancement depends primarily on the permeabilty of the ground, the rate of excavation and the size of the tunnel (Mair & Taylor 1997). In the present work, where consideration is given to argillaceous rocks with permeabilty lower than 10^{-7} m/s, undrained conditions are assumed to hold true at least for the time duration required effectively for a ground element at the tunnel periphery to experience the stress paths as described in Chapter 3.
Different stress paths were imposed to the specimens during testing in order to simulate either the sidewalls or crown/invert behaviour. These stress paths are illustrated again for convenience in **Figures 6.2** and **6.3** respectively for the sidewalls and crown/invert, in the *t*-*s* plane where *t* and *s* are those defined in Chapter 3. It is assumed that the initial total state of stress is defined by $\sigma_v = \sigma_h = 1$ MPa.
It is noted that in two dimensional conditions (i.e. no face advancement is simulated) and for an isotropic state of stress ($K_o = 1$), the stress path for a point at the sidewalls or crown/invert of a circular tunnel is vertical (s = constant). The stress path will differ only due the fact that at the sidewalls a "compression" condition will occur (Figure 6.2) whereas at the crown/invert the opposite is to take place, i.e. an "extension" condition (Figure 6.3).
The corresponding stress path in three dimensional conditions (i.e. face advancement is simulated), as illustrated in the same Figures 6.2 and 6.3, shows a continuos change in the

mean stress during excavation. These stress paths computed have been simplified for the purpose of testing by introducing three oriented segments respectively for the 3D stress path at the sidewalls and crown/invert. Also, each stress path has been scaled accordingly so as to make the initial state of stress the starting point for either the "compression " or the "

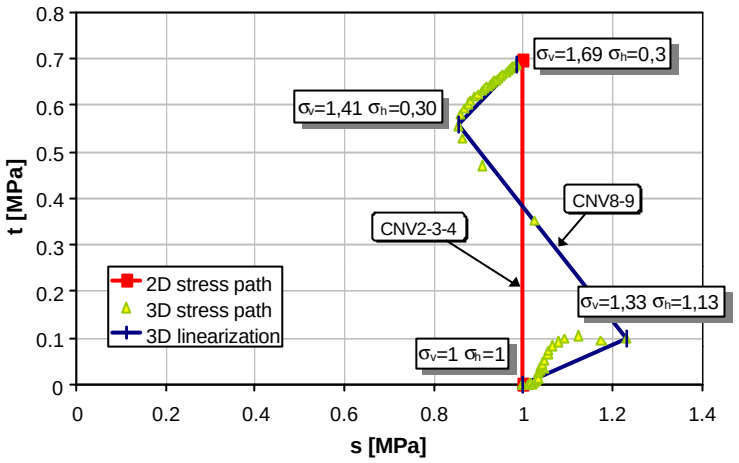

Figure 6.2 Stress paths applied during triaxial testing to simulate the state of stress at the tunnel sidewalls. "Compression " condition for K_o = 1.

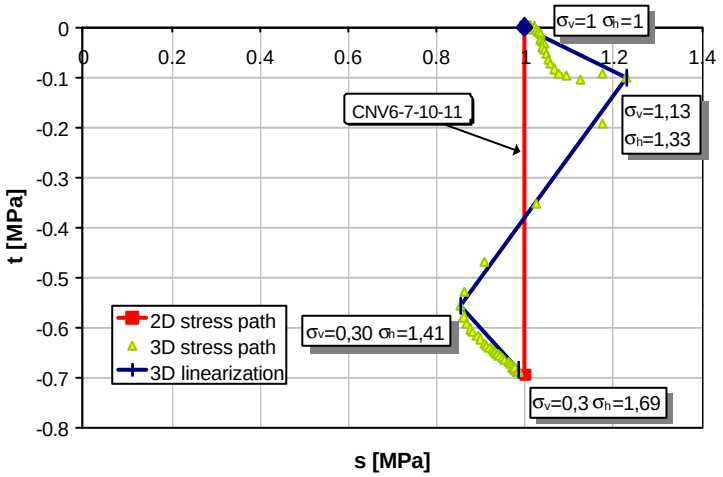

Figure 6.3 Stress paths applied during triaxial testing to simulate the state of stress at the tunnel crown/invert. "Extension " condition for K_o = 1.

To perform a triaxial test in controlled conditions so as to implement one of the stress paths described above is a rather difficult task. It requires both accurate pressure control and ability to follow continously any small stress change taking place as required. With the triaxial testing units used during this thesis, these tasks could be performed satisfactorily and effectively given the software programme developed and the special features of the pressure controller units adopted. In order to activate any desired stress path, the user need to input the following data:

- consolidation total vertical stress,
- consolidation total horizontal stress,
- displacement rate (mm/min) of the loading plate,
- K constant value, defining the desired stress path direction in the *t-s* plane (**Figure 6.4**).

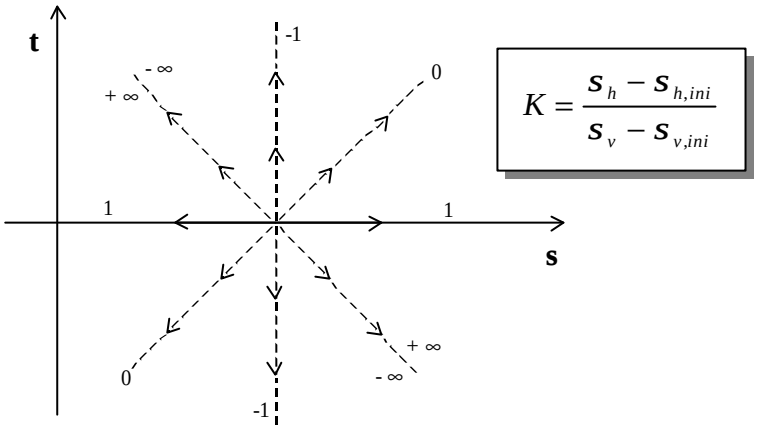

Figure 6.4 K values in the *t-s* plane to activate different stress paths from a starting point on the s axis.

With the appropriate input data, the computer of the control system (Figure 4.14) is to implement the desired condition of testing. The first step of a typical testing program consists in assigning to the loading machine the desired rate of axial displacement for either the "compression" or "extension" test to be performed (between 0.001 and 0.004 %/min for those described in this chapter). Then, as the axial stress applied to the specimen increases (in either "compression" or "extension"), the desired confining stress will be automatically computed so as to attain the chosen stress path. This value of the confining stress will be compared with that actually applied to the specimen and read at the pressure transducer; any difference within ± 0.4 kPa of the computed value will activate the servo-valve to change the applied pressure and bring it to the desired value in a stepwise manner by increments or decrements of pressure.

6.2.6 The swelling / consolidation phase

As described in the following, some tests have been performed up to failure. However, for a number of tests the chosen undrained stress path was carried out up to a defined value of the mobilised deviatoric strength. The intention in this latter case has been to study the subsequent swelling / consolidation phase. In fact, in line with the likely behaviour of the ground around a tunnel during excavation, drained conditions will occur in the section of interest in the case of a standstill or as the face moves away.
For these tests, at the end of the undrained stress path, before failure, the state of stress was maintained and creep deformation of the sample measured at a constant stress level up to attaining a creep rate lower than $\Delta\varepsilon < 0{,}05$ %/day. With this condition holding true, the drainage valve was opened and the deformations produced in the sample measured until final stabilisation.

6.3 Testing programme

A total of 10 triaxial tests were performed, as shown in **Table 6.1**, with the aim to simulate, "at laboratory scale", the tunnel behaviour in the undrained and drained phase. The two special devised triaxial apparatuses described in Chapter 4 were used.

Table 6.1 Triaxial tests performed*.

Name	Borehole	Depth [m]	w_n	Type of test	σ'_c [kPa]	B. P. [kPa]	Triaxial Apparatus
CNV1	CAEST4-3	37.51	14.49	CIU	718	243	GDS
CNV2	CAEST4-3	37.28	13.36	CIU-2D	650	350	GDS
CNV3	CAEST4-3	37.06	11.47	CIU-2D	670	310	GDS
CNV4	CAEST4-3	36.91	14.10	CID	657	320	GDS
CNV5	CAEST4-5	51.19	14.26	CIU	200	0	SRTA
CNV6	CAEST4-5	51.35	13.05	EIU-2D	815	200	SRTA
CNV7	CAEST4-5	51.49	12.28	EIU-2D	750	380	SRTA
CNV8	CAEST4-3	36.90	11.17	CIU-3D	635	350	GDS
CNV9	CAEST3-1	45.17	9.39	CIU-3D	1150	553	SRTA
CNV10	CAEST3-1	44.87	20.52	EIU-2D	695	405	SRTA

*Legend: w_n = natural water content, σ'_c = consolidation effective stress, B.P. = back pressure.

Tests CNV1 to CNV4 and CNV8 were performed on the specimens derived from the CAEST4-3 sample. This group of tests was carried out on the GDS triaxial apparatus, with the intent to reproduce the behaviour at the sidewalls of a circular tunnel during excavation. As indicated in Figure 6.2, the *s* = constant "compression" stress path was imposed to tests CNV2, CNV3 and CNV4. While the CNV2 test was carried out up to failure, the CNV3 stress path was interrupted at a value of the mobilised deviatoric strength factor $f = 0.5$. At this point

the drainage valve was opened and the swelling deformations measured. The CNV4 test was carried out up to $f = 0.33$ in drained conditions.
The three dimensional conditions were introduced for test CNV8 that followed the simplified three dimensional stress path (Figure 6.2). At a value of the mobilised factor $f = 0.5$, in order to compare the results with test CNV3, the stress path was interrupted and the drainage valve opened.
To investigate the behaviour at the crown/invert of the circular tunnel during excavation, two samples were opened: CAEST4-5 and CAEST3-1. CNV5, CNV6 and CNV7 pertain to CAEST4-5 sample while CNV9, CNV10 pertain to CAEST3-1. These two groups of tests were performed on the newly developed soft rock triaxial apparatus. The stress paths applied to these tests are shown in Figure 6.3. Also in this case, when a two dimensional condition is applied, the stress path is vertical (s = costant), however in "extension".
All the tests of this group, except for CNV5 and CNV9, followed the s = constant "extension" stress path in undrained conditions. For the CNV6, CNV7 and CNV10 tests the stress path was interrupted at a value of the mobilised factor $f = 0.5$. At this point the drainage valve was opened and the drained phase investigated. It is noted that the performance of the "extension" tests, as described above, requires a pressure cell able to stand a pressure greater than applied in the "compression" tests. This made it imperative to choose the newly developed triaxial cell that can stand a confining pressure up to 2 MPa in safe conditions. The CNV9 test was used to repeat the three dimensional stress path in "compression" by adopting the SRTA apparatus and was taken up to failure. The CNV5 specimen was sheared under a conventional compression loading stress path.

6.4 Brief description of the tests performed

A brief description of all the tests performed is reported in the following by pointing out the testing conditions and the problems encountered.

Test CNV1

The CNV1 specimen, saturated at a back pressure of 243 kPa, gave a B value higher than 0.95. It was isotropically consolidated to 718 kPa effective stress. Due to an error occurred in the control program, the stress path adopted in this case was not s = constant, but a condition near to compression unloading was effected. In order to obtain additional data at failure conditions as already available by the conventional triaxial tests described in Chapter 5, this specimen was sheared in undrained conditions.

Test CNV2

The CNV2 specimen, saturated at a back pressure of 350 kPa, gave a B value higher than 0.87. This specimen was isotropically consolidated to 650 kPa effective stress. After consolidation, according to a s = constant stress path this specimen was taken up to failure in undrained conditions. At failure a well defined shear plane was evidenced and a negative excess pore pressure of –350 kPa was measured.

Test CNV3

The CNV3 specimen was saturated at a back pressure of 310 kPa to give a B value higher than 0.90. Following consolidation in isotropic conditions to an effective stress of 670 kPa, the s = constant stress path was followed in undrained conditions up to 50% of the previously defined

failure strength. The specimen exhibited an incipient failure plane (Figure 6.5) and a negative excess pore pressure of about –60 kPa. After the complete dissipation of creep deformations, the drainage valve was opened and the swelling deformations versus time measured.

Test CNV4

The CNV4 specimen was saturated at a back pressure of 320 kPa with a B value higher than 0.95. Consolidation was done at 657 kPa effective stress. After consolidation, the s = constant stress path was followed with the drainage valve open up to 33% of the previously defined failure stress. The specimen showed the formation of an incipient sliding plane along which failure finally occurred during creep deformation.

Test CNV5

The CNV5 specimen, saturated at a back pressure of 400 kPa, gave a B value higher than 0.93. The sample was consolidated isotropically at 730 kPa effective stress. A problem was experienced at this time with the pressure chamber: a sudden leak at an o-ring during the night time caused a fall down of the confining pressure. The o-ring was to guarantee sealing at a hole for the electric cables on the top plate of the triaxial cell. Since the specimen at this point experienced an unloading of the effective state of stress attained, some degree of swelling is likely to have occurred. For this reason the test was abandoned and the specimen was sheared in compression with 200 kPa of confining pressure and 0 kPa of back pressure. The specimen failed by exhibiting a number of vertical failure planes.

Test CNV6

The CNV6 specimen, saturated at a back pressure of 100 kPa, gave a B value higher than 0.99. Saturation of this sample was much easier than in other cases. This is due to a higher sand content present in this specimen. Isotropic consolidation was done at 815 kPa effective stress. After consolidation the extension stress path was applied in undrained conditions with the aim to reach a mobilisation factor f = 0.5. One problem was encountered in this test and is related to the stress path which was interrupted by the computer before reaching the final state of stress. The stress path was then resumed, however some creep deformation could not be avoided. The excess pore pressure during the undrained phase was positive and had a value of 160 kPa. With the drainage valve open, the specimen showed a tendency to contract.

Test CNV7

The CNV7 specimen, saturated at a back pressure of 370 kPa, gave a B value higher than 0.90. Isotropic consolidation was done at 770 kPa effective stress. After consolidation the extension stress path in undrained conditions was applied with the aim to reach a mobilisation factor f = 0.7. In order to be sure that the results obtained with the previous test (CNV6) were not affected by errors due to migration of fluid from the pressure cell due to leaking of the lactic membrane, additional measures were taken. Two membranes were mounted on the specimen and a layer of grease with an aluminium foil were interposed between them. Even though, at the end of consolidation, when the drainage valve was closed for a while to verify if the pore pressure was stable, a positive excess pore pressure developed at a constant state of stress with the tendency to stabilise. During the stress path phase, the excess pore pressure was positive with a value of 160 kPa. When the drainage valve was opened the specimen showed a clear contraction. This test exhibited a behaviour substantially similar to that of the previous CNV6 test.

Test CNV8

The CNV8 specimen, saturated at a back pressure of 350 kPa, gave a B value higher than 0.90. Isotropic consolidation was done at 635 kPa effective stress. After consolidation the three dimensional compression stress path in undrained conditions (linearized in three different segments) was applied with the aim to reach a mobilisation factor f = 0.5. The pore pressure excess during the undrained phase was positive with a value of 100 kPa. Then the drainage valve was opened and the stress path was continued up to failure. For this test, at the consolidation stage, the increasing of pore pressure was measured to be around 5-10 kPa. Since the confining pressure during the stress path was reduced, this problem is believed not to have affected the results significantly.

CNV1

CNV2

CNV3

CNV4

CNV9

Figure 6.5 Selected specimens of interest after testing.

Test CNV9
The CNV9 specimen, saturated at a back pressure of 550 kPa, gave a B value higher than 0.77. Isotropic consolidation was done at 600 kPa effective stress. After consolidation the three dimensional "compression" stress path in undrained conditions (linearised in three different segments) was applied up to failure. The excess pore pressure during the undrained phase was initially positive, then started to decrease after the changing of the stress path direction and reached a value of -43 kPa at failure.
Test CNV10
The CNV10 specimen, saturated at a back pressure of 400 kPa, gave a B value higher than 0.88. Isotropic consolidation was done at 695 kPa effective stress. After consolidation the "extension" stress path in undrained conditions was applied with the aim to reach a mobilisation factor f = 0.5. The pore pressure excess which developed during the undrained phase was positive with a value of 124 kPa. With the drainage valve opened the specimen exhibited a contracting behaviour. It is noted that during consolidation the pore pressure was measured versus time before initiating the stress path, as for the previous tests. An increase in the pore pressure value, with the tendency to stabilise, was evidenced. The procedure was repeated a few times before starting the stress path phase. This allowed one to notice that each time the drainage valve was closed the excess pore pressure developed was smaller. As a consequence, the stress path phase was initiated when no more pore pressure was measured with closing of the drainage valve. This type of behaviour was interpreted as an indication that the excess pore pressure measured in tests CNV6, CNV7 and CNV8, at the end of consolidation, could be due to an incomplete dissipation of the excess pore pressure developed in the consolidation stage, in the inner part of the specimen and not related to leaking of the lactic membrane.

6.5 Results and discussion

In the present paragraph the results obtained with the triaxial testing programme will be discussed and the following aspects will be addressed:
- swelling stresses exhibited during the flushing phase,
- shear strength parameters,
- undrained behaviour (shearing phase),
- undrained creep behaviour,
- drained behaviour (swelling / consolidation phase).

Table 6.2 gives a summary of the results obtained for all the tests performed. The complete data sets available for all the tests are collected in Appendix A.

Table 6.2 Triaxial tests performed*.

Name	Borehole	Depth [m]	Type of test	B	σ'_c [kPa]	B.P. [kPa]	t_{max} [kPa]	s'_{max} [kPa]	Δu [kPa]
CNV1	CAEST4-3	37.51	CIU	0.94	718	243	270	558	-286
CNV2	CAEST4-3	37.28	CIU-2D	0.87	650	350	452	1000	-349
CNV3	CAEST4-3	37.06	CIU-2D	0.90	670	310	245	728	-60
CNV4	CAEST4-3	36.91	CID	0.95	657	320	135	661	0
CNV5	CAEST4-5	51.19	CIU	0.93	200	0	470	669	-
CNV6	CAEST4-5	51.35	EIU-2D	0.99	815	200	-317	632	175
CNV7	CAEST4-5	51.49	EIU-2D	0.90	750	380	-318	595	164
CNV8	CAEST4-3	36.90	CIU-3D	0.90	635	350	234	656	100
CNV9	CAEST3-1	45.17	CIU-3D	0.77	1150	553	317	735	-43
CNV10	CAEST3-1	44.87	EIU-2D	0.88	695	405	-132	479	124

*Where: B = Skempton's parameter, σ'_c = consolidation effective stress, B.P. = back pressure.

6.5.1 Swelling stresses from the flushing phase

Table 6.3 gives the final state of stress for the different specimens resulting from the flushing phase. The vertical and horizontal stresses given are those that prevent swelling of the specimens during the water flux and may depend on many factors. First of all the quality of the sample but also the type of soil, the swelling potential and the stress history need to be considered.

Table 6.3 Results of the flushing phase*.

	CNV1	CNV2	CNV3	CNV4	CNV5	CNV6	CNV7	CNV8	CNV9	CNV10
$\sigma_{v,fin}$	46.6	110.41	79.65	89.96	44.4	80.3	151.9	141	171.12	208
$\sigma_{h,fin}$	38.8	151.19	183.13	165	51.07	86.2	88.8	153	126.46	213

*Where: $\sigma_{v,fin}$ = final vertical stress, $\sigma_{h,fin}$ = final horizontal stress.

Figure 6.6 compares the vertical stress at the end of flushing with the data available for other soils which exhibit a different degree of swelling potential (Barla G. et al. 1990). These data pertain to the Varicolori clay-shales and to the Terravecchia claystone, previously mentioned in Chapter 5. They were obtained from oedometer tests giving the vertical pressure which prevents swelling (ISP). Even though the data cannot be directly compared, since the testing procedures are quite different, the Caneva clay is shown to exhibit a moderate to high swelling potential, in agreement with considerations drawn in Chapter 5.

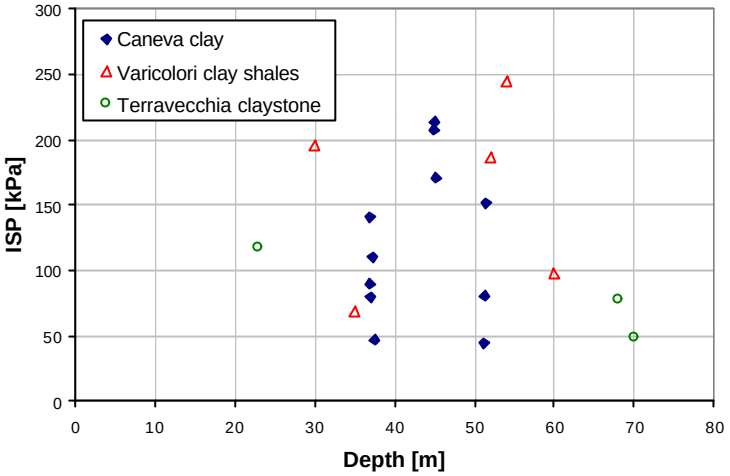

Figure 6.6 Swelling pressure for Caneva clay and other soils.

6.5.2 Shear strength parameters

The shear strength parameters determined for the Caneva clay, based on the results of conventional triaxial tests, were presented in paragraph 5.5. Moreover, given that some triaxial tests described in the present chapter were brought up to failure, some additional information on the strength parameters could be gained as described below.

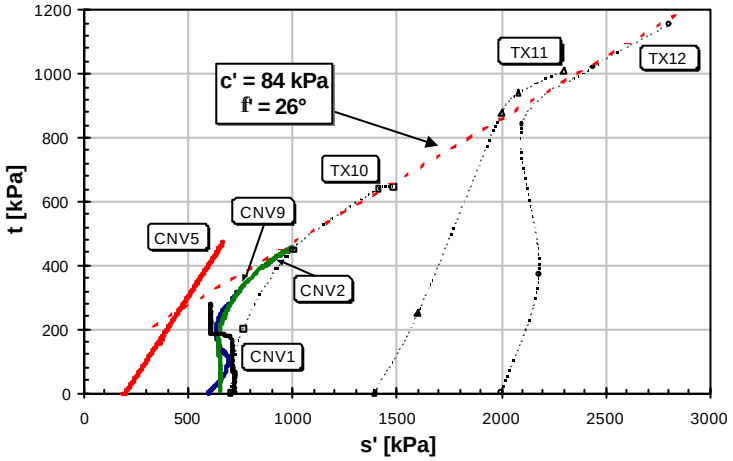

Figure 6.7 Effective stress paths for CNV1, CNV2, CNV5 and CNV9 tests and failure envelope for CAEST4-2 sample[1].

[1] Tests Tx10, Tx11, TX12 are conventional triaxial compression loading tests, previously described in paragraph 5.5 and performed at ISMES laboratory.

Figure 6.7 shows the stress path for tests CNV1, CNV2, CNV5 and CNV9 with specimens taken from samples CAEST4-3, CAEST4-5 and CASET3-1. Except for the CNV5 test, which was performed on a specimen taken from the CAEST4-5 sample, the data confirm the failure envelope as obtained with the conventional triaxial tests TX10 to TX12. It is worthwhile to notice that the CNV5 specimen is characterised by a slightly higher sand content than the other specimens which could justify the larger undrained strength obtained for the specimen.

6.5.3 Undrained shearing phase

6.5.3.1 Simulation of tunnel sidewall behaviour

To simulate the sidewall behaviour of a circular tunnel several tests were carried out. **Figure 6.8** shows the total stress path for the tests performed. The CNV2 and CNV3 tests were carried out according to the stress path holding true in two dimensional conditions and for K_o = 1. The CNV8 and CNV9 tests followed the corresponding stress path in three dimensional conditions. All the tests are undrained tests, except the CNV4 test which was carried out in drained conditions according to a two dimensional stress path. Also shown in Figure 6.8 is the stress path of the CNV1 undrained test.

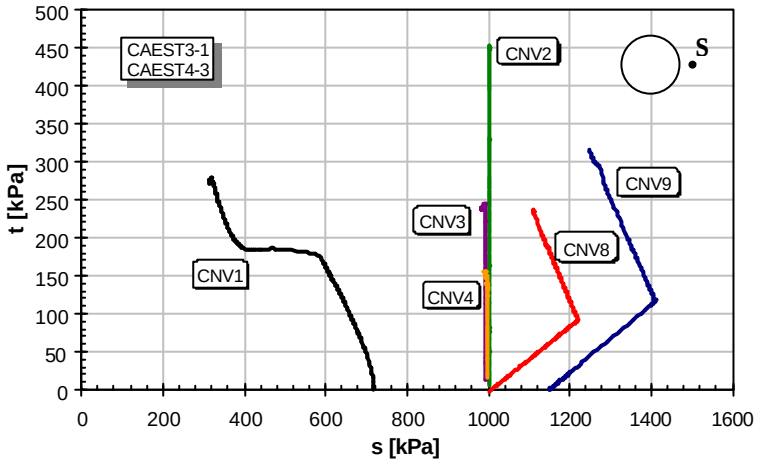

Figure 6.8 Total stress paths for the tests intended to simulate the behaviour at the sidewall of a circular tunnel (point S).

In order to give a more detailed representation of the results obtained and allow a better comparison between two dimensional and three dimensional conditions, as imposed with different stress paths, **Figures 6.9** and **6.10** give the effective stress path plot. Also shown is the excess pore pressure at the end of each test.

The comparison of total and effective stress paths allows one to clearly appreciate the excess pore pressure change which occurs during each test. It is noted that in two dimensional

conditions (tests CNV2 and CNV3, Figure 6.9) the excess pore pressure Δu is almost negligible in the first part of the test, as long as the *t* value remains small.
However, with *t* nearly equal to 200 kPa, a negative pore pressure develops, subsequently to increase in relation to the increase of *t*. The decreasing rate in the pore pressure for the CNV3 specimen appears to be higher than that for the CNV2 specimen, a likely consequence of the better saturation conditions obtained for the first specimen, confirmed by the B values given in Table 6.2.
Some further comments are possible if a closer view is taken to the tunnel problem, with the excavation process being simulated with the tests performed. According to the stress paths of tests CNV2 and CNV3 a final *t* value equal to 695 kPa would correspond to the excavation completed in the cross section of interest (Figure 6.2 and Chapter 3).
The CNV2 specimen is shown to have failed at t = 452 kPa, with a negative excess pore pressure Δu = -348 kPa (Figure 6.9). This is to say that the secondary state of stress, induced around the tunnel with the excavation process completed, would lead to the development of a failure zone with a negative excess pore pressure, unless a confining pressure was applied on the tunnel contour.
The CNV3 test was interrupted before failure for a mobilisation factor f = 0.5. This signifies that the tunnel excavation is not completed and the advancing face is at a small distance from the cross section of interest, where the ground element undergoing the test is supposed to be located. The same type of behaviour would be experienced by a ground element at a certain distance from the tunnel contour, in a cross section where excavation has however been completed.
It is noted that the results obtained in such a case are quite similar to those exhibited by the CNV2 test with a negative excess pore pressure Δu = -60 kPa (Figure 6.9). This would mean that if the excavation face is further advanced with respect to the cross section of interest, failure would occur with the development of a consistent negative excess pore pressure.

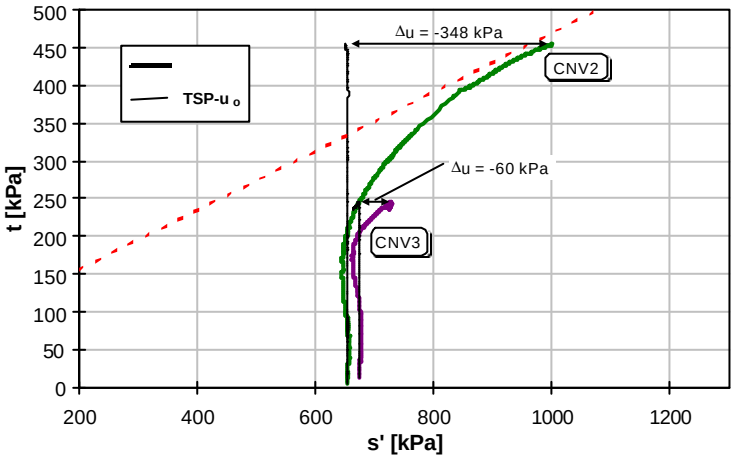

Figure 6.9 Effective stress paths and failure envelope for CNV2 and CNV3 tests.

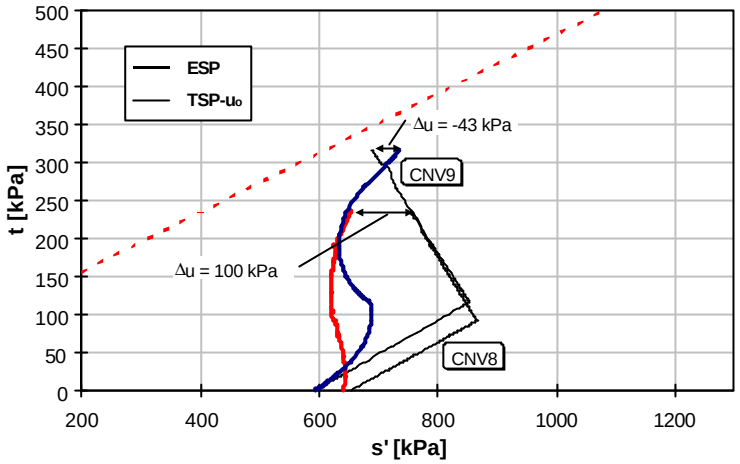

Figure 6.10 Effective stress paths and failure envelope for CNV8 and CNV9 tests.

If the attention is now posed on the CNV8 and CNV9 tests, which were carried out specifically to simulate three dimensional conditions during face advancement, the results obtained for the excess pore pressure show a significantly different response. During the first segment of the stress path both the axial and the confining pressures in the triaxial cell are increasing. This results in a positive excess pore pressure for low *t* values. For the CNV8 specimen, the positive excess pore pressure is greater than that for the CNV9 specimen as shown in **Figure 6.11**, where the pore pressure excess Δu is plotted versus *t*.

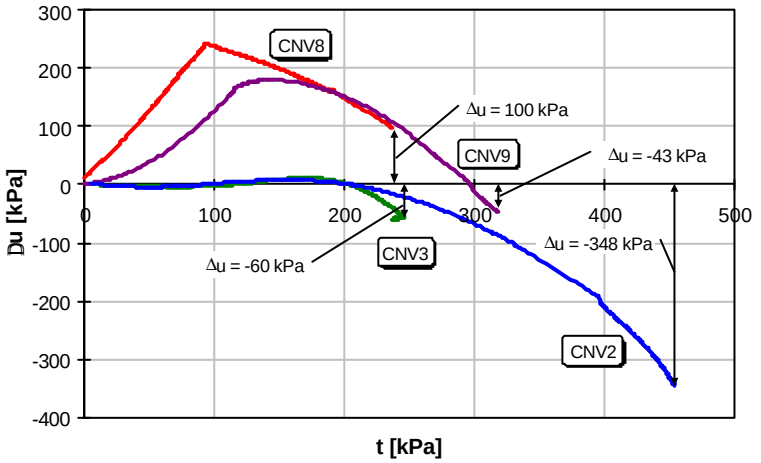

Figure 6.11 Excess pore pressure versus t value for tests CNV2, CNV3 and CNV8.

It is noted that this could be due to the fact that the pore pressure value was not completely stabilised in the inner part of the specimen, after consolidation for the CNV8 test. Nevertheless, when the stress path changes direction (i.e. when the tunnel passes the cross section of interest) the confining pressure decreases rapidly with a notable effect on the pore pressure.

When t is greater than 100 kPa for the CNV8 test and 140 kPa for test CNV9, the Δu value starts to decrease and this behaviour is maintained up to the end of the test. For the CNV8 specimen at the end of the test the excess pore pressure is positive with a value of 100 kPa. On the contrary, for the CNV9 specimen, which was taken up to failure, the negative excess pore pressure is -43 kPa.

As can be seen in Figure 6.11, that compares both tests in two dimensional and in three dimensional conditions, two different trends of behaviour are experienced. While for the two dimensional conditions the negative excess pore pressure develops at a t value of 200 kPa, when the influence of the advancing face is taken into account (i.e. in three dimensional conditions) a greater value of it is necessary to induce a negative excess pore pressure. In the latter case it is also seen that a positive excess pore pressure is developing in the first part of the stress path, which simulates the tunnel face approaching the cross section of interest.

If the negative excess pore pressure is connected to the amount of swelling that is expected, in the near vicinity of the sidewalls of a circular tunnel, the areas where swelling is likely to occur would be smaller when predicted with a three dimensional analysis instead of a two dimensional one. Moreover, at failure, for both cases, as a negative excess pore pressure around the tunnel results in a water inflow towards it, swelling is likely to occur as an inverse consolidation due to the interaction between water and swelling minerals when present in the ground. To investigate this behaviour for the CNV3 and CNV8 tests, the drainage valve was opened at the constant final state of stress. The results obtained will be discussed in the following paragraph 6.5.5.

6.5.3.2 Simulation of tunnel crown/invert behaviour

With the purpose to simulate the crown/invert behaviour of a circular tunnel three tests were performed as shown in **Figure 6.12**, which gives the total stress paths holding true in two dimensional conditions. These tests (CNV6, CNV7 and CNV10) were stopped for different values of t and were performed in undrained conditions. The corresponding effective stress paths are plotted in **Figure 6.13**, where also given is the excess pore pressure value at the end of each test.

It is clearly shown that the excess pore pressure Δu, negative at the sidewall of the tunnel, is instead positive at the invert/crown. The final value of Δu attained in each case at the end of the test is directly related to the stress level t.

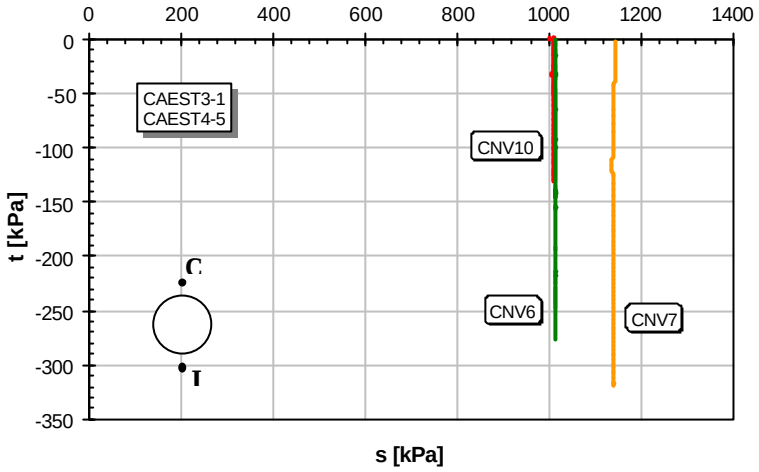

Figure 6.12 Total stress paths for the tests intended to simulate the behaviour at the crown/invert of a circular tunnel (point C and I).

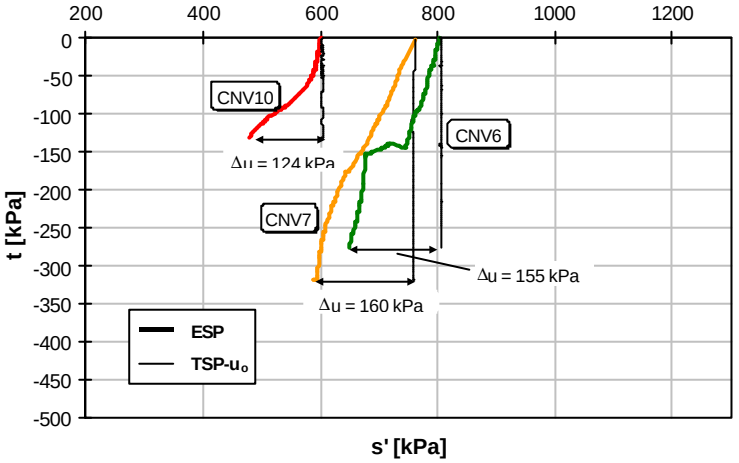

Figure 6.13 Effective stress paths and failure envelope for CNV6, CNV7 and CNV10 tests.

Figure 6.14 compares the positive excess pore pressure directly versus *t* and shows a quite similar trend of behaviour for the three specimens. As a consequence, during the drained phase, consolidation would take place with a decrease in volume. As shown in paragraph 6.5.5, this behaviour would occur, based upon the simulation undertaken, at the crown/invert of the tunnel.

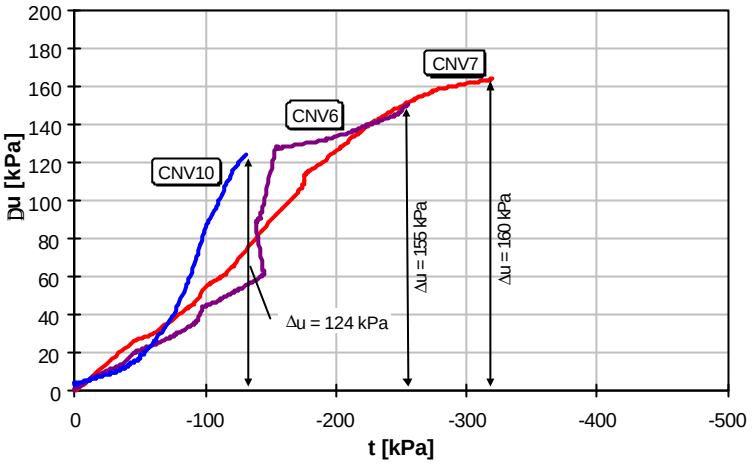

Figure 6.14 Excess pore pressure versus t value for CNV6, CNV7 and CNV10 tests.

6.5.4 Creep behaviour

Following the undrained phase for tests CNV3, CNV7, CNV8 and CNV10, and the drained stress path for test CNV4, the state of stress attained in each case was maintained constant in order to allow for undrained creep deformations to occur, before opening the drainage valve. The axial and radial strains are plotted in each case versus time as shown in **Figures 6.15** to **6.17**. It is noted that this type of behaviour could be related directly to the tunnel response during a standstill. As it is possible to see, the creep rate decreases progressively to a negligible value for all the tests.

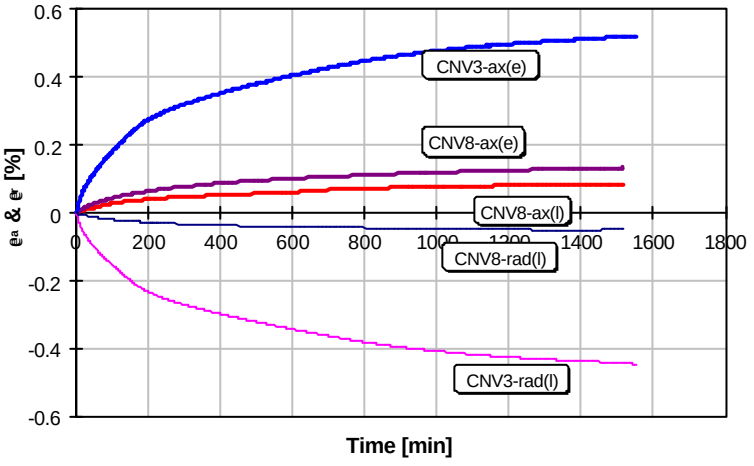

Figure 6.15 Axial and radial strains for CNV3 and CNV8 tests.

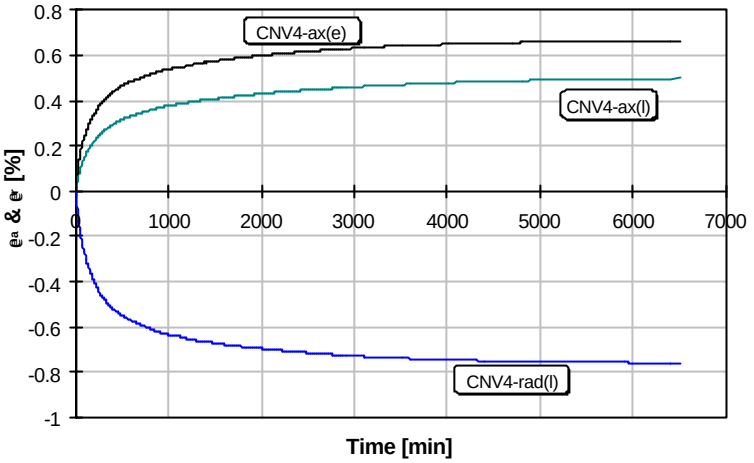

Figure 6.16 Axial and radial strains for test CNV4.

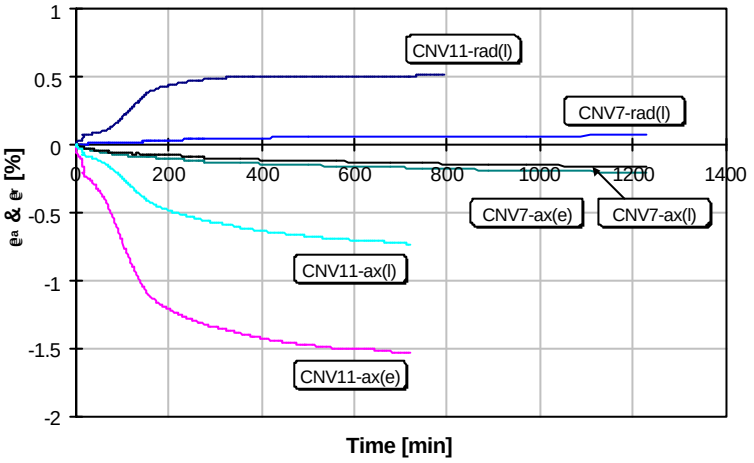

Figure 6.17 Axial and radial strains for CNV7 and CNV11 tests.

6.5.5 Drained phase

6.5.5.1 Simulation of the tunnel sidewall behaviour

Tests CNV3 and CNV8 were stopped before reaching failure and the actual state of stress was maintained constant with the drainage valve open. As already stated, this part of the test (drained phase) is intended to simulate the behaviour at the sidewalls, for a ground element at a certain distance from the tunnel periphery, in a cross section where stress concentrations are

no longer present, due to the advancing face. With a released state of stress and drainage occurring, deformation due to water adsorption and chemical reactions with the mineralogical constituents can take place. For this reason the axial, radial and volumetric deformations were measured, all the other conditions holding true.

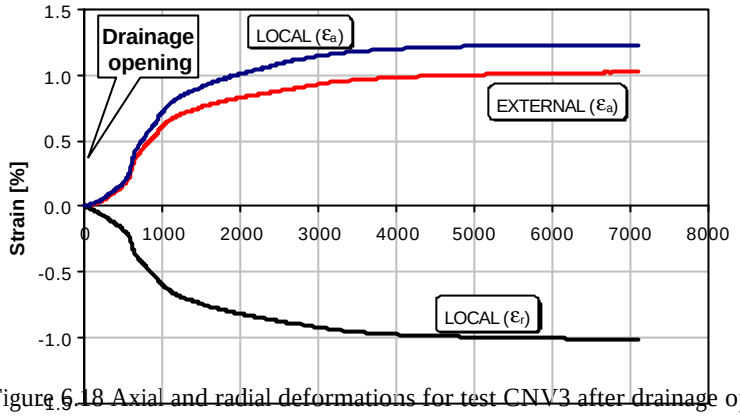

Figure 6.18 Axial and radial deformations for test CNV3 after drainage opening.

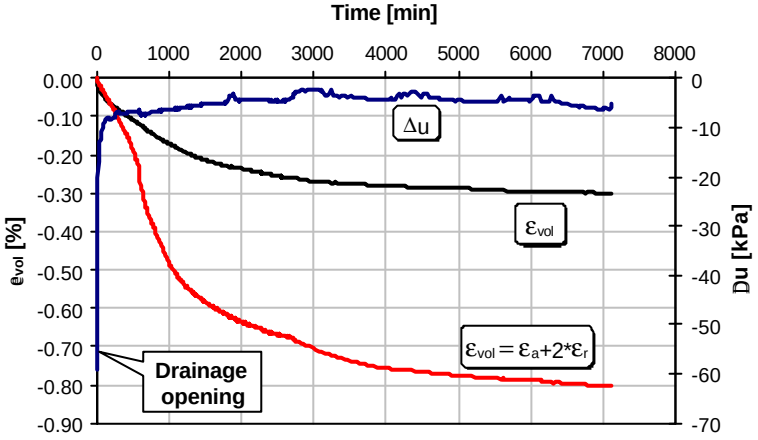

Figure 6.19 Volumetric deformation and pore pressure excess for test CNV3 after drainage opening.

Figure 6.18 illustrates for the CNV3 test a plot of the axial (ε_a) and radial (ε_r) strains versus time as derived from both local and external measurements. **Figure 6.19** gives the corresponding plot of the volumetric deformation (ε_{vol}), obtained by either direct measurement of volume change in the specimen (i.e. volume of water entering-positive or exiting-negative the specimen) or computation of the first invariant of strain in terms of ε_a and ε_r. Also shown

in the same Figure 6.19 is the plot of the excess pore pressure versus time. Finally, always with reference to the sidewalls, the results of the drained phase for test CNV8 are plotted in **Figures 6.20** and **6.21**; **Figure 6.22** reports the axial strain rate versus time for both tests CNV3 and CNV8.

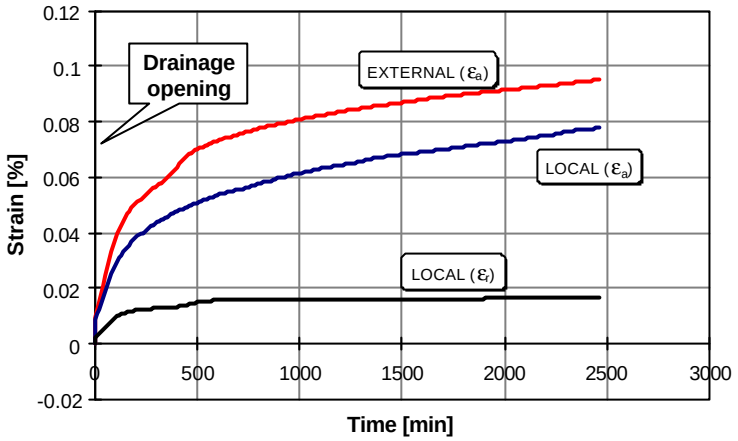

Figure 6.20 Axial and radial deformations for test CNV8 after drainage opening.

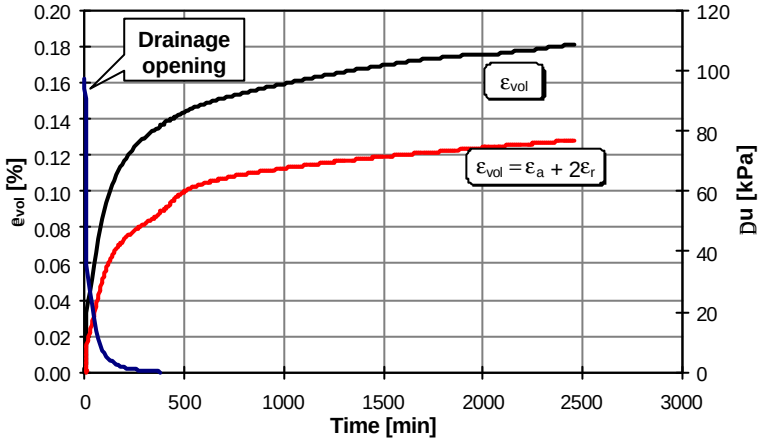

Figure 6.21 Volumetric deformation and excess pore pressure for test CNV8 after drainage opening.

It is of interest to point out the different trends of behaviour exhibited by the CNV3 and CNV8 specimens, depending on the excess pore pressure values attained at the end of the undrained phase. This excess pore pressure dissipates, under a constant state of stress, in a few

hours. The CNV3 test exhibits a dilatant behaviour (swelling) at the end of shearing, while the CNV8 test experiences a contracting behaviour (consolidation).

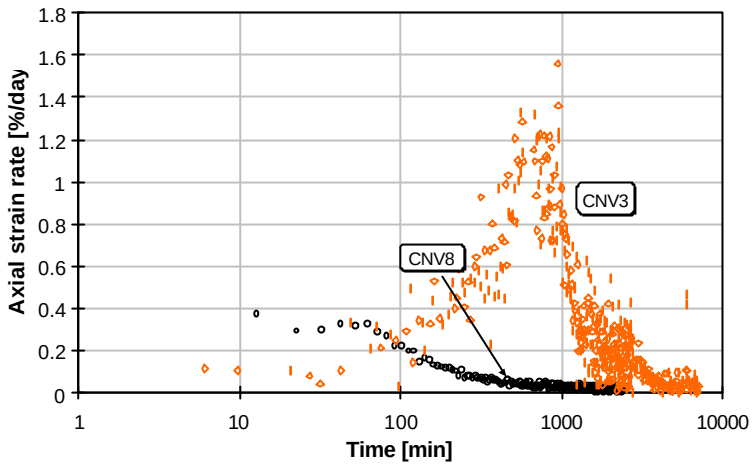

Figure 6.22 Axial strain rate for the CNV3 and CNV8 tests.

It is also to be noted that the increase in volume shown in test CNV3 (-0.80%) is greater than the corresponding decrease in volume (+0.13%) holding true for test CNV8. This occurs even though the excess pore pressure to dissipate in the latter case is greater. It appears as well that the CNV3 specimen takes a much longer time to dissipate the excess pore pressure than the CNV8 specimen.

Another point of interest to be observed as result of testing relates to the measurements of volume increase/decrease in each specimen. The direct measurement of volume for the two tests gives values which are not significantly different in modulus (-0.30% for CNV3 and +0.18% for CNV8). In contrast, the results derived by means of the local strain measurements exhibit a remarkable difference (-0.80% for CNV3 and +0.13% for CNV8). There is also a difference in the results of the two measurements of volumetric deformation for the same test.

These different trends of behaviour, which are well illustrated in Figures 6.19 and 6.21, are due to the barrel shape attained by the deformed specimen, which obviously causes a difference in the results of measurements. However, one could argue that another reason that might enhance the differences is the swelling of the expansive minerals in the specimen.

In the case of negative excess pore pressure, the water enters the sample during the drained phase and the water content will increase over time and swelling will occur. As the volume measuring device measures an increase in volume due to the water flowing into the specimen, the local measurement system will show a greater volume increase because of the chemical reactions with the swelling minerals. The opposite phenomenon will take place when the excess pore pressure is positive. The volume increase caused by the chemical reactions is opposite to the volume decrease measured, due to the water flowing out of the specimen.

6.5.5.2 Simulation of the tunnel crown/invert behaviour.

Some insights into the response of the tunnel to excavation during the drained phase at the crown/invert have been gained by means of tests CNV7 and CNV10. As **Figure 6.23** shows the axial and radial deformations for CNV7 test, **Figure 6.24** illustrates the corresponding volumetric deformation and excess pore pressure versus time. The same plots for the CNV10 test are shown in **Figures 6.25** and **6.26**. The strain rate for both tests is given in **Figure 6.27**.

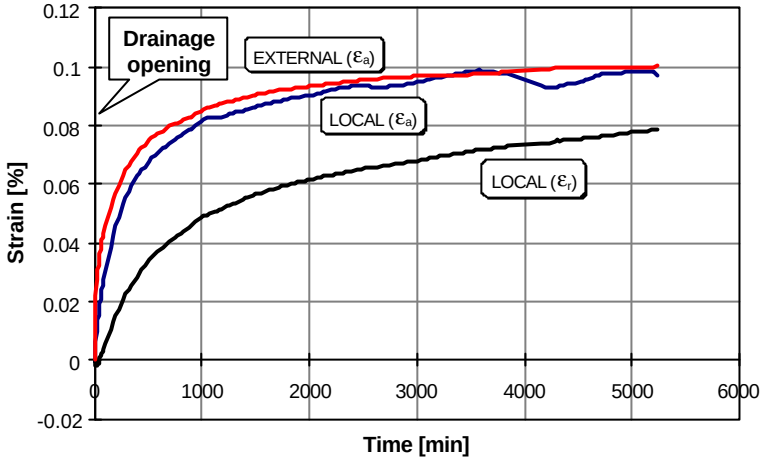

Figure 6.23 Axial and radial strain for test CNV7 after drainage opening.

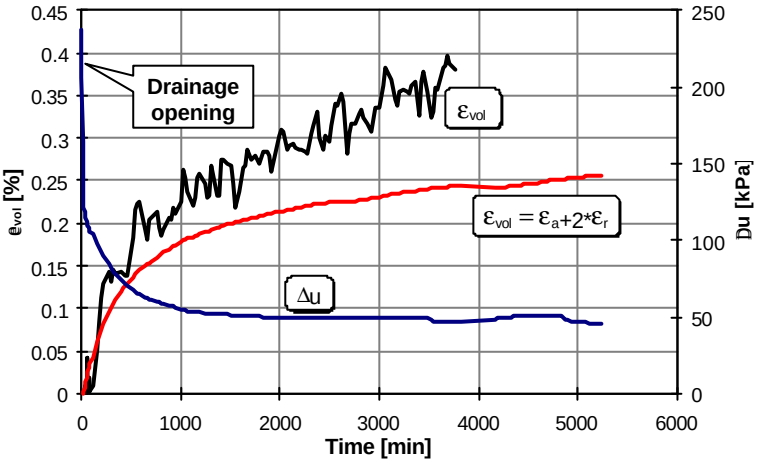

Figure 6.24 Volumetric deformation and pore pressure excess for test CNV7 after drainage opening.

The excess pore pressure developed for both tests CNV7 and CNV10 during the stress path phase resulted to be positive. As a consequence, during the drained phase, consolidation occurs with a volume decrease.

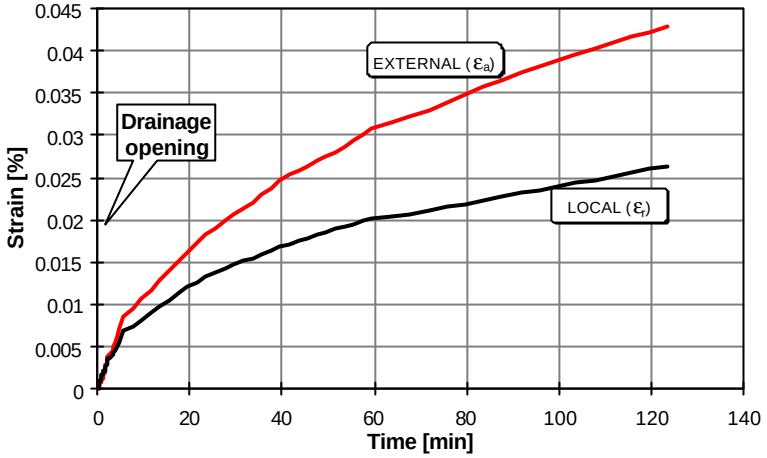

Figure 6.25 Axial and radial strains for test CNV10 after drainage opening.

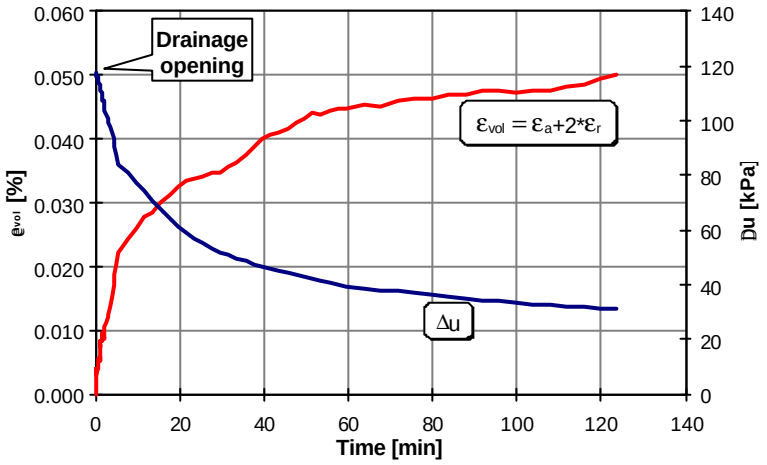

Figure 6.26 Volumetric deformation and pore pressure excess for test CNV10 after drainage opening.

The CNV7 specimen, which had the highest positive excess pore pressure at the end of the undrained phase (160 kPa), undergoes a greater volume decrease than that experienced by both the CNV10 and CNV8 tests. The latter one pertains to the sidewall simulation. Among the three, the CNV10 specimen has the smallest decrease in volume. In fact, the sample

CAEST3-1, from which the CNV10 specimen is taken, is shown to exhibit the most significant swelling behaviour, as evidenced during the flushing phase (Table 6.3).

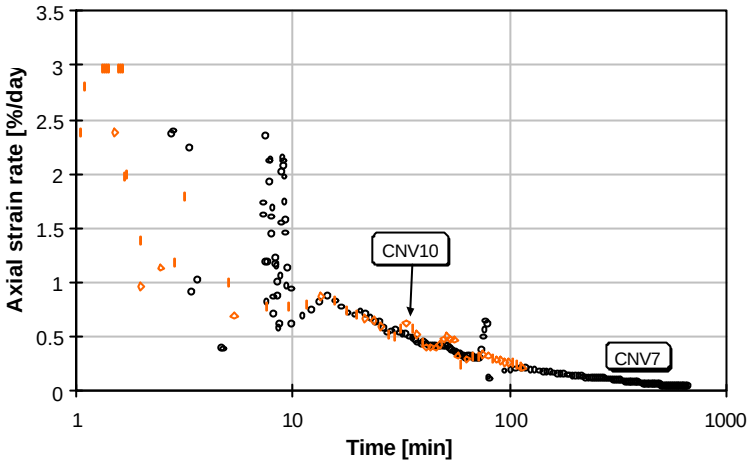

Figure 6.27 Strain rate for CNV7 and CNV10 tests.

6.6 Conclusions

The triaxial testing programme, developed with the main purpose to investigate the tunnel behaviour during excavation in swelling ground, has been described in the present chapter by taking an Italian stiff clay (Caneva clay) as representative material. On the basis of the work performed so far, the following main conclusions can be drawn.

- The testing procedures adopted are shown to be very effective in simulating the soil behaviour in the particular conditions and stress histories which are experienced by a ground element in the near vicinity of a circular tunnel.
- The specimens of Caneva clay tested up to failure (CNV1, CNV2, CNV5 and CNV9) give shear strength parameters in the same range as those obtained by conventional triaxial tests for the specimens taken from the CAEST4-2 sample, with the exception of the CNV5 test which is characterised by slightly higher strength parameters.
- From the results of the flushing phase, the Caneva clay is shown to exhibit a moderate to high swelling potential, as expected on the basis of its mineralogical composition.
- The Caneva clay specimens, isotropically consolidated to the in situ state of stress, exhibit a negative excess pore pressure during the undrained “compression” stress paths, typical of the tunnel sidewall response simulation. This behaviour is shown to hold true for both two dimensional (pure shear) and three dimensional conditions, when taking into account the influence of the advancing face.
- It is also shown that, when three dimensional conditions are simulated in the triaxial cell, a greater value of t is necessary to induce negative excess pore pressure in the specimen

since during the first portion of the stress path (i.e. when the tunnel face is approaching the cross section of interest) a positive excess pore pressure develops due to a stress increase.

- When the attention is taken to the tunnel crown/invert behaviour and the tests on the Caneva clay specimens are similarly carried out under "extension" conditions, following a pure shear stress path, a positive excess pore pressure is shown to develop during the undrained phase of the test.
- With the drained phase, which follows in each case a creep stage, swelling is shown to occur for specimens simulating the tunnel sidewall behaviour, as the negative excess pore pressure dissipates under the imposed constant state of stress. On the contrary, for specimens simulating the tunnel crown/invert response, as a consequence of development of positive excess pore pressure during the undrained phase, consolidation is shown to take place when the drainage valve is opened.

Chapter 7

Summary and conclusions

7.1 Summary

In the present thesis the following main tasks were undertaken.

- Stress analysis were carried out with the main objective to define the stress history around a circular tunnel during excavation and face advancement, as well represented in terms of stress paths for both the sidewalls and crown/invert zones.
- The results obtained, by using numerical simulations in both two dimensional and in three dimensional conditions, show a significantly different trend of behaviour for the above two zones in the near vicinity of the tunnel periphery.
- A new triaxial apparatus, specifically devoted to soft rocks and indurated soils, under any desired stress path conditions, was designed, constructed and calibrated. The software needed for automated testing and data acquisition was developed. Overall the triaxial apparatus was shown to perform very satisfactorily as desired.
- A stiff Italian clay (Caneva clay), taken as representative of a swelling indurated soil, was sampled in situ and laboratory tests were carried out on the specimens obtained. The main emphasis was placed on triaxial testing for a set of conditions (undrained, drained, time-dependent), as they occur during excavation in the vicinity of the tunnel face, according to predictions by numerical modelling. The interest was centered on the simulation of the stress paths at the sidewalls and crown/invert around the tunnel.

7.2 Conclusions

It is the purpose of the present chapter to draw some conclusions on the work performed so far. The following aspects will be considered:

- numerical simulation of typical stress paths for zones around a circular tunnel;
- development and calibration of a newly developed triaxial apparatus;
- laboratory simulation of the tunnel sidewalls and invert/crown behaviour;
- consequence of laboratory results on design analyses of tunnels in swelling ground.

7.2.1 Stress paths for zones around a circular tunnel

The numerical analyses were performed for a circular tunnel in an infinitely extended medium, in both two dimensional and three dimensional conditions, and for a set of assumptions for

the in situ state of stress and material behaviour. The results obtained show a significantly different response when the attention is paid to the influence of face advancement during excavation.
If two dimensional conditions are considered for a linearly elastic, continuous and isotropic medium, under the K_o stress ratio (horizontal to vertical in situ stress) equal to 1, the computed stress paths for points at the sidewalls and crown/invert, in the near vicinity of the tunnel contour, do not show any change in the mean normal stress. However, this is not the case, if three dimensional conditions are considered, when the influence of the tunnel face during excavation makes this stress to change significantly.
When the attention moves to the effects of the K_o ratio, and the $K_o = 2$ case is examined in detail, always in three dimensional conditions and under the assumptions above for the linearly elastic behaviour of the medium, the stress path response at the sidewalls differs quite significantly from that at the crown/invert of the tunnel. A global decrease in the mean normal stress is experienced in the first case, while an increase takes place for the crown/invert zones. The corresponding stress paths are shown to increase in complexity, with a decrease in the mean normal stress, whenever an elasto-plastic constitutive law is introduced for the medium, for both $K_o = 1$ and $K_o = 2$ conditions and for all the positions considered around the tunnel.
From the above considerations it becomes evident that the modified Huder-Amberg oedometer test, which is often used to characterise a swelling ground behaviour for the purpose of design analysis, is not representative of the real history undertaken by an element of ground surrounding a tunnel. It is therefore concluded that in order to simulate tunnel behaviour "at laboratory scale", it is imperative to undertake careful testing in triaxial conditions.

7.2.2 The new triaxial apparatus (SRTA)

One of the two triaxial apparatuses used in this thesis in order to perform triaxial testing was designed and constructed as part of the research work. The special features of the SRTA, as described in details in Chapter 4, were shown to be essential in order to perform appropriate triaxial tests in closely controlled conditions, whenever a special stress path need be followed during testing.
Most of the attention was posed, when developing the new triaxial apparatus, to a number of special features which make the equipment (presently available at the Rock Mechanics Laboratory of the Structural and Geotechnical Engineering Department of the Politecnico di Torino) innovative and well advanced in many aspects: need of local strain measurements, appropriateness of the sliding mechanism at the base pedestal, effective data acquisition and control system in the various stages of the test.
The calibration testing programme which was performed for the SRTA, also by means of performance tests and comparisons with results obtained by other laboratories (i.e. ISSMGE-TC29 Round Robin Test), confirmed the importance of using local strain versus global strain measurements, when assessing stiffness properties and creep deformations of soils. Also the effectiveness in the adoption of the sliding mechanism during testing was as well demonstrated.

7.2.3 Tunnel behaviour simulation "at laboratory scale"

The testing programme undertaken for the Caneva clay was intended to reproduce, "at laboratory scale", the behaviour of the ground in the surrounding of a circular tunnel. The typical stress paths for the sidewalls and for the invert/crown positions, computed by numerical analyses, were successfully reproduced in the triaxial apparatuses in both the undrained and the drained phase.

The results obtained from "compression" tests, with a stress history simulated which is typical for the sidewall behaviour of a tunnel, show the development of a negative excess pore pressure during the undrained stress path phase.

For the s = constant stress path simulated (i.e. in two dimensional conditions) under the stress ratio $K_o = 1$ (isotropic initial state of stress), the negative excess pore pressure starts to develop in the Caneva clay tested for a shear stress t greater than 200 kPa. However, a greater value of t is necessary in order to induce a negative excess pore pressure in the specimen, if the stress path implemented is chosen to account for the influence of the tunnel face (i.e. in three dimensional conditions).

The results of testing of the same soil, however in the "extension" conditions attained in the triaxial cell by keeping the mean normal stress s constant, showed a different trend of behaviour, with the development of positive excess pore pressure in the undrained phase. This would signify that during tunnel excavation a similar condition would occur at the crown/invert, which is not in agreement with the results of similar tests previously performed by Bellwald (1990) and Aristorenas (1992) on shales.

As a consequence of the excess pore pressure attained at the end of the shearing phase (negative, during the "compression" tests, and positive, during the "extension" tests), a swelling behaviour was experienced during the drained phase of the "compression" tests, in contrast with the corresponding consolidation behaviour shown however after the "extension" tests.

It is to be noted that a number of simplifications have been introduced during the present stage of the research work performed so far. These simplifying assumptions can be listed as follows.

- The stress paths implemented in the triaxial tests were computed by the numerical analyses under the assumption of a linearly elastic isotropic medium. The use of an elasto-plastic stress-strain law for the soil would however result into a substantially different trend of behaviour.
- No account is taken of the out of plane stress component, when describing the stress paths in the t-s plane. This is however considered in the three dimensional calculations carried out.
- The initial state of stress considered during testing was taken as isotropic ($K_o = 1$), even though the clay deposit under study gives a certain degree of over consolidation as described in Chapter 5.

7.2.4 Experimental evidences for design analyses of tunnels in swelling ground

The prediction of tunnel behaviour in a swelling ground is a difficult task. A number of important studies have been undertaken in recent years from the theoretical and experimental points of view, as summarised in Chapter 2. However, uncertainties remain and a fully satisfactory method for the design analysis of tunnels in swelling ground is not yet available. The present thesis was intended to provide some additional insights into the ground response in the near vicinity of the tunnel during face advancement, and for a set of conditions that occur in argillaceous soils and rocks. It is felt that the testing methods, including both the undrained and drained phases of the test, described in Chapter 6 and followed throughout the testing programme, are capable to reproduce effectively the real behaviour of the ground in the tunnel sourround, in particular if compared with the presently available oedometer tests.
If one pays attention to 2D stress distribution around a circular tunnel (**Figure 7.1**) in the linearly elastic case, as described in the previous pages, a practical implication of the results obtained for the Caneva clay is evident in terms of both the excess pore pressure, which is experienced during tunnel excavation, and the subsequent deformational response. From the complete set of tests performed in the "compression" conditions, i.e. at the sidewalls of a circular tunnel, a negative excess pore pressure is shown to develop for t greater than 200 kPa, whereas failure would be attained around the tunnel for t_{max} equal to 450 kPa.

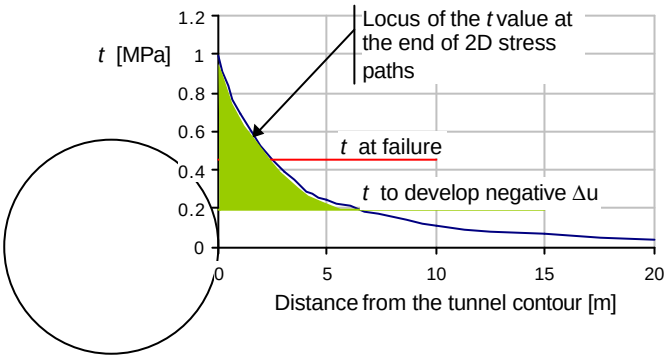

Figure 7.1 Maximum shear stress distribution around the tunnel.

One can therefore observe that a zone around the tunnel (as shown in Figure 7.1) extending at least more than its radius, would experience a negative excess pore pressure in undrained conditions, subsequently to be dissipated during a standstill or when the excavation is completed, thus resulting in swelling deformations. The amount of swelling strains can be assessed from the test at least "at laboratory scale".
An additional point of interest can be raised on the basis of the results of testing, when the 3D stress paths are considered. The extent of the swelling zone around the tunnel is expected to decrease due to face effects: the shear stress t needed to induce the negative excess pore

pressure is in fact significantly greater than that required in the corresponding 2D case. If one applies this concept further, then it would appear that any ground treatment ahead of the heading, made to inhibit instability from developing, would be beneficial by reducing the negative excess pore pressure in the zone behind.

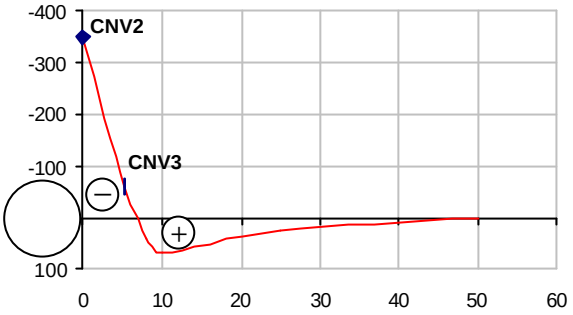

Figure 7.2 Negative pore pressure excess distribution around the tunnel.

Always keeping with the results of triaxial testing for the "compression" conditions, one would conclude that it is of great interest to conduct a series of tests, by following a similar stress path, to a different level of the *t* stress finally attained. As shown in **Figure 7.2**, a plot of the negative excess pore pressure can be drawn for points away from the tunnel contour, thus inferring a likely distribution of Δu in its surround (Bellwald 1990).

7.3 Recommendations for further developments

As already stated, further developments of the research work undertaken are needed, with the aim to be able to clarify the issues which could not be solved completely. This is to be done by keeping in mind the final objective, which is to provide the design engineer with better tools than presently available to deal with tunnelling in swelling ground. The following main aspects are to be considered.

- The different trend of behaviour shown with the "extension" tests on stiff clay with respect to the results of similar tests previously performed on clay-shales (Bellwald 1990, Aristorenas 1992) need be further investigated. It is important to understand if this behaviour is connected with the substantially different characteristics of the materials tested, or if other motivations need be invoked. This can be achieved by further testing, in particular by applying the 3D stress paths defined for the tunnel crown/invert. Also, it might be appropriate to test other argillaceous soils and rocks.
- The influence of the K_o stress ratio on the trends of behaviour evidenced so far need be investigated by performing triaxial tests of the same type carried out in both undrained and drained conditions. The stress paths to be considered are those computed in the

present thesis, which exhibit a different response in the near vicinity of the tunnel with respect to the corresponding isotropic case ($K_o = 1$).

- Additional triaxial tests are to be performed for different levels of the soil mobilised strength, in order to investigate the distribution of excess pore pressure in the tunnel surround. This is important with respect to the need, in argillaceous soils and rocks containing expansive minerals, to better understand the stability conditions of both the tunnel heading and of the zones behind, during and subsequent to excavation.
- With the main purpose to distinguish between mechanical and physico-chemical swelling during testing, it is proposed to stop the test during the shearing phase when the excess pore pressure attains a zero value. This would allow one to evaluate if any change in volume takes place, without any water adsorption determining it.
- Further attention need be paid in low permeability soils to the difficulty of measuring the excess pore pressure induced in the specimen as a direct result of the stress paths simulating tunnel response during excavation. From this point of view, additional insights into the soil behaviour are to be gained by using local measurements of excess pore pressure within the specimen.
- In order to clarify the practical implications of the results obtained on tunnel design methods (mainly with respect to tunnel stability, induced deformations, ground-support-stabilisation interaction, etc.), a behavioural model need be implemented which is capable to describe the response of a representative elementary volume as observed during triaxial testing. Then, the same model should be applied to a tunnel problem as observed in practice, in order to compare in a practical case, predictions and performance, for validation purposes.

References

ANAGNOSTOU, G. 1991. Untersuchungen zur Statik des Tunnelbaus in quellfähigem Gebirge. Dissertation No. 9553. ETH. Zurich, Switzerland.

ARISTORENAS, G. V. 1989. Rheological modelling of swelling rocks. Internal report, Massachusetts Institute of Technology. Boston, USA. Unpublished, included as Chap. 2 in Aristorenas 1992.

ARISTORENAS, G. V. 1992. Time-dependent behaviour of tunnels excavated in shale. PhD Thesis. Massachusetts Institute of Technology. Boston, USA.

BARLA, G., G. PAZZAGLI, U. RABAGLIATI 1986. The San Donato tunnel (Florence). *Proc. Int. Congress on Large Caverns*. Florence, Italy. Pp. 61-69.

BARLA, G., F. FORLATI, A. ZANINETTI 1990. Prove di laboratorio su rocce tenere: problematiche ed esempi. *Conferenze di Meccanica e Ingegneria delle Rocce, Mir '90*. pp 4.1-4.47. Politecnico di Torino. Torino, Italy.

BARLA, G. 1993. Metodi di analisi progettuale per gallerie in rocce rigonfianti e/o spingenti. *XVIII Convegno Nazionale di Geotecnica*. Rimini, Italy.

BARLA, G., G. ARDUINO, L. VAI 1997. Progetto di risistemazione del versante a monte della cava "Parè" di Cordignano (Tv) e delle cave "Piai" e "Dal Caneva (Pn). Relazione Tecnica No. 0086. Geodes S.r.l.

BARLA, G., M. BARBERO, M. CASTELLETTO 1999. Fenomeni di instabilità per scivolamento planare nella collina torinese. *Ital. Geotech. J.*: No. 2/99, pp. 5-25.

BARLA, M., G. BARLA, D.C.F. LO PRESTI, O. PALLARA, N. VANDENBUSSCHE 1999. Stiffness of soft rocks from laboratory tests. *Proceedings of the IS Torino '99, Second International Symposium on Pre-failure deformation characteristics of geomatrials*. Torino, Italy.

BARTON, N., R. LIEN, J. LUNDE 1974. Engineering classification of rock masses for the design of tunnel support. *Rock Mech.*, Vol. 6, pp. 189-236.

BARTON, N. 1976. Recent experiences with the Q-system of tunnel support design. *Proc. Symp. On Exploration for Rock Engineering*. Vol. 1, pp. 107-118. Balkema. Rotterdam, The Nederlands.

BELLWALD, P. 1987. Elasto plastic constitutive model. *Proc. of the 6th Int. Congress of the ISRM*. Montreal, Canada.

BELLWALD, P. 1990. A contribution to the design of tunnels in argillaceous rock. PhD Thesis. Massachusetts Institute of technology. Boston, USA.

BERNAUD, D., H. COLINA, G. ROUSSET 1993. Calculs de dimensionnement du soutenement du tunnel "Linea Alta Velocità" dans les argiles chaotiques. Techincal report, Groupement pour l'Etude des Structures Souterraines de Stockage. Palaiseau Cedex: Ecole Polytechnique.

BREKKE, T.L., T.R. HOWARD 1973. *Functional classification of gouge material from seams and faults in relation to stability*. 195 pp. Sponsored by ARPA, University of California, Berkley, California, USA.

BURLAND, J.B. 1989. Small is beautiful - The stiffness of soil at small strains. Ninth Laurits Bjerrum Memorial Lecture, *Canadian Geotechnical Journal*: Vol. 26, No 4, pp. 499-516.

CARTER, J.P., J.R. BROKER 1982. Elastic response around a deep circular tunnel. *Int. J. Solids Struct.*: Vol. 18, pp. 1059-1074.

CARTER, J.P. 1988. A semi-analytical solution for swelling around a borehole. *Int. J. Rock Mech. Min. Sci. & Geomech. Abstr.* Vol. 12, pp. 197-212.

CLAYTON, C.R.I., S.A. KHATRUSH 1986. A new device for measuring local axial strains on triaxial apparatus. *Géotechnique*: Vol. 36(4), pp. 593-597.

DETOURNAY E., A. H.-D. CHENG 1988. Poroelastic response of a borehole in a non hydrostatic stress field. *Int. J. Rock Mech. Min. Sci. & Geomech. Abstr.* Vol. 25, No. 3, pp. 171-182.

EINSTEIN, H. H., N. BISHOFF, E. HOFFMANN 1972. Behaviour of invert slabs in swelling shale. *Proc. Int. Symp. On Underground Openings.* Lucerne, Switzerland.

EINSTEIN, H. H. 1996. Tunnelling in difficult ground – Swelling behaviour and identification of swelling rocks. *Rock Mech. Rock Eng.* Vol. 28, No. 3, pp. 113-124.

FRANKLIN, J. A., C. LOUIS, P. MASURE 1974. Rock material classification. *Proc. 2nd Int. Congr. Eng. Geol. IAEG*. San Paolo, Brasil. Pp. 325-341.

FRÖHLICH, B. 1986. Anisotropes Quellverhalten diagenetisch verfestigter Tonsteine. Dr. Dissertation, Veröffentlichung des Inst. F. Boden und Felsmechnik der Univ. Friedericiana, Karlsruhe, Germany.

FUOCO, S., V. MAUGLIANI, M. TANZINI 1995. Deformability of a schistose rock mass from the interpretation of field and laboratory measurement data. *Proceedings of the FMGM (Field Measurement in GeoMechanics) '95 - 4th International Symposium.* Pp. 171-183. Bergamo, Italy.

GAUDIN, B., ET AL. 1981. Soutènement d'une galerie dans les Marnes du Cénomanien. *Proc. 10th Int. Conference on Soil Mechanics and Foundation Eng.* Vol. 1, pp. 293-296.

GOTO, S., F. TATSUOKA, S. SHIBUYA, Y.S. KIM, T. SATO 1991. A simple gauge for local small strain measurements in the laboratory. *Soils and Foundations*: Vol. 31, No 1, pp. 169-180.

GROB, H. 1972. Schwelldruck im Belchentunnel. Internationales Symposium für Untertagebau. Lucerna, Switzerland.

GYSEL, M. 1977. A contribution to the design of tunnel lining in swelling rock. *Rock mechanics*, Vol. 10, No 1-2, pp. 55-71. Errata, *Rock mechanics*, Vol. 11, No 3, pp. 132.

GYSEL, M. 1987. Design of tunnels in swelling rock. *Rock Mechanics and Rock Engineering*. Vol. 20, No. 4, pp. 219-242.

HAYANO, K., T. SATO, F. TATSUOKA 1997. Deformation characteristics of a sedimentary soft mudstone from triaxial compression tests using rectangular prism specimens. *Géotechnique*: Vol. 47, No. 3, pp. 439-449.

HEWLETT PACKARD, 1995. Getting started with HP VEE, Using HP VEE, HP VEE Advanced Programming Techniques. Ver. 3.12.

HUDER, J., G. AMBERG 1970. Quellung in Mergel, Opalinuston und anydrit. *Schweizerische Bauzeitung*. Vol. 88, No. 43, pp. 975-980.

ISRM 1983. Characterisation of Swelling Rock. Commission on Swelling Rock. Pergamon Press. Oxford, U.K.

ISRM 1989. Suggested methods for laboratory testing of argillaceous swelling rocks. Commission on Swelling Rock. Co-ordinator: H. Einstein. *Int. J. Rock Mech. Min. Sci. & Goemech. Abstr.* Vol. 26, No. 5, pp. 415-426.

ISRM 1994a. Comments and recommendations on design and analysis procedures for structures in argillaceous swelling rock. Commission on Swelling Rock. Co-ordinator: H. Einstein. *Int. J. Rock Mech. and Sci. & Geomech. Abstr.* Vol. 36, pp. 293-306.

ISRM 1994b. Suggested methods for rapid field identification of swelling and slaking rocks. Commission on Swelling Rock. Co-ordinator: H. Einstein. *Int. J. Rock Mech. and Min. Sci. & Geomech. Abstr.* Vol. 31, pp. 545-548.

ITASCA Inc., 1996. Flac2D Ver. 3.3. *User's Manual*. Minneapolis, USA.

ITASCA Inc., 1996. Flac3D Ver. 1.1. *User's Manual*. Minneapolis, USA.

JARDINE, R.J., M.J. SYMES, J.B. BURLAND 1984. The measurement of soil stiffness in the triaxial apparatus. *Géotechnique*: Vol. 34, pp 323-340.

KIEHL, J.R. 1990. Ein dreidimensionales Quellgesetz und seine Anwendung auf den Felshohlraumbau. *Proc. 9th Nat. Felsmechanik Symposium.* Aachen, Germany.

KOVARI, K. ET AL. 1981. Tunnelling with yielding support in swelling rock. *Proc. Int. Symp. on Weak Rock*. Tokyo, Japan. Pp. 1019-1029.

KOVARI, K., P. FRITZ. 1983. Rheo-staub users' manual. Version 30.04, 1983. Federal Institute of Technology. Zurich, Switzerland.

KOVARI, K., C. AMSTAD, G. ANAGNOSTOU 1987. Tunnelbau im quellfähigem Gebirge. Mitteilungen der schweizerischen Gesellschaft für Boden und Felsmechanik, Band 115, pp. 1019-1026.

LAMBE, T.W. 1967. The stress path method. JSMFD, ASCE, Nov., pp. 309-331.

LO, K.Y., R.S.C. WAI, J.H.L. PALMER, R.M. QUIGLEY 1978. Time dependent deformation of shaly rocks in southern Ontario. *Can. Geotech. J.* Vol. 15, pp. 537-547.

LO, K.Y., C.M.K. YUEN 1981. Design of tunnel lining in rock for long term time effects. *Can. Geotech. J.* Vol. 18, pp. 24-29.

LO PRESTI, D.C.F., O. PALLARA, D. COSTANZO, M. IMPAVIDO 1994. Small strain measurements during triaxial tests: many problems, some solutions. *Proc. IS Hokkaido*: Vol 1, pp. 11-16. Hokkaido, Japan.

LO PRESTI D.C.F., O. PALLARA, I. PUCI 1995. A modified commercial triaxial testing system for small strain measurements: preliminary results on Pisa Clay. *ASTM Geotechnical Testing Journal*: Vol. 18, N. 1, pp. 15-31. March 1995.

LO PRESTI D.C.F. 1997. Stress strain behaviour of clays in the laboratory. *Proc. 14th ICSMFE*. Hamburg, Germany. Vol. 4, pp. 2183-2186.

LO PRESTI D.C.F., G. BARLA, M. BARLA, A. GRIGORE, O. PALLARA, A. PLESCIA 1998. Development and use of a triaxial cell for soft rocks. *Proceedings of the 2nd International Symposium on Hard Soils Soft Rocks*. Napoli, Italy.

LO PRESTI D.C.F., O. PALLARA, A. CAVALLARO, M. JAMIOLKOWSKI 1999. Influence of reconsolidation techniques and strain rate on the stiffness of undisturbed clays from triaxial tests. *ASTM Geotechnical Testing Journal*, GTJODJ, Vol. 22, No. 3, September 1999, pp. 211-225.

LOMBARDI, G. 1974. Tunnel support. *Proc. 3rd Int. Congr. on Rock Mechanics*. Denver, USA. Vol. 1-B, pp. 1529-1541.

LOMBARDI, G. 1984. Underground openings in swelling rock. *Proc. 1st Nat. Conf. on Case Histories in Geotechnical Engineering*. Lahore, Pakistan.

MADSEN, F.T. 1999. Suggested methods for laboratory testing of swelling rocks. *Int. J. Rock Mech. Min. Sci. & Geomech.* Vol. 26, No. 3, pp. 211-225.

MAIR, R.J., R.N. TAYLOR 1997. Bored tunnelling in the urban environment. *Proc. 14th ICSMFE*. Hamburg, Germany. Pp. 2353-2385.

MATSUMOTO, M., K. HAYANO, T. SATO, J. KOSEKI, F. TATSUOKA 1999. Time effects on stress-strain properties at small strains of sedimentary soft mudstone. *Proceedings of the IS Torino '99, Second International Symposium on Pre-failure deformation characteristics of geomatrials*. Torino, Italy. Pp. 313-321.

NATIONAL INSTRUMENTS 1998. Lab View. User's manual.

NG, R.M.C., K.Y. LO 1985. The measurements of soil parameters relevant to tunnelling in clays. *Can. Geotech, J.* Vol. 22, pp. 375-391.

NGUYEN MINH, D., P. HABIB 1984. Time dependent behaviour of a pilot tunnel driven in hard marls. *Proc. Symp. on Design and Performance of Underground Excavations.* Paper 55.

PANET, M. 1979. Time dependent deformations in underground works. *Proc. 4th Int. Congress on Rock Mechanics.* Montreux. Vol. 3, pp. 279-290.

PECK, R.B. 1969. Deep excavation and tunnelling in soft ground. Proc. *7th ICSMFE*. State of the art Volume, pp. 225-290.

PREGL, O., M. FUCHS, H. MÜLLER, G. PETSCHL, G. RIEDMÜLLER, B. SCHWAIGHOFER 1980. Dreiaxiale Schwellversuche an Tongestein. *Geotechnik* 3, Heft 1.

PUCI, I. 1993. Modifica e miglioramento di una cella triassiale tipo GDS. M. Sc. Thesis. Department of Structural Engineering, Politecnico di Torino.

RENDULIC, L. 1935. Porenziffer und porenwasserdruck in tonen. *Der Bauingenieur*. Berlin, Germany. Vol. 17, No. 51/53, pp. 559-564.

ROCSCIENCE Inc., Univesity of Toronto 1998. Examine3D, *User's Manual.*

ROCSCIENCE Inc., Univesity of Toronto 1999. Phase2, *User's Manual.*

SAKURAI, S. 1977. Interpretation of field measurements in undersea tunnels with the aid of mathematical models. *Proc. Int. Symp. on Field Measurements in Rock Mechanics.* Zurich, Switzerland. Pp. 859-871.

SCHWEISIG, M., H. DUDDECK 1985. Beanspruchung des tunnelaus baus infolge Quellverhaltens von Tonsteingebirge. *Bericht*: No. 85-47, Institut für Statik, Technische Universität Braunschweig, 57 pp.

SINGH, A., J.K. MITCHELL 1968. General stress-strain-time function for soils. *ASCE, J. Of the Soil Mechanics and Foundation Eng. Division.* Vol. 194, SM1.

SIMPSON, B., N.J. O'RIORDAN, D.D. CROFT 1979. A computer model for the analysis of ground movements in London clay. *Geotechnique*: Vol. 29, pp. 149-175.

SEMPLE, R.M., A.J. HENDRON, G. MESRI 1973. The effect of time dependent properties of altered rock on tunnel support requirements. Report No. FRAORDD-74-30. University of Illinois at Urbana Champaign.

STEINER, W. 1980. Empirical methods in rock tunnelling – Review and recommendations. Ph.D. Thesis, Massachusetts Institute of Technology, 553 pp.

STEINER, W. 1992. Swelling rocks in tunnels: characterisation and effect of horizontal stresses. *Eurock '92*. pp. 163-168. Thomas Telford. London, U.K.

STEINER, W. 1993. Swelling rock in tunnels: rock characterisation, effect of horizontal stresse and construction procedures. *Int. J. Rock Mech. Min. Sci*. Vol. 30, No. 4, pp. 361-380.

SYMES, M.J., J.B. BURLAND 1984. Determination of local displacements on soil samples. *Geotechnical Testing Journal*. Vol. 7, No. 2, pp 49-59.

SUN JUN ET AL. 1986. The coupled creep effect of pressure tunnels interacting with its water osmotic swelling viscous elasto-plastic surrounding rocks. *Proc*. Peking, China.

SULEM, J. 1983. Comportement différé des galeries profondes. Thèse de Docteur Ingénieur en Génie Civil. Ecole Nationale des Ponts et Chaussées. Paris, France.

SULEM, J., M. PANET, A. GUENOT 1987a. Closure analysis in deep tunnels. *Int. J. Rock Mech. Min. Sci. & Goemech. Abstr.* Vol. 24, No. 3, pp. 145-154.

SULEM, J., M. PANET, A. GUENOT 1987b. An analytical solution for time dependent displacements in a circular tunnel. *Int. J. Rock Mech. in. Sci. & Goemech. Abstr.* Vol. 24, No. 3, pp. 155-164.

TATSUOKA, F. 1988 Some recent developments in triaxial testing systems for cohesionless soils. *Advanced Triaxial Testing of Soil and Rock, ASTM STP 977*: 7-67.

TATSUOKA, F., S. SHIBUYA 1992. Deformation characteristics of soil and rocks from field and laboratory tests. *Keynote Lecture, IX Asian Conference on SMFE, Bangkok, 1991*: Vol. 2, 101-190.

TATSUOKA, F., Y. KOHATA, K. OCHI, T. TSUBOUCHI 1995a. Stiffness of soft rocks in Tokyo metropolitan area from laboratory tests to full-scale behaviour. *International Workshop on Rock Foundation of Large Scaled Structures, Tokyo 30th Sept. 1995*.

TATSUOKA, F., D.C.F. LO PRESTI, Y. KOHATA 1995b. Deformation characteristics of soils and soft rocks under monotonic and cyclic loads and their relations. *3rd International Conference on Recent Advances in Geotechnical Earthquake Engineering and Soil Dynamic*: State of the Art 1, 2, pp. 851-879.

TATSUOKA, F., Y. KOHATA 1995. Stiffness of hard soils and soft rocks in engineering applications. *Keynote Lecture 8, IS Hokkaido 1994*: Vol. 2, 947-1066. Balkema.

TATSUOKA, F., R. JARDINE, D.C.F. LO PRESTI, H. DI BENEDETTO, T. KODAKA 1997. Testing and characterising per failure deformation properties of geomaterials. *14th ICSMFE*. Hamburg, Germany. Vol. 4, pp. 2129-2164.

TERZAGHI, K. 1923. Die berechnung der durchlässigkeitsziffer des tones aus dem verlauf der hydrodynamischen spannungserscheinungen. *Sitzungsberichte*, Akademie der Wissenschaften in Wien, Austria. Vol. 132, No. 3/4, pp. 125-138.

TERZAGHI, K. 1925. Erdbaumechanik auf bodenphysikalischer grundlage. Deuticke, Vienna, Austria.

TERZAGHI, K., R.V. PROCTOR, T.L. WHITE 1946. Rock tunnelling with steel supports. Commercial shearing and stamping company. Youngstown, Ohio, USA.

WITTKE, W., P. RISSLER 1976. Dimensioning of the lining of underground openings in swelling rock applying the finite element method. *Pubblications of the Institute for Foundation Engineering, Soil Mechanics, Rock mechanics and Water Ways Construction*. RWTH (University) Aachen. Vol. 2, pp. 7-48.

Appendix A

Triaxial tests' data

A.1 Contents

The present Appendix is to collect the data of the experimental programme carried out in this thesis and described in Chapter 6. For each test, a table is given by reporting the sample basic data and the phases of testing. Also given are complete data sets obtained and relevant for the stress-path phase and the swelling/consolidation. Data are organised in tables where the deviator stress (q), the water overpressure (Δu), the local ($\varepsilon_{a,l}$) and external ($\varepsilon_{a,e}$) axial strain and the local radial strain ($\varepsilon_{r,l}$) measurements are listed.
In **Table A.1** a complete list of the swelling triaxial tests performed is also reported.

Table A.1 Triaxial tests performed.

Name	Borehole	Depth	Type of test[1]
CNV1	CAEST4-3	37.51	CIU - CL (s' = constant)
CNV2	CAEST4-3	37.28	CIU – CL(2D)
CNV3	CAEST4-3	37.06	CIU – CL(2D)+D
CNV4	CAEST4-3	36.91	CID – CL(2D)
CNV5	CAEST4-5	51.19	CIU – CL
CNV6	CAEST4-5	51.35	CIU – EU(2D)
CNV7	CAEST4-5	51.49	CIU – EU(2D)+D
CNV8	CAEST4-3	36.90	CIU – CL(3D)+D
CNV9	CAEST3-1	45.17	CIU – CL(3D)
CNV10	CAEST3-1	44.87	CIU – EU(2D)+D

[1] The type of test is indicated as follows:
CIU indicates Isotropic Consolidation and Undrained conditions during the stress path while CID indicates Isotropic Consolidation but Drained conditions during stress path. Stress path is described as Compression Loading (CL) or Extension Unloading (EU). 2D indicates that stress path pertaining to two dimensional conditions (i.e. s = constant stress path) are applied, while 3D refers to three dimensional stress path (as explained in Chapter 3 and 6). CNV1 test was conducted at s' = constant. For those tests were drained swelling/consolidation phase have been simulated after completing stress path, the symbol +D is used.

Test CNV1

Borehole:	CAEST4-3
Depth of the sample [m]:	37.51
Type of test:	CIU – Stress path at s' = constant
Triaxial Apparatus:	GDS

LL:	39	Initial height [mm]:	140.30	Total unit weight [kN/m^3]:	21.7
LP:	21	Initial diameter [mm]:	69.60	Dry unit weight [kN/m^3]:	19.0
IC:	1.36	Initial volume [mm^3]:	533784.59	e_o:	0.47
G_s:	2.839	Total weight [g]:	1181.0	W_n [%]:	14.5
$CaCO_3$ [%]:	22.3	Dry weight [g]:	1031.5		

Phase of the test:	FLUSHING	Final height [mm]:	140.31
		Final diameter [mm]:	69.61
		Final volume [mm^3]:	533972.04
		Final total weight [g]:	21.7
		e (end of flushing):	0.47
		σ_v (end of flushing) [kPa]:	36.5
		σ_h (end of flushing) [kPa]:	36.6
Phase of the test:	SATURATION	Final height [mm]:	140.38
		Final diameter [mm]:	69.89
		Final volume [mm^3]:	538486.32
		Final total weight [g]:	21.52
		e (end of saturation):	0.48
		Skempton's B parameter:	0.94
Phase of the test:	CONSOLIDATION	Final height [mm]:	140.38
		Final diameter [mm]:	69.89
		Final volume [mm^3]:	538495.58
		Final total weight [g]:	21.51
		e (end of consolidation):	0.48
		σ'_v (end of cons.) [kPa]:	718
		σ'_h (end of cons.) [kPa]:	718
		u_o [kPa]:	243
Phase of the test:	SHEARING	t_{max} (at peak) [kPa]:	278
		s'_{max} (at peak) [kPa]:	602
		Δu (at peak) [kPa]:	-286

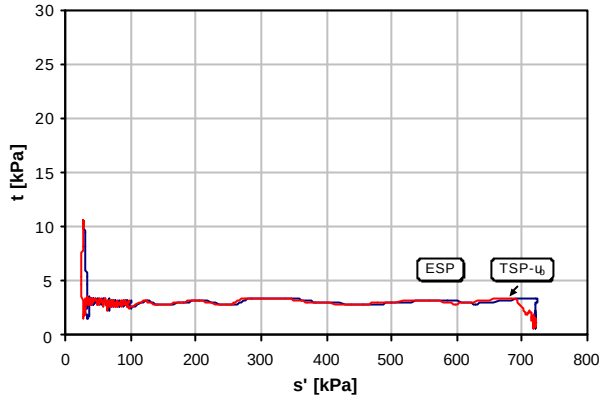

Figure A.1 Stress path during consolidation for CNV1 test.

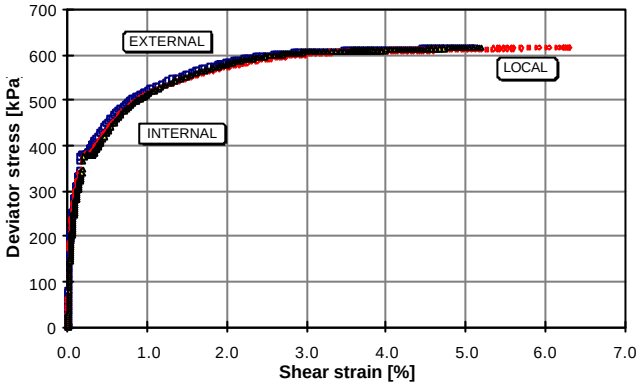

Figure A.2 Deviator stress versus shear strain for CNV1 test.

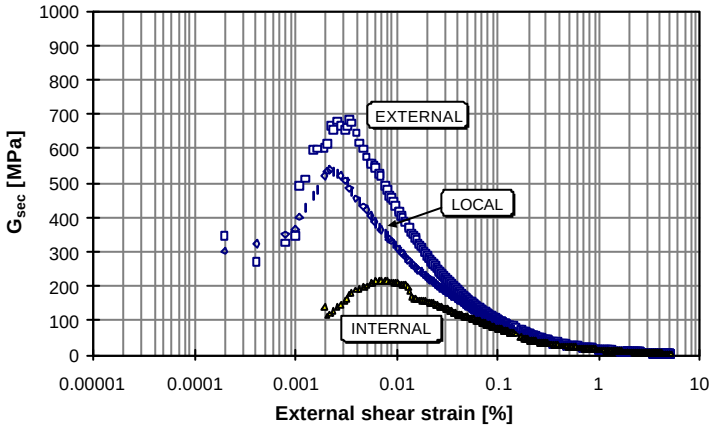

Figure A.3 Shear modulus versus external shear strain for CNV1 test.

Table A.2 Data for the shearing phase for test CNV1.

q [kPa]	Δu [kPa]	$\varepsilon_{a,l}$ [%]	$\varepsilon_{a,e}$ [%]	$\varepsilon_{r,l}$ [%]
2.25	0.00	0.00000	0.00000	0.00000
5.61	0.02	0.00042	0.00052	-0.00010
20.24	-0.61	0.00222	0.00182	0.00006
39.86	-3.28	0.00425	0.00380	0.00073
58.74	-6.92	0.00688	0.00569	0.00147
76.35	-10.86	0.00998	0.00765	0.00197
92.22	-14.86	0.01312	0.01021	0.00225
106.82	-19.08	0.01652	0.01222	0.00247
120.54	-23.32	0.01994	0.01514	0.00239
132.26	-27.29	0.02341	0.01782	0.00226
143.51	-31.27	0.02703	0.02040	0.00212
154.01	-34.96	0.03071	0.02353	0.00172
164.11	-38.37	0.03444	0.02673	0.00136
172.94	-41.82	0.03837	0.03040	0.00117
180.75	-44.93	0.04192	0.03387	0.00090
188.55	-47.99	0.04561	0.03672	0.00087
194.16	-50.73	0.04881	0.03964	0.00028
200.49	-52.77	0.05175	0.04257	-0.00026
207.16	-54.94	0.05493	0.04581	-0.00062
213.22	-57.10	0.05824	0.04867	-0.00100
218.25	-59.10	0.06149	0.05181	-0.00142
223.49	-61.06	0.06459	0.05497	-0.00185
228.47	-63.00	0.06785	0.05816	-0.00226
233.45	-64.93	0.07126	0.06129	-0.00278
239.48	-67.33	0.07576	0.06544	-0.00334
244.36	-69.29	0.07979	0.06889	-0.00399
249.09	-71.10	0.08369	0.07239	-0.00472
253.70	-73.06	0.08790	0.07618	-0.00531
257.87	-74.87	0.09172	0.07967	-0.00603
262.22	-76.67	0.09589	0.08335	-0.00684
266.38	-78.46	0.09981	0.08683	-0.00760
270.07	-80.16	0.10384	0.09031	-0.00835
274.31	-81.97	0.10802	0.09406	-0.00933
278.52	-83.65	0.11205	0.09748	-0.01030
282.17	-85.33	0.11612	0.10141	-0.01148
285.56	-86.97	0.12006	0.10481	-0.01244
289.00	-88.47	0.12384	0.10824	-0.01353
292.71	-90.02	0.12775	0.11147	-0.01446
295.79	-91.51	0.13162	0.11511	-0.01556
298.91	-92.96	0.13526	0.11877	-0.01668
301.98	-94.39	0.13902	0.12186	-0.01786
305.16	-95.81	0.14292	0.12522	-0.01892
308.25	-97.20	0.14674	0.12852	-0.02021
311.48	-98.62	0.15057	0.13201	-0.02134
314.47	-99.99	0.15443	0.13526	-0.02251
317.56	-101.33	0.15829	0.13863	-0.02397
320.60	-102.66	0.16202	0.14143	-0.02543
323.53	-103.96	0.16580	0.14488	-0.02707
325.91	-105.10	0.16949	0.14955	-0.02887
329.13	-106.38	0.17340	0.15294	-0.03051
334.13	-108.53	0.17985	0.15851	-0.03370
340.00	-111.99	0.19063	0.16799	-0.03952
377.01	-175.30	0.28995	0.20224	-0.07714

377.40	-185.45	0.29810	0.20714	-0.08532
378.02	-197.97	0.30962	0.21693	-0.09783
379.23	-202.27	0.31460	0.22134	-0.10312
380.22	-205.75	0.31938	0.22552	-0.10782
381.25	-208.74	0.32388	0.22964	-0.11233
382.57	-211.33	0.32839	0.23361	-0.11665
384.29	-213.61	0.33265	0.23763	-0.12082
386.41	-216.85	0.33983	0.24434	-0.12732
392.35	-221.59	0.35342	0.25585	-0.13881
395.50	-225.32	0.36621	0.26755	-0.14916
399.67	-228.35	0.37810	0.27758	-0.15905
404.12	-230.98	0.38968	0.28804	-0.16912
407.45	-233.20	0.40074	0.29793	-0.17860
412.19	-235.44	0.41376	0.30964	-0.18967
427.76	-241.96	0.46289	0.35521	-0.23072
443.01	-247.83	0.51799	0.40462	-0.27412
457.75	-252.25	0.57659	0.45693	-0.31730
471.08	-256.20	0.63438	0.51201	-0.36215
482.56	-259.48	0.69324	0.56679	-0.40740
491.45	-261.87	0.74900	0.61750	-0.44942
498.92	-263.85	0.80556	0.66748	-0.49172
505.65	-265.53	0.86141	0.71607	-0.53329
512.37	-267.07	0.91833	0.76480	-0.57490
518.80	-268.48	0.97709	0.81488	-0.61735
528.87	-269.99	1.09066	0.90985	-0.69578
539.83	-271.87	1.23158	1.02454	-0.78870
549.03	-273.87	1.37762	1.14085	-0.87894
557.52	-275.64	1.53004	1.25585	-0.96868
565.67	-277.30	1.68852	1.37305	-1.05748
573.07	-278.98	1.88457	1.51143	-1.16000
579.08	-279.77	2.01553	1.61353	-1.22967
580.85	-279.96	2.03927	1.63160	-1.24258
583.50	-280.47	2.12640	1.69877	-1.29141
587.74	-281.43	2.25426	1.79637	-1.36305
591.11	-282.04	2.38077	1.89313	-1.43279
594.06	-282.78	2.50678	1.98913	-1.50191
596.84	-283.28	2.63530	2.08607	-1.57392
599.57	-283.74	2.76087	2.18170	-1.64900
601.70	-284.41	2.89351	2.27962	-1.71995
603.31	-284.82	3.02709	2.37676	-1.79071
605.05	-285.16	3.16172	2.47337	-1.86176
606.09	-285.54	3.29556	2.57028	-1.93243
607.78	-286.12	3.56138	2.76152	-2.07357
608.08	-286.32	3.69599	2.85717	-2.14480
608.96	-286.71	3.96390	3.04643	-2.28680
609.40	-286.98	4.24205	3.23889	-2.43250
609.60	-287.03	4.38381	3.33461	-2.50514
610.53	-287.09	4.53152	3.43170	-2.57859
610.87	-287.15	4.68345	3.52712	-2.65102
611.43	-287.16	4.84317	3.62318	-2.72357
612.42	-287.19	5.01504	3.72073	-2.79653
613.12	-287.18	5.20034	3.81766	-2.86855
614.14	-287.15	5.64364	4.01033	-3.01207
615.04	-287.11	5.93982	4.10856	-3.08523
615.69	-287.09	6.18123	4.20631	-3.15832
616.55	-287.02	6.17861	4.30660	-3.23279

Test CNV2

Borehole:	CAEST4-3
Depth of the sample [m]:	37.28
Type of test:	CIU – CL(2D) - Sheared with s = const. stress paths
Triaxial Apparatus:	GDS

LL:	39	Initial height [mm]:	140.50	Total unit weight [kN/m^3]:	22.22
LP:	21	Initial diameter [mm]:	69.80	Dry unit weight [kN/m^3]:	19.61
IC:	1.42	Initial volume [mm^3]:	537622.02	e_o:	0.42
G_s:	2.839	Total weight [g]:	1218.0	W_n [%]:	13.36
$CaCO_3$ [%]:	22.3	Dry weight [g]:	1074.5		

Phase of the test:	FLUSHING	Final height [mm]:	140.56
		Final diameter [mm]:	69.80
		Final volume [mm^3]:	537867.12
		Final Total weight [g]:	22.21
		e (end of flushing):	0.42
		σ_v (end of flushing) [kPa]:	110.4
		σ_h (end of flushing) [kPa]:	151.2
Phase of the test:	SATURATION	Final height [mm]:	140.41
		Final diameter [mm]:	95.85
		Final volume [mm^3]:	538082.09
		Final Total weight [g]:	22.21
		e (end of saturation):	0.42
		Skempton's B parameter:	> 0.87
Phase of the test:	CONSOLIDATION	Final height [mm]:	138.95
		Final diameter [mm]:	69.49
		Final volume [mm^3]:	527035.08
		Final Total weight [g]:	22.67
		e (end of consolidation):	0.39
		σ'_v (end of cons.) [kPa]:	656
		σ'_h (end of cons.) [kPa]:	656
		u_o [kPa]:	351
Phase of the test:	SHEARING	t_{max} (at peak) [kPa]:	452
		s'_{max} (at peak) [kPa]:	998
		Δu (at peak) [kPa]:	-349

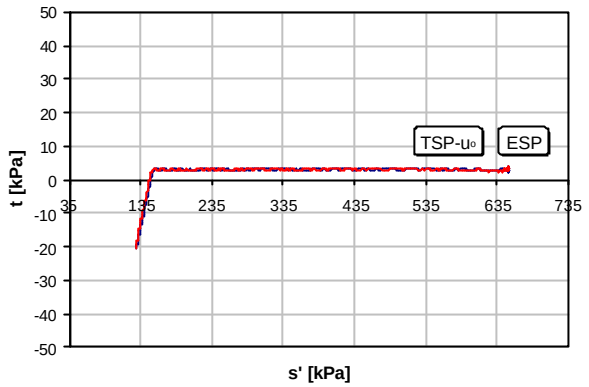

Figure A.4 Stress path during consolidation for CNV2 test.

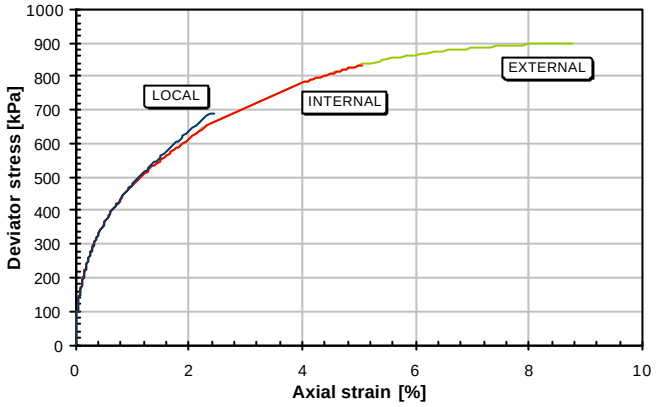

Figure A.5 Deviator stress versus axial strain for CNV2 test.

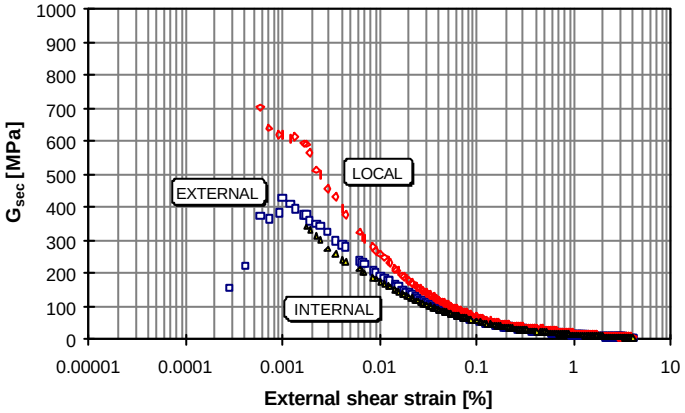

Figure A.6 Shear modulus versus external shear strain for CNV2 test.

Table A.3 Data for the shearing phase for test CNV2.

q [kPa]	Δu [kPa]	$\varepsilon_{a,l}$ [%]	$\varepsilon_{a,e}$ [%]	$\varepsilon_{r,l}$ [%]
7,89	0,00	0,00000	0,00000	0,00000
15,09	-0,44	0,00074	0,00120	0,00017
23,62	-1,16	0,00146	0,00217	0,00018
30,60	-1,72	0,00218	0,00325	-0,00002
36,79	-2,27	0,00300	0,00433	-0,00018
42,30	-2,84	0,00378	0,00551	-0,00053
46,79	-3,14	0,00455	0,00644	-0,00083
51,47	-3,49	0,00539	0,00786	-0,00133
55,71	-3,75	0,00620	0,00877	-0,00174
59,59	-3,93	0,00696	0,01000	-0,00212
63,20	-4,05	0,00776	0,01139	-0,00262
67,21	-4,26	0,00864	0,01249	-0,00301
70,51	-4,30	0,00941	0,01354	-0,00347
74,49	-4,55	0,01031	0,01480	-0,00402
78,01	-4,77	0,01134	0,01613	-0,00457
81,08	-4,89	0,01220	0,01722	-0,00521
83,64	-4,94	0,01297	0,01821	-0,00582
88,78	-4,95	0,01479	0,02069	-0,00698
91,60	-5,01	0,01589	0,02196	-0,00758
96,38	-5,12	0,01780	0,02450	-0,00873
100,96	-5,01	0,01964	0,02714	-0,00997
103,03	-5,03	0,02054	0,02836	-0,01050
109,22	-4,97	0,02323	0,03209	-0,01212
115,07	-4,73	0,02617	0,03586	-0,01396
116,97	-4,64	0,02721	0,03725	-0,01471
122,80	-4,46	0,03034	0,04107	-0,01674
124,74	-4,43	0,03143	0,04240	-0,01749
128,38	-4,35	0,03347	0,04508	-0,01870
130,21	-4,34	0,03457	0,04636	-0,01939
133,62	-4,16	0,03675	0,04908	-0,02075
135,23	-4,15	0,03786	0,05049	-0,02144
138,14	-3,93	0,03994	0,05307	-0,02284
139,75	-3,84	0,04096	0,05461	-0,02361
142,78	-3,59	0,04313	0,05739	-0,02495
144,21	-3,45	0,04432	0,05880	-0,02569
149,32	-3,24	0,04775	0,06308	-0,02786
150,69	-3,13	0,04880	0,06449	-0,02855
154,80	-2,88	0,05196	0,06848	-0,03071
156,19	-2,86	0,05311	0,06986	-0,03153
161,44	-2,29	0,05784	0,07541	-0,03458
162,75	-2,16	0,05887	0,07679	-0,03529
166,58	-1,91	0,06219	0,08087	-0,03732
168,02	-1,81	0,06332	0,08258	-0,03814
171,95	-1,62	0,06685	0,08699	-0,04038
175,62	-1,28	0,07064	0,09129	-0,04275
187,64	-0,35	0,08236	0,10588	-0,05063
193,76	1,11	0,09439	0,12068	-0,05856
204,27	2,07	0,10639	0,13538	-0,06667
209,05	2,54	0,11257	0,14281	-0,07075
218,03	3,46	0,12462	0,15709	-0,07866
226,95	4,22	0,13674	0,17153	-0,08648
235,92	4,72	0,14868	0,18622	-0,09445
240,05	4,99	0,15515	0,19370	-0,09846

247,93	5,47	0,16769	0,20803	-0,10646
251,60	5,71	0,17372	0,21538	-0,11032
259,28	6,16	0,18690	0,22978	-0,12040
266,58	6,42	0,19658	0,24464	-0,12874
277,00	6,77	0,20466	0,26695	-0,14065
283,59	6,93	0,21097	0,28138	-0,14858
290,25	7,03	0,21765	0,29601	-0,15658
296,77	7,00	0,22474	0,31100	-0,16455
306,27	6,92	0,23395	0,33337	-0,17712
311,77	6,93	0,23851	0,34799	-0,18510
323,00	6,63	0,24830	0,37763	-0,20132
327,92	6,55	0,24940	0,39244	-0,20963
346,89	5,81	0,28525	0,45043	-0,24270
353,89	5,28	0,30203	0,47237	-0,25573
367,24	4,05	0,33542	0,51568	-0,28136
373,79	3,30	0,35229	0,53759	-0,29471
386,71	1,52	0,38526	0,58277	-0,32240
392,59	0,72	0,40170	0,60532	-0,33636
404,65	-1,23	0,43485	0,65114	-0,36504
410,01	-2,15	0,45134	0,67397	-0,37949
420,76	-4,13	0,48405	0,71855	-0,40846
425,72	-5,16	0,50015	0,74044	-0,42296
435,77	-7,30	0,53245	0,78431	-0,45234
440,39	-8,37	0,54834	0,80608	-0,46708
450,98	-10,90	0,58308	0,85340	-0,49937
458,13	-12,79	0,60891	0,88841	-0,52367
472,91	-16,73	0,66343	0,96205	-0,57599
480,23	-18,87	0,69131	0,99941	-0,60273
495,84	-23,65	0,75526	1,08310	-0,66446
505,27	-26,67	0,79558	1,13560	-0,70370
522,93	-32,73	0,87687	1,23967	-0,78296
531,37	-35,71	0,91838	1,29089	-0,82295
548,13	-41,88	0,99974	1,39287	-0,90296
556,77	-45,24	1,02784	1,44540	-0,94411
572,36	-51,70	1,08492	1,54936	-1,02828
580,46	-54,96	1,11766	1,60025	-1,06987
595,97	-61,58	1,18362	1,70234	-1,15356
603,89	-64,97	1,22301	1,75360	-1,19569
618,62	-71,79	1,30149	1,85613	-1,28074
625,67	-74,99	1,33936	1,90585	-1,32244
640,93	-82,07	1,41615	2,00825	-1,40774
647,95	-85,51	1,45447	2,05968	-1,45082
662,15	-92,47	1,53024	2,16136	-1,53658
669,15	-95,98	1,56820	2,21231	-1,57947
682,96	-103,01	1,64397	2,31537	-1,66608
689,47	-106,44	1,68131	2,36669	-1,70893
697,08	-114,29	1,90729	2,66837	-1,96303
697,68	-115,26	1,94658	2,71805	-2,00525
698,89	-117,46	2,02825	2,81765	-2,09109
699,50	-118,61	2,07017	2,86731	-2,13423
701,32	-122,05	2,19895	3,01426	-2,26215
701,94	-123,31	2,24446	3,06313	-2,30544
703,85	-127,08	2,39185	3,21175	-2,43911
704,49	-128,41	2,44380	3,26038	-2,48350
706,44	-132,37	2,61477	3,40743	-2,61959
707,11	-133,79	2,67872	3,45674	-2,66615

728,55	-136,49	-	3,55371	-
728,55	-139,22	-	3,65099	-
728,55	-142,08	-	3,74932	-
728,55	-144,87	-	3,84728	-
758,86	-152,92	-	3,95014	-
863,60	-186,65	-	4,01148	-
882,60	-206,02	-	4,11403	-
886,98	-210,00	-	4,16534	-
893,89	-216,76	-	4,26777	-
898,01	-219,74	-	4,31803	-
905,16	-225,56	-	4,42231	-
908,77	-228,38	-	4,47334	-
915,44	-233,72	-	4,57474	-
918,72	-236,33	-	4,62642	-
926,21	-241,51	-	4,73132	-
929,46	-244,00	-	4,78402	-
935,11	-248,76	-	4,88697	-
938,69	-251,60	-	4,94959	-
949,82	-260,36	-	5,14801	-
955,71	-264,58	-	5,25025	-
965,72	-272,50	-	5,45461	-
970,39	-276,28	-	5,55547	-
979,05	-283,58	-	5,75647	-
983,29	-287,03	-	5,85721	-
991,57	-293,57	-	6,05562	-
995,46	-296,73	-	6,15416	-
1002,49	-302,63	-	6,35319	-
1005,73	-305,46	-	6,45463	-
1011,36	-310,77	-	6,66057	-
1013,98	-313,30	-	6,76217	-
1020,22	-318,11	-	6,96269	-
1023,42	-320,55	-	7,06409	-
1029,00	-325,13	-	7,26544	-
1031,77	-327,31	-	7,36618	-
1036,49	-331,42	-	7,57007	-
1038,56	-333,38	-	7,66932	-
1043,06	-337,09	-	7,87085	-
1045,14	-338,86	-	7,97273	-
1047,72	-340,47	-	8,07509	-
1049,43	-341,31	-	8,17655	-
1051,34	-341,65	-	8,25425	-
1051,95	-343,15	-	8,37789	-
1055,28	-344,59	-	8,48265	-
1057,13	-345,99	-	8,58728	-
1056,44	-346,94	-	8,69247	-
1061,65	-348,19	-	8,79711	-

Test CNV3

Borehole:	CAEST4-3
Depth of the sample [m]:	37.06
Type of test:	CIU – CL(2D) – s = constant stress paths with drained phase
Triaxial Apparatus:	GDS

LL:	39	Initial height [mm]:	142.2	Total unit weight [kN/m^3]:	21.88
LP:	21	Initial diameter [mm]:	69.2	Dry unit weight [kN/m^3]:	19.63
IC:	1.53	Initial volume [mm^3]:	534812.6	e_o:	0.42
G_s:	2.839	Total weight [g]:	1192.80	W_n [%]:	11.47
$CaCO_3$ [%]:	22.3	Dry weight [g]:	1070.10		

Phase of the test:	FLUSHING	Final height [mm]:	142.20
		Final diameter [mm]:	69.19
		Final volume [mm^3]:	534719.9
		Final Total weight [g]:	21.88
		e (end of flushing):	0.42
		σ_v (end of flushing) [kPa]:	107.71
		σ_h (end of flushing) [kPa]:	206.13
Phase of the test:	SATURATION	Final height [mm]:	142.01
		Final diameter [mm]:	69.21
		Final volume [mm^3]:	534266.2
		Final Total weight [g]:	21.90
		e (end of saturation):	0.42
		Skempton's B parameter:	0.90
Phase of the test:	CONSOLIDATION	Final height [mm]:	140.48
		Final diameter [mm]:	68.79
		Final volume [mm^3]:	522095.9
		Final Total weight [g]:	22.41
		e (end of consolidation):	0.39
		σ'_v (end of cons.) [kPa]:	661
		σ'_h (end of cons.) [kPa]:	661
		u_o [kPa]:	317
Phase of the test:	SHEARING	Final height [mm]:	132.24
		Final diameter [mm]:	72.14
		Final volume [mm^3]:	540462.4
		Final Total weight [g]:	21.65
		e (end of stress path):	0.43
		t_{max} (end of stress path) [kPa]:	215
		s'_{max} (end of stress path) [kPa]:	698
		Δu (end of stress path) [kPa]:	-60

Phase of the test:	DRAINED	Final height [mm]:	130.87
		Final diameter [mm]:	72.88
		Final volume [mm^3]:	545874.9
		Final Total weight [g]:	21.44
		e (end of saturation):	0.45

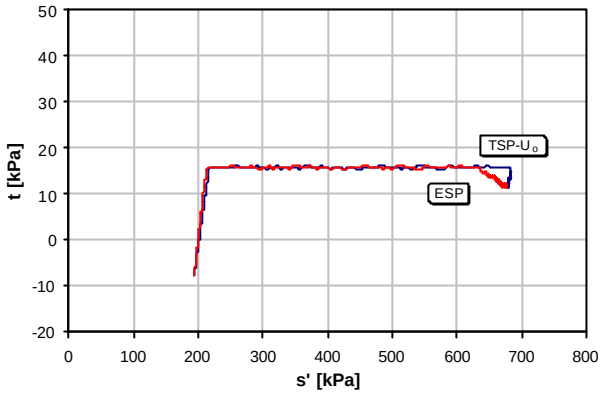

Figure A.7 Stress path during consolidation for CNV3 test.

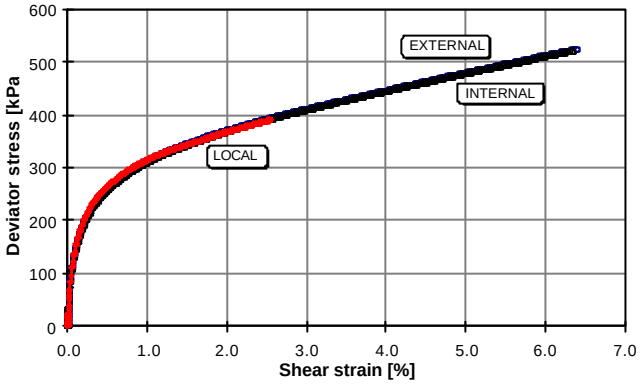

Figure A.8 Deviator stress versus shear strain for CNV3 test.

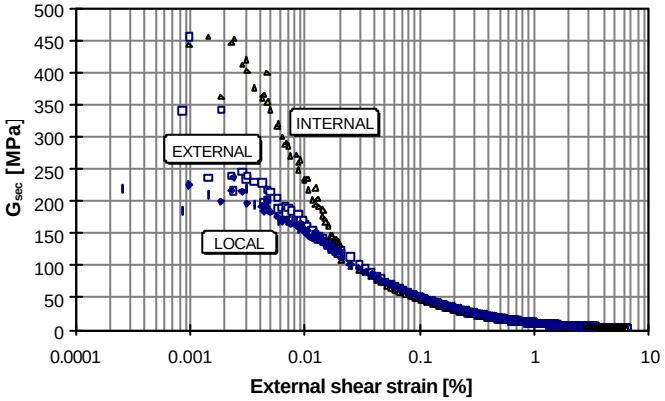

Figure A.9 Shear modulus versus external shear strain for CNV3 test.

Table A.4 Data for the shearing phase for test CNV3.

q [kPa]	Δu [kPa]	$\varepsilon_{a,l}$ [%]	$\varepsilon_{a,e}$ [%]	$\varepsilon_{r,l}$ [%]
-1,67	0,00	0,00000	0,00000	0,00000
-0,19	0,05	0,00020	-0,00036	0,00040
-0,21	0,06	0,00045	-0,00067	0,00027
13,85	0,14	0,00279	0,00293	-0,00048
19,88	-0,12	0,00434	0,00409	-0,00056
31,21	-0,46	0,00774	0,00661	-0,00191
51,59	-1,08	0,01352	0,01334	-0,00393
54,96	-1,16	0,01501	0,01496	-0,00495
62,28	-1,57	0,01812	0,01958	-0,00637
65,76	-1,66	0,01967	0,02057	-0,00701
107,80	-2,99	0,04881	0,05434	-0,02178
147,87	-2,32	0,09536	0,11269	-0,04763
159,25	-2,02	0,11171	0,13222	-0,05670
185,29	-0,25	0,15899	0,18858	-0,08535
193,67	0,34	0,17643	0,20925	-0,09661
206,82	1,79	0,20984	0,24724	-0,11923
229,04	4,40	0,27864	0,32514	-0,16814
233,78	5,07	0,29629	0,34439	-0,18123
241,64	6,23	0,33071	0,38312	-0,20586
245,05	6,83	0,34853	0,40249	-0,21706
254,61	8,36	0,40316	0,46116	-0,24970
257,91	8,52	0,42203	0,47988	-0,26162
267,02	9,84	0,47765	0,53949	-0,29649
275,18	10,67	0,53415	0,59764	-0,33690
278,03	10,87	0,55207	0,61756	-0,35262
282,92	11,29	0,59073	0,65490	-0,38069
285,46	11,45	0,60902	0,67416	-0,39431
291,77	11,86	0,66750	0,73193	-0,43428
298,61	11,95	0,72605	0,78837	-0,47322
300,18	12,02	0,74598	0,80917	-0,48637
305,83	12,11	0,80475	0,86617	-0,52585
308,49	12,15	0,82583	0,88486	-0,53999
311,27	12,17	0,86733	0,92494	-0,56916
318,08	12,04	0,95030	1,00158	-0,62431
320,07	12,03	0,97160	1,02101	-0,63877
322,72	12,03	1,01490	1,06105	-0,66769
328,63	11,95	1,10451	1,13742	-0,72641
330,06	12,01	1,12745	1,15776	-0,74197
333,18	11,76	1,17479	1,19729	-0,77815
338,98	11,26	1,27222	1,27425	-0,84990
340,07	11,28	1,29797	1,29426	-0,86622
342,96	10,68	1,34839	1,33274	-0,89894
348,29	10,04	1,44290	1,41262	-0,96460
349,35	9,95	1,46365	1,43169	-0,98016
351,73	9,74	1,50517	1,46973	-1,01203
356,65	8,83	1,58844	1,54703	-1,05914
357,90	8,85	1,60941	1,56608	-1,07455
360,16	8,40	1,65156	1,60574	-1,10677
364,01	7,43	1,73490	1,68227	-1,17811
366,09	7,37	1,75620	1,70151	-1,19526
368,69	6,88	1,79907	1,74197	-1,22983
372,82	5,90	1,88467	1,82109	-1,29805
373,20	5,90	1,90518	1,84035	-1,31453

375,94	5,33	1,94778	1,87999	-1,34846
379,67	4,31	2,03448	1,95827	-1,41630
381,11	4,13	2,05563	1,97829	-1,43286
382,95	3,69	2,09947	2,01642	-1,46572
386,84	2,52	2,18528	2,09354	-1,53147
388,33	2,42	2,20625	2,11307	-1,54617
389,91	1,83	2,25112	2,15286	-1,58019
393,40	0,88	-	2,22947	-1,64728
394,29	0,49	-	2,24931	-1,66459
396,51	0,04	-	2,28963	-1,69915
400,75	-1,03	-	2,36847	-1,76748
401,37	-1,31	-	2,38683	-1,78416
403,51	-1,92	-	2,42548	-1,81792
404,27	-2,13	-	2,44545	-1,83499
406,99	-3,16	-	2,50590	-1,88707
407,58	-3,40	-	2,52450	-1,90429
410,20	-4,15	-	2,58305	-1,97197
413,74	-5,08	-	2,64196	-2,02382
413,92	-5,28	-	2,66190	-2,04093
416,71	-6,37	-	2,72195	-2,09369
419,30	-7,12	-	2,78025	-2,14415
420,02	-7,43	-	2,80101	-2,16111
423,74	-8,62	-	2,86009	-2,21735
425,33	-9,64	-	2,92059	-2,27196
426,98	-9,87	-	2,94088	-2,28932
429,06	-10,80	-	2,99915	-2,34129
432,29	-11,90	-	3,05964	-2,39454
433,21	-12,26	-	3,08095	-2,41271
435,78	-13,25	-	3,13975	-2,46453
437,94	-14,27	-	3,19928	-2,51786
439,04	-14,54	-	3,21850	-2,53604
441,44	-15,71	-	3,27751	-2,58874
443,67	-16,60	-	3,33520	-2,64176
444,78	-17,02	-	3,35488	-2,65955
446,93	-18,13	-	3,41405	-2,71296
449,73	-19,13	-	3,47378	-2,76735
451,09	-19,54	-	3,49366	-2,78565
453,07	-20,84	-	3,55224	-2,83947
455,71	-21,72	-	3,61192	-2,89316
456,52	-22,06	-	3,63171	-2,91121
458,97	-23,24	-	3,69110	-2,96432
461,84	-24,32	-	3,74815	-3,01599
462,57	-24,68	-	3,76762	-3,03289
465,43	-25,89	-	3,82798	-3,08654
467,49	-27,02	-	3,88706	-3,13952
468,19	-27,49	-	3,90680	-3,15712
471,02	-28,55	-	3,96472	-3,21086
474,04	-29,71	-	4,02314	-3,26481
474,73	-30,15	-	4,04293	-3,28425
475,70	-30,91	-	4,08271	-3,33432
478,89	-32,58	-	4,16054	-3,40901
480,38	-32,89	-	4,18077	-3,42745
482,07	-33,79	-	4,21916	-3,46280
485,06	-35,28	-	4,29584	-3,53238
486,05	-35,62	-	4,31574	-3,54968
487,40	-36,37	-	4,35413	-3,58445

490,58	-38,09	-	4,43247	-3,65486
491,51	-38,42	-	4,45208	-3,67179
493,35	-39,13	-	4,48954	-3,70499
496,39	-40,93	-	4,56960	-3,77588
497,14	-41,26	-	4,58959	-3,79358
498,86	-42,05	-	4,62889	-3,82883
501,93	-43,52	-	4,70596	-3,89726
502,60	-43,97	-	4,72580	-3,91507
504,60	-44,77	-	4,76527	-3,94982
507,44	-46,30	-	4,84397	-4,01736
507,78	-46,60	-	4,86321	-4,03368
509,64	-47,58	-	4,90355	-4,06890
514,36	-49,42	-	4,98457	-4,13961
514,09	-49,76	-	5,00434	-4,15675
515,28	-50,43	-	5,04249	-4,18405
518,88	-52,01	-	5,12382	-4,25800
520,05	-52,55	-	5,14296	-4,27676
520,68	-53,27	-	5,18353	-4,31179
524,66	-54,77	-	5,26587	-4,38212
525,04	-55,27	-	5,28613	-4,40002
524,79	-55,88	-	5,32346	-4,43216
520,63	-56,47	-	5,36791	-4,47039
521,34	-56,61	-	5,37769	-4,47792
520,77	-56,71	-	5,39323	-4,49094
520,10	-56,99	-	5,42281	-4,51589
519,79	-57,07	-	5,42994	-4,52185
520,70	-57,07	-	5,44275	-4,53215
520,23	-57,31	-	5,46618	-4,55181
520,56	-57,33	-	5,47196	-4,55834
520,09	-57,20	-	5,48267	-4,56648
521,66	-57,15	-	5,50575	-4,58582
520,76	-57,26	-	5,51138	-4,59017
521,43	-57,45	-	5,52166	-4,59880
519,91	-57,59	-	5,53918	-4,61430
519,79	-57,79	-	5,54356	-4,61725
519,76	-57,78	-	5,55049	-4,62324
518,75	-58,00	-	5,56160	-4,63296
518,92	-58,15	-	5,56598	-4,63541
517,03	-58,29	-	5,57088	-4,64043
516,67	-58,18	-	5,57999	-4,64830
516,57	-58,25	-	5,58257	-4,65018
516,53	-58,12	-	5,58651	-4,65337
516,37	-58,11	-	5,59485	-4,66058
516,19	-58,23	-	5,59679	-4,66195
516,27	-58,16	-	5,59989	-4,66467
516,19	-58,18	-	5,60662	-4,67089
516,02	-58,27	-	5,60965	-4,67251
516,59	-58,35	-	5,61277	-4,67536
515,15	-58,11	-	5,61951	-4,68124
515,61	-57,99	-	5,62114	-4,68211
515,28	-58,06	-	5,62439	-4,68540
515,20	-57,85	-	5,63063	-4,69066
516,08	-57,86	-	5,63245	-4,69166
515,68	-57,72	-	5,63537	-4,69442
514,99	-57,73	-	5,64192	-4,69978
515,67	-57,65	-	5,64332	-4,70124

515,65	-57,57	-	5,64651	-4,70385
515,29	-57,42	-	5,65120	-4,70822
514,63	-57,18	-	5,65250	-4,70941
515,42	-57,19	-	5,65627	-4,71201
515,65	-57,18	-	5,66052	-4,71631
515,09	-57,13	-	5,66193	-4,71752
515,19	-57,35	-	5,66566	-4,72012
515,80	-57,01	-	5,67081	-4,72432
516,10	-56,98	-	5,67140	-4,72569
515,51	-56,99	-	5,67504	-4,72843
515,77	-56,93	-	5,67990	-4,73245
515,53	-56,89	-	5,68186	-4,73405
515,72	-56,77	-	5,68390	-4,73607
516,21	-56,85	-	5,68793	-4,74019
515,47	-56,67	-	5,68958	-4,74118
515,53	-56,73	-	5,69159	-4,74304
515,79	-56,61	-	5,69739	-4,74771
516,16	-56,65	-	5,69739	-4,74859
514,99	-56,74	-	5,70026	-4,75085
515,55	-56,65	-	5,70440	-4,75487
515,34	-56,53	-	5,70617	-4,75601
516,05	-56,58	-	5,70763	-4,75752
516,51	-56,58	-	5,71300	-4,76202
516,02	-56,62	-	5,71336	-4,76300
516,02	-56,72	-	5,71545	-4,76464
515,43	-56,80	-	5,71984	-4,76868
515,92	-56,70	-	5,72088	-4,76938
515,22	-56,74	-	5,72299	-4,77128
515,87	-56,86	-	5,72767	-4,77478
516,30	-56,94	-	5,72750	-4,77516
516,39	-57,02	-	5,72940	-4,77690
515,37	-57,11	-	5,73367	-4,78041
515,66	-57,13	-	5,73463	-4,78141
515,39	-57,10	-	5,73555	-4,78269
515,25	-57,20	-	5,73950	-4,78585
515,10	-57,21	-	5,73974	-4,78639
514,49	-57,45	-	5,74199	-4,78864
515,13	-57,54	-	5,74388	-4,79024
514,72	-57,48	-	5,74529	-4,79103
514,25	-57,57	-	5,74693	-4,79294
514,08	-57,79	-	5,74940	-4,79497
514,92	-57,75	-	5,74926	-4,79506
513,87	-57,81	-	5,75157	-4,79684
514,07	-58,08	-	5,75366	-4,79876
514,59	-58,05	-	5,75418	-4,79926
513,88	-58,02	-	5,75598	-4,80080
514,25	-58,17	-	5,75759	-4,80238
514,63	-58,29	-	5,75849	-4,80279
514,51	-58,39	-	5,76127	-4,80481
514,16	-58,49	-	5,76270	-4,80655
513,57	-58,47	-	5,76303	-4,80696
513,72	-58,56	-	5,76383	-4,80812
514,14	-58,71	-	5,76699	-4,81015
514,16	-58,82	-	5,76862	-4,81161
513,27	-58,93	-	5,76964	-4,81285
514,43	-59,00	-	5,76980	-4,81305

513,99	-59,01	-	5,77221	-4,81539
513,14	-59,04	-	5,77327	-4,81584
513,69	-59,15	-	5,77438	-4,81698
512,82	-59,27	-	5,77594	-4,81831
513,68	-59,25	-	5,77570	-4,81840
512,30	-59,29	-	5,77871	-4,82053
512,81	-59,35	-	5,77885	-4,82063
513,81	-59,49	-	5,78038	-4,82191
513,52	-59,44	-	5,78170	-4,82286
513,12	-59,58	-	5,78256	-4,82352
512,43	-59,58	-	5,78400	-4,82463
512,73	-59,50	-	5,78468	-4,82519
512,42	-59,59	-	5,78538	-4,82586
512,98	-59,54	-	5,78546	-4,82651
513,06	-59,54	-	5,78733	-4,82745
512,74	-59,51	-	5,78774	-4,82817
512,05	-59,48	-	5,78884	-4,82889
512,78	-59,56	-	5,79057	-4,82976
512,73	-59,50	-	5,79066	-4,83054
512,13	-59,65	-	5,79232	-4,83169
512,36	-59,52	-	5,79364	-4,83256
512,09	-59,67	-	5,79341	-4,83283
512,22	-59,57	-	5,79557	-4,83452
512,22	-59,45	-	5,79574	-4,83458
511,97	-59,49	-	5,79750	-4,83838

Table A.5 Data for the drained phase for test CNV3.

q [kPa]	Δu [kPa]	$\varepsilon_{a,l}$ [%]	$\varepsilon_{a,e}$ [%]	$\varepsilon_{r,l}$ [%]
493,87	-59,37	0,00000	0,00000	0,00000
495,61	-51,74	0,00092	-0,00019	-0,00086
493,25	-12,58	0,00818	0,00294	-0,01420
493,45	-11,31	0,01178	0,00600	-0,01904
492,63	-10,09	0,01541	0,00881	-0,02349
492,72	-8,12	0,02942	0,01959	-0,03913
492,76	-7,81	0,03381	0,02474	-0,04490
492,49	-8,22	0,04589	0,03454	-0,05616
493,18	-8,04	0,05875	0,04687	-0,06933
492,81	-7,25	0,07268	0,05943	-0,08287
493,22	-6,75	0,07974	0,06616	-0,09024
492,65	-7,24	0,10339	0,08708	-0,11214
492,56	-7,05	0,11032	0,09390	-0,11930
492,59	-7,05	0,11857	0,10244	-0,12772
493,45	-6,88	0,14439	0,12591	-0,15002
493,87	-6,84	0,15431	0,13622	-0,15903
495,34	-6,82	0,17686	0,15547	-0,17854
496,04	-6,76	0,20365	0,17953	-0,20143
497,48	-6,74	0,23483	0,20822	-0,22672
499,40	-6,64	0,25132	0,22270	-0,24044
504,42	-7,37	0,39329	0,34241	-0,34585
504,45	-7,35	0,42138	0,36536	-0,36745
502,81	-7,32	0,44394	0,38479	-0,38587
500,56	-6,99	0,49205	0,42714	-0,42588
500,72	-6,96	0,50663	0,43943	-0,43790

500,52	-6,64	0,53553	0,46328	-0,46134
501,97	-6,71	0,56686	0,48937	-0,48547
501,56	-6,68	0,59617	0,51349	-0,50849
501,59	-6,54	0,61265	0,52483	-0,51931
501,92	-6,47	0,65494	0,55737	-0,55082
504,64	-6,33	0,67548	0,57546	-0,56705
502,90	-6,56	0,69596	0,59117	-0,58161
501,59	-6,37	0,73736	0,62243	-0,61264
500,23	-6,46	0,74744	0,63261	-0,62141
500,84	-6,17	0,77119	0,65006	-0,63848
499,16	-6,26	0,79219	0,66461	-0,65273
498,61	-6,09	0,80720	0,67764	-0,66583
498,76	-5,98	0,81423	0,68371	-0,67205
497,00	-5,95	0,83251	0,69849	-0,68773
497,09	-5,82	0,84061	0,70298	-0,69194
496,11	-5,72	0,84614	0,70766	-0,69661
496,03	-5,70	0,86218	0,72039	-0,70933
494,64	-5,70	0,86723	0,72338	-0,71297
494,22	-5,62	0,87709	0,72980	-0,72051
494,20	-5,41	0,88248	0,73620	-0,72706
493,68	-5,27	0,89173	0,74315	-0,73386
495,36	-5,18	0,89733	0,74739	-0,73799
494,79	-5,20	0,91573	0,76031	-0,75045
494,62	-5,14	0,91815	0,76371	-0,75377
494,51	-5,23	0,92341	0,76754	-0,75726
493,95	-5,18	0,93632	0,77596	-0,76679
493,88	-5,17	0,94070	0,77870	-0,76990
492,31	-5,03	0,94851	0,78463	-0,77550
492,60	-5,02	0,95462	0,78956	-0,78072
492,63	-5,11	0,96129	0,79413	-0,78631
492,63	-5,04	0,96575	0,79615	-0,78841
491,71	-4,60	0,97339	0,80430	-0,79602
491,48	-3,91	0,97946	0,80714	-0,79850
491,85	-3,59	0,97904	0,80935	-0,80132
490,79	-3,36	0,99152	0,81735	-0,80955
486,36	-4,16	0,99469	0,81989	-0,81200
485,98	-4,48	1,00131	0,82443	-0,81682
486,01	-4,42	1,00708	0,82769	-0,82095
486,29	-4,43	1,01309	0,83170	-0,82532
486,15	-4,44	1,01725	0,83475	-0,82767
485,35	-4,51	1,02523	0,84001	-0,83361
485,87	-4,44	1,02737	0,84123	-0,83551
485,56	-4,43	1,02867	0,84398	-0,83761
485,26	-4,48	1,03836	0,84884	-0,84344
485,04	-4,49	1,04077	0,85072	-0,84534
486,09	-4,35	1,04508	0,85399	-0,84936
486,03	-4,43	1,05076	0,85782	-0,85340
485,48	-4,49	1,05537	0,86199	-0,85836
485,85	-4,47	1,05939	0,86445	-0,86020
486,01	-4,59	1,07056	0,86905	-0,86630
486,35	-4,54	1,07062	0,87164	-0,86850
485,86	-4,49	1,07486	0,87344	-0,87072
486,55	-4,62	1,08536	0,87821	-0,87653
486,39	-4,55	1,08653	0,88074	-0,87838
485,66	-4,51	1,09329	0,88468	-0,88250
486,25	-4,61	1,09947	0,88684	-0,88589

485,42	-4,48	1,10571	0,89122	-0,88942
485,69	-4,16	1,10693	0,89320	-0,89115
485,22	-4,09	1,11587	0,89829	-0,89641
485,12	-3,76	1,11429	0,90003	-0,89800
485,74	-3,11	1,11508	0,90238	-0,89978
484,62	-2,48	1,12880	0,91529	-0,91162
484,67	-2,32	1,13663	0,92130	-0,91784
484,02	-2,28	1,15120	0,93555	-0,93204
483,12	-2,55	1,16578	0,94845	-0,94233
481,97	-3,69	1,17348	0,95783	-0,95198
481,30	-3,69	1,17776	0,96207	-0,95637
478,87	-3,97	1,18883	0,97127	-0,96673
478,74	-4,24	1,19167	0,97446	-0,96974
477,59	-4,23	1,19387	0,97801	-0,97278
476,93	-4,37	1,20124	0,98327	-0,97963
476,06	-4,23	1,20274	0,98465	-0,98095
476,42	-3,15	1,20654	0,98857	-0,98454
475,35	-2,72	1,20998	0,99093	-0,98727
474,89	-3,01	1,21302	0,99551	-0,99036
474,86	-4,03	1,21423	0,99682	-0,99159
474,10	-4,30	1,21891	1,00103	-0,99615
474,55	-4,38	1,22022	1,00204	-0,99732
474,37	-4,46	1,22084	1,00298	-0,99856
474,54	-4,72	1,22344	1,00507	-1,00127
473,51	-4,91	1,22424	1,00672	-1,00248
473,33	-4,86	1,22554	1,00791	-1,00449
473,69	-4,51	1,22665	1,00834	-1,00553
472,64	-4,47	1,23012	1,01233	-1,00843
472,93	-4,56	1,23006	1,01246	-1,00834
472,56	-3,50	1,23062	1,01411	-1,00891
472,06	-4,35	1,23107	1,01381	-1,00986
472,69	-4,70	1,23270	1,01644	-1,01148
472,12	-5,03	1,23034	1,01641	-1,01255
472,62	-5,25	1,23055	1,01797	-1,01342
472,43	-5,68	1,23223	1,01880	-1,01541
471,94	-5,85	1,23258	1,01976	-1,01636
472,74	-6,24	1,23337	1,02139	-1,01731
471,76	-5,26	1,23416	1,02224	-1,01805

Test CNV4

Borehole:	CAEST4-3
Depth of the sample [m]:	36.91
Type of test:	CID – CL(2D) sheared with s = constant stress path
Triaxial Apparatus:	GDS

LL:	39	Initial height [mm]:	142.2	Total unit weight [kN/m^3]:	22.19
LP:	21	Initial diameter [mm]:	70.0	Dry unit weight [kN/m^3]:	19.45
IC:	1.38	Initial volume [mm^3]:	547249.7	e_o:	0.43
G_s:	2.839	Total weight [g]:	1238	W_n [%]:	14.10
$CaCO_3$ [%]:	22.3	Dry weight [g]:	1085		

Phase of the test:	FLUSHING	Final height [mm]:	141.9
		Final diameter [mm]:	70.0
		Final volume [mm^3]:	546419.2
		Final Total weight [g]:	22.23
		e (end of flushing):	90
		σ_v (end of flushing) [kPa]:	165
		σ_h (end of flushing) [kPa]:	
Phase of the test:	SATURATION	Final height [mm]:	142.1
		Final diameter [mm]:	70.0
		Final volume [mm^3]:	546946.7
		Final Total weight [g]:	22.20
		e (end of saturation):	0.43
		Skempton's B parameter:	0.95
Phase of the test:	CONSOLIDATION	Final height [mm]:	-
		Final diameter [mm]:	-
		Final volume [mm^3]:	-
		Final Total weight [g]:	-
		e (end of consolidation):	
		σ'_v (end of cons.) [kPa]:	662
		σ'_h (end of cons.) [kPa]:	659
		u_o [kPa]:	320
Phase of the test:	SHEARING	t_{max} (at peak) [kPa]:	142
		s'_{max} (at peak) [kPa]:	666
		Δu (at peak) [kPa]:	-11

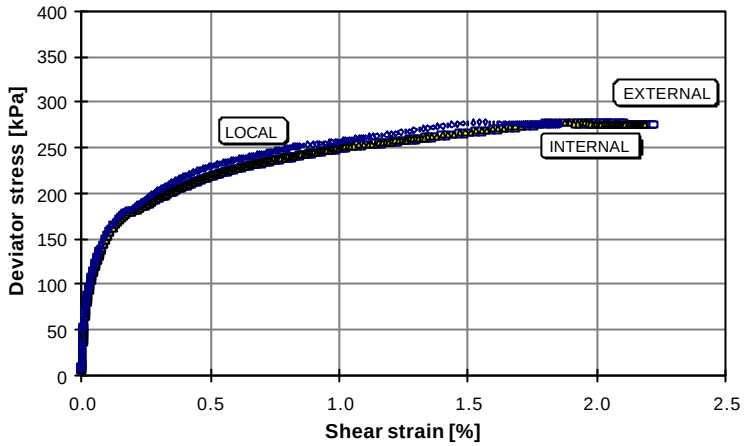

Figure A.10 Deviator stress versus shear strain for CNV4 test.

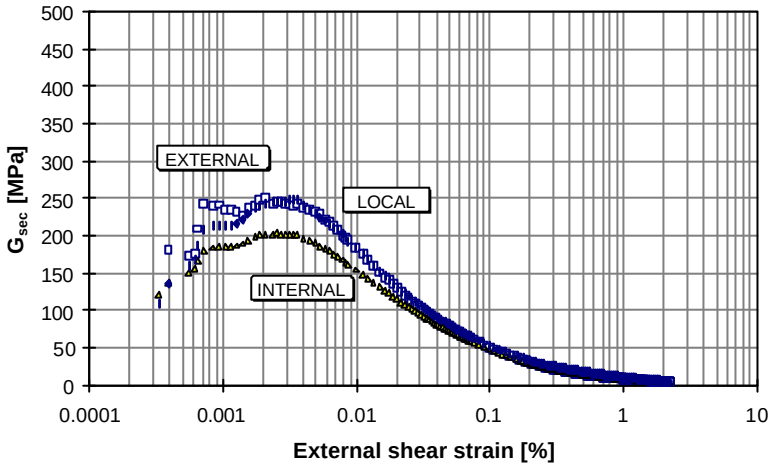

Figure A.11 Shear modulus versus external shear strain for CNV4 test.

Table A.6 Data for the shearing phase for test CNV4.

Q [kPa]	Δu [kPa]	$\varepsilon_{a,l}$ [%]	$\varepsilon_{a,e}$ [%]	$\varepsilon_{r,l}$ [%]
5,46	0,00	0,00000	0,00000	0,00000
12,01	0,24	0,00124	0,00124	-0,00033
19,25	0,13	0,00255	0,00259	-0,00038
45,83	-1,36	0,00847	0,00861	-0,00109
54,53	-1,92	0,01115	0,01129	-0,00191
58,64	-2,25	0,01254	0,01262	-0,00236
71,18	-3,14	0,01770	0,01814	-0,00449
74,46	-3,33	0,01909	0,01954	-0,00515
79,72	-3,77	0,02175	0,02217	-0,00617
89,26	-4,28	0,02719	0,02786	-0,00911
91,26	-4,39	0,02844	0,02943	-0,00985
93,23	-4,54	0,02978	0,03085	-0,01060
101,31	-5,01	0,03538	0,03684	-0,01353
104,68	-5,18	0,03817	0,03981	-0,01511
106,44	-5,22	0,03947	0,04113	-0,01590
113,53	-5,47	0,04525	0,04752	-0,01912
115,11	-5,55	0,04675	0,04902	-0,01998
118,53	-5,69	0,04970	0,05219	-0,02179
124,18	-5,88	0,05578	0,05848	-0,02521
125,53	-5,91	0,05722	0,06001	-0,02617
126,97	-5,92	0,05870	0,06166	-0,02704
131,92	-6,01	0,06455	0,06813	-0,03039
134,14	-6,00	0,06742	0,07118	-0,03211
135,45	-6,01	0,06892	0,07290	-0,03308
148,80	-6,10	0,08729	0,09340	-0,04380
153,27	-6,05	0,09469	0,10150	-0,04831
161,20	-5,83	0,10902	0,11798	-0,05718
173,05	-5,10	0,13732	0,15161	-0,07533
175,20	-4,89	0,14449	0,16036	-0,08006
177,02	-4,63	0,15156	0,16931	-0,08466
179,40	-4,07	0,16568	0,18750	-0,09307
182,89	-2,75	0,19166	0,22352	-0,10482
184,04	-2,44	0,19807	0,23275	-0,10698
185,06	-2,20	0,20446	0,24205	-0,10887
188,86	-1,24	0,22843	0,27747	-0,11494
191,12	-0,87	0,24068	0,29533	-0,11752
192,27	-0,71	0,24689	0,30472	-0,11878
196,24	-0,14	0,27175	0,34163	-0,12324
197,16	0,00	0,27781	0,35064	-0,12421
198,79	0,19	0,29002	0,36829	-0,12601
200,58	0,46	0,30213	0,38656	-0,12789
203,18	0,63	0,32031	0,41303	-0,13069
203,87	0,72	0,32627	0,42182	-0,13162
207,41	0,97	0,35067	0,45794	-0,13537
208,73	1,12	0,36305	0,47618	-0,13731
211,64	1,25	0,38695	0,51161	-0,14051
212,25	1,31	0,39288	0,52039	-0,14136
214,51	1,52	0,41104	0,54719	-0,14451
215,80	1,58	0,42319	0,56487	-0,14659
217,83	1,68	0,44145	0,59145	-0,14968
218,55	1,73	0,44763	0,60043	-0,15080
220,86	1,86	0,47250	0,63670	-0,15598
222,13	1,83	0,48510	0,65458	-0,15904

224,61	2,00	0,51031	0,69081	-0,16576
225,66	2,00	0,52313	0,70875	-0,16975
226,73	2,00	0,53605	0,72680	-0,17404
228,94	2,06	0,56238	0,76313	-0,18367
229,45	2,10	0,56893	0,77247	-0,18626
231,62	2,07	0,59584	0,80917	-0,19791
232,06	2,06	0,60243	0,81820	-0,20098
233,62	2,17	0,62258	0,84473	-0,21110
234,97	2,15	0,64281	0,87132	-0,22173
236,01	2,14	0,65623	0,88929	-0,22900
237,12	2,09	0,67018	0,90744	-0,23684
238,97	2,15	0,69827	0,94433	-0,25243
239,39	2,13	0,70525	0,95326	-0,25623
241,06	2,18	0,73239	0,98932	-0,27180
242,46	2,09	0,75277	101,629	-0,28318
244,24	2,13	0,77955	105,224	-0,29807
245,01	2,11	0,79308	107,004	-0,30567
246,84	2,00	0,81958	110,588	-0,32026
248,03	2,05	0,83976	113,277	-0,33198
249,74	1,96	0,86648	116,846	-0,34815
250,93	1,96	0,88649	119,520	-0,36120
252,68	1,88	0,91298	123,070	-0,40428
253,66	1,78	0,92618	124,849	-0,44146
255,32	1,78	0,95254	128,430	-0,48851
256,66	1,73	0,97231	131,067	-0,51804
258,27	1,55	0,99916	134,697	-0,55406
259,42	1,59	101,917	137,341	-0,57786
261,06	1,45	104,611	140,926	-0,60984
262,01	1,38	106,094	143,133	-0,63192
264,96	1,18	110,777	150,151	-0,69370
267,35	1,03	114,388	155,506	-0,74003
270,41	0,61	119,170	162,742	-0,79840
272,54	0,32	122,713	168,115	-0,84514
275,40	0,02	127,435	175,347	-0,91246
276,71	-0,12	129,772	178,955	-0,94849
276,86	0,04	133,870	185,063	-103,579
276,65	0,43	135,880	187,776	-107,764
276,31	0,49	138,020	190,576	-111,968
276,11	0,56	139,332	192,214	-114,684
275,86	0,68	140,808	194,064	-117,819
276,02	0,63	141,474	194,925	-119,138
275,67	0,78	142,660	196,410	-121,549
275,56	0,62	143,437	197,374	-123,069
275,53	0,54	144,383	198,520	-126,461
275,51	0,52	145,021	199,294	-127,611
275,36	0,48	145,796	200,291	-129,014
275,30	0,49	146,163	200,703	-129,684
275,19	0,53	146,828	201,487	-130,970
288,08	-0,13	0,31219	202,880	-228,350
295,12	-2,06	0,35767	212,013	-239,201
300,05	-3,13	0,41854	223,167	-252,530
281,49	-2,79	-0,47142	243,787	0,60329
282,59	-2,69	-0,43570	248,873	0,54146
282,44	-3,06	-0,38518	255,740	0,45438
283,70	-3,51	-0,35422	260,171	0,40083
283,83	-3,83	-0,32698	263,644	0,35703

284,14	-4,10	-0,31055	265,773	0,33116
284,35	-4,86	-0,29258	268,015	0,30777
284,50	-5,12	-0,28476	268,952	0,29673
284,56	-5,52	-0,27210	270,477	0,28038
284,34	-5,91	-0,26381	271,383	0,26874
284,67	-6,29	-0,25375	272,594	0,25440
285,38	-6,37	-0,24625	273,469	0,24388
284,99	-6,34	-0,23867	274,419	0,23082
285,00	-6,32	-0,23385	274,998	0,22552
284,38	-5,34	-0,22695	275,751	0,21701
284,56	-5,51	-0,22280	276,287	0,21145
284,44	-6,43	-0,21742	276,725	0,20702
284,94	-6,59	-0,21336	277,345	0,19980
285,15	-5,74	-0,20774	278,132	0,19210
284,24	-4,91	-0,20485	278,407	0,18829
283,92	-4,92	-0,20111	278,827	0,18619
284,65	-5,83	-0,19831	279,087	0,18310
284,40	-6,19	-0,19405	279,582	0,17828
285,19	-6,65	-0,19100	279,979	0,17476
284,88	-6,71	-0,18701	280,435	0,16963
284,96	-7,06	-0,18514	280,653	0,16763
284,74	-7,29	-0,18161	281,007	0,16381
285,00	-7,45	-0,17932	281,281	0,16123
285,49	-7,73	-0,17598	281,638	0,15800
285,08	-7,98	-0,17349	281,928	0,15535
285,21	-8,23	-0,17069	282,279	0,15211
285,01	-8,36	-0,16907	282,369	0,15070
285,09	-8,41	-0,16641	282,664	0,14767
285,24	-8,44	-0,16451	282,851	0,14604
285,10	-8,40	-0,16158	283,188	0,14341
285,13	-8,38	-0,15985	283,373	0,14121
285,30	-8,00	-0,15738	283,625	0,13800
285,42	-7,59	-0,15603	283,731	0,13652
285,36	-7,08	-0,15368	284,162	0,13329
284,72	-7,79	-0,15247	284,169	0,13235
285,73	-8,31	-0,15046	284,507	0,12994
284,56	-7,81	-0,14875	284,658	0,12851
285,02	-8,28	-0,14720	284,843	0,12705
285,70	-9,57	-0,13961	285,545	0,11878
285,06	-10,89	-0,12540	286,846	0,10706
284,94	-11,04	-0,11796	287,546	0,10080
284,82	-13,07	-0,11122	287,833	0,09695
284,77	-11,98	-0,10747	288,017	0,09345

Test CNV5

Borehole:	CAEST4-5
Depth of the sample [m]:	51.19
Type of test:	CIU-CL
Triaxial Apparatus:	SRTA

LL:	33	Initial height [mm]:	124.5	Total unit weight [kN/m^3]:	21.63
LP:	21	Initial diameter [mm]:	69.7	Dry unit weight [kN/m^3]:	18.93
IC:	1.56	Initial volume [mm^3]:	475034.1	e_o:	-
G_s:	-	Total weight [g]:	1047.3	W_n [%]:	14.3
$CaCO_3$ [%]:	-	Dry weight [g]:	916.6		

Phase of the test:	FLUSHING	Final height [mm]:	124.45
		Final diameter [mm]:	69.70
		Final volume [mm^3]:	474857.9
		Final Total weight [g]:	21.64
		e (end of flushing):	-
		σ_v (end of flushing) [kPa]:	64.1
		σ_h (end of flushing) [kPa]:	74.1
Phase of the test:	SATURATION	Final height [mm]:	124.40
		Final diameter [mm]:	69.65
		Final volume [mm^3]:	473915.5
		Final Total weight [g]:	21.68
		e (end of saturation):	-
		Skempton's B parameter:	0.93
Phase of the test:	CONSOLIDATION	Final height [mm]:	124.63
		Final diameter [mm]:	69.35
		Final volume [mm^3]:	470788.9
		Final Total weight [g]:	21.82
		e (end of consolidation):	-
		σ'_v (end of cons.) [kPa]:	200
		σ'_h (end of cons.) [kPa]:	200
		u_o [kPa]:	0
Phase of the test:	SHEARING	t_{max} (at peak) [kPa]:	471
		s'_{max} (at peak) [kPa]:	666
		Δu (at peak) [kPa]:	0

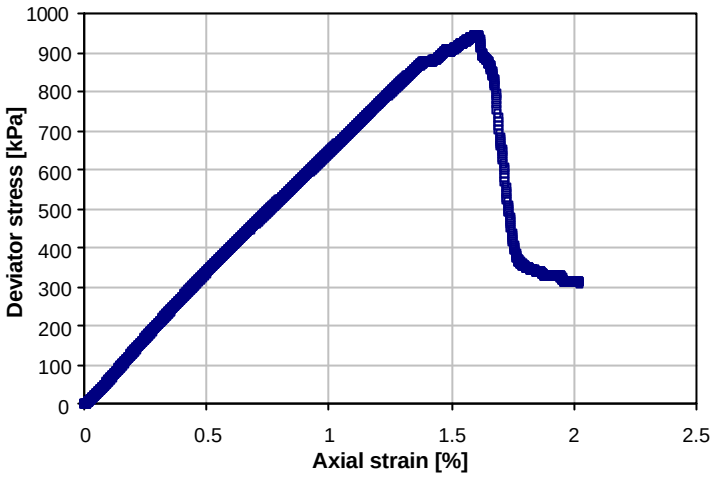

Figure A.12 Shear strain versus deviator stress for CNV5 test.

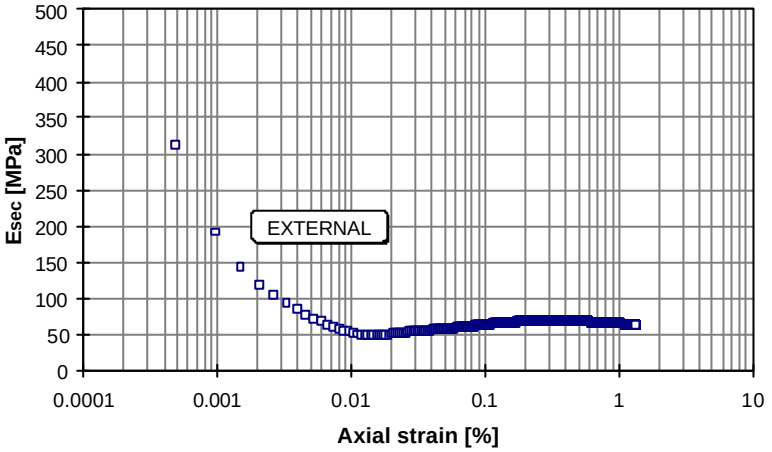

Figure A.13 Shear modulus versus external shear strain for CNV5 test.

Table A.7 Data for the shearing phase for test CNV5.

q [kPa]	$\varepsilon_{a,e}$ [%]	$\varepsilon_{r,l}$ [%]
-2,40	0,00000	0,00000
-2,41	-0,00422	0,00125
0,23	-0,00184	0,00014
7,03	0,01465	-0,01959
11,32	0,02190	-0,02144
29,76	0,05146	-0,01862
34,57	0,05880	-0,01734
47,42	0,07791	-0,01377
63,28	0,09985	-0,00941
74,38	0,11518	-0,00913
85,36	0,13011	-0,01070
107,79	0,16100	-0,02345
112,92	0,16849	-0,02802
134,75	0,19855	-0,04334
140,16	0,20601	-0,04756
156,99	0,22919	-0,05981
173,63	0,25284	-0,07153
185,39	0,26957	-0,07996
196,34	0,28517	-0,08781
215,28	0,31429	-0,10178
221,42	0,32193	-0,10528
243,15	0,35347	-0,12042
248,51	0,36129	-0,12446
265,08	0,38521	-0,13582
280,84	0,40880	-0,14675
291,52	0,42495	-0,15442
302,03	0,44139	-0,16242
323,44	0,47407	-0,17635
328,78	0,48226	-0,17950
349,46	0,51437	-0,19278
354,54	0,52234	-0,19632
370,28	0,54688	-0,20657
385,51	0,57117	-0,21689
395,82	0,58773	-0,22432
405,89	0,60385	-0,23064
426,19	0,63644	-0,24485
431,40	0,64472	-0,24817
451,29	0,67723	-0,26125
456,26	0,68536	-0,26460
471,25	0,71015	-0,27546
486,02	0,73458	-0,28650
496,10	0,75129	-0,29321
506,54	0,76830	-0,30082
527,54	0,80354	-0,31725
532,48	0,81182	-0,32025
552,04	0,84465	-0,33528
557,05	0,85289	-0,33853
572,65	0,87862	-0,34949
588,18	0,90450	-0,36035
598,34	0,92147	-0,36753
608,33	0,93796	-0,37439
628,57	0,97132	-0,38764
634,48	0,98081	-0,39142

655,32	1,01545	-0,40542
660,28	1,02390	-0,40856
676,16	1,04996	-0,42042
692,09	1,07598	-0,43260
702,61	1,09324	-0,44146
713,49	1,11063	-0,44981
734,52	1,14426	-0,46696
739,66	1,15250	-0,47153
768,89	1,20039	-0,50324
773,90	1,20862	-0,50824
793,35	1,24143	-0,53024
808,63	1,26664	-0,54731
819,41	1,28491	-0,55867
829,35	1,30163	-0,56874
848,96	1,33513	-0,58849
854,09	1,34437	-0,59381
872,44	1,37843	-0,61406
876,42	1,38684	-0,61899
874,94	1,41277	-0,63467
884,45	1,43904	-0,65528
894,03	1,45731	-0,66857
906,90	1,47936	-0,68522
911,87	1,51473	-0,72080
916,08	1,52339	-0,72855
929,87	1,55979	-0,76912
933,51	1,56818	-0,77669
942,49	1,59388	-0,79937
909,78	1,62119	-0,83553
884,37	1,63953	-0,86003
865,20	1,65812	-0,88700
651,04	1,70548	-1,17486
571,26	1,71914	-1,20697
372,82	1,76939	-1,21210
363,70	1,77905	-1,21245
350,06	1,80721	-1,21545
343,45	1,83518	-1,21663
340,72	1,85312	-1,21749
333,67	1,87222	-1,21845
329,63	1,91005	0,91712
329,61	1,91895	0,91665
317,67	1,95537	0,91444
313,21	1,96458	0,91355
312,40	1,99121	0,91237
312,80	2,01778	0,88041

Test CNV6

Borehole:	CAEST4-5
Depth of the sample [m]:	51.35
Type of test:	CIU – EU(2D) - s = constant stress path
Triaxial Apparatus:	SRTA

LL:	33	Initial height [mm]:	133.94	Total unit weight [kN/m³]:	22.15
LP:	21	Initial diameter [mm]:	69.77	Dry unit weight [kN/m³]:	19.56
IC:	1.66	Initial volume [mm³]:	512079.8	e_o:	-
G_s:	-	Total weight [g]:	1156.0	W_n [%]:	13.1
$CaCO_3$ [%]:	-	Dry weight [g]:	1022.6		

Phase of the test:	FLUSHING	Final height [mm]:	133.61
		Final diameter [mm]:	69.67
		Final volume [mm³]:	510815.5
		Final Total weight [g]:	22.20
		e (end of flushing):	-
		σ_v (end of flushing) [kPa]:	80.3
		σ_h (end of flushing) [kPa]:	86.2

Phase of the test:	SATURATION	Final height [mm]:	133.61
		Final diameter [mm]:	69.88
		Final volume [mm³]:	512416.9
		Final Total weight [g]:	22.13
		e (end of saturation):	-
		Skempton's B parameter:	0.99

Phase of the test:	CONSOLIDATION	Final height [mm]:	132.17
		Final diameter [mm]:	68.42
		Final volume [mm³]:	485922.3
		Final Total weight [g]:	23.34
		e (end of consolidation):	-
		σ'_v (end of cons.) [kPa]:	804
		σ'_h (end of cons.) [kPa]:	804
		u_o [kPa]:	209

Phase of the test:	SHEARING	Final height [mm]:	132.80
		Final diameter [mm]:	68.26
		Final volume [mm³]:	486057.7
		Final Total weight [g]:	23.33
		e (end of stress path):	-
		t_{max} (end of stress path) [kPa]:	-276
		s'_{max} (end of stress path) [kPa]:	648
		Δu (end of stress path) [kPa]:	158

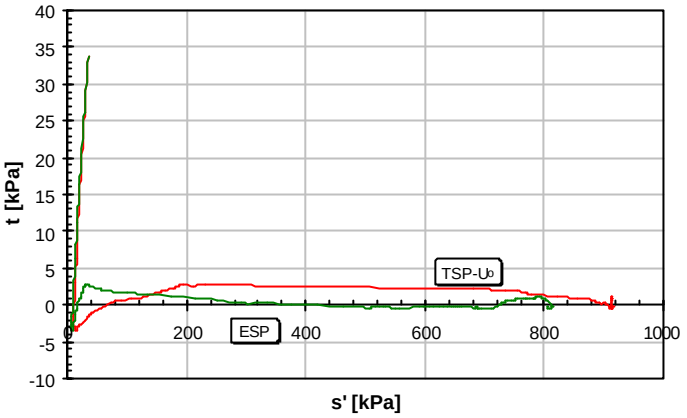

Figure A.14 Stress path during consolidation for CNV6 test.

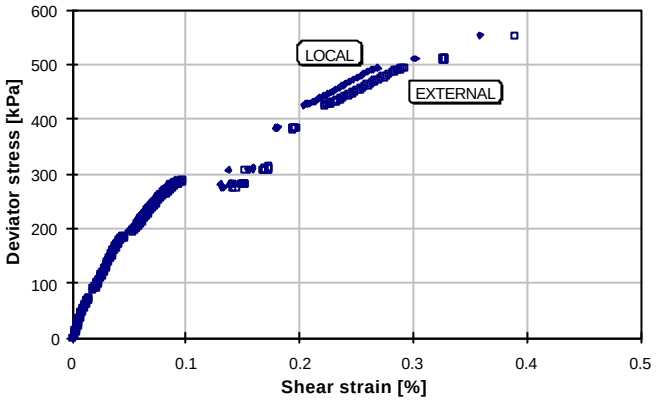

Figure A.15 Deviator stress versus shear strain for CNV6 test.

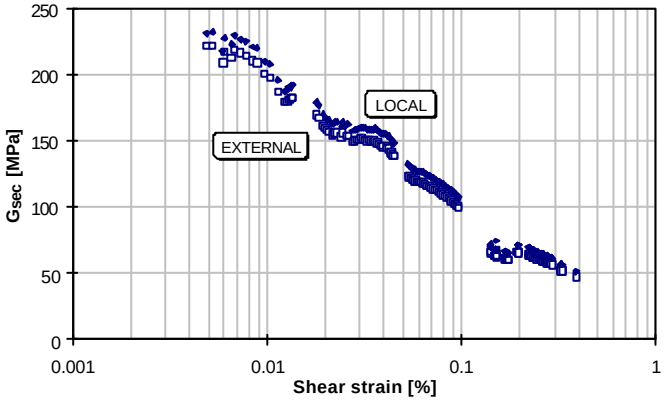

Figure A.16 Shear modulus versus external shear strain for CNV6 test.

Table A.8 Data for the shearing phase for test CNV6.

q [kPa]	Δu [kPa]	$\varepsilon_{a,l}$ [%]	$\varepsilon_{a,e}$ [%]	$\varepsilon_{r,l}$ [%]
0,29	0,00	0,00000	0,00000	0,00000
1,29	0,20	0,00014	0,00017	0,00000
-1,15	1,00	-0,00011	0,00025	0,00000
-4,09	1,68	-0,00034	0,00013	0,00114
-6,77	2,32	-0,00060	-0,00002	0,00161
-9,28	2,89	-0,00082	-0,00024	0,00168
-11,39	3,44	-0,00102	-0,00037	0,00211
-13,79	4,04	-0,00125	-0,00054	0,00250
-16,45	4,60	-0,00150	-0,00076	0,00282
-18,88	5,10	-0,00172	-0,00102	0,00282
-20,91	5,56	-0,00193	-0,00125	0,00296
-23,10	6,00	-0,00214	-0,00153	0,00336
-25,44	6,45	-0,00240	-0,00182	0,00353
-27,98	6,87	-0,00267	-0,00220	0,00357
-30,29	7,28	-0,00295	-0,00255	0,00371
-32,34	7,67	-0,00321	-0,00287	0,00414
-34,62	8,07	-0,00349	-0,00321	0,00436
-36,86	8,45	-0,00378	-0,00356	0,00511
-39,29	8,82	-0,00412	-0,00396	0,00496
-41,61	9,21	-0,00446	-0,00433	0,00536
-44,19	9,61	-0,00487	-0,00476	0,00528
-46,97	9,99	-0,00527	-0,00526	0,00564
-49,77	10,41	-0,00570	-0,00578	0,00596
-52,76	10,79	-0,00623	-0,00639	0,00635
-55,41	11,18	-0,00674	-0,00695	0,00657
-58,09	11,55	-0,00722	-0,00755	0,00735
-60,90	11,93	-0,00773	-0,00818	0,00771
-63,42	12,30	-0,00824	-0,00881	0,00878
-65,86	12,66	-0,00874	-0,00944	0,00971
-67,96	13,00	-0,00919	-0,01002	0,00978
-69,96	13,33	-0,00963	-0,01061	0,00975
-71,28	13,51	-0,00990	-0,01097	0,00982
-72,43	13,69	-0,01016	-0,01131	0,00978
-73,29	13,82	-0,01041	-0,01162	0,00971
-73,64	13,97	-0,01054	-0,01183	0,00968
-73,96	14,10	-0,01066	-0,01202	0,00964
-91,22	19,98	-0,01489	-0,01808	0,01203
-92,65	20,15	-0,01516	-0,01850	0,01257
-93,91	20,30	-0,01538	-0,01890	0,01375
-94,92	20,46	-0,01557	-0,01925	0,01425
-95,87	20,62	-0,01578	-0,01956	0,01460
-97,21	20,79	-0,01604	-0,01997	0,01493
-99,63	21,11	-0,01648	-0,02073	0,01578
-102,21	21,47	-0,01694	-0,02152	0,01607
-104,60	21,80	-0,01741	-0,02235	0,01610
-107,10	22,25	-0,01793	-0,02316	0,01643
-110,21	22,71	-0,01854	-0,02417	0,01753
-113,61	23,13	-0,01925	-0,02538	0,01725
-116,85	23,57	-0,01995	-0,02662	0,01807
-120,20	24,02	-0,02073	-0,02798	0,01828
-123,60	24,48	-0,02156	-0,02943	0,01975
-127,17	24,99	-0,02242	-0,03097	0,02000
-130,45	25,51	-0,02330	-0,03253	0,02007

-134,01	26,04	-0,02424	-0,03423	0,02025
-137,42	26,57	-0,02520	-0,03599	0,02010
-140,82	27,13	-0,02616	-0,03780	0,02028
-144,27	27,60	-0,02714	-0,03976	0,02078
-147,08	28,06	-0,02810	-0,04163	0,02092
-149,48	28,59	-0,02900	-0,04336	0,02075
-152,14	29,11	-0,02993	-0,04519	0,02082
-154,74	29,70	-0,03085	-0,04696	0,02114
-157,85	30,30	-0,03184	-0,04889	0,02107
-160,86	30,83	-0,03286	-0,05095	0,02078
-163,72	31,37	-0,03386	-0,05294	0,02121
-166,56	31,92	-0,03491	-0,05495	0,02132
-169,22	32,46	-0,03596	-0,05691	0,02174
-171,82	33,00	-0,03701	-0,05882	0,02199
-174,39	33,56	-0,03811	-0,06074	0,02139
-177,10	34,15	-0,03921	-0,06261	0,02174
-179,84	34,68	-0,04034	-0,06453	0,02185
-181,97	35,23	-0,04140	-0,06623	0,02181
-183,33	35,49	-0,04198	-0,06723	0,02249
-184,32	35,73	-0,04252	-0,06813	0,02281
-185,24	36,00	-0,04304	-0,06890	0,02335
-186,26	36,25	-0,04357	-0,06973	0,02335
-187,14	36,53	-0,04408	-0,07046	0,02331
-196,64	44,00	-0,05531	-0,08399	0,02438
-198,25	44,22	-0,05569	-0,08457	0,02506
-199,94	44,44	-0,05608	-0,08520	0,02595
-201,79	44,67	-0,05658	-0,08595	0,02660
-203,27	44,89	-0,05704	-0,08663	0,02720
-204,71	45,08	-0,05751	-0,08733	0,02799
-207,68	45,49	-0,05835	-0,08861	0,02831
-210,33	45,95	-0,05918	-0,08982	0,02913
-213,13	46,36	-0,06008	-0,09116	0,02945
-215,54	46,80	-0,06099	-0,09244	0,02952
-218,13	47,24	-0,06193	-0,09379	0,02963
-220,61	47,64	-0,06293	-0,09521	0,02977
-222,92	48,05	-0,06398	-0,09664	0,03038
-225,16	48,49	-0,06502	-0,09804	0,03063
-227,20	48,94	-0,06604	-0,09938	0,03084
-229,74	49,39	-0,06716	-0,10087	0,03142
-232,24	49,88	-0,06830	-0,10239	0,03170
-234,90	50,38	-0,06956	-0,10401	0,03174
-237,92	50,83	-0,07091	-0,10581	0,03234
-240,73	51,36	-0,07230	-0,10760	0,03284
-243,73	51,88	-0,07375	-0,10951	0,03320
-246,58	52,41	-0,07533	-0,11151	0,03363
-249,95	52,97	-0,07703	-0,11370	0,03399
-253,31	53,56	-0,07879	-0,11597	0,03445
-256,76	54,14	-0,08065	-0,11833	0,03495
-260,18	54,71	-0,08258	-0,12078	0,03527
-263,27	55,32	-0,08453	-0,12318	0,03570
-266,35	55,92	-0,08650	-0,12559	0,03652
-269,74	56,53	-0,08857	-0,12812	0,03670
-272,97	57,17	-0,09070	-0,13069	0,03716
-275,94	57,77	-0,09277	-0,13319	0,03731
-278,80	58,39	-0,09484	-0,13566	0,03788
-281,51	59,00	-0,09686	-0,13801	0,03834

-283,45	59,63	-0,09871	-0,14006	0,03920
-284,77	59,94	-0,09970	-0,14120	0,03948
-285,92	60,23	-0,10069	-0,14232	0,03959
-287,08	60,55	-0,10165	-0,14342	0,03991
-288,30	60,85	-0,10261	-0,14454	0,04070
-289,59	61,14	-0,10362	-0,14570	0,04105
-276,55	89,06	-0,15779	-0,17575	0,05688
-276,55	89,06	-0,15779	-0,17575	0,05305
-282,07	90,27	-0,16040	-0,17896	0,05048
-282,12	90,32	-0,16064	-0,17913	0,06442
-282,14	90,38	-0,16088	-0,17926	0,06116
-282,19	90,45	-0,16104	-0,17937	0,06199
-282,21	90,53	-0,16119	-0,17945	0,06249
-282,32	90,59	-0,16133	-0,17952	0,06263
-282,72	90,65	-0,16220	-0,18011	0,06284
-283,42	90,74	-0,16250	-0,18028	0,06277
-283,42	90,80	-0,16251	-0,18029	0,06309
-283,51	90,90	-0,16253	-0,18031	0,06320
-283,58	90,98	-0,16257	-0,18033	0,06316
-283,73	91,07	-0,16261	-0,18036	0,06313
-283,94	91,15	-0,16270	-0,18040	0,06345
-307,42	127,27	-0,20982	-0,24550	0,01592
-308,19	127,29	-0,21088	-0,24653	0,04222
-308,82	127,38	-0,21165	-0,24730	0,03901
-309,34	127,48	-0,21228	-0,24790	0,03997
-309,78	127,57	-0,21280	-0,24837	0,04047
-309,78	127,57	-0,21280	-0,24837	0,04043
-310,38	127,92	-0,21688	-0,25152	0,04108
-309,76	128,39	-0,21725	-0,25162	0,04140
-312,27	128,02	-0,21704	-0,25238	0,04165
-313,31	127,82	-0,21720	-0,25272	0,04165
-383,41	131,99	-0,24002	-0,28348	0,05007
-384,56	132,16	-0,24086	-0,28443	0,05011
-384,56	132,16	-0,24086	-0,28443	0,05025
-384,56	132,16	-0,24086	-0,28443	0,05075
-384,56	132,16	-0,24086	-0,28443	0,05143
-384,56	132,16	-0,24086	-0,28443	0,05157
-385,41	132,32	-0,24175	-0,28536	0,05182
-426,53	136,52	-0,27428	-0,31973	0,05693
-427,74	136,63	-0,27576	-0,32092	0,05771
-428,56	136,76	-0,27712	-0,32202	0,05832
-429,16	136,90	-0,27832	-0,32304	0,05857
-429,66	137,05	-0,27944	-0,32399	0,05950
-430,41	137,21	-0,28057	-0,32505	0,06010
-432,09	137,55	-0,28309	-0,32732	0,06053
-433,60	137,95	-0,28547	-0,32943	0,06093
-435,82	138,24	-0,28791	-0,33175	0,06125
-438,49	138,48	-0,29058	-0,33429	0,06153
-440,61	138,76	-0,29321	-0,33677	0,06239
-442,48	139,07	-0,29573	-0,33913	0,06335
-444,42	139,43	-0,29819	-0,34158	0,06385
-446,74	139,73	-0,30075	-0,34414	0,06428
-449,11	140,06	-0,30340	-0,34675	0,06524
-451,73	140,38	-0,30615	-0,34949	0,06592
-454,10	140,67	-0,30893	-0,35213	0,06642
-456,47	140,89	-0,31171	-0,35479	0,06703

-458,99	141,09	-0,31454	-0,35754	0,06749
-461,20	141,38	-0,31738	-0,36019	0,06814
-463,29	141,72	-0,31990	-0,36302	0,06853
-465,57	142,05	-0,32249	-0,36588	0,06910
-468,07	142,37	-0,32514	-0,36880	0,06939
-470,66	142,65	-0,32787	-0,37178	0,07042
-473,24	142,96	-0,33060	-0,37477	0,07117
-475,93	143,22	-0,33347	-0,37788	0,07246
-478,40	143,53	-0,33632	-0,38091	0,07353
-481,08	143,84	-0,33925	-0,38404	0,07431
-483,82	144,17	-0,34224	-0,38721	0,07496
-486,48	144,49	-0,34531	-0,39041	0,07570
-489,01	144,83	-0,34837	-0,39361	0,07642
-490,20	144,99	-0,34999	-0,39503	0,07713
-491,41	145,13	-0,35157	-0,39644	0,07785
-492,62	145,26	-0,35321	-0,39787	0,07860
-493,72	145,40	-0,35486	-0,39932	0,07945
-494,66	145,57	-0,35653	-0,40072	0,08038
-511,07	151,32	-0,40054	-0,43889	0,08713
-511,07	151,32	-0,40054	-0,43889	0,08781
-511,07	151,32	-0,40054	-0,43889	0,08895
-511,07	151,32	-0,40054	-0,43889	0,08945
-511,07	151,32	-0,40054	-0,43889	0,09002
-553,91	157,98	-0,47158	-0,50609	0,10995

Test CNV7

Borehole:	CAEST4-5
Depth of the sample [m]:	37.51
Type of test:	CIU - EU(2D) – s = constant stress path with drained phase
Triaxial Apparatus:	SRTA

LL:	33	Initial height [mm]:	136.2	Total unit weight [kN/m³]:	22.29
LP:	21	Initial diameter [mm]:	69.68	Dry unit weight [kN/m³]:	19.86
IC:	1.73	Initial volume [mm³]:	519377.7	e_o:	-
G_s:	-	Total weight [g]:	1180.3	W_n [%]:	12.3
$CaCO_3$ [%]:	-	Dry weight [g]:	1051.2		

Phase of the test:	FLUSHING	Final height [mm]:	136.20
		Final diameter [mm]:	69.68
		Final volume [mm³]:	519387.2
		Final Total weight [g]:	22.29
		e (end of flushing):	-
		σ_v (end of flushing) [kPa]:	151.9
		σ_h (end of flushing) [kPa]:	88.8
Phase of the test:	SATURATION	Final height [mm]:	136.19
		Final diameter [mm]:	69.67
		Final volume [mm³]:	519243.0
		Final Total weight [g]:	22.30
		e (end of saturation):	-
		Skempton's B parameter:	0.91
Phase of the test:	CONSOLIDATION	Final height [mm]:	134.93
		Final diameter [mm]:	68.79
		Final volume [mm³]:	501454.5
		Final Total weight [g]:	23.09
		e (end of consolidation):	-
		σ'_v (end of cons.) [kPa]:	760
		σ'_h (end of cons.) [kPa]:	760
		u_o [kPa]:	379
Phase of the test:	SHEARING	Final height [mm]:	136.01
		Final diameter [mm]:	68.42
		Final volume [mm³]:	500098.0
		Final Total weight [g]:	23.15
		e (end of stress path):	-
		t_{max} (end of stress path) [kPa]:	-319
		s'_{max} (end of stress path) [kPa]:	579
		Δu (end of stress path) [kPa]:	178

Phase of the test:	DRAINED	Final height [mm]:	135.87
		Final diameter [mm]:	68.31
		Final volume [mm^3]:	497991.8
		Final Total weight [g]:	23.25
		e (end of saturation):	-

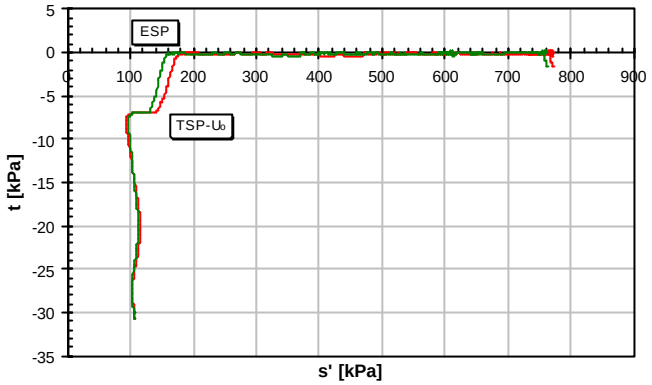

Figure A.17 Stress path during consolidation for CNV7 test.

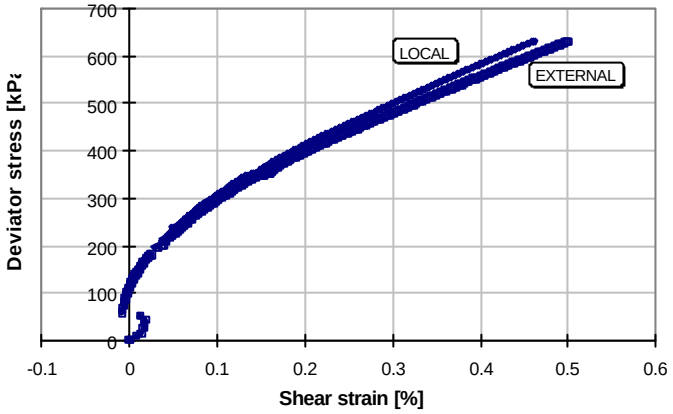

Figure A.18 Deviator stress versus shear strain for CNV7 test.

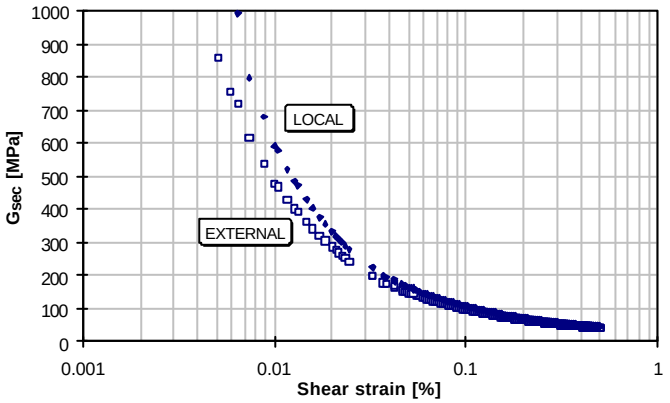

Figure A.19 Shear modulus versus external shear strain for CNV7 test.

Table A.9 Data for the shearing phase for test CNV7.

q [kPa]	Δu [kPa]	$\varepsilon_{a,l}$ [%]	$\varepsilon_{a,e}$ [%]	$\varepsilon_{r,l}$ [%]
-2.49	0.00	0.00000	0.00000	0.00000
-48.76	17.62	-0.00223	-0.00858	-0.01451
-94.58	27.03	-0.00898	-0.02055	-0.01487
-108.19	28.18	-0.01266	-0.02602	-0.01462
-122.87	30.57	-0.01756	-0.03332	-0.01445
-128.44	31.64	-0.01981	-0.03671	-0.01463
-138.93	34.48	-0.02427	-0.04326	-0.01316
-146.60	36.61	-0.02776	-0.04813	-0.01267
-161.84	40.83	-0.03411	-0.05712	-0.01206
-164.92	41.58	-0.03556	-0.05902	-0.01174
-180.43	45.62	-0.04302	-0.06844	-0.00896
-185.17	46.89	-0.04535	-0.07124	-0.00688
-203.82	55.44	-0.06105	-0.08773	-0.00238
-207.10	56.31	-0.06279	-0.08962	-0.00096
-223.83	59.88	-0.07074	-0.09919	0.00204
-228.56	60.96	-0.07378	-0.10272	0.00404
-239.24	64.25	-0.08085	-0.11058	-0.00117
-241.28	65.04	-0.08231	-0.11211	0.00722
-252.46	70.47	-0.09001	-0.11982	0.01072
-260.37	73.72	-0.09520	-0.12527	0.01290
-269.96	77.17	-0.10250	-0.13289	0.01579
-274.53	78.90	-0.10597	-0.13671	0.01676
-283.27	82.32	-0.11305	-0.14425	0.01951
-289.58	84.96	-0.11831	-0.14994	0.02215
-299.48	89.12	-0.12749	-0.15928	0.02526
-301.41	89.99	-0.12937	-0.16116	0.02558
-310.93	93.65	-0.13858	-0.17059	0.02929
-316.67	95.69	-0.14411	-0.17629	0.03058
-324.09	98.13	-0.15139	-0.18387	0.03283
-327.85	99.40	-0.15509	-0.18768	0.03412
-335.12	102.13	-0.16228	-0.19512	0.03629
-340.43	103.92	-0.16793	-0.20070	0.03790
-347.57	107.13	-0.17683	-0.20942	0.04062
-348.52	107.73	-0.17853	-0.21100	0.04112
-351.02	110.58	-0.18547	-0.21738	0.04319
-351.56	111.91	-0.18881	-0.22041	0.04404
-352.31	113.51	-0.19271	-0.22407	0.04405
-353.04	114.22	-0.19436	-0.22588	0.04558
-357.00	115.54	-0.19771	-0.23000	0.04344
-361.51	116.47	-0.20095	-0.23337	0.04530
-371.19	118.30	-0.20814	-0.24020	0.05015
-373.07	118.83	-0.20980	-0.24167	0.05108
-381.52	121.10	-0.21839	-0.24948	0.05501
-386.58	122.42	-0.22385	-0.25464	0.05722
-393.10	124.30	-0.23116	-0.26197	0.06112
-396.42	125.30	-0.23495	-0.26578	0.06226
-403.30	127.31	-0.24279	-0.27382	0.06608
-408.54	128.73	-0.24878	-0.27998	0.06879
-416.96	130.98	-0.25876	-0.29014	0.07308
-418.58	131.52	-0.26067	-0.29204	0.07412
-426.29	133.57	-0.27031	-0.30163	0.07805
-430.74	134.68	-0.27596	-0.30717	0.08037
-436.54	136.03	-0.28356	-0.31463	0.08394

-439.38	136.75	-0.28732	-0.31830	0.08605
-445.10	138.42	-0.29449	-0.32557	0.08905
-449.35	139.57	-0.29976	-0.33112	0.09151
-456.55	141.35	-0.30920	-0.34054	0.09573
-458.03	141.74	-0.31109	-0.34246	0.09687
-465.14	143.03	-0.32073	-0.35199	0.10055
-469.50	144.14	-0.32662	-0.35777	0.10308
-475.37	145.31	-0.33454	-0.36561	0.10648
-478.30	145.93	-0.33853	-0.36956	0.10776
-484.05	147.16	-0.34635	-0.37743	0.11119
-488.39	147.86	-0.35239	-0.38348	0.11383
-495.64	149.16	-0.36224	-0.39363	0.11762
-497.10	149.34	-0.36430	-0.39568	0.11805
-504.28	150.56	-0.37402	-0.40566	0.12176
-508.63	151.44	-0.38013	-0.41173	0.12376
-514.33	152.49	-0.38845	-0.41989	0.12727
-517.18	153.02	-0.39267	-0.42396	0.12852
-522.71	153.99	-0.40062	-0.43197	0.13112
-526.84	154.49	-0.40649	-0.43799	0.13341
-533.80	155.44	-0.41629	-0.44804	0.13684
-535.20	155.57	-0.41833	-0.45009	0.13734
-542.19	156.47	-0.42830	-0.46017	0.14098
-546.37	157.06	-0.43431	-0.46630	0.14355
-551.93	158.29	-0.44239	-0.47444	0.14598
-554.74	158.75	-0.44656	-0.47864	0.14773
-560.31	159.24	-0.45481	-0.48701	0.15005
-564.44	159.29	-0.46093	-0.49330	0.15245
-571.22	159.93	-0.47081	-0.50344	0.15566
-572.53	160.01	-0.47276	-0.50546	0.15613
-579.16	160.56	-0.48266	-0.51552	0.15945
-583.08	160.63	-0.48866	-0.52157	0.16188
-588.41	161.00	-0.49692	-0.52962	0.16431
-591.06	161.20	-0.50098	-0.53366	0.16595
-596.40	161.54	-0.50934	-0.54190	0.16816
-600.41	161.78	-0.51541	-0.54811	0.17024
-607.05	162.22	-0.52551	-0.55839	0.17409
-608.38	162.31	-0.52752	-0.56043	0.17456
-614.86	162.61	-0.53758	-0.57050	0.17799
-619.03	162.83	-0.54375	-0.57661	0.17963
-627.17	163.31	-0.55625	-0.58913	0.18374
-631.15	163.28	-0.56243	-0.59548	0.18617
-635.49	163.25	-0.56967	-0.60286	0.19020
-637.98	164.42	-0.57947	-0.61228	0.19145
-638.33	164.81	-0.58584	-0.61809	0.19385
-639.21	164.75	-0.58968	-0.62152	0.19470
-639.58	165.11	-0.59606	-0.62704	0.19624
-639.77	165.20	-0.59885	-0.62938	0.19717
-638.21	165.91	-0.60360	-0.63308	0.19828
-637.85	166.17	-0.60592	-0.63487	0.19895
-638.92	166.22	-0.61019	-0.63842	0.20060
-639.18	166.24	-0.61212	-0.64005	0.20163
-639.57	166.31	-0.61599	-0.64319	0.20271
-639.33	166.51	-0.61778	-0.64450	0.20317
-638.62	166.99	-0.62069	-0.64664	0.20399
-638.44	167.18	-0.62209	-0.64766	0.20424
-638.40	167.42	-0.62519	-0.64974	0.20492

-638.45	167.50	-0.62688	-0.65078	0.20531
-638.68	167.61	-0.62966	-0.65281	0.20599
-638.78	167.67	-0.63094	-0.65388	0.20628
-639.15	167.74	-0.63342	-0.65600	0.20688
-639.29	167.77	-0.63476	-0.65712	0.20724
-639.57	167.93	-0.63815	-0.65970	0.20810
-639.62	168.00	-0.63979	-0.66100	0.20856
-638.39	168.59	-0.64225	-0.66268	0.20906
-637.50	168.97	-0.64326	-0.66318	0.20946
-636.38	169.81	-0.64543	-0.66428	0.20992
-636.30	170.14	-0.64642	-0.66498	0.21010
-636.21	170.64	-0.64825	-0.66638	0.21049
-636.73	170.62	-0.64932	-0.66721	0.21046
-638.31	170.33	-0.65154	-0.66911	0.21121
-639.05	170.12	-0.65278	-0.67008	0.21146
-639.45	170.05	-0.65478	-0.67180	0.21178
-639.48	170.12	-0.65577	-0.67256	0.21189
-638.93	170.66	-0.65744	-0.67379	0.21267
-638.48	170.96	-0.65825	-0.67431	0.21278
-637.63	171.13	-0.65953	-0.67534	0.21317
-637.44	171.33	-0.66010	-0.67580	0.21299
-637.28	171.82	-0.66166	-0.67679	0.21360
-637.05	172.17	-0.66236	-0.67726	0.21378
-631.80	174.58	-0.66318	-0.67697	0.21442
-627.05	176.88	-0.66345	-0.67626	0.21410
-630.06	176.89	-0.66569	-0.67804	0.21560
-640.29	173.48	-0.66859	-0.68171	0.21617
-638.49	174.08	-0.66969	-0.68234	0.21646
-635.78	175.09	-0.67026	-0.68241	0.21660
-633.82	176.27	-0.67093	-0.68254	0.21671
-632.15	177.65	-0.67151	-0.68272	0.21699
-630.60	178.55	-0.67207	-0.68291	0.21699
-629.16	179.20	-0.67266	-0.68309	0.21707
-627.83	179.67	-0.67310	-0.68323	0.21724
-626.61	180.11	-0.67355	-0.68332	0.21735
-625.51	180.65	-0.67389	-0.68343	0.21739
-624.55	181.20	-0.67432	-0.68353	0.21739
-623.45	181.78	-0.67491	-0.68366	0.21749
-622.38	182.34	-0.67525	-0.68377	0.21760
-621.41	182.88	-0.67558	-0.68387	0.21764
-620.50	183.47	-0.67598	-0.68393	0.21757
-619.60	184.05	-0.67650	-0.68400	0.21767
-618.83	184.61	-0.67678	-0.68409	0.21764
-624.01	183.24	-0.67768	-0.68563	0.21774
-629.16	181.83	-0.67920	-0.68763	0.22003
-630.69	181.64	-0.68076	-0.68922	0.21989
-637.79	179.24	-0.68343	-0.69236	0.22193
-647.55	176.06	-0.68664	-0.69750	0.23600
-646.59	176.45	-0.68877	-0.70003	0.23515
-640.85	178.17	-0.68914	-0.69954	0.23497
-640.33	178.23	-0.68987	-0.69998	0.23515
-639.75	178.42	-0.69070	-0.70034	0.23518
-640.13	178.19	-0.69356	-0.70274	0.23679
-640.31	178.21	-0.69611	-0.70476	0.23708
-640.05	178.95	-0.69703	-0.70529	0.23725
-639.43	179.41	-0.69783	-0.70582	0.23750

-639.45	180.69	-0.70378	-0.71054	0.23783
-638.57	186.42	-0.72826	-0.72935	0.25022
-637.90	198.19	-0.76399	-0.75845	0.25775

Table A.10 Data for the drained phase for test CNV7.

q [kPa]	Δu [kPa]	$\varepsilon_{a,l}$ [%]	$\varepsilon_{a,e}$ [%]	$\varepsilon_{r,l}$ [%]
-643.07	175.15	-0.00009	0.00074	0.00018
-644.95	154.38	-0.00029	0.00130	0.00050
-648.39	123.22	-0.00057	0.00276	0.00054
-647.39	123.19	-0.00037	0.00495	0.00039
-645.27	123.18	0.00001	0.00683	0.00018
-641.15	123.20	0.00031	0.00877	-0.00014
-638.82	123.21	0.00062	0.01024	-0.00029
-638.92	123.18	0.00096	0.01108	-0.00050
-639.07	123.12	0.00152	0.01223	-0.00061
-639.19	123.03	0.00199	0.01368	-0.00111
-639.80	122.75	0.00247	0.01548	-0.00157
-639.48	122.53	0.00288	0.01682	-0.00164
-639.22	122.45	0.00317	0.01724	-0.00175
-639.22	122.35	0.00336	0.01761	-0.00172
-639.76	122.24	0.00365	0.01787	-0.00168
-639.53	122.16	0.00388	0.01824	-0.00175
-639.08	122.08	0.00403	0.01860	-0.00182
-639.28	121.72	0.00473	0.01966	-0.00186
-639.19	120.39	0.00677	0.02287	-0.00211
-639.13	119.75	0.00771	0.02426	-0.00218
-638.94	117.77	0.01054	0.02773	-0.00182
-639.01	116.51	0.01227	0.02961	-0.00150
-638.87	114.69	0.01483	0.03213	-0.00086
-638.89	114.11	0.01565	0.03288	-0.00065
-638.78	112.45	0.01796	0.03490	0.00003
-638.78	111.45	0.01930	0.03618	0.00053
-638.93	110.03	0.02119	0.03801	0.00132
-638.99	109.58	0.02181	0.03854	0.00157
-638.99	108.32	0.02356	0.04006	0.00225
-639.00	107.53	0.02470	0.04103	0.00275
-638.85	106.26	0.02674	0.04275	0.00353
-638.80	105.47	0.02793	0.04376	0.00375
-638.73	101.71	0.03353	0.04811	0.00739
-638.70	98.56	0.03772	0.05131	0.01000
-638.81	94.22	0.04321	0.05531	0.01353
-638.68	92.87	0.04484	0.05653	0.01464
-638.59	88.97	0.04934	0.05977	0.01757
-638.64	86.47	0.05183	0.06169	0.01946
-638.61	82.87	0.05514	0.06440	0.02225
-638.61	81.69	0.05618	0.06525	0.02314
-638.59	78.44	0.05907	0.06757	0.02539
-638.67	76.53	0.06072	0.06893	0.02682
-638.59	73.96	0.06301	0.07078	0.02875
-638.60	73.17	0.06365	0.07134	0.02947
-638.65	70.91	0.06529	0.07283	0.03111
-638.54	69.50	0.06625	0.07372	0.03225
-638.32	67.58	0.06779	0.07500	0.03411

-638.33	66.99	0.06826	0.07538	0.03457
-638.25	65.43	0.06974	0.07632	0.03582
-638.29	64.60	0.07054	0.07685	0.03672
-638.32	63.47	0.07173	0.07774	0.03782
-638.35	63.11	0.07210	0.07801	0.03818
-638.30	62.00	0.07293	0.07885	0.03947
-638.27	61.36	0.07352	0.07936	0.04015
-638.14	60.48	0.07449	0.08002	0.04118
-638.10	60.23	0.07481	0.08024	0.04161
-638.07	59.46	0.07589	0.08082	0.04261
-638.06	58.98	0.07656	0.08123	0.04343
-637.99	58.24	0.07749	0.08187	0.04422
-637.99	57.99	0.07774	0.08210	0.04440
-638.02	57.29	0.07858	0.08270	0.04540
-638.06	56.94	0.07895	0.08305	0.04600
-637.99	56.41	0.07959	0.08367	0.04711
-637.98	56.17	0.07982	0.08392	0.04747
-637.95	55.31	0.08107	0.08482	0.04818
-637.86	54.75	0.08196	0.08564	0.04879
-637.81	54.12	0.08263	0.08643	0.04968
-637.83	53.96	0.08258	0.08648	0.04993
-637.91	53.61	0.08261	0.08670	0.05018
-637.75	53.12	0.08283	0.08725	0.05104
-637.75	53.02	0.08294	0.08734	0.05140
-637.65	52.50	0.08354	0.08796	0.05247
-637.46	52.22	0.08452	0.08873	0.05365
-637.44	52.13	0.08472	0.08892	0.05408
-637.48	51.84	0.08519	0.08942	0.05504
-637.39	51.27	0.08623	0.09029	0.05633
-637.36	51.20	0.08628	0.09039	0.05650
-637.31	50.82	0.08710	0.09090	0.05704
-637.25	50.49	0.08771	0.09145	0.05804
-637.30	50.45	0.08789	0.09160	0.05836
-637.32	50.33	0.08824	0.09191	0.05893
-637.15	50.07	0.08896	0.09244	0.05975
-637.16	50.03	0.08916	0.09250	0.06004
-637.29	49.89	0.08951	0.09282	0.06058
-637.11	49.62	0.09000	0.09326	0.06129
-637.24	49.62	0.09009	0.09335	0.06143
-637.07	49.49	0.09043	0.09364	0.06179
-637.23	49.44	0.09141	0.09398	0.06258
-637.26	49.43	0.09147	0.09403	0.06275
-637.00	49.26	0.09218	0.09433	0.06318
-636.85	49.16	0.09282	0.09457	0.06383
-636.85	49.14	0.09305	0.09467	0.06393
-636.80	49.12	0.09334	0.09494	0.06425
-636.81	49.27	0.09341	0.09534	0.06515
-636.80	49.30	0.09345	0.09538	0.06526
-636.67	49.42	0.09329	0.09564	0.06543
-636.55	49.47	0.09311	0.09593	0.06586
-636.52	49.47	0.09302	0.09601	0.06601
-636.40	49.50	0.09307	0.09614	0.06608
-636.43	49.59	0.09350	0.09637	0.06686
-636.50	49.63	0.09364	0.09638	0.06679
-636.47	49.75	0.09391	0.09648	0.06711
-636.50	49.81	0.09435	0.09672	0.06768

-636.50	49.78	0.09457	0.09681	0.06783
-636.44	49.70	0.09481	0.09683	0.06818
-636.34	49.62	0.09576	0.09695	0.06897
-636.36	49.62	0.09591	0.09699	0.06893
-636.21	49.56	0.09621	0.09715	0.06922
-636.07	49.49	0.09689	0.09712	0.06972
-636.02	49.50	0.09711	0.09717	0.06990
-635.97	49.49	0.09738	0.09726	0.07047
-636.26	49.65	0.09799	0.09739	0.07086
-636.26	49.66	0.09804	0.09739	0.07083
-636.10	49.02	0.09845	0.09740	0.07108
-636.05	46.64	0.09871	0.09752	0.07154
-636.15	46.52	0.09858	0.09752	0.07172
-636.02	46.50	0.09852	0.09761	0.07193
-635.98	46.36	0.09809	0.09785	0.07236
-635.95	46.27	0.09801	0.09797	0.07258
-635.87	46.34	0.09750	0.09868	0.07293
-637.67	49.12	0.09273	0.09924	0.07386
-638.01	49.22	0.09287	0.09915	0.07411
-638.55	49.55	0.09294	0.09937	0.07476
-638.69	50.13	0.09384	0.09963	0.07501
-638.66	50.17	0.09397	0.09969	0.07515
-638.71	50.47	0.09421	0.09999	0.07536
-638.74	50.74	0.09471	0.09966	0.07554
-638.80	50.81	0.09508	0.09961	0.07565
-638.78	50.97	0.09559	0.09955	0.07586
-638.78	50.96	0.09713	0.09963	0.07622
-638.78	50.95	0.09730	0.09963	0.07618
-638.76	50.94	0.09779	0.09961	0.07633
-638.69	50.06	0.09761	0.09957	0.07676
-638.65	49.11	0.09761	0.09955	0.07701
-638.61	47.67	0.09796	0.09959	0.07718
-638.67	46.89	0.09847	0.09958	0.07772
-638.67	46.85	0.09848	0.09958	0.07779
-638.66	46.44	0.09864	0.09963	0.07801
-638.72	46.00	0.09839	0.09977	0.07826
-638.69	46.03	0.09816	0.09985	0.07854
-638.78	46.05	0.09727	0.10012	0.07886

Test CNV8

Borehole:	CAEST4-3
Depth of the sample [m]:	36.76
Type of test:	CIU – CL(3D) with drained phase
Triaxial Apparatus:	GDS

LL:	39	Initial height [mm]:	140.18	Total unit weight [kN/m^3]:	22.79
LP:	21	Initial diameter [mm]:	69.75	Dry unit weight [kN/m^3]:	20.49
IC:	1.54	Initial volume [mm^3]:	535629.3	e_o:	0.36
G_s:	2.839	Total weight [g]:	1244	W_n [%]:	11.2
$CaCO_3$ [%]:	22.3	Dry weight [g]:	1119		

Phase of the test:	FLUSHING	Final height [mm]:	140.94
		Final diameter [mm]:	69.10
		Final volume [mm^3]:	528610.4
		Final Total weight [g]:	23.09
		e (end of flushing):	0.34
		σ_v (end of flushing) [kPa]:	141
		σ_h (end of flushing) [kPa]:	153
Phase of the test:	SATURATION	Final height [mm]:	140.69
		Final diameter [mm]:	69.49
		Final volume [mm^3]:	533543.74
		Final Total weight [g]:	22.87
		e (end of saturation):	0.35
		Skempton's B parameter:	0.90
Phase of the test:	CONSOLIDATION	Final height [mm]:	139.54
		Final diameter [mm]:	69.11
		Final volume [mm^3]:	523403.81
		Final Total weight [g]:	23.32
		e (end of consolidation):	0.33
		σ'_v (end of cons.) [kPa]:	650
		σ'_h (end of cons.) [kPa]:	650
		u_o [kPa]:	350
Phase of the test:	SHEARING	Final height [mm]:	138.20
		Final diameter [mm]:	69.58
		Final volume [mm^3]:	525519.40
		Final Total weight [g]:	23.22
		e (end of stress path):	0.33
		t_{max} (end of stress path) [kPa]:	234
		s'_{max} (end of stress path) [kPa]:	656
		Δu (end of stress path) [kPa]:	98

Phase of the test:	DRAINED	Final height [mm]:	138.09
		Final diameter [mm]:	69.56
		Final volume [mm^3]:	524752.62
		Final Total weight [g]:	23.26
		e (end of saturation):	0.33

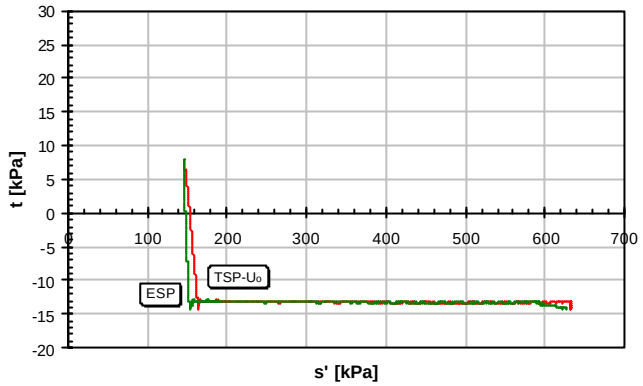

Figure A.20 Stress path during consolidation for CNV8 test.

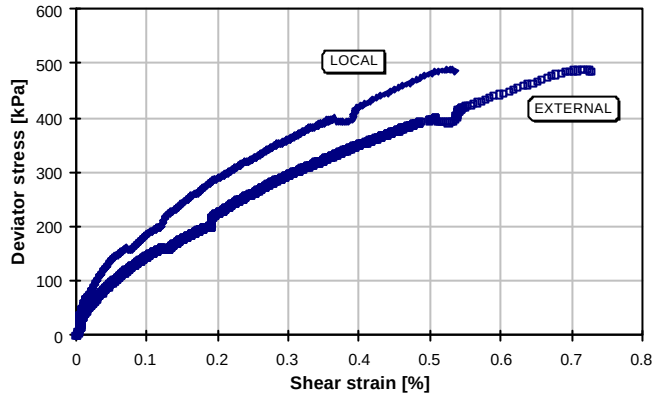

Figure A.21 Deviator stress versus shear strain for CNV8 test.

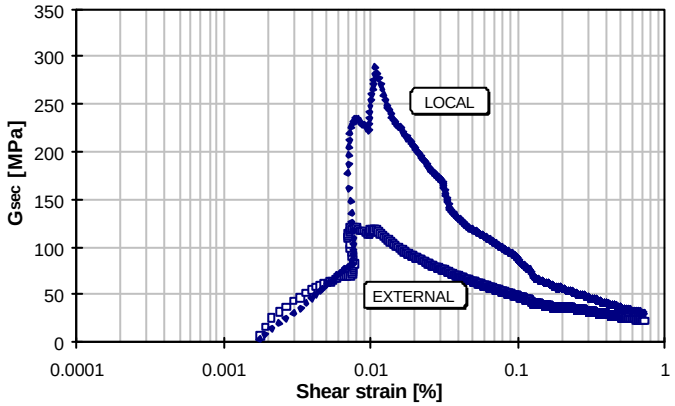

Figure A.22 Shear modulus versus external shear strain for CNV8 test.

Table A.11 Data for the shearing phase for test CNV8.

q [kPa]	Δu [kPa]	$\varepsilon_{a,l}$ [%]	$\varepsilon_{a,e}$ [%]	$\varepsilon_{r,l}$ [%]
0.00	0.00	0.00000	0.00000	0.00000
14.03	1.26	0.00596	0.00693	-0.00314
17.23	4.09	0.00651	0.00858	-0.00288
20.37	7.00	0.00710	0.01022	-0.00100
26.52	12.99	0.00822	0.01343	0.00235
31.84	18.57	0.00922	0.01600	0.00221
34.42	21.32	0.00981	0.01754	0.00268
39.47	26.69	0.01098	0.02088	0.00386
41.84	29.36	0.01163	0.02258	0.00324
44.34	32.03	0.01217	0.02415	0.00272
51.29	39.88	0.01324	0.02916	0.00107
53.75	42.55	0.01374	0.03055	0.00061
56.16	45.15	0.01424	0.03206	0.00010
58.46	47.76	0.01481	0.03360	-0.00044
62.89	53.07	0.01591	0.03736	-0.00152
65.26	55.79	0.01647	0.03928	-0.00205
69.56	61.03	0.01741	0.04206	-0.00297
73.33	65.87	0.01983	0.04487	-0.00396
75.32	68.34	0.02199	0.04676	-0.00451
77.20	70.78	0.02317	0.04860	-0.00507
79.29	73.22	0.02404	0.05051	-0.00567
81.31	75.74	0.02486	0.05224	-0.00628
87.22	83.15	0.02716	0.05710	-0.00797
88.94	85.45	0.02794	0.05892	-0.00855
90.87	87.77	0.02873	0.06067	-0.00910
95.00	92.54	0.03011	0.06419	-0.01016
97.06	95.02	0.03075	0.06616	-0.01077
99.01	97.49	0.03138	0.06806	-0.01140
102.63	102.19	0.03280	0.07191	-0.01253
106.27	106.79	0.03421	0.07565	-0.01360
108.06	109.10	0.03497	0.07755	-0.01418
109.75	111.38	0.03567	0.07930	-0.01477
113.29	115.88	0.03717	0.08322	-0.01595
116.58	120.22	0.03865	0.08708	-0.01713
118.13	122.30	0.03938	0.08851	-0.01764
119.68	124.42	0.04014	0.09028	-0.01827
124.70	130.93	0.04253	0.09590	-0.02011
126.27	132.96	0.04333	0.09791	-0.02069
127.82	134.95	0.04413	0.09995	-0.02128
129.37	136.99	0.04481	0.10198	-0.02193
134.11	143.15	0.04714	0.10794	-0.02390
135.70	145.22	0.04795	0.10984	-0.02449
137.33	147.24	0.04878	0.11191	-0.02512
138.92	149.20	0.04960	0.11383	-0.02577
143.06	154.88	0.05203	0.11932	-0.02776
144.54	156.91	0.05358	0.12125	-0.02846
146.13	159.00	0.05595	0.12333	-0.02917
148.96	162.86	0.05931	0.12781	-0.03058
151.61	166.49	0.06149	0.13158	-0.03194
154.07	169.92	0.06339	0.13528	-0.03405
155.43	171.73	0.06431	0.13734	-0.03566
156.92	173.63	0.06522	0.13917	-0.03660
159.38	178.25	0.06841	0.14571	-0.03950

157.81	178.34	0.07119	0.14943	-0.04349
161.48	181.45	0.07461	0.15356	-0.04621
163.40	183.57	0.07605	0.15527	-0.04706
168.43	189.43	0.07985	0.16100	-0.04939
169.84	191.21	0.08099	0.16267	-0.05007
171.38	193.01	0.08215	0.16474	-0.05082
174.47	196.76	0.08431	0.16864	-0.05232
177.03	200.19	0.08640	0.17293	-0.05382
179.69	203.55	0.08834	0.17707	-0.05531
181.06	205.10	0.08918	0.17906	-0.05604
182.37	206.67	0.09000	0.18112	-0.05677
185.89	211.53	0.09247	0.18671	-0.05891
187.05	213.01	0.09334	0.18860	-0.05964
189.80	216.16	0.09551	0.19275	-0.06114
191.15	217.96	0.09779	0.19490	-0.06197
194.41	222.51	0.10289	0.20089	-0.06424
195.54	223.95	0.10400	0.20282	-0.06503
196.75	225.41	0.10507	0.20474	-0.06576
198.89	228.46	0.10722	0.20919	-0.06683
199.21	230.41	0.10908	0.21282	-0.06788
199.47	231.51	0.11073	0.21623	-0.06887
200.76	232.06	0.11172	0.21754	-0.06949
206.53	231.11	0.11399	0.21715	-0.06999
220.43	225.81	0.12009	0.22148	-0.07188
222.60	224.77	0.12173	0.22426	-0.07278
225.98	223.41	0.12476	0.22911	-0.07450
227.68	222.78	0.12627	0.23176	-0.07523
231.62	221.70	0.13433	0.23915	-0.07600
234.02	220.84	0.13639	0.24146	-0.07682
235.71	220.12	0.13817	0.24398	-0.07769
238.30	219.29	0.14136	0.24904	-0.07933
242.61	217.74	0.14456	0.25415	-0.08093
246.35	216.40	0.14754	0.25903	-0.08240
247.78	215.80	0.14905	0.26157	-0.08328
249.34	215.29	0.15055	0.26431	-0.08421
253.32	214.10	0.15464	0.27191	-0.08655
255.96	213.04	0.15623	0.27458	-0.08716
258.39	212.21	0.15988	0.27960	-0.08905
259.57	211.89	0.16279	0.28209	-0.09003
263.54	210.53	0.16919	0.28956	-0.09215
265.22	209.77	0.17095	0.29230	-0.09272
267.41	209.06	0.17260	0.29509	-0.09281
271.01	207.76	0.17581	0.29992	-0.09396
272.25	207.12	0.17846	0.30504	-0.09526
278.05	204.94	0.18304	0.31260	-0.09771
279.32	204.40	0.18461	0.31528	-0.09852
284.28	202.37	0.18918	0.32312	-0.10056
285.95	201.62	0.19070	0.32570	-0.10150
287.72	201.03	0.19382	0.33066	-0.10352
289.40	200.64	0.19704	0.33321	-0.10465
294.24	198.60	0.20480	0.34129	-0.10802
297.42	197.38	0.20856	0.34667	-0.11012
300.62	195.86	0.21196	0.35193	-0.11219
302.21	195.05	0.21481	0.35708	-0.11367
306.04	193.64	0.21795	0.36259	-0.11502
307.19	193.07	0.21943	0.36509	-0.11613

307.67	192.60	0.22067	0.36765	-0.11720
310.88	191.39	0.22470	0.37482	-0.12004
311.42	191.18	0.22598	0.37747	-0.12122
317.77	188.29	0.23075	0.38539	-0.12388
318.32	188.05	0.23734	0.39267	-0.12637
320.87	187.38	0.24079	0.39501	-0.12697
323.31	186.48	0.24323	0.39765	-0.12766
325.88	185.05	0.24687	0.40264	-0.12957
328.11	183.81	0.25025	0.40794	-0.13163
332.73	181.76	0.25485	0.41583	-0.13443
333.81	181.27	0.25629	0.41844	-0.13551
337.89	179.12	0.26081	0.42599	-0.13828
339.15	178.54	0.26219	0.42828	-0.13923
340.51	177.62	0.26506	0.43328	-0.14135
341.63	177.17	0.26652	0.43595	-0.14239
346.97	174.59	0.27104	0.44395	-0.14531
348.67	173.66	0.27354	0.44905	-0.14717
351.53	172.33	0.27622	0.45425	-0.14880
353.16	171.51	0.28167	0.45982	-0.15095
355.25	170.59	0.28744	0.46518	-0.15308
356.70	169.92	0.28948	0.46775	-0.15415
358.58	169.15	0.29145	0.47056	-0.15525
362.90	166.79	0.29703	0.47893	-0.15900
364.74	165.83	0.29874	0.48166	-0.16048
367.47	164.08	0.30308	0.48936	-0.16404
371.03	162.25	0.30737	0.49688	-0.16682
371.99	161.62	0.30875	0.49962	-0.16759
373.38	160.96	0.31021	0.50240	-0.16851
375.85	159.60	0.31293	0.50735	-0.17047
377.58	158.84	0.31555	0.51230	-0.17239
380.67	157.16	0.31845	0.51701	-0.17400
382.49	156.04	0.32315	0.52239	-0.17623
385.45	154.56	0.33083	0.52959	-0.18030
386.11	154.08	0.33252	0.53206	-0.18098
388.81	152.58	0.33575	0.53708	-0.18264
389.89	152.17	0.33730	0.53972	-0.18353
397.17	153.73	0.35138	0.56366	-0.19223
398.57	152.11	0.35287	0.56639	-0.19323
393.86	153.55	0.35729	0.56904	-0.19584
401.70	147.30	0.37938	0.59717	-0.20826
413.27	141.13	0.38236	0.60111	-0.20915
418.09	137.24	0.38529	0.60759	-0.21147
425.76	131.44	0.39487	0.62439	-0.21750
470.16	101.90	0.46258	0.72718	-0.25953

Table A.12 Data for the drained phase for test CNV8.

q [kPa]	Δu [kPa]	$\varepsilon_{a,l}$ [%]	$\varepsilon_{a,e}$ [%]	$\varepsilon_{r,l}$ [%]
485.45	100.63	0.00000	0.00000	0.00000
485.30	94.31	0.00019	0.00046	-0.00001
485.39	87.04	0.00047	0.00081	-0.00001
485.44	80.06	0.00071	0.00108	0.00004
485.35	71.62	0.00093	0.00140	0.00013
485.31	65.07	0.00123	0.00201	0.00020

485.28	59.13	0.00159	0.00252	0.00030
485.16	48.72	0.00374	0.00450	0.00063
484.86	35.56	0.00961	0.00883	0.00198
484.80	22.22	0.01782	0.01460	0.00409
484.49	10.95	0.02752	0.02123	0.00660
484.59	6.33	0.03552	0.02657	0.00888
484.73	4.03	0.04113	0.03078	0.01024
484.84	2.74	0.04540	0.03393	0.01118
484.72	1.91	0.04874	0.03651	0.01170
484.76	1.35	0.05138	0.03879	0.01208
484.74	0.98	0.05366	0.04073	0.01231
484.59	0.72	0.05542	0.04224	0.01256
484.57	0.52	0.05703	0.04370	0.01280
484.35	0.34	0.05844	0.04496	0.01304
484.29	0.20	0.06042	0.04619	0.01324
484.43	0.07	0.06293	0.04743	0.01336
484.37	-0.03	0.06545	0.04838	0.01360
484.31	-0.11	0.06797	0.04926	0.01407
484.28	-0.21	0.06932	0.05023	0.01458
484.19	-0.27	0.07043	0.05108	0.01514
484.28	-0.32	0.07140	0.05192	0.01538
484.20	-0.29	0.07233	0.05274	0.01552
484.09	-0.29	0.07319	0.05347	0.01560
484.31	-0.32	0.07396	0.05420	0.01567
484.33	-0.37	0.07466	0.05493	0.01575
484.31	-0.40	0.07529	0.05545	0.01583
484.33	-0.43	0.07595	0.05590	0.01591
484.41	-0.40	0.07659	0.05655	0.01593
484.28	-0.37	0.07721	0.05718	0.01593
484.38	-0.38	0.07777	0.05797	0.01594
484.53	-0.40	0.07831	0.05854	0.01593
484.49	-0.41	0.07880	0.05909	0.01598
484.55	-0.21	0.07929	0.05980	0.01595
484.56	-0.01	0.07972	0.06020	0.01591
484.35	-0.01	0.08021	0.06084	0.01588
484.35	-0.14	0.08069	0.06135	0.01591
484.30	-0.43	0.08119	0.06185	0.01594
484.43	-0.50	0.08163	0.06236	0.01597
484.51	-0.51	0.08205	0.06283	0.01598
484.30	-0.54	0.08247	0.06325	0.01594
484.43	-0.59	0.08287	0.06364	0.01596
484.41	-0.66	0.08326	0.06410	0.01596
484.32	-0.67	0.08364	0.06456	0.01596
484.32	-0.72	0.08403	0.06484	0.01599
484.24	-0.76	0.08441	0.06514	0.01603
484.08	-0.78	0.08476	0.06546	0.01604
484.09	-0.79	0.08513	0.06605	0.01602
484.11	-0.75	0.08544	0.06663	0.01599
484.12	-0.75	0.08578	0.06695	0.01600
484.22	-0.76	0.08606	0.06733	0.01602
484.23	-0.78	0.08638	0.06757	0.01604
484.17	-0.78	0.08667	0.06785	0.01609
484.20	-0.74	0.08696	0.06824	0.01610
484.12	-0.74	0.08731	0.06851	0.01613
484.15	-0.75	0.08759	0.06877	0.01616
484.23	-0.77	0.08794	0.06903	0.01614

484.26	-0.75	0.08829	0.06937	0.01613
484.37	-0.69	0.08854	0.06953	0.01611
484.31	-0.67	0.08881	0.06998	0.01608
484.18	-0.64	0.08911	0.07015	0.01608
484.19	-0.68	0.08938	0.07049	0.01608
484.25	-0.71	0.08963	0.07091	0.01606
484.35	-0.74	0.08985	0.07106	0.01611
484.39	-0.81	0.09017	0.07144	0.01615
484.22	-0.84	0.09037	0.07166	0.01621
484.11	-0.85	0.09064	0.07204	0.01623
484.11	-0.86	0.09087	0.07216	0.01628
484.15	-0.85	0.09109	0.07246	0.01629
484.12	-0.85	0.09129	0.07275	0.01632
484.24	-0.86	0.09146	0.07298	0.01636
484.28	-0.86	0.09167	0.07335	0.01637
484.42	-0.85	0.09191	0.07344	0.01643
484.36	-0.78	0.09219	0.07380	0.01643
484.31	-0.72	0.09244	0.07415	0.01645
484.32	-0.61	0.09265	0.07456	0.01648
484.20	-0.46	0.09284	0.07500	0.01649
484.21	-0.18	0.09309	0.07528	0.01649
484.27	-0.11	0.09338	0.07555	0.01646
484.24	-0.13	0.09367	0.07611	0.01643
484.33	-0.35	0.09396	0.07651	0.01642
484.34	-0.56	0.09419	0.07686	0.01646
484.20	-0.60	0.09444	0.07709	0.01648
484.14	-0.63	0.09471	0.07708	0.01651
484.09	-0.66	0.09493	0.07743	0.01647
482.35	-0.61	0.09529	0.07797	0.01633

Test CNV9

Borehole:	CAEST3-1
Depth of the sample [m]:	45.17
Type of test:	CIU – CL(3D) sheared in 3D conditions
Testing apparatus:	SRTA

LL:	63	Initial height [mm]:	132.10	Total unit weight [kN/m^3]:	22.43
LP:	23	Initial diameter [mm]:	69.80	Dry unit weight [kN/m^3]:	20.50
IC:	1.34	Initial volume [mm^3]:	505479.5	e_o:	0.29
G_s:	2.69	Total weight [g]:	1155.6	W_n [%]:	9.39
$CaCO_3$ [%]:	1.9	Dry weight [g]:	1056.4		

Phase of the test:	FLUSHING	Final height [mm]:	132.10
		Final diameter [mm]:	69.80
		Final volume [mm^3]:	505468.45
		Final Total weight [g]:	22.43
		e (end of flushing):	0.29
		σ_v (end of flushing) [kPa]:	171.12
		σ_h (end of flushing) [kPa]:	126.46
Phase of the test:	SATURATION	Final height [mm]:	132.19
		Final diameter [mm]:	69.64
		Final volume [mm^3]:	507870.98
		Final Total weight [g]:	22.32
		e (end of saturation):	0.29
		Skempton's B parameter:	0.78
Phase of the test:	CONSOLIDATION	Final height [mm]:	131.68
		Final diameter [mm]:	69.46
		Final volume [mm^3]:	499018.32
		Final Total weight [g]:	22.72
		e (end of consolidation):	0.27
		σ'_v (end of cons.) [kPa]:	1150
		σ'_h (end of cons.) [kPa]:	1150
		u_o [kPa]:	553
Phase of the test:	SHEARING	t_{max} (end of stress path) [kPa]:	317
		s'_{max} (end of stress path) [kPa]:	735
		Δu (end of stress path) [kPa]:	-43

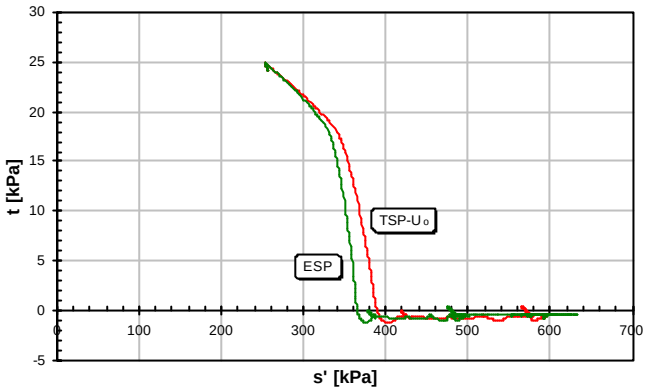

Figure A.23 Stress path during consolidation for CNV9 test.

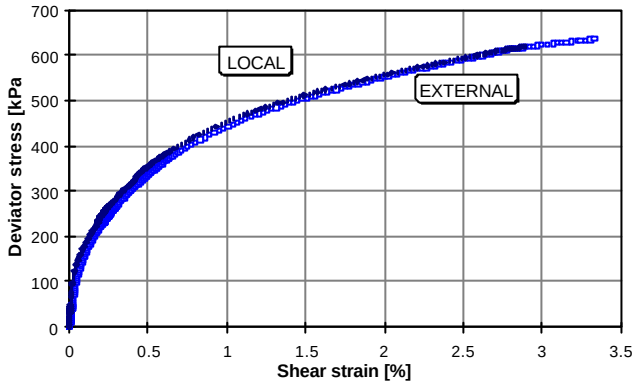

Figure A.24 Deviator stress versus shear strain for CNV9 test.

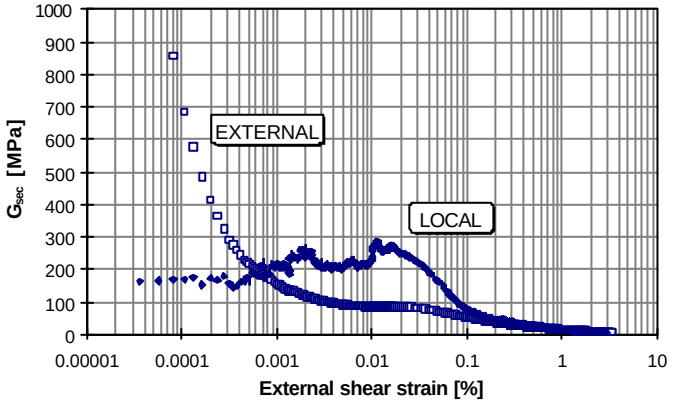

Figure A.25 Shear modulus versus external shear strain for CNV9 test.

Table A.13 Data for the shearing phase for test CNV9.

q [kPa]	Δu [kPa]	$\varepsilon_{a,l}$ [%]	$\varepsilon_{a,e}$ [%]	$\varepsilon_{r,l}$ [%]
-0.76	3.35	0.00000	0.00000	0.00000
-0.76	3.37	0.00036	-0.00006	0.00012
-0.78	3.35	0.00015	-0.00005	0.00017
-0.92	3.40	0.00028	-0.00007	0.00023
-0.94	3.42	0.00027	-0.00006	0.00026
-0.94	3.44	0.00042	-0.00006	0.00026
-0.97	3.48	0.00051	-0.00005	0.00027
-0.89	3.50	0.00064	-0.00004	0.00025
-0.82	3.50	0.00062	-0.00004	0.00023
-0.64	3.50	0.00075	-0.00003	0.00021
-0.40	3.51	0.00071	-0.00004	0.00025
-0.11	3.52	0.00069	-0.00002	0.00029
0.20	3.54	0.00060	0.00001	0.00034
0.45	3.54	0.00056	0.00009	0.00038
0.69	3.55	0.00070	0.00018	0.00038
0.89	3.56	0.00081	0.00028	0.00038
1.05	3.58	0.00096	0.00036	0.00038
1.27	3.59	0.00097	0.00045	0.00036
1.50	3.60	0.00098	0.00053	0.00033
1.80	3.62	0.00106	0.00065	0.00029
2.07	3.64	0.00124	0.00077	0.00026
2.37	3.63	0.00118	0.00091	0.00023
2.66	3.64	0.00111	0.00103	0.00022
3.26	3.66	0.00118	0.00131	0.00021
3.64	3.81	0.00144	0.00171	0.00041
4.32	3.91	0.00145	0.00206	0.00028
4.71	4.07	0.00172	0.00234	0.00033
5.05	4.35	0.00177	0.00271	0.00058
5.79	4.54	0.00174	0.00310	0.00047
6.60	4.72	0.00187	0.00352	0.00036
7.43	4.99	0.00219	0.00404	0.00032
8.48	5.23	0.00238	0.00459	0.00011
9.66	5.52	0.00254	0.00527	0.00000
10.95	5.83	0.00259	0.00601	-0.00017
12.36	6.15	0.00288	0.00678	-0.00032
13.93	6.52	0.00288	0.00764	-0.00048
15.52	6.91	0.00292	0.00851	-0.00067
17.19	7.31	0.00341	0.00942	-0.00081
18.98	7.71	0.00364	0.01040	-0.00096
21.20	8.12	0.00363	0.01138	-0.00155
23.46	8.57	0.00370	0.01258	-0.00173
25.49	9.19	0.00351	0.01390	-0.00146
27.60	9.80	0.00351	0.01512	-0.00155
29.89	10.43	0.00402	0.01639	-0.00165
32.25	11.12	0.00472	0.01775	-0.00174
34.62	11.83	0.00504	0.01915	-0.00179
36.85	12.60	0.00537	0.02051	-0.00178
39.23	13.48	0.00570	0.02195	-0.00170
41.85	14.33	0.00615	0.02339	-0.00171
49.51	17.00	0.00845	0.02796	-0.00152
68.77	25.13	0.01426	0.04095	-0.00082
94.20	38.70	0.02472	0.06163	-0.00099
118.28	54.78	0.03931	0.08592	-0.00313

138.96	71.12	0.06294	0.11095	-0.00586
157.12	87.19	0.08987	0.13648	-0.00949
173.09	102.70	0.11495	0.16228	-0.01388
187.40	117.55	0.14040	0.18833	-0.01877
200.42	131.52	0.16642	0.21448	-0.02420
212.46	144.63	0.19258	0.24069	-0.02950
223.67	156.97	0.21830	0.26694	-0.03474
230.53	166.79	0.23177	0.28895	-0.03935
232.20	170.59	0.23059	0.29766	-0.04128
234.11	171.24	0.23228	0.29940	-0.04174
235.53	171.85	0.23354	0.30107	-0.04224
236.71	172.40	0.23476	0.30281	-0.04277
237.75	172.88	0.23657	0.30450	-0.04340
238.72	173.31	0.23835	0.30610	-0.04402
239.67	173.73	0.23988	0.30777	-0.04457
240.50	174.10	0.24147	0.30937	-0.04515
241.31	174.45	0.24309	0.31105	-0.04578
242.13	174.83	0.24505	0.31287	-0.04629
242.83	175.23	0.24676	0.31459	-0.04674
243.54	175.63	0.24850	0.31628	-0.04723
244.25	176.01	0.25019	0.31799	-0.04774
244.97	176.28	0.25155	0.31958	-0.04841
245.63	176.48	0.25353	0.32115	-0.04903
246.31	176.73	0.25545	0.32282	-0.04959
247.03	176.97	0.25700	0.32450	-0.05020
247.68	177.26	0.25902	0.32621	-0.05074
248.39	177.52	0.26048	0.32802	-0.05134
249.12	177.71	0.26193	0.32980	-0.05194
249.73	177.97	0.26351	0.33150	-0.05241
250.34	178.20	0.26531	0.33316	-0.05292
251.00	178.42	0.26691	0.33486	-0.05339
251.70	178.65	0.26850	0.33654	-0.05387
252.37	178.85	0.27029	0.33821	-0.05440
253.06	179.03	0.27201	0.33998	-0.05495
253.83	179.18	0.27361	0.34177	-0.05555
254.49	179.36	0.27515	0.34349	-0.05608
255.15	179.45	0.27678	0.34510	-0.05672
255.74	179.53	0.27850	0.34682	-0.05730
256.37	179.73	0.28020	0.34865	-0.05777
257.02	179.92	0.28149	0.35037	-0.05820
257.62	180.14	0.28276	0.35206	-0.05865
258.20	180.34	0.28413	0.35369	-0.05919
258.83	180.53	0.28625	0.35536	-0.05977
259.56	180.69	0.28825	0.35710	-0.06031
260.23	180.86	0.28977	0.35883	-0.06074
260.88	180.98	0.29149	0.36048	-0.06126
261.40	181.09	0.29320	0.36220	-0.06176
261.86	181.23	0.29509	0.36390	-0.06227
262.49	181.35	0.29664	0.36560	-0.06282
263.16	181.50	0.29804	0.36735	-0.06328
263.68	181.53	0.30003	0.36897	-0.06392
264.22	181.56	0.30191	0.37066	-0.06453
264.80	181.71	0.30313	0.37245	-0.06495
265.46	181.86	0.30496	0.37426	-0.06548
266.09	181.96	0.30681	0.37600	-0.06608
266.82	182.09	0.30874	0.37821	-0.06672

272.71	182.78	0.32683	0.39556	-0.07177
284.03	183.39	0.36047	0.42998	-0.08190
294.94	183.15	0.39266	0.46499	-0.09204
305.23	182.48	0.42710	0.49986	-0.10168
314.98	181.38	0.46454	0.53485	-0.11099
324.15	179.83	0.49781	0.56975	-0.12007
333.01	177.97	0.51387	0.60460	-0.12888
341.62	175.93	0.53630	0.63959	-0.13727
349.74	173.77	0.57293	0.67483	-0.14535
358.07	171.27	0.61258	0.71292	-0.15373
367.27	168.39	0.65548	0.75481	-0.16266
375.13	165.76	0.69430	0.79386	-0.17052
390.20	159.41	0.78187	0.88229	-0.18661
418.64	145.70	0.96561	1.07224	-0.21766
447.55	129.37	1.18828	1.30180	-0.25077
471.18	113.24	1.41286	1.52486	-0.28013
491.07	97.54	1.63693	1.74467	-0.30694
508.67	82.49	1.86028	1.96446	-0.33254
524.69	68.35	2.08644	2.18414	-0.35761
539.85	53.46	2.31932	2.40824	-0.38317
554.13	40.84	2.54646	2.63066	-0.40714
567.12	33.09	2.76655	2.84799	-0.42950
579.39	23.89	2.98862	3.06599	-0.45477
591.11	6.64	3.22197	3.29268	-0.47433
601.31	-9.78	3.45914	3.51022	-0.44807
609.79	-19.50	3.68266	3.70815	-0.39859
614.42	-23.98	3.81370	3.83146	-0.38154
616.51	-26.07	3.88404	3.89671	-0.39088
622.58	-31.36	-	4.07847	-0.41892
63.78	-43.19	-	4.48943	-0.50981

Test CNV10

Borehole:	CAEST3-1
Depth of the sample [m]:	44.87
Type of test:	CIU – EU(2D) with drained phase
Triaxial Apparatus:	SRTA

LL:	63	Initial height [mm]:	133.9	Total unit weight [kN/m^3]:	20.75
LP:	23	Initial diameter [mm]:	69.7	Dry unit weight [kN/m^3]:	17.22
IC:	1.06	Initial volume [mm^3]:	510900.1	e_o:	0.53
G_s:	2.69	Total weight [g]:	1080.9	W_n [%]:	20.52
$CaCO_3$ [%]:	1.9	Dry weight [g]:	896.9		

Phase of the test:	FLUSHING	Final height [mm]:	133.91
		Final diameter [mm]:	69.72
		Final volume [mm^3]:	511300.9
		Final Total weight [g]:	20.74
		e (end of flushing):	0.53
		σ_v (end of flushing) [kPa]:	208
		σ_h (end of flushing) [kPa]:	213
Phase of the test:	SATURATION	Final height [mm]:	133.93
		Final diameter [mm]:	69.62
		Final volume [mm^3]:	509827.7
		Final Total weight [g]:	20.80
		e (end of saturation):	0.53
		Skempton's B parameter:	0.88
Phase of the test:	CONSOLIDATION	Final height [mm]:	132.48
		Final diameter [mm]:	69.04
		Final volume [mm^3]:	495922.3
		Final Total weight [g]:	21.38
		e (end of consolidation):	0.49
		σ'_v (end of cons.) [kPa]:	695
		σ'_h (end of cons.) [kPa]:	695
		u_o [kPa]:	405
Phase of the test:	SHEARING	Final height [mm]:	135.81
		Final diameter [mm]:	69.12
		Final volume [mm^3]:	509660.6
		Final Total weight [g]:	20.81
		e (end of stress path):	0.53
		t_{max} (end of stress path) [kPa]:	-132
		s'_{max} (end of stress path) [kPa]:	479
		Δu (end of stress path) [kPa]:	124

Phase of the test:	DRAINED	Final height [mm]:	135.75
		Final diameter [mm]:	69.09
		Final volume [mm^3]:	508902.3
		Final Total weight [g]:	20.84
		e (end of saturation):	0.53

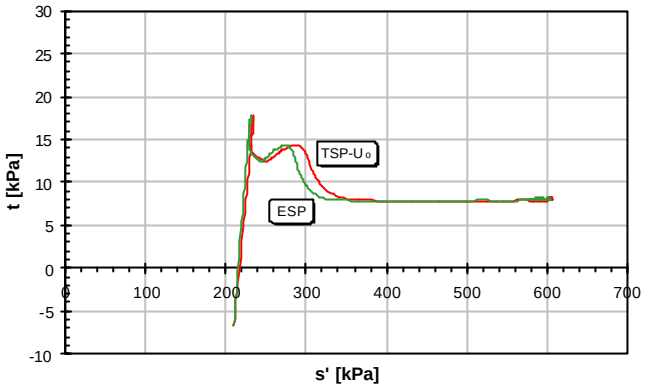

Figure A.26 Stress path during consolidation for CNV10 test.

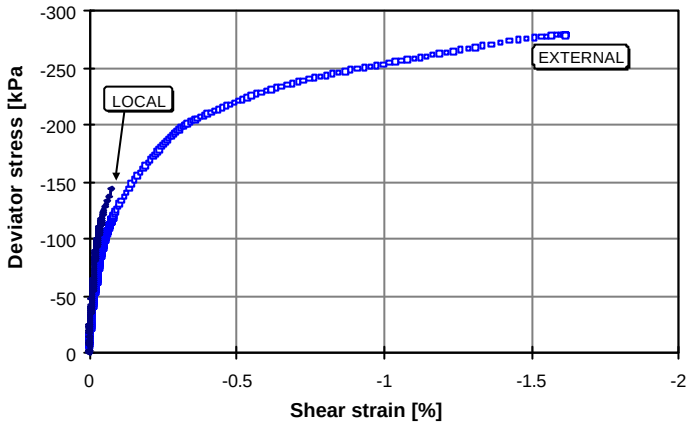

Figure A.27 Deviator stress versus shear strain for CNV10 test.

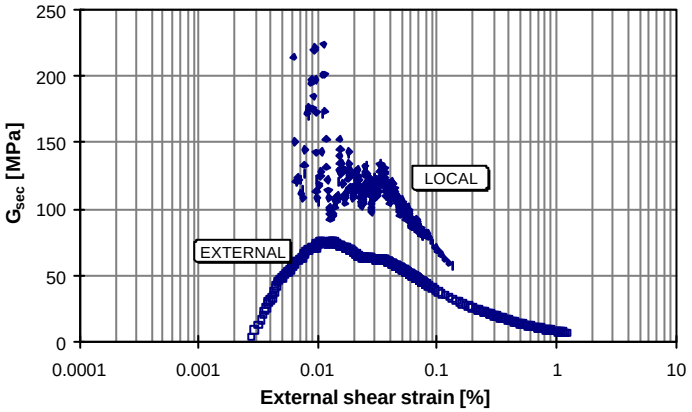

Figure A.28 Shear modulus versus external shear strain for CNV10 test.

Table A.15 Data for the shearing phase for test CNV10.

q [kPa]	Δu [kPa]	$\varepsilon_{a,l}$ [%]	$\varepsilon_{a,e}$ [%]	$\varepsilon_{r,l}$ [%]
-14.64	0.00	0.00000	0.00000	0.00000
-13.13	0.07	-0.00481	0.00043	-0.00026
-3.75	0.63	-0.00456	0.00372	-0.00075
-1.20	0.73	-0.00111	0.00475	-0.00078
-1.20	0.50	0.00162	0.00516	-0.00068
-1.28	0.50	0.00075	0.00530	-0.00065
-1.41	0.68	-0.00216	0.00530	-0.00068
-1.33	0.86	-0.00153	0.00530	-0.00062
-0.80	1.32	0.00181	0.00530	-0.00049
-0.48	1.54	0.00136	0.00516	-0.00055
0.21	1.86	0.00134	0.00455	-0.00097
-0.75	1.86	0.00132	0.00365	-0.00130
-3.03	1.63	0.00014	0.00117	-0.00208
-4.52	1.68	0.00042	-0.00028	-0.00234
-5.99	2.45	0.00185	-0.00165	-0.00205
-7.08	2.86	0.00119	-0.00207	-0.00172
-9.02	3.04	-0.00193	-0.00296	-0.00153
-9.98	3.04	-0.00123	-0.00331	-0.00149
-12.32	3.27	0.00022	-0.00413	-0.00123
-13.89	3.59	0.00052	-0.00461	-0.00094
-16.71	3.91	0.00234	-0.00578	-0.00062
-17.86	3.77	0.00086	-0.00627	-0.00065
-19.96	3.54	-0.00241	-0.00709	-0.00052
-21.10	3.68	-0.00351	-0.00744	-0.00042
-23.23	4.13	-0.00178	-0.00840	-0.00020
-24.19	4.22	-0.00090	-0.00888	-0.00010
-26.35	4.27	-0.00481	-0.00971	0.00003
-27.46	4.36	-0.00516	-0.01026	0.00013
-30.05	4.72	-0.00544	-0.01116	0.00036
-31.32	4.91	-0.00443	-0.01171	0.00042
-33.69	5.22	-0.00485	-0.01288	0.00058
-34.57	5.27	-0.00373	-0.01343	0.00078
-36.51	5.50	-0.00932	-0.01398	0.00078
-37.44	5.50	-0.00882	-0.01446	0.00081
-39.33	5.59	-0.00522	-0.01556	0.00094
-40.32	5.86	-0.00632	-0.01611	0.00107
-42.39	6.36	-0.01242	-0.01735	0.00130
-43.46	6.31	-0.01431	-0.01777	0.00133
-45.08	6.27	-0.01440	-0.01866	0.00156
-45.85	6.36	-0.01269	-0.01928	0.00172
-47.37	6.50	-0.01073	-0.02045	0.00198
-48.04	6.63	-0.00937	-0.02093	0.00214
-49.47	6.86	-0.01215	-0.02190	0.00247
-50.24	6.81	-0.01394	-0.02245	0.00256
-51.84	7.00	-0.01233	-0.02362	0.00289
-52.51	7.22	-0.01028	-0.02417	0.00299
-53.78	7.50	-0.01216	-0.02520	0.00324
-54.48	7.50	-0.01384	-0.02582	0.00344
-55.70	7.50	-0.01216	-0.02693	0.00389
-56.10	7.50	-0.01383	-0.02761	0.00399
-56.87	7.50	-0.01348	-0.02906	0.00396
-57.38	7.50	-0.01506	-0.02954	0.00393
-58.79	7.68	-0.01693	-0.03058	0.00412

-59.51	7.95	-0.01697	-0.03099	0.00425
-60.97	8.31	-0.01530	-0.03230	0.00438
-61.53	8.27	-0.01355	-0.03299	0.00422
-62.73	8.31	-0.01486	-0.03429	0.00419
-63.44	8.41	-0.01651	-0.03491	0.00412
-64.75	8.31	-0.01815	-0.03595	0.00389
-65.31	8.18	-0.01669	-0.03657	0.00373
-66.58	8.22	-0.01992	-0.03774	0.00357
-67.12	8.36	-0.02286	-0.03843	0.00354
-68.31	8.50	-0.02172	-0.03946	0.00347
-68.98	8.50	-0.02092	-0.04022	0.00341
-70.68	8.63	-0.02062	-0.04153	0.00331
-71.40	8.91	-0.02082	-0.04221	0.00337
-72.49	9.41	-0.02297	-0.04338	0.00347
-73.10	9.50	-0.02199	-0.04394	0.00328
-74.41	9.50	-0.02350	-0.04490	0.00292
-75.26	9.50	-0.02371	-0.04552	0.00298
-77.15	9.50	-0.02004	-0.04669	0.00337
-78.11	9.50	-0.02041	-0.04717	0.00354
-79.44	9.59	-0.02355	-0.04827	0.00363
-80.00	9.86	-0.02372	-0.04882	0.00376
-81.19	10.41	-0.02164	-0.05006	0.00393
-81.75	10.50	-0.02307	-0.05068	0.00399
-82.92	10.50	-0.02598	-0.05172	0.00415
-83.48	10.50	-0.02725	-0.05234	0.00412
-84.81	10.72	-0.02673	-0.05365	0.00422
-85.43	10.86	-0.02756	-0.05447	0.00422
-86.68	11.18	-0.02993	-0.05578	0.00438
-87.24	11.27	-0.02763	-0.05633	0.00444
-88.41	11.72	-0.02645	-0.05743	0.00467
-88.97	11.86	-0.02627	-0.05798	0.00490
-89.98	12.00	-0.02745	-0.05929	0.00545
-90.46	12.00	-0.02837	-0.06005	0.00561
-91.76	12.00	-0.02962	-0.06143	0.00574
-92.27	12.04	-0.03096	-0.06205	0.00584
-93.30	12.50	-0.03071	-0.06322	0.00626
-94.02	12.77	-0.03029	-0.06384	0.00639
-95.06	13.00	-0.03270	-0.06528	0.00668
-95.54	13.00	-0.03477	-0.06590	0.00672
-96.44	13.00	-0.03408	-0.06714	0.00675
-97.00	13.00	-0.03368	-0.06776	0.00688
-98.01	13.09	-0.03263	-0.06900	0.00714
-98.52	13.13	-0.03345	-0.06962	0.00727
-99.58	13.63	-0.03515	-0.07086	0.00746
-99.93	13.86	-0.03595	-0.07148	0.00762
-100.67	14.04	-0.03579	-0.07286	0.00775
-101.13	14.18	-0.03710	-0.07348	0.00779
-101.93	14.45	-0.03930	-0.07451	0.00785
-102.35	14.50	-0.03749	-0.07520	0.00788
-103.26	14.72	-0.03664	-0.07671	0.00801
-103.66	14.86	-0.03700	-0.07747	0.00814
-104.45	15.00	-0.03842	-0.07892	0.00840
-104.80	15.00	-0.03960	-0.07968	0.00853
-105.76	15.00	-0.04089	-0.08098	0.00876
-106.24	15.00	-0.04108	-0.08160	0.00886
-107.03	15.04	-0.04349	-0.08298	0.00899

-107.43	15.04	-0.04442	-0.08353	0.00909
-108.21	15.27	-0.04387	-0.08477	0.00944
-108.66	15.54	-0.04283	-0.08546	0.00957
-109.43	15.95	-0.04311	-0.08677	0.00983
-109.72	16.00	-0.04437	-0.08746	0.00993
-110.52	16.00	-0.04374	-0.08890	0.00999
-111.00	16.00	-0.04291	-0.08952	0.01006
-111.67	16.00	-0.04416	-0.09090	0.01022
-111.93	16.04	-0.04561	-0.09152	0.01032
-112.46	16.40	-0.04855	-0.09255	0.01071
-112.92	16.68	-0.04830	-0.09310	0.01103
-113.69	17.04	-0.04847	-0.09441	0.01181
-114.11	17.04	-0.04755	-0.09496	0.01214
-114.73	17.00	-0.04614	-0.09648	0.01262
-115.63	17.27	-0.04900	-0.09841	0.01324
-116.03	17.50	-0.04925	-0.09889	0.01350
-116.78	18.09	-0.04815	-0.10020	0.01379
-117.09	18.36	-0.04827	-0.10089	0.01396
-117.89	18.54	-0.04885	-0.10240	0.01425
-118.88	18.54	-0.04927	-0.10433	0.01467
-119.20	18.54	-0.05005	-0.10495	0.01477
-122.07	19.68	-0.05222	-0.11128	0.01587
-128.30	22.18	-0.06201	-0.12719	0.01818
-148.39	30.72	-0.09703	-0.19069	0.02506
-158.66	35.68	-0.11421	-0.23132	0.02694
-174.58	45.45	-0.14360	-0.31478	0.01967
-180.91	50.00	-0.15858	-0.35637	0.00948
-191.13	58.59	-0.18496	-0.44232	-0.02045
-195.15	62.31	-0.19529	-0.48405	-0.03681
-201.70	68.90	-0.21257	-0.57075	-0.07070
-205.15	72.86	-0.22458	-0.62894	-0.09080
-212.66	81.72	-0.24851	-0.77700	-0.13907
-216.97	85.95	-0.26296	-0.86163	-0.16461
-225.94	92.50	-0.29236	-1.03166	-0.20528
-230.22	95.36	-0.30562	-1.11753	-0.21669
-238.10	100.68	-0.33583	-1.28700	-0.22540
-241.67	103.40	-0.35318	-1.37123	-0.22538
-248.45	108.86	-0.39312	-1.54208	-0.21233
-251.57	111.09	-0.41189	-1.62974	-0.20066
-257.53	114.99	-0.45487	-1.79743	-0.17789
-260.56	116.90	-0.47871	-1.88110	-0.16580
-267.35	120.40	-0.53119	-2.06331	-0.13596
-271.07	121.72	-0.56168	-2.16427	-0.11873
-277.67	123.99	-0.62620	-2.37947	-0.08167
-279.22	124.63	-0.64598	-2.44599	-0.06949
-279.24	124.68	-0.65521	-2.48297	-0.06282
-279.23	124.49	-0.65446	-2.48376	-0.06268

Table A.16 Data for the drained phase for test CNV10.

q [kPa]	Δu [kPa]	$\varepsilon_{a,l}$ [%]	$\varepsilon_{a,e}$ [%]	$\varepsilon_{r,l}$ [%]
-278.98	117.52	0.00000	0.00000	0.00000
-280.03	116.92	0.00379	0.00000	0.00014
-280.48	116.80	0.00269	0.00000	0.00015
-281.00	116.70	0.00311	0.00021	0.00029

-281.29	116.61	0.00297	0.00028	0.00036
-281.53	116.43	0.00275	0.00034	0.00045
-281.98	116.15	0.00203	0.00055	0.00068
-282.04	115.97	0.00261	0.00062	0.00078
-282.09	115.79	0.00282	0.00069	0.00084
-282.14	115.61	0.00289	0.00069	0.00091
-282.30	115.15	0.00279	0.00076	0.00107
-282.30	114.61	0.00273	0.00076	0.00120
-282.30	114.42	0.00272	0.00076	0.00123
-282.36	113.88	0.00248	0.00083	0.00136
-282.25	113.61	0.00283	0.00083	0.00140
-282.20	113.42	0.00305	0.00090	0.00143
-282.04	112.70	0.00237	0.00110	0.00159
-281.98	112.51	0.00315	0.00117	0.00166
-281.93	112.24	0.00314	0.00124	0.00172
-281.93	111.97	0.00386	0.00131	0.00179
-281.93	111.51	0.00363	0.00145	0.00188
-281.80	110.97	0.00432	0.00172	0.00205
-281.72	110.69	0.00388	0.00179	0.00211
-281.59	110.24	0.00504	0.00193	0.00221
-281.45	109.97	0.00432	0.00200	0.00227
-281.32	109.69	0.00404	0.00207	0.00231
-280.97	109.06	0.00394	0.00234	0.00240
-280.92	108.78	0.00415	0.00241	0.00247
-280.79	108.60	0.00446	0.00248	0.00250
-280.79	108.42	0.00383	0.00255	0.00253
-280.65	107.87	0.00419	0.00269	0.00266
-280.65	107.42	0.00345	0.00282	0.00279
-280.60	107.24	0.00316	0.00289	0.00283
-280.33	106.14	0.00355	0.00317	0.00305
-280.17	105.42	0.00342	0.00337	0.00318
-279.94	104.51	0.00333	0.00358	0.00331
-279.67	101.05	0.00433	0.00434	0.00387
-279.67	99.59	0.00441	0.00461	0.00409
-279.67	98.04	0.00496	0.00489	0.00432
-279.62	95.86	0.00602	0.00544	0.00464
-279.38	90.31	0.00754	0.00702	0.00559
-279.64	84.12	0.00871	0.00861	0.00679
-279.64	80.94	0.00952	0.00957	0.00747
-279.56	74.29	0.00983	0.01171	0.00893
-279.75	70.93	0.00911	0.01274	0.00974
-279.70	67.56	0.00888	0.01391	0.01056
-279.27	59.01	0.00815	0.01722	0.01267
-279.40	56.91	0.00727	0.01818	0.01325
-279.22	55.09	0.00652	0.01908	0.01380
-279.11	53.55	0.00612	0.01997	0.01426
-279.22	50.72	0.00547	0.02142	0.01510
-278.79	48.54	0.00569	0.02300	0.01591
-278.66	47.63	0.00603	0.02383	0.01630
-278.66	45.81	0.00635	0.02527	0.01718
-278.79	44.99	0.00588	0.02582	0.01754
-278.66	44.17	0.00590	0.02638	0.01790
-278.87	42.08	0.00619	0.02810	0.01890
-278.82	41.44	0.00553	0.02879	0.01919
-278.74	40.81	0.00534	0.02947	0.01955
-278.79	40.08	0.00520	0.03009	0.01981

-278.87	38.80	0.00451	0.03147	0.02036
-278.74	37.53	0.00373	0.03305	0.02111
-278.87	36.89	0.00343	0.03388	0.02150
-278.71	35.71	0.00216	0.03574	0.02231
-278.71	35.07	0.00156	0.03657	0.02273
-278.58	34.44	0.00109	0.03739	0.02316
-278.45	32.89	-0.00106	0.03960	0.02433
-278.58	32.43	-0.00206	0.04035	0.02478
-278.74	32.07	-0.00237	0.04104	0.02523
-278.98	31.71	-0.00273	0.04166	0.02566
-279.22	31.07	-0.00276	0.04283	0.02644

ERRATA CORRIGE

Page 75, line 16: **(0±0.0015)** instead of *(0±0.0015%)*

Page 76, line 27: **10^{-9} m/s** instead of *10^{-7} m/s*

Page 112, line 25: **stresses** instead of *stresse*